FINAL REPORT

Watershed to Local Scale Characteristics and Function of Intermittent and Ephemeral Streams on Military Lands

SERDP Project RC-1725

JULY 2015

David Cooper
Jeremy Shaw
Department of Forest and Rangeland Stewardship

Ellen Wohl
Dennis Harry
Nicholas Sutfin
Department of Geosciences

Stephanie Kampf
Joshua Faulconer
Department of Ecosystem Science and Sustainability
Colorado State University

SERDP
DOD ▪ EPA ▪ DOE

REPORT DOCUMENTATION PAGE

Form Approved
OMB No. 0704-0188

PLEASE DO NOT RETURN YOUR FORM TO THE ABOVE ADDRESS.

1. REPORT DATE *(DD-MM-YYYY)*	2. REPORT TYPE	3. DATES COVERED *(From - To)*
07/31/2015	Final Report	01/28/2010 - 07/31/2015

4. TITLE AND SUBTITLE

Watershed To Local Scale Characteristics And Function Of Intermittent And Ephemeral Streams On Military Lands

5a. CONTRACT NUMBER

10-C-0007

5b. GRANT NUMBER

5c. PROGRAM ELEMENT NUMBER

6. AUTHOR(S)

Cooper, D.J.; Wohl E.C.; Kampf, S.; Harry, D.; Shaw, J.; Sutfin, N.; Faulconer, J.

5d. PROJECT NUMBER

RC-1725

5e. TASK NUMBER

5f. WORK UNIT NUMBER

7. PERFORMING ORGANIZATION NAME(S) AND ADDRESS(ES)

Colorado State University
1472 Campus Delivery
Fort Collins, CO 80523

8. PERFORMING ORGANIZATION REPORT NUMBER

9. SPONSORING/MONITORING AGENCY NAME(S) AND ADDRESS(ES)

Strategic Environmental Research and Development Program
4800 Mark Center Drive, Ste 17D08
Alexandria, VA 22350

10. SPONSOR/MONITOR'S ACRONYM(S)

SERDP

11. SPONSOR/MONITOR'S REPORT NUMBER(S)

12. DISTRIBUTION/AVAILABILITY STATEMENT

Unlimited

13. SUPPLEMENTARY NOTES

14. ABSTRACT

The objective of this project is to determine the characteristics of intermittent and ephemeral streams and develop a stream hydrogeomorphic classification incorporating key physical process drivers that create and support riverine and riparian landforms, hydrologic regimes, and biota. We hypothesized that differences in channel planform, lateral confinement, and boundary materials would produce distinctive physical environments and biotic patterns in ephemeral stream networks. We outlined five hydrogeomorphic stream types, based on the above criteria, that are widespread throughout arid regions of North America: bedrock, bedrock with alluvium, incised alluvium, braided, and piedmont headwater streams. Our analyses of physical and biological patterns and processes were framed within this stream typology. Our hydrogeomorphic stream classification characterizes variation in fluvial form and function throughout stream networks, and can be used to facilitate management and restoration of ephemeral streams of the southwestern United States. Resource managers could use this conceptual framework to infer basic information on physical and ecological characteristics fluvial ecosystems, plan the types and locations of land use and human disturbance in order to minimize long-term environmental impacts, and improve the efficiency of resource inventories and mapping projects.

15. SUBJECT TERMS

Sonoran Desert, Ephemeral Stream, stream classification, rainfall-runoff, braided channel; channel geometry; arid region, riparian ecology, ecohydrology

16. SECURITY CLASSIFICATION OF:			17. LIMITATION OF ABSTRACT	18. NUMBER OF PAGES	19a. NAME OF RESPONSIBLE PERSON
a. REPORT	b. ABSTRACT	c. THIS PAGE			David J Cooper
U	U	U	UU	228	19b. TELEPHONE NUMBER *(Include area code)* 970-491-5430

Table of Contents

List of Figures

List of Tables

List of Acronyms

ANOVA = Analysis of Variance

BA = bedrock with alluvium channels

BD = braided channels

BMGR – Barry M Goldwater Range

BK = Bedrock channels

CT = Classification tree

DEM = Digital Elevation Model

DTM = Digital Terrain Model

IA = Incised alluvium channel

LDA = Linear discriminant analysis

NMS = non-metric multidimensional scaling ordination

PerManova = permutational multivariate analysis of variance

PC-Ord = computer program for multivariate statistics

TER-S = threatened, endangered and rare species

YPG = Yuma proving ground, Arizona

Keywords

Sonoran Desert, Ephemeral Stream, stream classification, rainfall-runoff, braided channel; channel geometry; arid region, riparian ecology, ecohydrology

Acknowledgements

Funding for this research was provided by the Strategic Environmental Research and Development Program (SERDP contract RC-1725), under the Resource Conservation and Climate Change program area. We greatly appreciate the opportunity to conduct this research, and thank the Program Manager, John Hall, his staff, and the staff at HydroGeoLogic for their support and guidance. We also thank Aaron Alvidrez of BMGR; Laura Merrill of YPG; and Meg McDonald, Ruben Hernandez, Chris Black, Mauricio Nicolls, Brian Bledsoe, Andrew Carlson, Whitney Mowl, Elise Mulder, Cole Green-Smith, and Dave Dust for assistance with various aspects of the project. For CMIP3 data, we acknowledge the modeling groups, the Program for Climate Model Diagnosis and Intercomparison (PCMDI), and the World Climate Research Programme (WCRP) Working Group on Coupled Modelling (WGCM) for their roles in making available the WCRP CMIP3 multimodel dataset. Support of this dataset is provided by the Office of Science, U.S. Department of Energy. For CMIP5, we also acknowledge WCRP's WGCM and thank the MPI climate modeling group for producing and making available their model output. For CMIP, the U.S. Department of Energy's Program for Climate Model Diagnosis and Intercomparison provides coordinating support and led development of software infrastructure in partnership with the Global Organization for Earth System Science Portals.

Abstract

Objectives

We describe the physical and biological characteristics of ephemeral streams of the Sonoran Desert and develop a stream hydrogeomorphic classification incorporating key physical processes (drivers) that create and support riverine and riparian landforms, hydrologic regimes and biota. We developed this classification on the Yuma Proving Ground by analyzing geomorphic, hydrogeologic, hydrologic, and ecological characteristics of ephemeral stream networks. We tested which stream classes and physical drivers were meaningful for identifying habitat characteristics and riparian biota on the Barry M. Goldwater Range.

We collected and analyzed 3 years of field data for representative streams to quantify physical patterns and processes, and the factors influencing the distribution of biota. We analyzed streamflow, groundwater, and volumetric water content data from the full range of stream types to develop a 3-dimensional perspective on surface water and ground water interactions, hyporheic zone characteristics, and the seasonality of surface, ground and soil water that supports and riparian biota. We also examined seasonal water relations of dominant riparian trees to understand how hydrologic variability affects their growth, survival, and reproduction. These data were used to develop a model of hydrologic processes and patterns that support key biota. A factorial experiment was used to determine the physical and biotic limitations to riparian tree reproduction.

Our analyses was used to build a climate and hydrology model to understand how climate changes may affect stream flow, subsurface water content, and riparian ecohydrology. We also describe the effects of hydrologic and geomorphic alterations associated with roads and other military land uses on fluvial landforms, hydrology, and riparian structure and function. Our stream classification provides tools for rapid, long-term and cost effective monitoring and management. Our analysis of factors limiting seedling survival can be used to improve revegetation efforts, and could be used as the basis for scaling up to restore entire stream systems.

Technical Approach

We hypothesized that differences in channel planform, lateral confinement, and boundary materials would produce distinctive physical environments and biotic patterns in ephemeral stream networks. We outlined five hydrogeomorphic stream types, based on the above criteria, that are widespread throughout arid regions of North America: bedrock, bedrock with alluvium, incised alluvium, braided, and piedmont headwater streams. Our analyses of physical and biological patterns and processes were framed within this stream typology.

We collected and analyzed field data describing geomorphic characteristics and composition of riparian plant communities on 86 stream reaches throughout YPG, and verified these observations on 15 stream reaches at BMGR. At a subset of 18 representative study reaches at YPG, we measured the timing, magnitude and frequency of rainfall and streamflow events. Eight intensively instrumented study reaches on YPG were used to clarify the interactions of surface water, groundwater, and unsaturated water content. Subsurface alluvial structure and stratigraphy of these sites was also investigated. Ecohydrological relations of riparian trees, including seasonal water sources, patterns of water stress, and sap flow were documented and related to streamflow and subsurface moisture dynamics. The importance of herbivory, nurse plant shading, and infrequent wet periods on riparian tree seedling survival was determined in a factorial field experiment.

Results

Differences in channel planform, lateral confinement, and boundary materials reflect distinctive geomorphic process domains within ephemeral watersheds, resulting in consistent patterns of channel morphology and hydraulics among the five stream types (Chapter 1). Patterns in subsurface stratigraphy and alluvial characteristics were evident at broader spatial scales (Chapter 2). Incised alluvium and braided streams that occur within lowland valley settings contain deep (~1 m) active alluvial deposits underlain by consolidated sedimentary strata, while bedrock with alluvium streams in narrow mountain valleys exhibit thinner active alluvium and complex subsurface stratigraphy bounded by bedrock. Bedrock and piedmont headwater channels lack persistent alluvium. Differences in streamflow responses among stream types correspond to network position and channel boundary materials (Chapter 3). Bedrock and piedmont headwater streams, which drain small watersheds with low infiltration rates, experience runoff most

frequently. Streamflow occurs less frequently in channels containing unconsolidated alluvial deposits, such as bedrock with alluvium, incised alluvium, and braided streams, where floods occur almost exclusively during intense summer thunderstorms. Direct precipitation from storm events briefly increase water content within the upper 100 cm of alluvial deposits, but deep recharge occurs only after periodic summer floods (Chapter 4). In all stream types, streamflow and saturation of shallow alluvium typically lasts for only a few hours, but deeper recharge (2-3 m) beneath incised alluvium and braided streams can persist for months after flow events.

The stream types support distinctive riparian plant communities, and differences in community composition closely mirror the distinctive morphological attributes of stream types, highlighting the critical role of geomorphic disturbance in shaping riparian vegetation of arid ephemeral streams (Chapter 5). Compositional differences among stream types correspond primarily to variation in channel gradient and width:depth. Within the study area, large woody plants rely primarily on water from near-surface (0-50 cm) alluvial sediments, but riparian trees access water from different depths, following seasonal shifts in water availability (Chapter 6). All riparian trees access water from greater depths during drought periods, when plant water stress is greatest (Chapter 7). In braided and incised alluvium streams, periodic large floods can improve riparian tree water status for several seasons, while limited storage capacity in the shallow substrate of bedrock with alluvium and piedmont headwater streams results in more regular seasonal dynamics. Herbivory by small mammals appears to be the primary limitation to riparian tree establishment within the study area, and significant seedling survival requires protection from herbivores and shading by nurse plants, both of which can be provided by shrubs with dense canopies (Chapter 8). Infrequent wet years substantially increase seedling survival rates, and likely influence desert tree population dynamics over timescales of decades to centuries. Integrated climate and hydrology models suggest that increasing frequency of extreme storm events can result in greater deep recharge, while shallow alluvial water content is relatively insensitive to model parameters (Chapter 9). However, many uncertainties remain in predicting the effects of global climate changes on monsoon rainfall patterns that drive ecohydrological dynamics, and resource managers should focus on minimizing hydrologic alterations and maintaining streamflow connectivity to avoid ecological degradation.

Benefits

Our hydrogeomorphic stream classification characterizes variation in fluvial form and function throughout stream networks, and can be used to facilitate management and restoration of ephemeral streams of the southwestern United States (Chapter 10). Resource managers could use this conceptual framework to infer basic information on physical and ecological characteristics fluvial ecosystems, plan the types and locations of land use and human disturbance in order to minimize long-term environmental impacts, and improve the efficiency of resource inventories and mapping projects. Our analyses also demonstrated that improved revegetation and stream restoration efforts require providing protection from herbivores and shade, while planting larger seedlings during infrequent wet years maximizes survival rates. This information provides a better understanding for managing and restoring ephemeral streams on southwestern DoD installations, thereby increasing the capacity for sustainable ranges in the context of military training and testing, maintenance of critical riparian habitat for listed and at-risk species, and enabling appropriate restoration of degraded stream systems.

Objectives

This work responds to the SERDP FY 2010 Statement of Need (SISON-10-02) to develop scientific understanding to support the management and restoration of intermittent and ephemeral streams on Department of Defense (DoD) installations in the southwestern United States. Our overall objectives were to improve understanding of ecological variation in ephemeral stream networks, and develop tools that provide insight into the effects of hydrologic alterations due to climate change. We addressed this need by implementing a wide range of hydrological, geomorphic and ecological investigations. The objectives of this suite of studies were to provide a broad understanding of ephemeral streams on the two military installations, their sensitivity to climate changes, and human disturbances, and a set of tools that could be used for continued study and restoration. Specific objectives included:

1. Characterize the spatial and temporal variation of physical and ecological properties of ephemeral stream systems that occur on DoD installations in the southwestern United States. This need was addressed by developing a stream classification system that characterized spatial variation in geomorphology and riparian plant communities at Yuma Proving Ground (YPG) and Barry M. Goldwater Range (BMGR). Within the context of this stream classification, local-scale studies were used to characterize variation in streamflow and subsurface moisture regimes, and riparian tree ecohydrologic relations at YPG.
2. Improve understanding of the interactions between contemporary hydrologic regimes and non-native invasive species on the composition, structure, and function of native communities in southwestern ephemeral stream systems. We used the stream classification system to relate spatial patterns in streamflow, soil moisture dynamics, and geomorphology to the composition, structure, and function of riparian plant communities. We also identified linkages between seasonal patterns of water stress and water use in the dominant riparian trees of the Sonoran desert to contemporary rainfall, streamflow, and soil moisture dynamics.
3. Determine how projected climate change may impact ephemeral stream systems, and the implications for managing these systems. Hydrologic models were developed to determine potential changes in runoff and subsurface moisture dynamics due to climate change, and we outlined implications for management.
4. Develop adaptive management interventions that can mitigate the adverse ecological effects of current stresses and future climate changes. To address mitigation of disturbances from military training activities, we designed and implemented a factorial analysis to determine the requirements for reestablishing the dominant woody plants along ephemeral streams. We also provided general guidelines on management interventions to mitigate future impacts associated with training and infrastructure development, as well as climate change.

Introduction & Background

Hydro-ecological research has focused largely on perennial rivers (Nanson et al., 2002) while relatively little is known about the factors controlling hydrologic or geomorphic processes, or the distribution of riparian vegetation and other biota, in ephemeral stream networks (Zimmerman, 1969; Zimmerman et al., 1999; Williams 2006). Few perennial streams occur in the southwestern US, and on a landscape-scale stream networks may be composed entirely of intermittent and ephemeral streams. The processes and properties of intermittent and ephemeral streams that affect riparian vegetation may contrast strongly with those of perennial streams (Hupp and Osterkamp, 1996; Tooth, 2000). Stream flow variability is typically greater in ephemeral basins (Poff, 1996; Bull and Kirkby, 2002), and the magnitude and frequency of floods commonly decrease downstream due to high transmission losses and asynchronous tributary inflows (Yair and Lavee, 1985; Goodrich et al., 1997). These streams have surface flows for hours to weeks each year, yet provide many of the same critical ecological and geomorphic functions as perennial streams, including habitat for threatened, endangered and at-risk species (TER-S), ground water recharge, bank stability, and maintenance of floodplains and riparian vegetation. Studies of ephemeral streams in the Southwest demonstrate that as watershed area and stream length increases, drainage density and watershed slope decreases, producing wider and deeper stream channels (Leopold and Miller, 1956; Miller et al., 1996; Youberg et al., 1998; Shaw and Cooper, 2008) with more attenuated stream flow (Murphey et al., 1977; Goodrich et al., 1997).

Stream channel morphology and runoff characteristics in turn dictate alluvial aquifer recharge and subsurface hydrologic regime (Walter, 1990; Sorman et al., 1997; Dunkerley and Brown, 1999; Lange, 2005; Shaw and Cooper, 2008). The frequency and duration of flow, intensity of flood disturbance, and the thickness of alluvium determine many aspects of how intermittent and ephemeral streams function, and the riparian vegetation and animal species that can be supported. By understanding the physical drivers of these streams, the landforms and hydrologic systems they create, and response of riparian plants to these characteristics, a model of stream hydrology, geomorphology and biota as well as a stream classification can be developed. This model and classification could be used as the basis for understanding landscape physical characteristics, the distribution of biota including native species, TER-S, and exotic species, as well as the impacts of hydrologic and climatic changes. The model could also be used to identify the relative sensitivity of different stream segments to natural and human-induced disturbances.

Relatively minor modifications in the frequency and duration of flow, or characteristics of the alluvial channel and hyporheic zone, may significantly perturb a stream and riparian ecosystem. Understanding the effects of water diversions, roads, off-road vehicle use, and other impacts on stream hydrologic regimes, landforms and the biota that depend upon them is a critical need for understanding and managing streams. Invasive species are another concern for many military bases. Heavy maneuvering of troops and equipment may cause disturbances that impact native vegetation and channel landforms, allowing invasive plants to succeed. Replacing stands of invasive plants with native plants on military training grounds will improve habitat for TER-S, create more sustainable ecological systems, and maintain mission readiness.

Flow in dry land ephemeral channels typically results from high-intensity rainfall that generates Hortonian overland flow. Sparse vegetation and thin soils promote rapid runoff resulting in flashy hydrographs. Streamflow exhibits high spatial variability due to poor connectivity of drainage networks (Nanson et al., 2002), transmission losses through channels, and high spatial and temporal variability of convective storms (Goodrich et al., 1997). Because runoff in ephemeral streams is infrequent, floods and other disturbances can have long-lasting effects on channel form (Bull and Kirkby, 2002). Due to the importance of floods in ephemeral channels, hydrologic modeling in these systems typically focuses on simulating runoff during isolated rainfall events (Shannon et al., 2002).

Riparian vegetation relies not only on infrequent surface runoff but also on the long-term availability of subsurface water. By incorporating measurements of soil water and ground water in the riparian zone, we will study continuous hydrologic dynamics of ephemeral streams rather than relying solely on inferences from runoff events. Continuous soil water measurements indicate timescales of soil water response to precipitation and runoff, and distinguish the persistence of water availability in different channel types. These measurements will allow us to develop metrics to describe both soil water and surface water dynamics in terms of their “flashiness” or time scales of response to hydrologic inputs. Supplementary measurements of local microclimate and unsaturated zone soil moisture and temperature will help us further characterize how water use by riparian plants interacts with these ground and surface water dynamics.

Description of conceptual model

Five primary types of stream channels are present on military installations in the Sonoran Desert; (1) bedrock, (2) bedrock with alluvium, (3) incised alluvium, (4) braided, and (5) piedmont headwaters (Figure 1). We posit a downstream progression in channel characteristics in relation to, (i) composition of channel boundaries, (ii) lateral confinement, (iii) depth of alluvium, and (iv) flow characteristics.

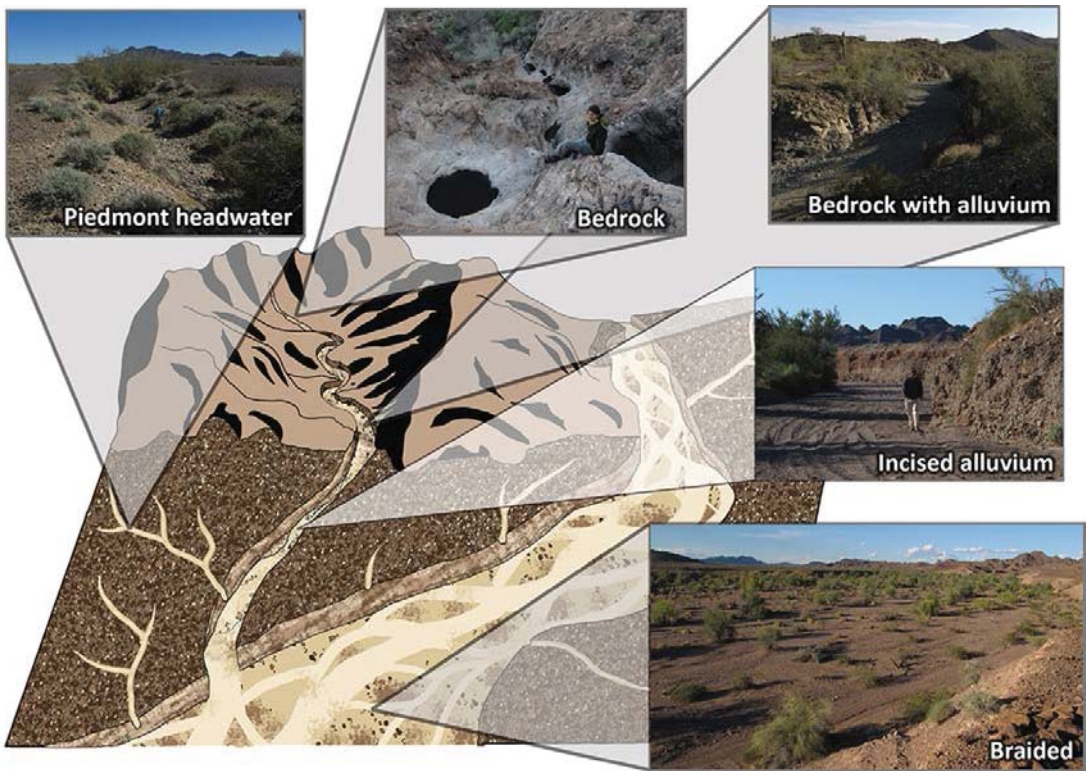

Figure 0-1. Schematic illustration of conceptual model for longitudinal distribution of stream types on military installations in the Sonoran Desert.

Bedrock streams are formed in cohesive bedrock, are closely confined between steep valley walls, and have little or no alluvial sediment present along the streambed. Surface flow in these streams may be perennial or intermittent, and is often spatially discontinuous. *Perennial* stream segments, which are of very limited longitudinal extent in the study area (< 1 km long), are supplied by springs and flow throughout the year. *Intermittent* streams, which may be supplied by springs or the gradual release of floodwater stored in alluvium (Meinzer 1923), flow seasonally when subsurface moisture availability exceeds evapotranspiration demands. Flow typically starts at the source springs but continues only a few tens to hundreds of meters downstream before disappearing. In many instances, streams are *discontinuously* perennial or intermittent, where surface flow may infiltrate in reaches of thick alluvium and reappear further downstream along channel segments with shallow alluvium. Relative to other channel types, runoff will occur most frequently in bedrock channels, but infiltration capacities are low except along fracture zones. Therefore, bedrock channels are likely to have the lowest availability of subsurface moisture. A special subset of bedrock streams contain *tinajas*, which are deep, narrow depressions in bedrock that can hold water for much longer times than adjacent stream segments (sometimes throughout the year). These sites support aquatic organisms and provide important water sources for terrestrial species from birds to bighorn sheep. Little research has been done on the physical processes by which tinajas form, or the characteristics of the bedrock substrate and channel geometry necessary to create these features. We will evaluate controls on form, process, and location for tinajas as part of the study of geologic-geomorphic controls on channel systems in the study area.

Streams designated as ***bedrock with alluvium*** are also form in cohesive bedrock and are closely confined between steep valley walls, but sufficient alluvial sediment is present to create bedforms such as pools and riffles and to store subsurface water. These streams can be perennial, but are most likely to be intermittent or discontinuously

intermittent. As alluvium accumulates downstream, infiltration capacity increases, providing greater opportunity for surface water infiltration. Of the channels with alluvial sediments, bedrock with alluvium channels will have the highest supply of surface water for infiltration, but the lowest capacity for ground water storage.

As stream channels cross the mountain front into the piedmont environment characterized by alluvial fans and pediments, streams are likely to be ***incised*** into alluvium. In addition, ***piedmont*** surfaces form significant headwater areas similar to bedrock mountain systems. This alluvium may be cohesive as a result of secondary calcium carbonate sedimentation, but the streambed is typically non-cohesive sand- to boulder-sized sediment. Although the valley walls are no longer present, the active channel is narrowly confined within alluvial banks that may be overtopped during rare floods, depending on the depth of incision. The depth of alluvium below the streambed increases substantially, facilitating infiltration and subsurface flow, causing these streams to be *ephemeral*, with flow that is discontinuous in time. These streams are not spring-fed and flow only briefly in response to rainfall. Because of increased infiltration capacity, incised alluvium channels experience less surface runoff.

Further from the mountain front, stream gradient decreases and, although the streams may remain incised, they are more likely to be shallow ***braided*** channels with very little lateral confinement, thick alluvium, and ephemeral flow. Braided streams are also formed in non-cohesive sand- to boulder-sized sediment and have the potential for substantial erosion and deposition during floods. High transmission losses limit stream flow in these channels, but because they occupy the lowest portions of stream networks, they are supplied by down-slope flow of alluvial ground water.

Average annual precipitation at Yuma Proving Ground is 93 mm (NOAA, 1998). Over half of annual rainfall comes from summer convective storms that are brief but intense. These storms generate large floods within the upper channel segments (bedrock, bedrock with alluvium), but the flood wave generally dissipates within the incised alluvium or braided reaches. More extensive floods result from the rare dissipating tropical storm during the autumn months, such as Hurricane Nora in 1997. Frontal storm systems pass through the region during winter, bringing widespread, low-intensity rainfall. Winter frontal storms or autumn tropical storms are more likely to produce longitudinally continuous flow throughout a drainage network, although this flow will be brief in duration (hours to days). All types of floods are typically erosive within the confined, steep geometries of the upper channel segments. Localized erosion and deposition alternate within the lower alluvial segments, creating a greater diversity of habitats for plants and animals.

Riparian and aquatic organisms respond to, and influence, the downstream progressions described above. Aquatic species that require year-round surface water are confined to pools immediately downstream from springs and tinajas. Tinajas are also critical to terrestrial species such as the desert bighorn sheep (*Ovis canadensis nelsoni*) and Sonoran pronghorn antelope (*Antilocapra americana sonoriensis*). Distinctive riparian and wetland communities are typically present in the vicinity of ephemeral pools that form in alluvium, although riparian communities are of limited extent and diversity within the bedrock, piedmont headwaters, and bedrock with alluvium, channel types.

The extent and diversity of riparian vegetation increases in a downstream direction. From a distance, incised and braided channels may be visible because of the darker green woody riparian vegetation lining the channels. Vegetation cover in upland areas is only 1-5%, but increases to an average of 31% within the incised and braided portions of Yuma Wash at Yuma Proving Ground (Merritt and Wohl, 2003). Dominant vegetation in the channels is composed of xeric woody species and phreatophytes such as ironwood (*Olneya tesota*), blue palo verde (*Cercidium floridum*), mesquite (*Prosopis juliflora*), smoke-tree (*Dalea spinosa*), and catclaw acacia (*Acacia greggii*). Spatial distribution of these plants likely reflects the combined effects of fluvial disturbance and availability of surface (during ephemeral flows) and subsurface water. The plants thus reflect downstream increases in alluvial deposition and variation in disturbance regime, but also influence channel characteristics by increasing hydraulic resistance within the channel and increasing shear strength of the channel substrate. Merritt and Wohl (2003) inferred a threshold relationship between flow and riparian vegetation along braided portions of Yuma Wash during flooding from Hurricane Nora. The Nora flood eroded confined portions of the braided channel, but when stage increased sufficiently to overtop vegetated bars, the resulting increase in hydraulic resistance facilitated deposition, causing channels to aggrade.

Natural disturbances along channels of the Sonoran desert take the form of debris flows and floods. Debris flows may extend into the incised channels of the piedmont, but are typically confined to the upper channel segments. They occur where sufficient weathered material has accumulated on hillslopes to be mobilized *en masse* by intense

rainfall. Because of the extreme aridity and slow bedrock weathering in the study region, debris flows are relatively rare, with recurrence intervals of centuries. Floods, although also recurring at intervals of a decade or more, are the primary natural disturbance. Although erosion and deposition during floods can kill individual aquatic and riparian organisms, most riparian plants have adaptations to flooding that lead to recruitment and population increase following a flood. For example, riparian plants may resprout after sediment burial or stem breakage, and bare moist sediments provide sites for riparian plant germination.

Anthropogenic disturbances to stream systems in the Sonoran Desert take the form of changes in land cover, selective removal of woody riparian vegetation, withdrawal of ground water at rates exceeding natural recharge, and introduction and spread of invasive exotic species. Changes in land cover can result from domestic grazing, cropping, urbanization, or military training exercises, each of which has the potential to change vegetation type and distribution, as well as infiltration and runoff potential. Selective removal of woody riparian vegetation for firewood and construction materials, along with declining soil water availability can stress riparian plants, has resulted in substantial declines in the extent of woody riparian communities throughout the Sonoran Desert during the past 150 years (Turner et al., 2003). Lowered water tables caused by ground water withdrawals may alter the ability of riparian vegetation to persist along channels, and may exacerbate channel incision where formerly intermittent or perennial channels become ephemeral (Waters and Haynes, 2001). Invasive exotic plants such as *Tamarix* spp. compete with native species that may already be stressed by changes in land cover and water tables. Anthropogenic disturbances are typically most severe in the lower (incised alluvium, braided) channel segments where most intensive land use occurs, although disruption of an isolated spring or tinaja can severely affect aquatic and terrestrial species dependent on that single water source.

Research Goals

1. Develop a stream hydrogeomorphic classification incorporating key physical processes (drivers) that create and support riverine and riparian landforms and biota. Our goal was to develop and test this classification in the Yuma Proving Ground by doing an inventory/baseline analysis of 86 streams over 3 years. We wanted to test which stream classes and physical drivers were biologically meaningful for identifying the habitat characteristics and ecological thresholds for key taxa, especially riparian and wetland habitat for threatened, endangered and at-risk species (TER-S).

2. Test the classification by analyzing geomorphology and riparian plant communities of 15 streams on the Barry M. Goldwater Range. Our goal was to verify that the general patterns among stream types at BMGR were consistent with those observed at YPG.

3. Characterize the geomorphic, hydrologic, and ecological controls on stream and riparian function at reference sites that represent the types of streams identified in our classification. Our goal was to measure stream stage, flow duration and volumetric soil water content data from the range of stream types to develop a 3-dimensional perspective on surface water and ground water interactions, hyporheic zone characteristics, and the seasonality of surface, ground, and soil water that supports aquatic and riparian biota. We also sought to model hydrologic processes and patterns that support key biota.

4. Analyze the effects of hydrologic and geomorphic alterations associated with roads and other military land uses and feral burros on fluvial landforms, stream characteristics, floodplain formation, non-native species, TER-S, and riparian structure and function. Our goal was to assess the downstream patterns in channel form and function, and associated hydrology and biota, in drainages least affected by land use within or adjacent to the channel network, and use these as reference conditions.

5. Develop and test options for long-term and cost effective monitoring, management of streams and riparian resources, and restoration techniques. This task sought to identify the processes necessary to establish native woody plants in disturbed riparian lands, and provide guidance on the restoration of desert stream biota.

Study Area Description

Study reaches were located within the US Army Yuma Proving Ground (YPG) and US Air Force Barry M. Goldwater Range (BMGR) in the Sonoran Desert of southern Arizona, USA. This portion of the Sonoran Desert lies within the Basin and Range Physiographic Province, a region characterized by low igneous mountain ranges separated by broad alluvial valleys (Shreve and Wiggins 1964, McAuliffe 1999). These linear intrusive and volcanic mountain ranges were formed during mid-Tertiary crustal extension and regional magmatism, while valley fill and

piedmont sediments were deposited during the Miocene to Pleistocene epochs (Eberly and Stanley 1978, Richard et al. 2000). Modern drainages contain reworked Plio-Pleistocene sediments and Holocene alluvium, consisting of gravel to cobbles supported in a sandy matrix.

The Yuma Proving Ground is within the Lower Colorado Valley subdivision (also known as Colorado Desert), the most arid portion of the Sonoran Desert (Shreve and Wiggins 1964, Turner and Brown 1994). This area consists of level plains and gently sloping bajadas, with low mountain ranges composed of primarily extrusive rocks, and elevations between 60 to 845 m. The Barry M. Goldwater Range lies at the interface of the Lower Colorado Valley and Arizona Uplands subdivisions, with elevations between 260 and 1250 m. Aside from the allogenic Colorado and Gila rivers, streamflow throughout the region is ephemeral (Shreve and Wiggins 1964).

The Sonoran Desert within southwestern Arizona is a hyperthermic arid region, where potential evapotranspiration exceeds precipitation throughout the year (Sellers and Hill 1974). Biseasonal rainfall is derived from Pacific frontal storms from November to March, while convective thunderstorms of the North American Monsoon occur from July to September. Mean annual precipitation increases with elevation, and ranges from 93 to 103 mm at YPG, and from 156 to 213 mm at BMGR (NCDC station IDs #29654, 26865, 23393, 20080). Temperatures throughout the region are more uniform, with mean annual daily minima and maxima of 13˚C and 32˚C.

Upland vegetation consists of scattered microphyllous shrubs and subshrubs, primarily *Larrea tridentata* (creosote) and *Ambrosia dumosa* (white bursage) (Shreve and Wiggins 1964, Turner and Brown 1994, Turner et al. 1995). Riparian plant communities are largely composed of xerophytic shrubs such as *Acacia* spp., *Ambrosia* spp., *Lycium* spp., *Encelia farinosa* (brittlebush), and *L. tridentata*. Common tree species throughout ephemeral stream networks of the Sonoran Desert include *Olneya tesota* (ironwood), *Parkinsonia microphylla* (foothills paloverde), and *P. florida* (blue paloverde), while *Psorothamnus spinosus* (smoketree) and *Prosopis velutina* (velvet mesquite) are locally abundant along larger alluvial streams. With the exception of smoketree, these trees occupy upland surfaces within the wetter portions of their ranges, and may be considered facultative riparian species (Turner and Brown 1994, Turner et al. 1995, Smith et al. 1997).

Chapter 1. A Geomorphic Classification of Ephemeral Channels in a Mountainous, Arid Region, Southwestern Arizona, USA

Abstract

Despite the global abundance of arid-region ephemeral streams, hydrologic and geomorphic data for these systems are limited compared to their perennial counterparts. High spatial and temporal variability in flow make hydrologic and geomorphic aspects of dryland ephemeral channels difficult to characterize. Perennial stream classifications have been extended to dryland ephemeral streams but do not adequately describe observed differences in channel geometry and characteristics of ephemeral channels in desert environments. We present a geomorphic classification for ephemeral streams in mountainous regions based on planform, degree of confinement, and composition of confining material. Five stream types were identified in the Sonoran desert of southwestern Arizona: (1) piedmont headwater, (2) bedrock, (3) bedrock with alluvium, (4) incised alluvium, and (5) braided channels. Nonparametric permutational multivariate analysis of variance for 101 surveyed reaches indicated differences ($p < 0.001$) in channel geometry and hydraulics among the five stream types. Nonmetric multidimensional scaling ordination identified the strongest channel geometry and hydraulic variables capable of distinguishing the five channel types, and a classification tree determined relative importance of these variables in the following order: width-to-depth ratio (*W/D*), stream gradient (*S*), stream power (Ω), and shear stress (τ). A classification tree and discriminant analysis used *W/D*, *S*, Ω, and τ for 86 study reaches on the U.S. Army Yuma Proving Ground (77% and 77% internal validation hit rate, respectively) to predict stream type of 15 separate study reaches on Barry Goldwater Air Force Range with 67% and 73% external validation hit rates, respectively. Differences in channel geometry among the five stream types reflect likely differences in hydrology, hydraulics, and sediment transport with implications for disturbance regime, channel adjustment to disturbance, and ecological sensitivity.

Introduction

Understanding the relationships between physical and biological characteristics of fluvial ecosystems is crucial to assessing their sensitivity to natural and anthropogenic disturbances. Our knowledge of hydrologic, geomorphic, and ecological relationships in dryland ephemeral channels, however, is hindered by limited data sets. In addition, classifications created for perennial streams are commonly used for intermittent and ephemeral streams, even though the classifications do not adequately address the geomorphic characteristics of channel networks in arid regions.

In this chapter, we developed and tested an *a priori* channel classification based on the physical characteristics of ephemeral channels in a mountainous desert region. The classification focuses on channel geometry, as reflected in differences among channel planform, lateral confinement, and composition of boundary materials. We emphasize these characteristics because they persist for tens to hundreds of years and are readily identified in the field. Channel geometry also strongly influences the distribution of hydraulic forces and the transport of sediment and nutrients (Hassan, 1990; Powell et al., 1998). A classification based on channel geometry can provide insights into the processes occurring during infrequent and episodic flows, which are typically of short duration and difficult to observe or measure. This classification provides a foundation for investigating the relationships between channel geometry and geomorphic processes.

Ephemeral streams in arid regions

Ephemeral streams constitute a significant portion of river networks in arid regions, which cover approximately one-third of Earth's land surface (Cooke and Warren, 1973). Spatial and temporal relationships of fluvial processes vary greatly between dryland rivers and those in humid regions (Graf, 1988a; Reid and Larrone, 1995; Tooth, 2000; Bull and Kirkby, 2002; Reid and Frostick, 2011). Recurrence intervals for bankfull flows in arid-zone rivers range from ~ 1 to 32 years, as opposed to ~ 1.5-year recurrence intervals typical of temperate zone rivers (Graf, 1988a; Bull and Kirkby, 2002). Infrequent, sporadic, and segmented flows in arid regions reflect spatial variability in precipitation significant enough to produce runoff, and the discontinuity of flow conveyance.

Ephemeral streams typically exhibit large downstream decreases in unit discharge (Babcock and Cushing, 1941; Cornish, 1961; Lane et al., 1971; Walters, 1989; Hughes and Sami, 1992; Goodrich et al., 1997) as a result of storms covering only a portion of a watershed. In addition, substantial transmission losses result from high rates of evapotranspiration and infiltration into dry, unconsolidated alluvial beds, creating a positive feedback (Keppel and Renard, 1962; Constantz et al, 1994; Bull, 1997; Goodrich et al., 1997; Tooth, 2000). Infiltration losses decrease flow depth and sediment transport capacity, cause aggradation in low-gradient channel segments, and increase the volume of stored alluvium. Enhanced sediment deposition within channels maintains high infiltration rates and subsurface storage capacity, increasing the potential for further transmission losses (Graf, 1988a; McDonald et al., 2004; Reid and Frostick, 2011). Downstream increases in the extent and thickness of alluvium, and associated transmission losses, can lead to increased subsurface moisture storage in ephemeral channels, supporting more abundant and functionally diverse vegetation (Shaw and Cooper, 2008).

Decreased transport capacity associated with transmission losses and flow obstruction by vegetation creates a positive feedback for instream aggradation (Graf, 1988a; Reid and Frostick, 2011; Merritt and Wohl, 2003). Aggradation increases storage capacity of subsurface water and promotes vegetation establishment and increased flow resistance (Bull, 1977; Knighton, 1998; Graf, 1981, 1988a; Stanley et al., 1997; Tooth, 2000; Tooth and Nanson, 2000; Comporeale et al., 2006; Reid and Frostick, 2011). Woody vegetation can limit channel adjustment during subsequent flows by enhancing the erosional resistance of banks and bars (Merritt and Wohl, 2003; Perucca et al., 2007; Camporeale et al., 2013).

Perennial streams with coarse-grained sediment are reportedly more ecologically productive than those composed of finer silt- and clay- sized particles (Allan, 1995; Waters, 1995), but the accumulation of silt in dryland channels may facilitate storage of water in micropores on annual time scales (Brooks et al., 2009). The filling of pore spaces with fine sediment on alluvial streambeds following transmission losses (Knighton, 1998; Bull and Kirkby, 2002; Reid and Frostick, 2011) can result in complex layering that limits downward flow (Graf, 1981; Ronan et al., 1998) and results in water retention closer to the surface.

In contrast to alluvial washes, adjacent upland surfaces in arid regions are commonly characterized by desert pavement underlain by a relatively impermeable silty, clay-rich A_z vesicular horizon (McFadden et al., 1987, 1998). These surfaces limit infiltration capacity, increase overland flow, and contribute to the flashy runoff response of ephemeral channels (Graf, 1988a; McAuliffe, 1994; Tooth, 2000; Bevens, 2002; Bull and Kirkby, 2002; Young et al., 2004; Wood et al., 2005). Surface runoff and channel patterns on upland piedmont surfaces reflect past depositional environments or inherited memories (*sensu* Sidorchuk, 2003) by concentrating flow and facilitating channel initiation in topographic depressions.

Complex response to short-lived infrequent flows in arid-region ephemeral streams results in progressive episodes of cutting and filling (Schumm, 1977; Patton and Schumm, 1981) accompanied by channel widening (Hooke, 1967; Bull, 1997; Powell et al., 2005). Progressive aggradation in braided channels commonly results in the development of secondary channels perched above the main channel (Keppel and Renard, 1962; Graf, 1988a; Reid and Frostick, 2011). During periods of relatively more frequent and lower magnitude flows, braided channels typically develop compound meandering channels inset across the braided valley bottom (Graf, 1988b). Infrequent, high-magnitude floods can completely restructure ephemeral channel geometry and temporary flow characteristics in arid regions (Graff 1988a), but ephemeral streams tend to maintain similar flow characteristics over longer periods of time (Bull and Kirkby, 2002).

Despite the relative long-term stability of flow characteristics in ephemeral streams, channel characteristics commonly exhibit spatial variability and longitudinal discontinuity in arid regions. Longitudinal changes in channel planform commonly occur with changes in lithology and valley characteristics. For example, single-thread channels can transition into braided as valleys widen (Leopold et al., 1964; Graf, 1981; Bull, 1997). This adjustment in planform is accompanied by decreased flow depth and velocity, abrupt decreases in channel gradient, increased infiltration losses, declining unit discharge, and abundant sediment input resulting in part from bank erosion (Graf, 1988a; Knighton, 1998; Bull and Kirkby, 2002; Reid and Frostick, 2011).

Regional setting

Study sites included ephemeral watersheds ranging in size from 0.0014 to 23,000 ha within the U.S. Army Yuma Proving Ground (YPG; > 3300 km^2) and Barry M. Goldwater Air Force Range (BMGR; > 6800 km^2) in

southwestern Arizona within the Sonoran desert (Fig. 1-1). The primary study area and source of the calibration data set for the stream classification was the western portion of YPG within watersheds ranging in elevation from 90 to 860 m. Data used for verification and testing of the classification system were collected and derived from the eastern side of BMGR in watersheds of 260 to 1250 m elevation.

The YPG and BMGR lie within the Basin and Range physiographic province, where broad alluvial lowlands separate individual mountain ranges. Heterogeneous soil characteristics on various surfaces result in highly variable infiltration rates (Bacon et al., 2008). The most common surface types within the study areas are (i) exposed intrusive and extrusive igneous bedrock of primarily felsic composition (Eberly and Stanley, 1978), (ii) unconsolidated alluvial sediments in washes with relatively frequent hydrologic and anthropogenic disturbances, and (iii) desert pavement on relict alluvial fan and piedmont surfaces. The YPG and BMGR are used for various military training activities and contain limited public access roads.

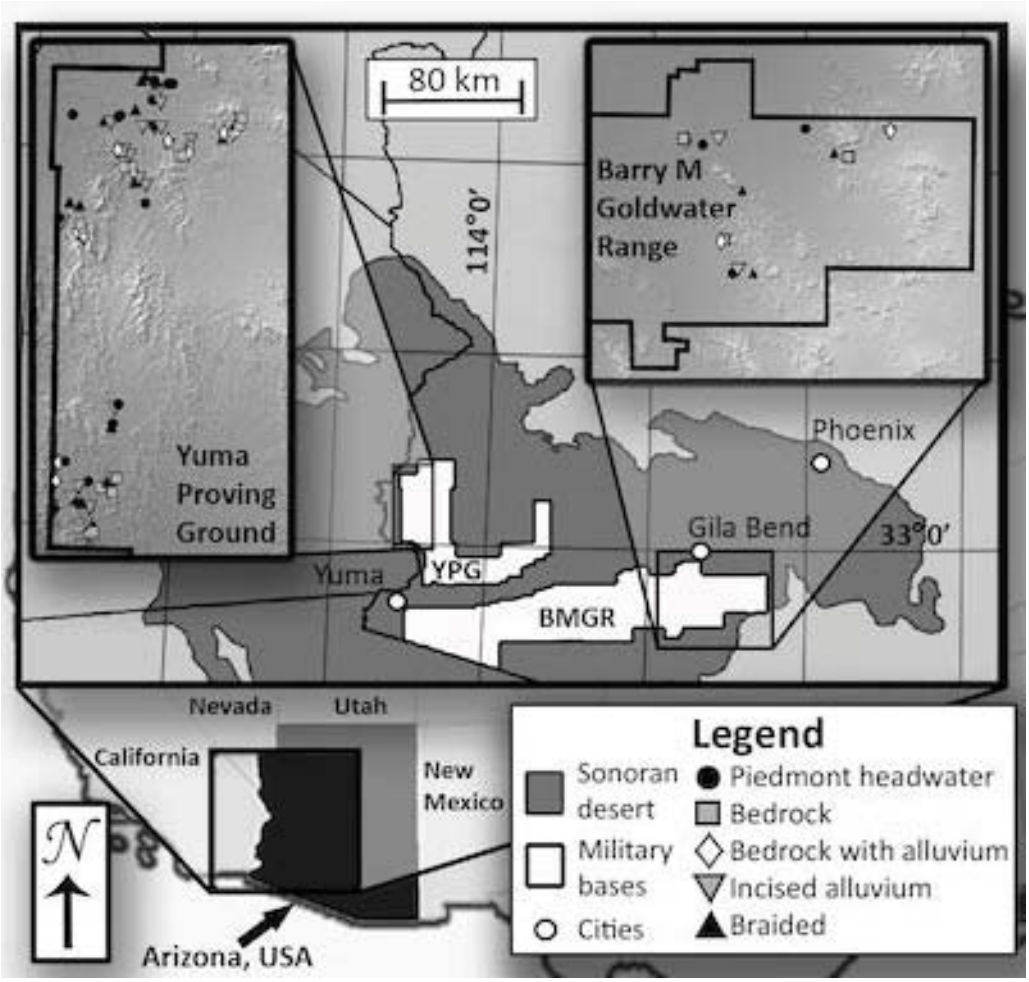

Figure 1-1. Locations of 101 study reaches within the U.S. Army Yuma Proving Ground (YPG) and Barry Goldwater Air Force Range (BMGR) in southern Arizona within the extent of the U.S. Sonoran desert, as defined by Brown et al. (2007).

Convective summer storms and dissipating tropical cyclones create temporally and spatially variable warm-season precipitation in the Sonoran desert, while Pacific frontal storms generate widespread, low-intensity rainfall during winter months. A distinct dry season occurs from April to June, and a wet season occurs from November to March; but approximately half of annual precipitation in the research area falls during the period from July to September (National Weather Service, 2012; Western Regional Climate Center, 2012a, b). Total average annual rainfall at YPG is 95 mm, whereas total average annual rainfall in Gila Bend (~ 30 km north of BMGR) is 156 mm (Western Regional Climate Center, 2012a, b). Abundant vegetation and dense stands of trees are restricted to riparian areas. Common woody xeroriparian vegetation includes ironwood (*Olneya tesota*), palo verde (*Parkinsonia florida* and *P.*

microphylla), acacia (*Acacia* spp.), mesquite (*Prosopis* spp.), white bursage (*Ambrosia dumosa*), and creosote (*Larrea tridentata*). Uplands are dominated by creosote bush and white bursage.

Materials and methods

Proposed ephemeral stream classification

Existing geomorphic classifications refer primarily to characteristics of perennial streams and do not adequately describe relevant, reach-scale, geomorphic characteristics of ephemeral channels. Bankfull stage and width provide examples of concepts that are important in classifications developed for perennial streams but are difficult to apply to ephemeral channels. Bankfull stage in perennial channels is typically associated with a channel-forming flow that occupies the entire channel on average every 1.5 years (Leopold et al., 1964; Dunne and Leopold, 1978; Knighton, 1998) and transports the majority of suspended sediment (Simon et al., 2004). Ephemeral streams may experience continuous aggradation during decades without significant flows (Graf, 1981) and undergo substantial erosion during large floods (Graf, 1988a; Kondolf et al., 2001; Friedman and Lee, 2002; Merritt and Wohl, 2003). This makes it difficult to identify a single flow magnitude, or associated channel width or flow stage, that adequately represents channel adjustment over a period of decades (Graf, 1988b; Tooth, 2000). Lack of information on flow magnitude and recurrence intervals for ephemeral streams is exacerbated by the paucity of flow data in arid environments.

Our ephemeral channel classification is based on channel planform, the degree of lateral confinement and composition of confining material. These criteria represent relatively persistent features, unlike alluvial bedforms that can change substantially during a single flood. Planform, lateral confinement and channel boundary composition influence hydraulics and sediment dynamics (Hassan, 1990; Powell et al., 1998), which are difficult to measure in ephemeral channels (Bull and Kirkby, 2002). Channel geometry, hydraulics, and sediment dynamics influence riparian structure and function via habitat creation and destruction (Birkeland, 1996; Hupp and Osterkamp, 1996; Merritt and Wohl, 2003). The classification presented here focuses on persistent aspects of channel geometry that can be used as indicators of transient channel processes, just as the Montgomery and Buffington (1997) channel classification for mountainous perennial channels focuses on persistent bedforms as indicators of relative sediment supply and mobility. The channel types proposed here could be applied to rivers in diverse environments, but they are particularly suitable for arid-region ephemeral channels in mountainous areas.

Our classification draws on existing classifications that describe planform (Leopold et al., 1964), longitudinal zonation within drainage basins (Schumm, 1977; Bull, 1979), and process domains (Montgomery, 1999; Polvi et al., 2011). As channel slope decreases from mountainous uplands toward broad lowland valleys, progressively higher order streams exhibit decreases in stream power (Bull, 1979). This creates an idealized spectrum where upland channels are confined primarily by bedrock along the bed and banks, which transition into alluvial bed channels confined by bedrock. As distance from the mountainous uplands increases, these channels incise through previously deposited sediment and alluvial fans, which compose the piedmont. We initially developed an *a priori* classification of five channel types distinguished based on simple visual characteristics. The goal of this paper is to objectively test whether differences in channel geometry and hydraulic parameters existed between our channel types.

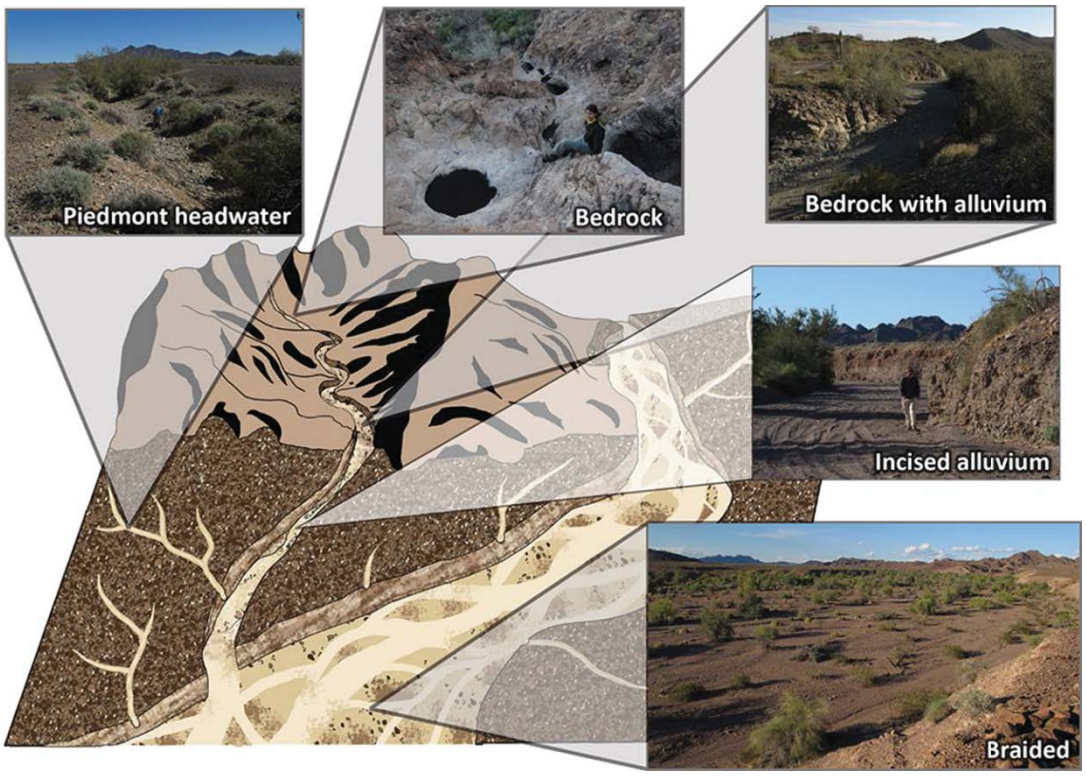

Figure 1-2. Five arid-region ephemeral channel types depicted as an idealized progression include primarily erosive piedmont headwater (A) and bedrock (B) channels, those located in intermediate transfer zones along the transition from the mountain front to the piedmont or adjacent to the piedmont (bedrock with alluvium (C) and incised alluvium (D)) and primarily depositional braided channels (E).

Our *a priori* classification included five channel types. *Piedmont headwater* channels initiate on piedmont surfaces and are incised into partially consolidated alluvium, yet lack persistent active alluvium on the channel bed and do not exhibit significant point bar or floodplain development (Fig. 1-2A). Montane *bedrock* channels are entirely confined by exposed bedrock and devoid of persistent alluvium (Fig. 1-2B). *Bedrock with alluvium* channels are confined by bedrock, but contain a persistent bed of active alluvium for at least 50% of the study reach length, and may exhibit point bars and narrow floodplain benches (Fig. 1-2C). *Incised alluvium* channels contain active alluvial beds that are bound only by the partially consolidated alluvium composing the piedmont into which they are incised (Fig. 1-2D). These channels may exhibit significant floodplain and point bar development, or have narrow floodplain benches. Depositional *braided* washes exhibit multiple channels and transient gravel bars, regardless of the degree and composition of confining material (Fig. 1-2E). Primary qualitative differences between channel types are those pertaining to valley confinement. The relative degrees of valley confinement are captured in typical cross sections of each proposed channel type, where multiple channels and relatively well-developed floodplains are evident in braided and incised alluvial reaches, respectively (Figs. 1-3, 1-4).

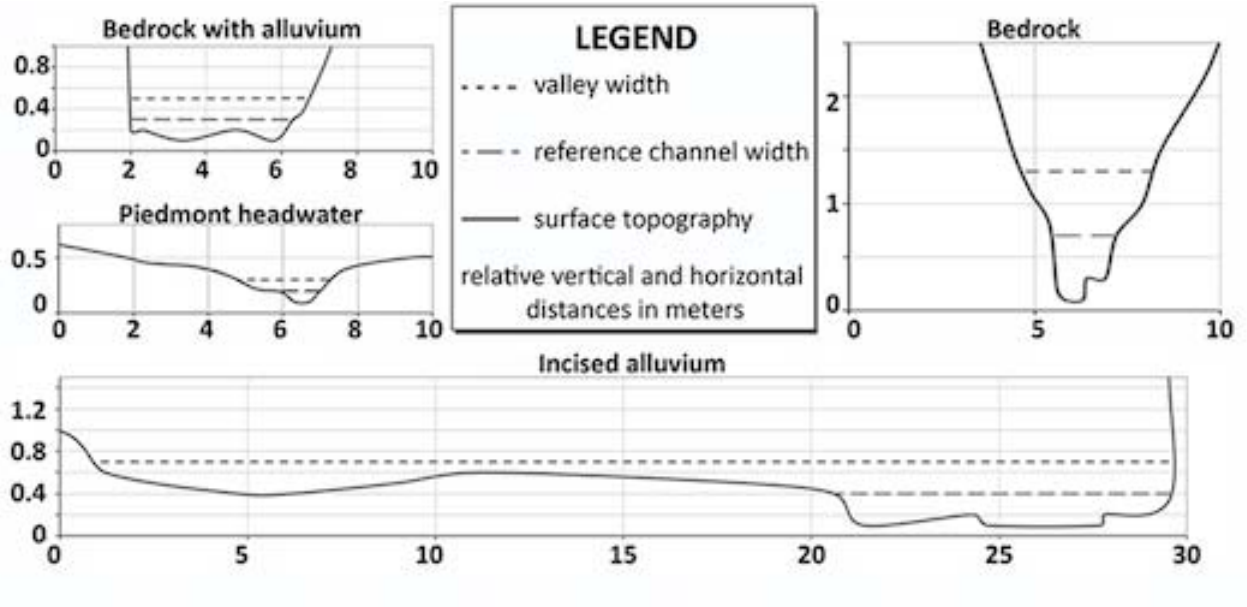

Figure 1-3. Representative cross-sectional profiles for bedrock, bedrock with alluvium, piedmont headwater, and incised alluvium channel types. Figures are in relative scale to one another with vertical and horizontal axes in meters. Refer to Fig. 1-4 for a typical cross section of a braided wash at a significantly different scale.

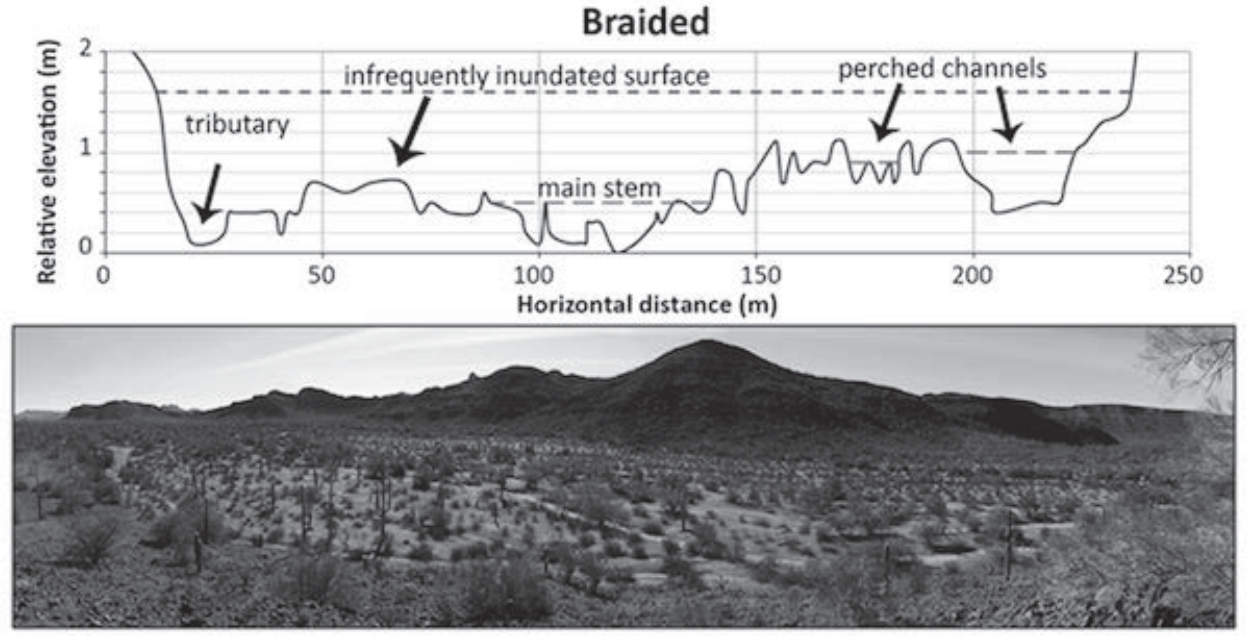

Figure 1-4. Braided wash cross-sectional profile from Yuma Proving Ground illustrating typical features of a braided channel. The photograph depicts the view of a braided wash in Barry M. Goldwater Range from valley right.

The five channel types thus represent an idealized downstream progression from eroding channel segments that initiate on the piedmont (A) or in the mountains (B), downstream channel segments on the piedmont that have larger drainage area, numerous tributaries and at least some depositional features and potential for subsurface water storage (C and D), and larger channels in the alluvial basins between mountain ranges that have extensive deposition and greater potential for subsurface water storage (E; Fig. 1-2). Channel characteristics reflect many aspects of the

climate and landscape including antecedent features and accommodation space as described by Fryirs and Brierley (2010), which are a function of the lithotopographic footprint (Montgomery, 1999; Beechie et al., 2010) and geomorphic memory (Sidorchuk, 2003) from past processes. Reach-scale channel characteristics and spatial transitions between channel types are dependent upon discontinuity of upland geomorphic surfaces, exposure and lithology of bedrock, and location of tributary junctions. This heterogeneity of the landscape controls process domains — analogous to those described by Montgomery (1999) for humid temperate environments — and associated channel characteristics in locations where channel dimensions can be strongly influenced by debris flow, sheet flow, confined channelized flow, or minimal confinement. We emphasize that the longitudinal progression mentioned above is idealized in the sense that it represents very broad-scale patterns. An individual channel could change downstream from bedrock to incised alluvium to bedrock with alluvium and then braided, for example, as a function of downstream variations in surface bedrock exposure.

Objectives and hypothesis

The objective of this paper is to identify the characteristics of measured channel geometry and inferred hydraulics among five *a priori* proposed ephemeral channel types. We address this by (i) testing the hypothesis that the five proposed stream types exhibit significantly different channel geometry and reach-scale hydraulics, (ii) determining ranges of values in reach-scale hydraulics and channel geometry for each channel type in this study area, and (iii) testing the validity of such a classification by predicting channel types for an external validation data set using discriminant analysis and a classification tree.

Reach surveys

Stratified sampling and field visits were used to select study reaches that were representative of each channel type. We attempted to select study sites that encompassed the full range of variability in physical characteristics of each channel type (e.g., scale, stream gradient, lithology, width/depth ratio) observed in the field, but avoided study reaches that exhibited evidence of possible transitional states between stream types. Study reaches were located to avoid confounding effects of tributary junctions and intensive anthropogenic disturbance.

Channel geometry and reach characteristics for 101 study reaches at YPG and BMGR were surveyed using a Laser Technology TruPulse 360B laser rangefinder with 10-cm accuracy. Data collection at 86 study reaches in YPG consisted of channel surveys for 19 piedmont headwater (PH), 18 bedrock (BK), 18 bedrock with alluvium (BA), 18 incised alluvium (IA), and 13 braided (BD) study reaches. Sufficiently long braided study reaches were difficult to find that did not have large tributary confluences or changes in channel characteristics. Downstream changes in channel characteristics, for example, included the loss of a well-defined channel resulting from transmission losses. This smaller sample size for BD reaches, however, reflects the lower abundance of this stream type in the study area. Reach surveys conducted at BMGR included three study reaches representing each of the five channel types, totaling 15 study reaches in the external validation data set.

Cross sections were surveyed with respect to a reference stage, which we assume represents the discharge responsible for maintaining contemporary channel geometry. We make no attempt to define specific discharges for channel-forming flows and avoid the use of bankfull stage because it has become associated with recurrence interval in perennial streams (Leopold et al., 1964; Knighton, 1998; Benda et al., 2005). We refer instead to a reference stage using topographic features in a way that is analogous to bankfull stage, defined as the change in slope of the stage-discharge rating curve (Williams, 1978). We delineated reference stage based on development of desert varnish and desert pavement on adjacent upland surfaces as an upper limit, height of fluvial depositional surfaces as a lower limit, and staining on bedrock within the channel. The reference flow stages identified in the field may not represent the large floods responsible for scouring and shaping the channel prior to numerous depositional events. However, this stage likely represents the most common (median) flow depth under modern climate responsible for creating and maintaining current channel geometry. In this respect, reference flows likely represent the hydrologic and geomorphic conditions responsible for maintaining contemporary riparian vegetation community structure rather than specific events with distinct magnitudes or recurrence intervals.

Four cross sections were spaced approximately four mean channel widths apart, with the exception of braided washes where cross sections were spaced by one width of the entire fluvial corridor (wash width). Cross-sectional profiles based on identification of reference flows provide information about channel geometry for estimates of

width-to-depth ratio, ratio of valley-to-channel width, shear stress, dimensionless shear stress, stream power, and unit stream power.

Length of each study reach was defined as 3 wash widths for braided channels and 12 mean channel widths for all other reach types. Longitudinal streambed profiles for all reach types except braided reaches were surveyed at consecutive points along the best approximation of the thalweg for a distance of at least one channel-width beyond the upstream- and downstream most cross sections. Topographic elevation was surveyed at slope breaks, changes in grain size, and bends in the channel. The GIS-derived slopes were preferred for stream gradient calculations in BD reaches because of the large scale of braided valley bottoms and difficulty in achieving accurate thalweg slope estimates. Longitudinal profiles for BD reaches were calculated using 5-m digital terrain models (DTM) (McDonald and Hernandez, 2011) for YPG and 10-m digital elevation models (DEM) (ALRIS, 2012) for BMGR.

Streambed surface pebble counts of at least 100 clasts were made at every study reach with the exception of bedrock channels devoid of alluvium. Sample intervals were scaled according to channel width. Using a modified Wentworth scale, each pebble was classified by the length of the median axis into one of eight grain size categories ranging from sand (i.e., 0.33 to 2 mm) to boulders (i.e., > 128mm; Wentworth, 1922).

Reach-scale channel hydraulics

Reach-scale estimates of channel geometry and hydraulic parameters were derived by averaging values across the four surveyed cross sections within each reach. Flow depth was based on reference stage. Average velocity (V) and discharge (Q) were calculated using the Manning equation (Manning, 1889, as cited in Knighton, 1998) for each study reach,

$$V = (k/n)R^{2/3}S^{1/2} \qquad (1)$$

where $k = 1$ in SI units, R is the hydraulic radius, S is stream gradient estimated as slope of the channel bed, and n is the roughness coefficient. Estimates of Manning's roughness coefficient (n) were initially derived using an adapted version of the Cowan method (Arcement and Schneider, 1989), yielding estimated n values within the range of 0.03 to 0.06. Because visual estimation of roughness values is subjective, survey accuracy is limited, and the Manning equation assumes steady, uniform flow, we considered all estimates of hydraulic variables to be first-order approximations. Discharge (Q) was estimated as the product of V and A. Discharge estimates were used to calculate stream power (Ω) and unit stream power (ω) as a proxy for hydraulic driving forces:

$$\Omega = \gamma QS \qquad (2)$$

$$\omega = (\gamma QS)/w = \Omega/w \qquad (3)$$

where γ is the specific weight of water. In order to focus our analyses on measured variation in channel morphology and to standardize uncertainties in estimating roughness coefficients, our first-order approximations of Ω and ω used the lowest estimate of Manning's roughness coefficient for all study reaches ($n = 0.03$) to examine relative differences between channel types. Shear stress was calculated using

$$\tau = \gamma RS \qquad (4)$$

To incorporate median grain size (d_{50}) in the analysis of hydraulics, dimensionless shear stress was calculated using

$$\tau^* = (RS)/(1.65d_{50}) \qquad (5)$$

The ratio W_v/W_c was calculated for all stream types using entrenchment ratio and the reference flow width and depth (Rosgen, 1994). Entrenchment ratio is the floodprone width (width of the channel/valley at two times the bankfull depth) over the bankfull width (Rosgen, 1994). Floodprone width was measured for braided reaches at two times the maximum depth of the channel highest in elevation along the valley bottom.

Statistical analyses

Eight metrics (stream gradient S, width/depth ratio W/D, ratio of valley width to channel width W_v/W_c, shear stress τ, dimensionless shear stress τ^*, median grain size d_{50}, stream power Ω, and unit stream power ω) were calculated and examined for strength as predictor variables in multivariate analyses. A combination of univariate and multivariate statistical methods were used to (i) examine the strength of variables in distinguishing channel types, (ii) test the hypothesis that the five channel types exhibit significantly different values of channel geometry and inferred

hydraulics, (iii) examine potential range of values for variables of interest between channel types, and (iv) validate the basis of the channel classification by predicting channel type using indicator variables. These statistical methods include one-way analysis of variance (ANOVA) with multiple contrasts and comparisons, nonparametric permutational multivariate analysis of variance (PerMANOVA) (Anderson, 2001), nonmetric multidimensional scaling (NMS) (Clarke, 1993), classification trees (Breiman et al., 1984; De'ath and Fabricius, 2000), and linear discriminant analysis (LDA).

Variables were $\log_{10}$ transformed to achieve approximate normality and homoscedasticity that satisfied the assumptions of our statistical analyses. Individual one-way analysis of variance (ANOVA) and multiple comparisons and contrasts were conducted between channel-type group means for each of the eight variables (ω, τ, W/D, S, Ω, W_w/W_c, τ^*, d_{50}) to determine potential strength of variables for distinguishing channel type.

We tested the hypothesis that the five *a priori* channel types exhibit differences in channel geometry using PerMANOVA (Anderson, 2001, 2005) via the *adonis* function within the *vegan* package in R (Oksanen et al., 2011; R Core Team, 2012). Euclidean was the distance measure, and 9999 permutations were used (Oksanen et al., 2011).

Nonmetric multidimensional scaling using the Euclidean distance measure and random starting coordinates, Monte Carlo tests for dimensionality were performed with 250 permutations of observed and randomized data from the 86 study reaches in YPG. Dimensionality of the final solution was selected to minimize stress values. Applicability of the ordination was verified using axis scores for the validation data set of 15 study reaches in BMGR. Reach-scale geomorphic and hydraulic variables were correlated against axis scores, using Pearson correlation. Ordination was performed using PC-Ord (McCune and Mefford, 1999; version 5.10, MjM Software, Gleneden Beach, OR, USA).

Classification tree analysis was used to provide the potential ranges of values for hydraulics and geometry that can be expected for each channel type. The classification tree was grown with training data from the 86 study reaches in YPG, using 15-fold cross-validation and the Gini index as the splitting rule, and validated using the 15 study reaches from BMGR. The final tree was pruned to minimize the relative cost (0.417) (Salford Predictive Model Builder, 1998). This analysis provides a way to test the basis of the *a priori* classification by predicting channel type based on hydraulics and channel geometry.

Linear discriminant analysis (LDA) was used to investigate the potential strength in the classification by predicting channel type based on channel geometry and hydraulics. The LDA was conducted using moment calculations in the *lda* function of the *MASS* package in R statistical software (Ripley et al., 2012; R Core Team, 2012). The discriminant criterion was developed using 86 study reaches at YPG, while 15 study reaches at BMGR were used as an external validation data set. Internal validation of the discriminant function was conducted using *predict* in the *MASS* package of R-studio to determine the stream type of the 86 study reaches used to develop the discriminant function. External validation of the discriminant function was conducted by predicting the stream type for 15 study reaches surveyed at BMGR. Internal and external validation results in optimal and actual hit rates (Manly, 2000), which indicates the ratio of successful predictions of stream type over the total number of classification attempts.

Results

Study reach characteristics

Contributing drainage areas and stream gradients (0.004–0.58) for all 101 study reaches capture the progression of channel types through distinct zones from small, steep, erosional mountainous bedrock channels to broad, depositional braided alluvial valleys. Boxplots illustrate relative differences in the five stream types with respect to all eight variables examined, particularly strong differences in W/D, S, Ω, τ, and ω (Fig. 1-5). The most pronounced differences in channel geometry and hydraulics occur between bedrock (BK) and braided (BD) channels. The BD and BK reaches are easily distinguished from other channel types by W/D and τ, respectively. As expected, BK channels have much higher gradients and lower W/D ratios, whereas BD channels have lower gradients and higher W/D ratios. The BD, BK, and PH channels form relatively tight groups with respect to W/D and Ω, whereas the BA and IA channels contain more variability and overlap with less distinct grouping (Fig. 6). The BA and IA channels are more closely related and not easily distinguished from one another (Figs. 1-5, 1-6).

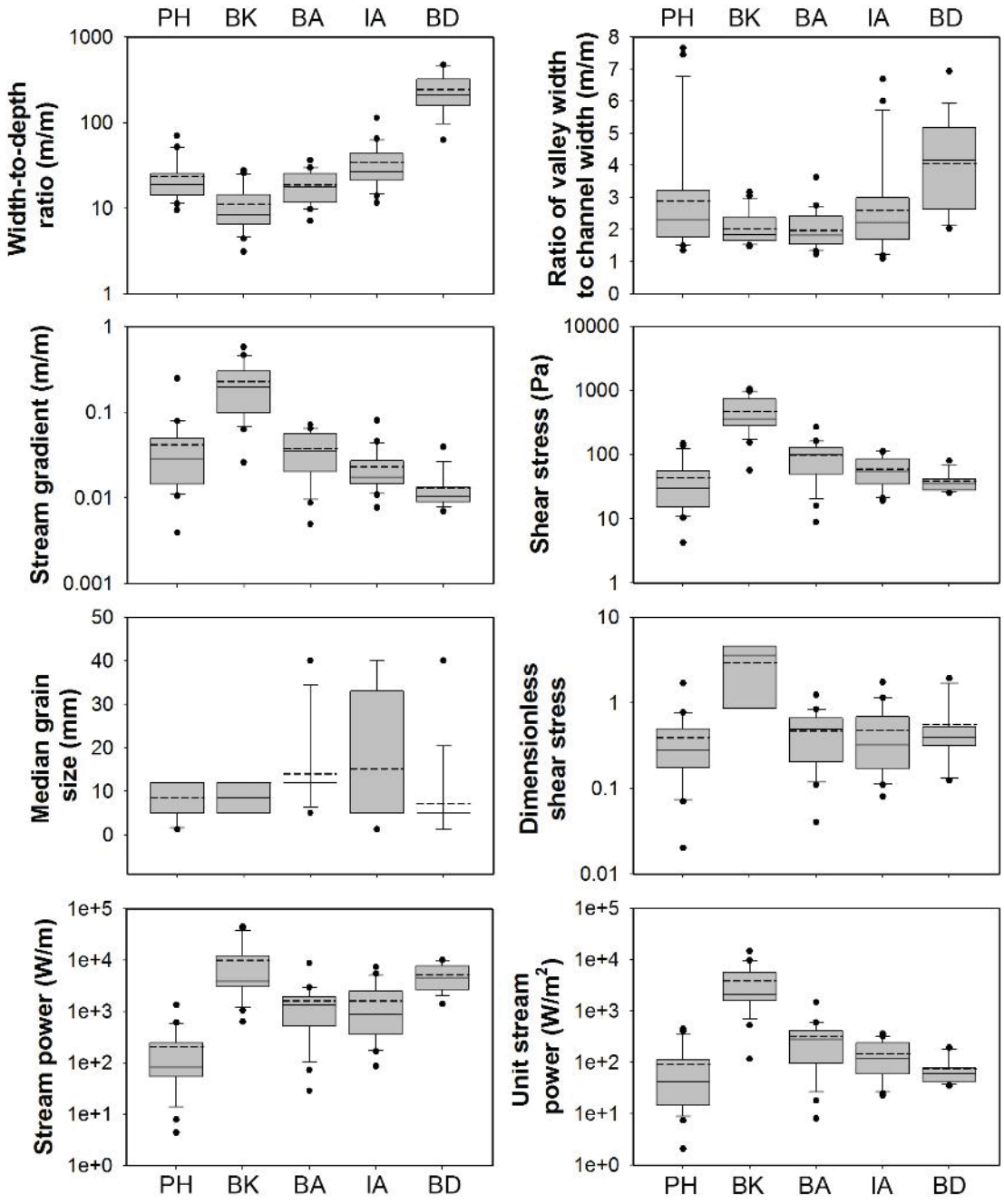

Figure 1-5. Box plots of eight variables (W/D, W_v/W_c, S, τ, d_{50}, τ*, Ω, ω) for the five channel types on the horizontal axis; bedrock (BK), bedrock with alluvium (BA), incised alluvium (IA), braided (BD), and piedmont headwater (PH) channels from 101 study reaches surveyed at YPG and BMGR. Values are log-transformed, box center lines indicate the median, dashed lines indicate means, box ends are the 25th and 75th percentiles, and whiskers extend to the 5th and 95th percentiles.

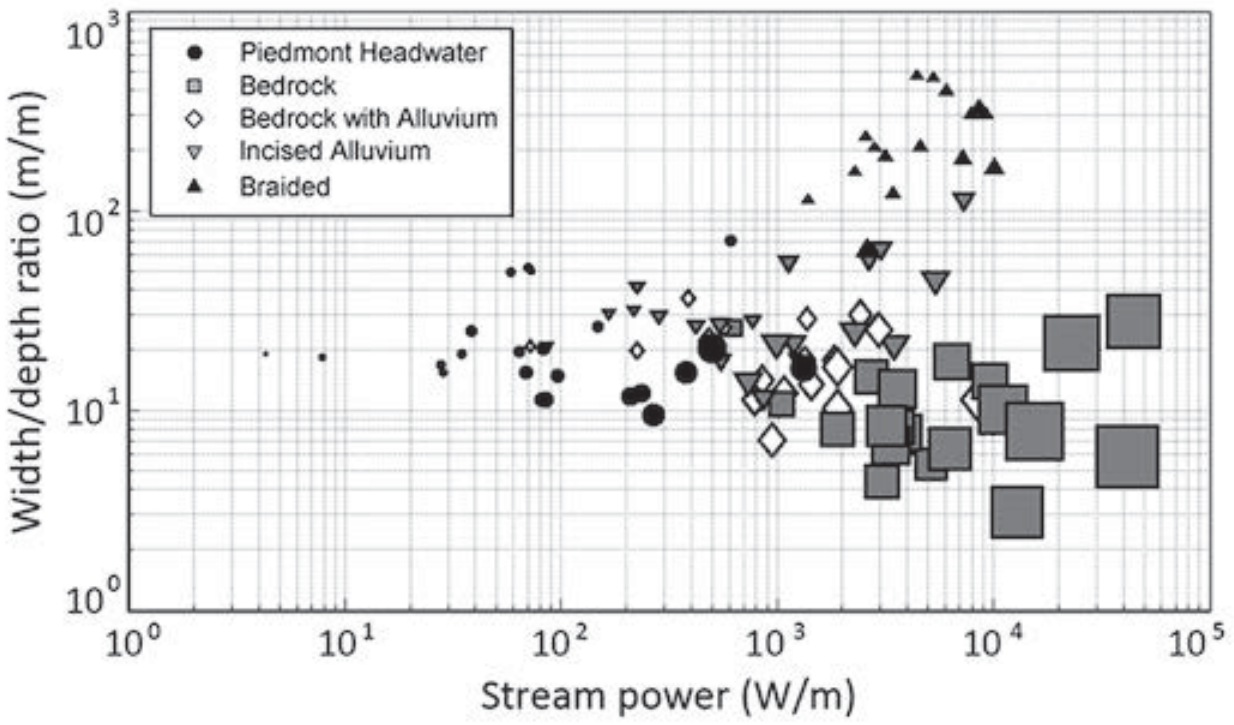

Figure 1-6. A scatter plot of reach-average width-to-depth ratio versus stream power for 101 study reaches illustrates grouping among stream types. Marker size indicates estimated relative reach-average shear stress.

Variable selection

Individual one-way analysis of variance (ANOVA) indicated that group means of each predictor variable differed significantly between the five stream types ($p \leq 0.001$), with the exception of median grain size (d_{50}, $p = 0.147$). Multiple comparisons of group means of each variable indicated that the best variables for distinguishing between channel types are width-to-depth ratio (*W/D)*, stream gradient (*S)*, stream power *(Ω),* shear stress (*τ),* and unit stream power (*ω)*. Median grain size (d_{50}*)* and dimensionless shear stress *(*τ^**)* lacked the power to distinguish stream types and were eliminated from the analyses. To reduce the likelihood of confounding cross correlation between predictor variables, measures of stream competence (*τ, Ω, ω*) were reduced to *τ* and *Ω.* Although both *Ω* and *τ* incorporate channel slope (*S*) by definition and are correlated with *S* (R^2 = 0.25 and 0.82, respectively), each of these variables provided information crucial for distinguishing particular channel types. Shear stress (*τ*) was retained as a predictor variable in the model because it encompasses depth of flow and easily distinguishes bedrock from other channel types. First-order approximations of stream power (*Ω*) could be used to distinguish piedmont headwater channels from other stream types.

A two-dimensional NMS ordination minimized mean stress at 3.52 ($p = 0.004$) for 86 study reaches in YPG. The NMS scores for the validation data set from BMGR using this solution exhibited a mean stress of 3.53 and corresponded closely to those from YPG (Fig. 1-7). Separation of study reaches along axis 1 was dominated by differences in *τ* (r = -0.93) and *Ω* (r = -0.91), whereas separation along axis 2 was driven by width-to-depth ratio (r = 0.94) (Fig. 1-7; Table 1-2). Stream gradient exhibited moderate correlations with both axes scores (r_1 = -0.71, r_2 = -0.68). Entrenchment ratio was weakly correlated with both axes and is a poor indicator variable. These ordination results validate the use of *W/D*, *S, Ω,* and *τ* for additional multivariate analyses.

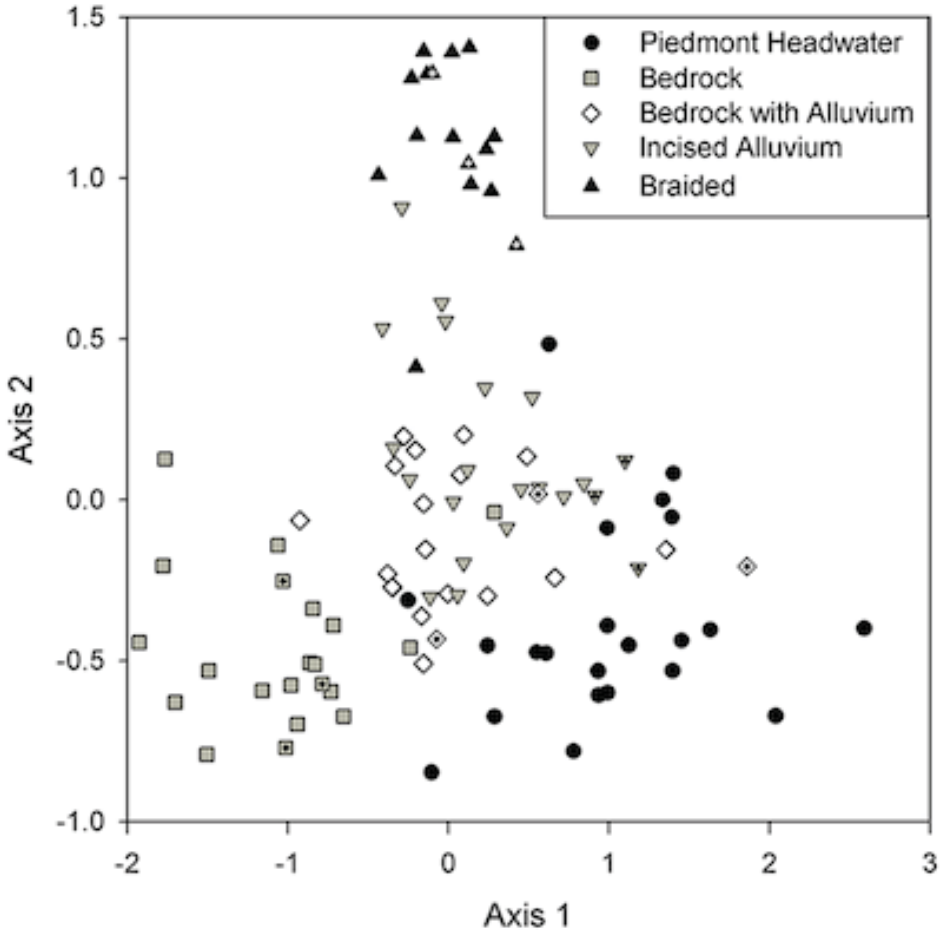

Figure 1-7. Nonmetric multidimensional scaling ordination plot of 101 study reaches for five variables (S, τ, W/D, Ω, and W_v/W_c). Crossed symbols denote the external validation data set of 15 study reaches from BMGR, whereas solid symbols (without crosses) indicate the calibration data set of 86 study reaches from YPG.

Table 1-1. Pearson correlation coefficients for nonmetric multidimensional scaling ordination among reach-scale geomorphic and hydraulic variables for 86 study reaches at YPG

Axis	1	2
Stream gradient	- 0.71	- 0.68
Width/depth	+0.24	+0.94
Entrenchment ratio	+0.23	+0.30
Shear stress	- 0.93	- 0.41
Stream power	- 0.91	+0.36

Hydraulic and geomorphic differences among channel types

We used multivariate analyses to address our primary objective and to test our hypothesis described in section 3.2. PerMANOVA results indicated that multivariate mean channel geometry and hydraulics are not equal for all five stream types (p = 0.0001, F-statistic = 362). This allowed us to reject the null hypothesis that channel types were identical.

To identify differences in channel type, linear discriminant analysis (LDA) was conducted using *W/D*, *S*, *Ω,* and *τ* for the learning data set of 86 study reaches at YPG. This discriminant function correctly predicted 77% of sites

(Table 1-2). The BA and IA channel types were misclassified more than other channel types using LDA on the data from YPG. The majority of misclassifications occurred within prediction of BA (67% BA hit rate) and IA (50% IA hit rate) study reaches, such that these stream types were confused for one another.

External validation for the testing data set using the same discriminant function resulted in successful prediction of 73% of the 15 study reaches surveyed at BMGR (Table 1-2). The PH, BK, and BD channels were correctly classified through external validation in every case (100% hit rate). Misclassifications occurred for BA and IA channels when they were confused for one another or misclassified as PH channels.

The classification tree (CT) determined the relative strength of variables to be the following: $S > W/D > \Omega > \tau$. The CT model distinguished 92% of BD reaches by $W/D > 118$ (Fig. 1-8). For channels with $W/D \leq 118$, 94% of BK reaches were identified by $\tau > 152$ Pa. Approximately 68% of PH channels were distinguished by $\Omega \leq 217$ W/m, $\tau \leq 152$ Pa, and $W/D \leq 118$. Of the remaining study reaches, 67% of IA channels had $S < 0.02$. The areas under the receiver operator curves for the entire CT were 0.93 and 0.88 for the learning and test data sets, respectively. Successful prediction in the learning data set from YPG for correctly identifying PH (68%), BK (94%), BA (67%), IA (67%), and BD channels (92%) resulted in an overall hit rate of 77%, which equates to an overall prediction error of 23%.

Table 1-2. A confusion matrix for prediction of channel types based on W/D, S, Ω, and τ for linear discriminant analysis (LDA; values on top) and a classification tree model (CT; values in parentheses); Numbers before each comma indicate results for the training data set of 86 study reaches at YPG, whereas bold numbers following each comma indicate results for the test data set of 15 study reaches at BMGR

		Predicted channel type					**Hit rate**		
		Piedmont headwater	**Bedrock**	**Bedrock with alluvium**	**Incised alluvium**	**Braided**	**Learning data set (YPG)**	**Test data set (BMGR)**	**Model**
Actual channel type	**Piedmont headwater**	17, **3** (13, **3**)	0, **0** (0, **0**)	1, **0** (5, **0**)	1, **0** (1, **0**)	0, **0** (0, **0**)	90% (68%)	100% (100%)	LDA CT
	Bedrock	0, **0** (0, **0**)	16, **3** (17, **3**)	1, **0** (1, **0**)	1, **0** (0, **0**)	0, **0** (0, **0**)	89% (94%)	100% (100%)	LDA CT
	Bedrock with alluvium	3, **1** (1, **1**)	0, **0** (2, **0**)	12, **1** (12, **1**)	3, **1** (3, **1**)	0, **0** (0, **0**)	67% (67%)	33% (33%)	LDA CT
	Incised alluvium	2, **1** (0, **2**)	0, **0** (0, **0**)	6, **0** (6, **0**)	9, **1** (12, **1**)	1, **1** (0, **0**)	50% (67%)	33% (33%)	LDA CT
	Braided	0, **0** (0, **0**)	0, **0** (0, **0**)	0, **0** (1, **0**)	1, **0** (0, **1**)	12, **3** (12, **2**)	92% (92%)	100% (67%)	LDA CT
					Total prediction hit rate		**77% (77%)**	**73% (67%)**	**LDA CT**

1

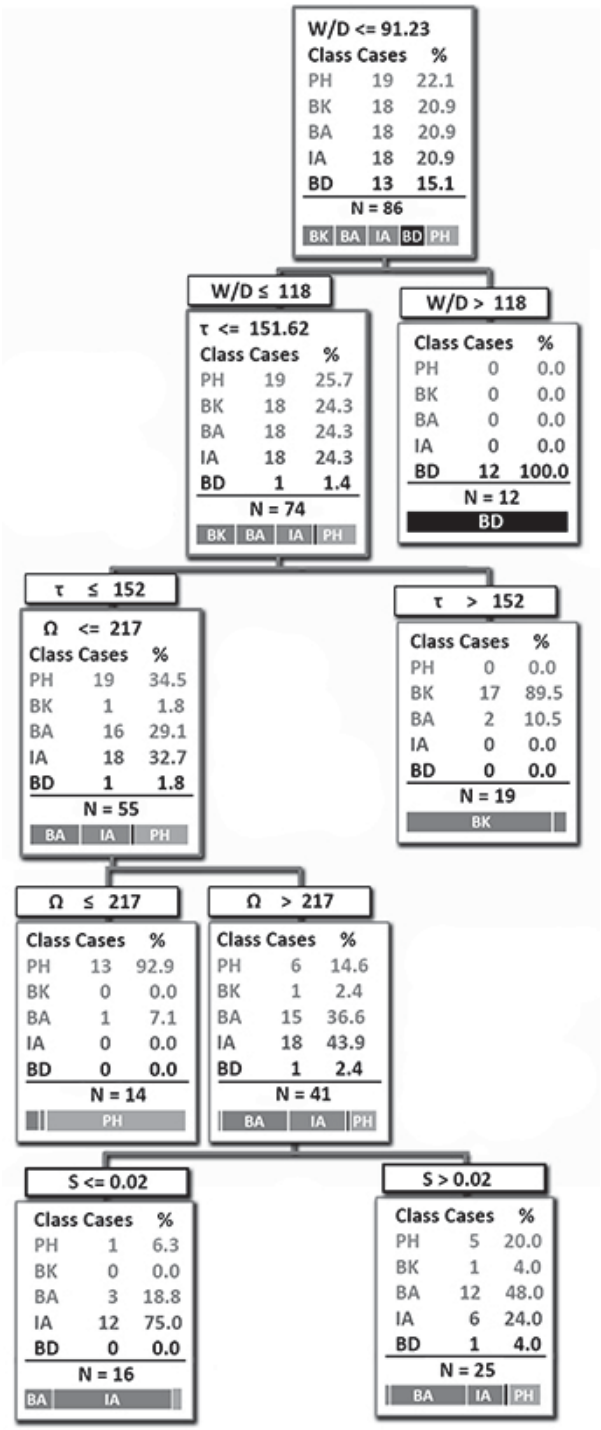

Figure 1-8. Classification tree (Salford Predictive Modeler v6.6, 1998) based on 86 study reaches at YPG identifying cutoff points for W/D, S, Ω, and τ used to distinguish the five channel types: piedmont headwater (PH), bedrock (BK), bedrock with alluvium (BA), incised alluvium (IA), and braided (BD) channels. N represents the sample size for each node, and percentages indicate the relative distribution of each stream type within each node.

Discussion

Channel geometry and reach-scale hydraulics can allow the differentiation of ephemeral stream types in arid regions and form the basis for a channel classification. We observed higher stream gradient and shear stress in bedrock channels than in alluvial channel segments, which is known for streams in diverse environments (Tinkler and Wohl, 1998; Wohl and David, 2008). Lower shear stress and stream gradient, and greater width-to-depth ratios and stream power, are known to occur in braided alluvial ephemeral channels (Bull, 1977; Graf, 1988a; Tooth, 2000; Reid and Frostick, 2011). Because channel parameters influence sediment transport (Powell et al., 1998; Tucker et al., 2006), surface/subsurface hydrologic interactions (Schick, 1986), structure and function of riparian habitat and vegetation communities (Birkeland, 1996; Hupp and Osterkamp, 1996; Merritt and Wohl, 2003; Al-Rowaily et al., 2012), and sensitivity to disturbance (Montgomery, 1999; Brierley and Fryirs, 2005), they provide insight into the physical and biological processes occurring in dryland ephemeral channels.

Channel geometry and hydraulic parameters can be used to infer differences in disturbance regime, channel adjustment to disturbance, and ecological sensitivity. Water and sediment storage appear to increase from negligible amounts in bedrock channels to progressively higher amounts in piedmont headwater, bedrock with alluvium, incised alluvium, and braided channels based on relative values of shear stress, stream power, and width/depth ratio among these channel types. Consequently, disturbances such as floods or debris flows that alter water and sediment inputs to channel segments are more likely to completely restructure channel and riparian habitat in piedmont headwater and bedrock with alluvium channels, whereas incised alluvium and braided channels more likely experience localized erosion, deposition, and restructuring of habitat. In contrast, the resistant channel boundaries and high transport capacity of bedrock reaches would probably result in minimal geomorphic adjustments to allogenic disturbances. We also expect the smaller drainage areas of bedrock, piedmont headwater, and bedrock with alluvium reaches to result in more frequent flood disturbance than in incised alluvium and braided reaches occupying the lower portions of channel networks. Small headwater catchments experience more frequent storm coverage and rapid runoff generation than downstream portions of larger channel networks, which require more spatially extensive and prolonged rainfall to generate floods (Tucker et al., 2006; Shaw and Cooper, 2008).

The combined effects of localized erosion and deposition during flow events, infrequent disturbance, and greater alluvial storage capacity are reflected in the greater diversity of woody riparian vegetation along incised alluvium and braided channel segments within the study area (Merritt and Wohl, 2003) and in other ephemeral channel networks (Hupp and Osterkamp, 1996; Shaw and Cooper, 2008). Braided and incised alluvium channels are more geomorphically complex (Figs. 1-5, 1-6) than steeper, confined reaches and therefore have more capacity to absorb changes in water and sediment inputs without substantial morphologic change. Because flood disturbances are less likely to completely replace existing alluvial surfaces and remove riparian vegetation in braided channel segments, this channel type may be more resilient to natural disturbances. However, human-induced disturbances such as vehicular traffic and military training are more likely to alter channel geomorphology and remove riparian vegetation. Braided channels could be considered less resilient to such disturbances compared to bedrock channels, which mostly lack riparian vegetation and have resistant channel boundaries. Our classification of channel geometry may be a useful proxy for river ecosystem characteristics, such as riparian vegetation extent and sensitivity to disturbances, when managing riverine ecosystems in the study area.

Misclassifications

The bedrock with alluvium and incised alluvium channels are the most similar based on field measures, and our analyses often misclassified them. However, we believe that these two channel types warrant distinction. Aggregating bedrock with alluvium and incised alluvium channels into a single reach type resulted in decreased hit rates for all stream types using the linear discriminant function. Additionally, we observed geomorphic differences between these two reach types that were not captured by our data. These differences between bedrock with alluvium and incised alluvium channels likely have implications for channel evolution, riparian vegetation community structure, and disturbance. Incised alluvium channels often have more vegetated point bars and well-developed floodplain surfaces with abundant riparian vegetation compared to bedrock with alluvium channels. Although the measured channel geometry and reach-scale hydraulics of these reach types are similar, differences in boundary material erodability would likely lead to different sensitivity to natural and anthropogenic disturbance.

Transitional states

Spatial and temporal transitional states can pose difficulties in identifying the appropriate ephemeral channel type through quantification of the data and qualitative identification in the field. Although visual distinction of most channel types in the field are relatively straightforward (e.g., bound by bedrock, braided, initiate on the piedmont), ambiguity lies in the distinction between bedrock and bedrock with alluvium channels. For this reason, we define bedrock with alluvium channels to contain a persistent, significant cover of continuous alluvium for > 50% of the channel reach. This, however, is subjective to the time scale at which channels of interest are considered. We add the additional modifier for presence of bedforms and/or point bar development, which should indicate some level of persistence of the alluvial cover.

Although attempts were made to minimize inclusion of transitional reaches in the data, difficulties arise with transitional states along the spectrum of channel evolution on which we have imposed a discrete classification. Users must consider potential transitional states when applying this classification. When the designation of channel type is in question as a result of a potential transitional state, we recommend considering the range of S, W/D, , and τ values found in this study for more than one possible channel type (Fig. 5). It may also be of interest to investigate the direction in which the transition is trending in order to improve land management or restoration efforts.

Floodout zones

Transitional states may also create conditions where channel characteristics become undefined or indistinct, such as the phenomenon referred to as floodout zones in Australia (Tooth, 1999, 2000; Grenfell, 2012). Braided channels exist at BMGR as short segments that develop distributary channels and disappear into unconsolidated alluvium. We did not find this pattern at YPG, but it may occur in surrounding regions. Braided channel reaches located at BMGR appeared to occur only in partially confined zones bounded by mountains. As confinement of bedrock uplands decreased and valley width increased along a study reach in BMGR, for example, infiltration appeared to result in a floodout zone downstream of the study reach where the wash became entirely unconfined. Dust and Wohl (2010) identified thresholds for braiding, which distinguish channel types with regard to width-to-depth ratio and unit stream power. A similar threshold may exist for floodout zones, such that accommodation space becomes infinitely large and shallow sheet flow infiltrates readily into unconsolidated alluvium, leaving minimal to no trace of channelized flow. The lack of surface channel geometry in floodouts limit their comparison and inclusion in our classification, and we suggest that these features be considered as a landscape unit rather than a channel type.

Application of the classification system

Both the classification tree and discriminant analysis provide a way to test the strength of this *a priori* classification by predicting channel type based on channel geometry and hydraulics. This alone is not the way we intend the classification to be used, but rather use it to test the validity of such a classification. Given a high success rate of prediction using these methods, land use managers can then assume a range of values in channel geometry and hydraulics that can be expected for a channel of interest given qualitative identification of the channel type in the field or using remotely sensed imagery and DEMs.

We provide a dichotomous key to distinguish channel types (Fig. 1-9). Channel type can be identified in the field using the dichotomous key or GIS data if the necessary imagery, geologic layers, and DEMs are available. Braided channels are easily distinguished using channel planform from aerial imagery. Bedrock with alluvium and incised alluvium channels can be identified using geologic maps or field reconnaissance to separate bedrock versus unconsolidated alluvium channel boundaries. Piedmont and alluvial fan surfaces are distinguishable using aerial imagery and may be apparent in some regions when contrasted with adjacent desert pavement. Headwater channels that initiate on piedmont or bedrock surfaces are easily distinguished from one another using geologic and geomorphic surfaces with the appropriate surveys and GIS layers mentioned above. We encourage remotely sensed applications of this classification to include field visits for a subset of channel segments in the field to ensure correct identification of channel types

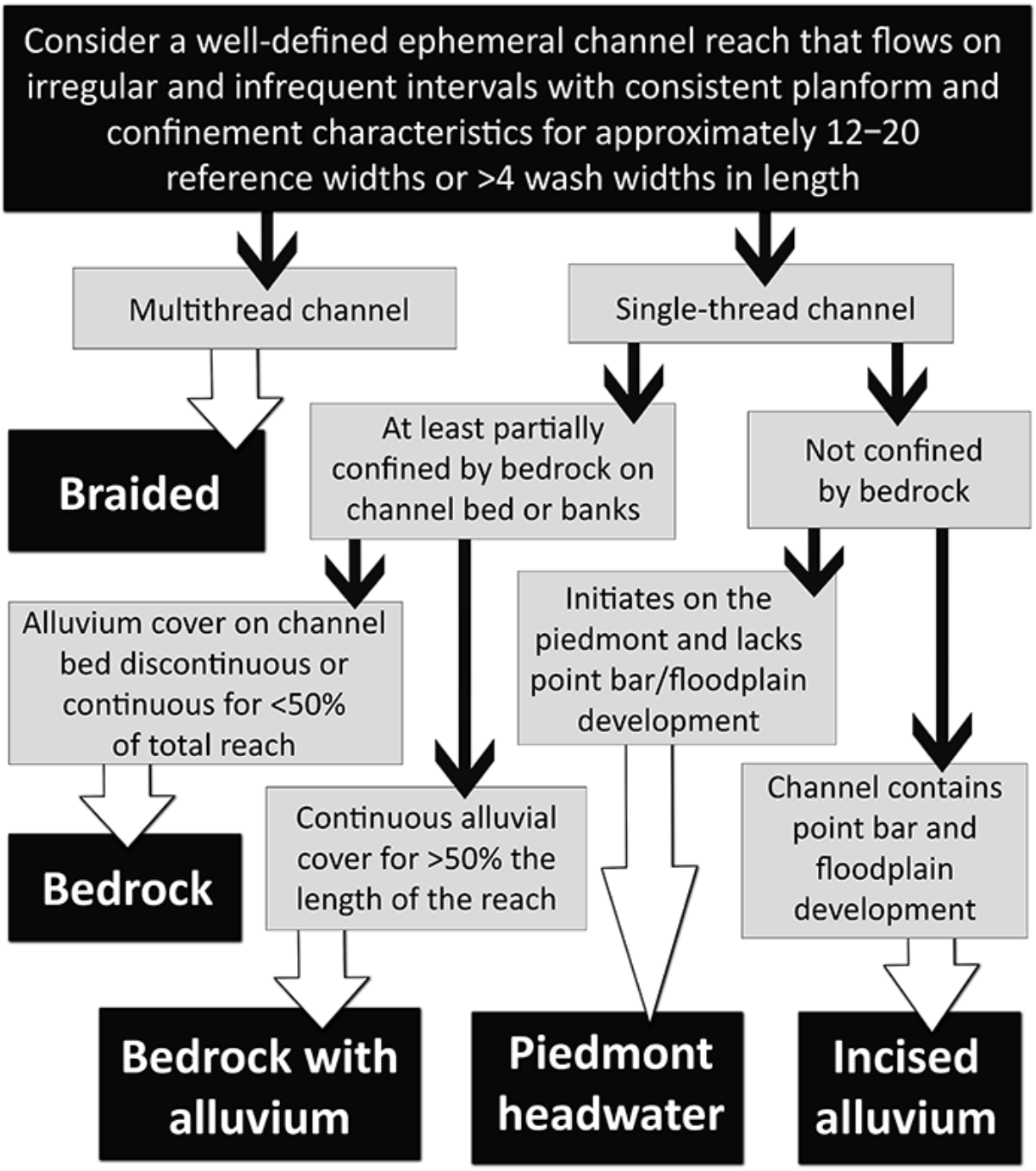

Figure 1-9. Dichotomous key to identify arid-region ephemeral stream geomorphic channel types based on qualitative descriptors. Reference widths refer to the width of the channel at a stage that represents a discharge responsible for maintaining contemporary channel geometry. Wash width refers to the valley bottom width at the confining boundaries of a braided channel.

Although we did not formally analyze the spatial distribution of each channel type, qualitative analysis from field observations, digital elevation models, geologic maps, and aerial imagery indicate a generalized spatial distribution

of channel types relative to mountainous uplands. Within YPG and BMGR, exposed bedrock is limited to mountain highlands, while unconsolidated alluvial bodies are more prevalent with increasing distance from mountains. Thus braided and incised alluvium channels increase in abundance with distance from mountains. Piedmont headwater channels occur most commonly along the margins of broad valleys and intermountain basins. The spatial distributions of reach types will likely differ in other physiographic regions. For example, bedrock or bedrock with alluvium channels may occur in incised canyons commonly found in lowlands of flat sedimentary landscapes such as the Colorado Plateau.

Our classification should be tested and applied in other arid regions. We anticipate this channel classification to be applicable to dryland ephemeral streams around the world, even though the range of values in channel geometry and hydraulic variables associated with each channel type will vary with climate, physiography, geology, and vegetation. Applications in arid regions that differ substantially from the Sonoran Desert may require similar analyses to determine parameter ranges of channel types.

Conclusions

Stream classifications provide guidance to understanding and measuring the physical response in channel geometry and structure and function of aquatic and riparian habitat with regard to anticipated frequency and magnitude of flows. A dearth of data concerning the temporal and spatial variability of ephemeral streams in arid regions currently limits understanding of channel response and associated riparian habitat, and researchers lack the broadly applicable vocabulary necessary to discuss these relationships. We have presented a geomorphic classification of ephemeral channels in arid regions based on planform, the degree of confinement, and the composition of confining material to contribute to understanding of dryland fluvial systems. Our analyses indicate that five *a priori* channel types differ significantly with respect to width-to-depth ratio, stream gradient, stream power, and shear stress despite limited accuracy of a few measured and derived variables based on the reference stage. These results illustrate meaningful differences in channel geometry among the five stream types and provide a conceptual framework to infer fluvial processes, assess hydrologic and ecological sensitivity to disturbance and climate change, and guide management and restoration activities throughout ephemeral stream networks.

Chapter 2. Alluvial Stratigraphy of Ephemeral Streams in the Sonoran Desert, Southwestern Arizona, USA: Constraints from DC Electrical Resistivity and Ground Penetrating Radar

Abstract

Ground penetrating radar and DC electrical resistivity profiles image the upper 4 m of the subsurface beneath ephemeral streams in Yuma and Mohave Washes in the Sonoran Desert, 30 km northeast of Yuma, Arizona. The geophysical data are tied to trenches to establish a lithostratigraphic interpretation. Archie's Law, calibrated to resistivity measurements on soil samples from each site, is used to estimate in-situ soil pore saturation. Three different stream types are surveyed. Increasing in stream order, these are incised bedrock with alluvium fill, incised alluvium, and braided streams. Three radar facies are identified on the basis of reflection amplitude, continuity, and dip. Near the surface, RF1 (0.5-1.5 m thick) contains laterally continuous sheetlike deposits interpreted to be active channel gravel, sand, and cobble deposits reworked during floods. Below, RF2 contains moderately continuous downlapping and onlapping reflections interpreted to be partially lithified Pleistocene gravel and cobble valley fill deposits. The underlying facies RF3 is nearly reflection free, but at the larger washes contains weak reflection similar in character to RF2. In the smaller washes, RF3 contains abundant diffractions. Two electrofacies are identified. The shallowest, EF1, extends from the surface to ~2.5 m deep. EF1 encompasses radar facies RF1 and RF2, with resistivity ranging from 250-1500 ohm-m. Electrofacies EF1 is inferred to represent a relatively dry surficial layer that includes the modern channel deposits and the upper ~1 m of the Pleistocene strata. Estimated soil moisture in this facies ranges from 2-40%, and varies up to 20% laterally over 2-5 m distances in the smallest washes. Electrofacies EF2 coincides with radar facies RF3, and has resistivity ranging from 10-300 ohm-m. At the larger washes, facied EF2 is interpreted to be Pleistocene valley fill, distinguishable from the overlying lithologically equivalent Pleistocene deposits by lower resistivity resulting from higher moisture content. Near surface lateral soil moisture variations in the smaller washes is strongly influenced by the subsurface stratigraphic architecture (facies RF2). In the larger washes, soil moisture variations are more subtle, changing gradationally with depth and downstream.

Introduction

Complex geomorphic processes and subsurface stratigraphic architecture likely play important roles in controlling the storage and transportation of groundwater and the ecohydrological dynamics of ephemeral stream networks in arid regions. Sediment thickness, texture, sorting, and cementation profoundly influence plant community dynamics in these regions, where water availability for riparian vegetation is severely limited [McAuliffe, 1994; Noy-Meir, 1973; Shreve and Wiggins, 1964; Yang and Lowe, 1956]. In general, a greater sediment thickness creates greater water storage capacity, providing more stable resource availability to vegetation [McAuliffe, 1994]. In arid regions, near-surface variations in sediment grain size, sorting, and stratigraphic layering have a strong effect on the storage and mobility of subsurface moisture, greatly impacting the distribution of desert biota. Coarse surficial sediments retain little moisture, but facilitate rapid and deep infiltration of rainfall that minimizes subsequent evaporation [Noy-Meir, 1973]. Fine-grained surficial sediments result in low infiltration rates and shallow wetting that is rapidly evaporated [Noy-Meir, 1973]. Fine-grained facies at greater depths may provide long-term storage of moisture on annual time scales {Brooks, 2010 #2248}. Variations in ephemeral stream subsurface structure and alluvial thickness between mountainous headwaters and lowland settings likely exert a fundamental control on subsurface moisture regime and riparian community composition.

In this study, we use ground penetrating radar, electrical resistivity, and trenching to characterize spatial variations in sedimentation patterns, sediment thickness, and subsurface water content in ephemeral streams in the Sonoran Desert of southwestern North America. Our purpose is to assess the geomorphic and ecological processes controlling stream morphology and subsurface moisture storage, and how these processes vary between different types of streams found in different positions in the watershed. We use the stream classification of Sutfin et al. [Sutfin et al., 2014], who distinguished five types of ephemeral streams in the northern Sonoran Desert on the basis of channel planform, lateral confinement, and composition of the confining material. This stream classification

includes piedmont headwater, montane bedrock, bedrock with alluvium, incised alluvium, and braided channels. Piedmont headwater channels are incised into partially consolidated alluvium on piedmont surfaces, and lack significant accumulations of active alluvium. Montane bedrock channels are confined by bedrock and devoid of persistent alluvium. Bedrock with alluvium channels occur in mountain valleys and foothills. These channels are confined by bedrock but contain a continuous bed of alluvium within the channel for at least 50% of a study reach length. Incised alluvium channels are found in relatively large alluvium-filled valleys and on piedmonts. These channels are confined by partially consolidated alluvium and contain active alluvial deposits extensive enough for floodplain and point bar development. Braided washes occur on lowland valley floors and exhibit multiple channels, with bars, islands, and broad floodplain surfaces along channel margins. In this paper we focus on the bedrock with alluvium, incised alluvium and braided channel systems that contain sufficient fluvial sediments to support riparian ecosystems. Our objectives in this paper are to determine the subsurface hydrostratigraphic characteristics of each channel type (bedrock with alluvium, incised alluvium, and braided channels) and to assess the implications in regards to ecohydrological processes and riparian vegetation,

Description of the Yuma Proving Grounds Study Area

This study focuses on ephemeral streams in the southern Sonoran Desert of southwestern North America. The study area is located on the U.S. Army Yuma Proving Ground (YPG) in the Lower Colorado River Valley of the southwestern United States Basin and Range physiographic province, 10-20 km east of the Colorado River and 160 to 200 km upstream of the Gulf of California (Fig. 2-1). Topography in the area is dominated by fault bounded mountain ranges and intervening valleys initially formed during mid-Tertiary crustal extension and regional magmatism [Eberly and Stanley, 1978; Richard et al., 2000]. The ranges expose mid-Tertiary and older crystalline bedrock, consisting primarily of felsic intrusive and extrusive rocks. Miocene to Pleistocene age sediments eroded from the mountains form extensive piedmonts on the flanks of the ranges and fill the intervening valleys. The modern drainages contain reworked Plio-Pleistocene sediments and Holocene alluvium consisting dominantly of cobbles, gravel, and sand. Elevations within the study area range between 845 m in the mountains to 60 m in the valley floors. Upland vegetation consists of widely spaced low shrubs and cacti, with denser vegetation and riparian trees along active channels [Shreve and Wiggins, 1964]. Annual rainfall measured at climate stations surrounding the study area ranges from 93 to 103 mm. Precipitation is biseasonal, resulting primarily from low intensity Pacific frontal storms during winter months and brief summer convective storms [Sellers and Hill, 1974]. Daily high and low temperatures average 40 □C and 27 □C respectiv
winter.

Study sites are located in bedrock within alluvium, incised alluvium, and braided channels in two different watersheds, known as Yuma Wash and Mohave Wash (Fig. 2-1). The study sites are typical of channels found in narrow montane valleys and broad alluvial valley floors throughout the northern Sonoran Desert. The Yuma Wash watershed has a catchment area of 174 km2. Bedrock in the upper portion of Yuma Wash consists primarily of Jurassic granite and granodiorite of the Kitt Peak-Trigo Peaks Super-unit and Oligocene to Middle Miocene dacite and rhyolite of the Fresnal Canyon Sequence [Richard et al., 2000; Tosdal et al., 1989]. The lower portion of the watershed is dominated by Middle Miocene to Pliocene conglomerates and sandstone underlain by moderately to strongly consolidated Pliocene-Pleistocene sediments. The bedrock with alluvium channel studied in the Yuma Wash watershed investigated in this study drains 2.21 km^2, and is incised into porphyritic granodiorite, diorite and gneiss (Tosdal, unpublished map). The incised alluvium reach investigated here is incised into a pediment composed of Pliocene to Pleistocene sand and gravel and has a drainage area of 3.60 km^2. The braided channel study reach drains 170 km^2 and contains Pleistocene to Holocene alluvium that is bounded by Pliocene-Pleistocene sediments, Miocene fanglomerate, and Oligocene porphyritic andesite with interbedded tuff of the Quechan Formation (Tosdal, unpublished map).

The Mohave Wash watershed has a catchment area of 225 km^2. Bedrock in the upper part of Mohave Wash consists primarily of dacite and rhyolite of the Fresnal Canyon Sequence, with isolated granitic outcrops of the Kitt Peak-Trigo Peaks Super-unit[Richard et al., 2000; Tosdal et al., 1989]. Piedmont and valley fill materials consist of Late Pliocene to Early Pleistocene consolidated gravel and sand deposits, with localized exposures of underlying Middle Miocene to Pliocene conglomerate, sandstone, siltstone, mudtstone of the Bouse Formation [Eberly and Stanley, 1978; Richard et al., 2000; Tosdal et al., 1989; Youberg et al., unpublished]. The Mohave bedrock with alluvium

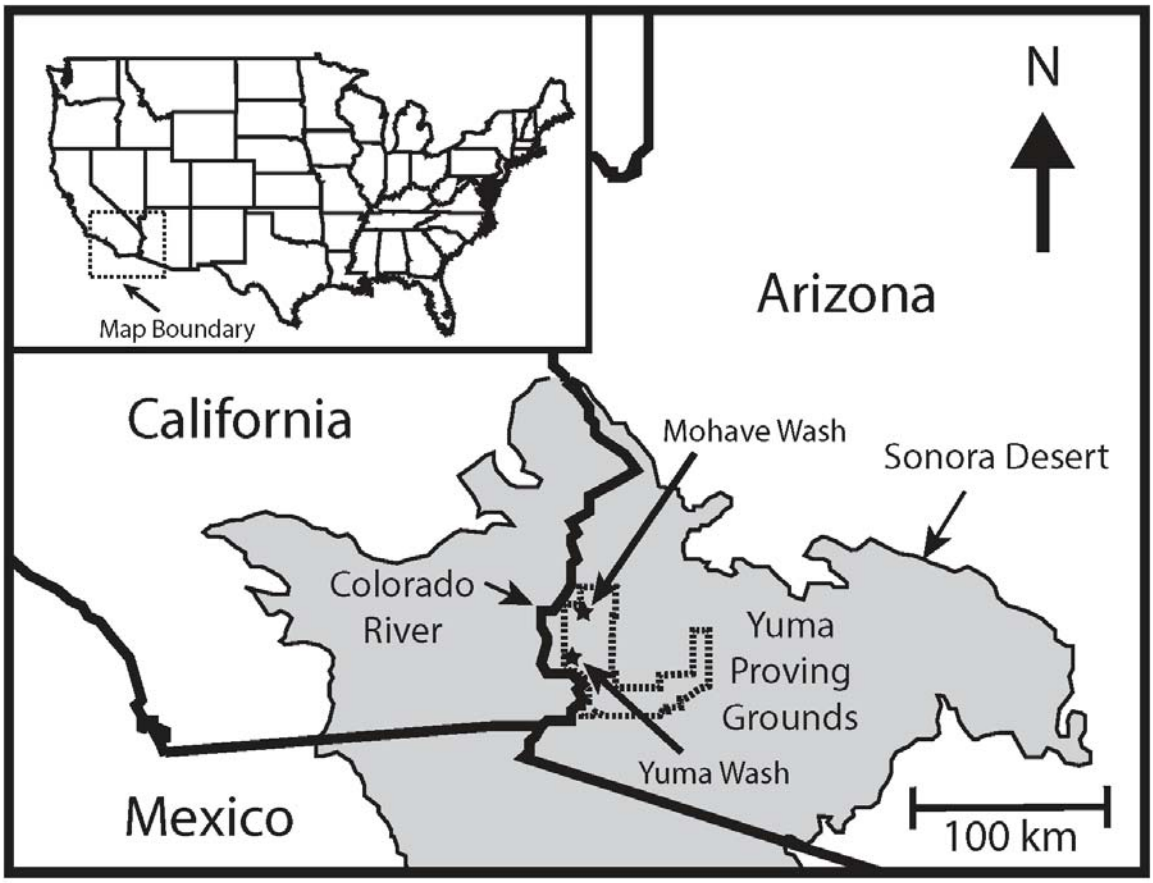

Figure 2-1. Location of Yuma Proving Grounds (YPG) and Mohave Wash and Yuma Wash study areas. Inset shows regional location of study area (dashed box). Yuma Proving Grounds (dashed outline) lies within the Sonoran Desert (gray shading) in the western North American Basin and Range province and is bounded on the west by the Colorado River.

study reach drains 0.91 km^2 of rhyolitic terrain at the foothills of the Trigo Mountains. The incised alluvium study reach has a drainage area of 170 km^2, and is bounded by Pliocene-Pleistocene consolidated sediments and, in some areas, granite outcrops. The braided study reach at Mohave Wash drains 225 km^2, and is incised into relict fan and terrace deposits composed of Pliocene-Pleistocene consolidated alluvium.

Methods

Twenty-five Ground Penetrating Radar (GPR) and 23 DC Electrical Resistivity (ERT) profiles were collected during January 2011 at each of the six study sites, representing each of the three channel types investigated in Yuma and Mohave Washes. The GPR and ERT profiles were co-located where possible. Lithological interpretation of the geophysical data is constrained by correlation to sediment profiles in three trenches 1.5 to 4.6 m deep at each of the incised alluvium and braided channel sites, and seven soil pits at each bedrock with alluvium site. Trenching was conducted during three campaigns in November 2011 to January 2012, October 2012, and May 2013.

The GPR data were collected using a Sensors & Software Pulse Ekko Pro system with 100 MHz antennae and a recording time of 400 ns. A minimum of four common offset profiles with a 0.25 m trace spacing were collected at each site, with three cross sectional profiles crossing the drainage perpendicular to the channel and one longitudinal profile parallel to the drainage. The cross sectional transects were spaced approximately four channel widths apart at the bedrock with alluvium and incised alluvium channel sites. The spacing between transects across the braided channels was approximately equal to the width of the wash. Common Midpoint (CMP) surveys collected at each of

the study sites indicate an average subsurface radar velocity of 0.045 m ns^{-1}, with little variation between sites. This equates to a maximum imaging depth of 3.5 m and a bed minimum thickness resolution (one fourth of the wavelength) of 0.16 m. Automatic Gain Control (AGC) and Spherical and Exponential (SEC) Gain Corrections were separately applied to the data to enhance reflection geometries and amplitude variations, respectively.

DC Electrical Resistivity surveys were collected along profiles coincident with all but one of the GPR profiles (the narrowness of the channels at the Yuma Wash bedrock with alluvium site precluded collection of ERT data at the upstream end of the reach). The data were collected with a 10-channel 48 electrode Syscal Pro system. A dipole-dipole array was used with a 2 m electrode spacing except for two profiles at the Yuma Wash bedrock with alluvium site, where 1 m electrode spacing was tested to verify that the electrode spacing was capturing subsurface heterogeneity at the bedform scale. The subsurface resistivity structure was estimated by tomographic inversion using the Res2D software program by Geotomo Software, Ltd. [Loke and Barker, 1996; Loke and Dahlen, 2002]. Data were filtered prior to inversion to remove measurements with low voltage drops and measurements with large standard deviations. A rectangular mesh was used to parameterize the subsurface during the tomographic inversion. The thickness of the rows in the mesh is 0.2 times the electrode spacing near the surface and increases 10% with each row down to a maximum depth of 30 m. The width of the columns in the mesh is equal to the electrode spacing. Inverse models using both L1 and L2 norms (minimizing the mean absolute misfit and mean squared misfit between modeled and measured voltage drops, respectively) were tested [Loke et al., 2003]. The L1 inversion yielded an inverse model with a sharp resistivity gradient at a depth coinciding with abrupt changes in AGC radar amplitude, and so was chosen as the basis for interpretation. The fidelity of the inverse models was assessed by calculating the sensitivity of the predicted surface voltage drops to variations in the resistivity within each portion of the model mesh [Loke and Barker, 1995], and by examining the Depth of Investigation (DOI) Index [Oldenburg and Li, 1999], which identifies portions of the model domain in which the solution is heavily dependent upon the initial model (and is therefore deemed to be poorly constrained). Both the DOI Index and the model sensitivity are relatively uniform at depths shallower than about 3.5 m, and diminish rapidly at greater depths. Consequently, we confine our interpretation of the ERT data to depths shallower than 3.5 m.

Laboratory measurements of resistivity as a function of water saturation were conducted on surficial sediment samples from each site to establish an empirical basis for estimating in-situ water content from the ERT data. Sediment samples were collected by shovel in all of the active channels except the Mohave Wash bedrock with alluvium site, where the channel was composed primarily of large cobbles. Samples were also collected from adjacent floodplains and/or bars at all sites except the Yuma Wash bedrock with alluvium and incised alluvium sites. The samples were sieved to determine the grain size distribution by weight (Fig. 2-2a). Porosity was determined by volumetric balance for three separate portions of each sample [Lee et al., 2003]. These were averaged to determine a mean porosity for the sediment at each sample location (Table 2-1). Resistivity for each of the samples was measured using a protocol similar to that described by [Telford et al., 1990]. A simplified form of Archie's Law [Archie, 1942] is used to describe the relationship between resistivity and saturation:

$$\text{Eqn. 1} \qquad \rho = B \times S^{-n} \times \rho_w$$

where ρ is the sample bulk resistivity, S is the volumetric pore saturation, and ρ_w is the resistivity of the pore fluid. B and n are empirically determined coefficients that were estimated by least squares regression (Fig. 2-2b; Table 2-1). Equation 1 is used to estimate volumetric pore saturation at each site based on the ERT data.

Facies Identification and Geophysical Attributes

Three distinctive radar facies are recognized in the GPR profiles on the basis of reflection amplitude, continuity, and dip. Radar facies RF1 is the surficial unit, and is characterized by high amplitude, sub-horizontal to horizontal parallel reflections (Fig. 2-3a, b) that can be correlated over several tens to hundreds of meters distance. An abrupt decrease in signal amplitude on the SEC data at the base of this facies (radar horizon RH1) separates facies RF1 from underlying radar facies RF2 (Fig. 2-3a). Horizon RH1 lies at depths ranging from 0.5 to 1.1 m, with the depth increasing progressively from the bedrock with alluvium, to the incised alluvium, and finally to the braided channels. Radar facies RF2 is characterized by high amplitude on the AGC data, lower frequency content than RF1, and distinctive undulatory and in places bidirectionally dipping reflections correlatable over distances of 10 to 20 m, with abundant downlapping and onlapping relationships (Fig. 2-3b). Weak to moderate amplitude diffractions are common at the top of this facies in the larger streams (braided and incised alluvium channel sites), and throughout

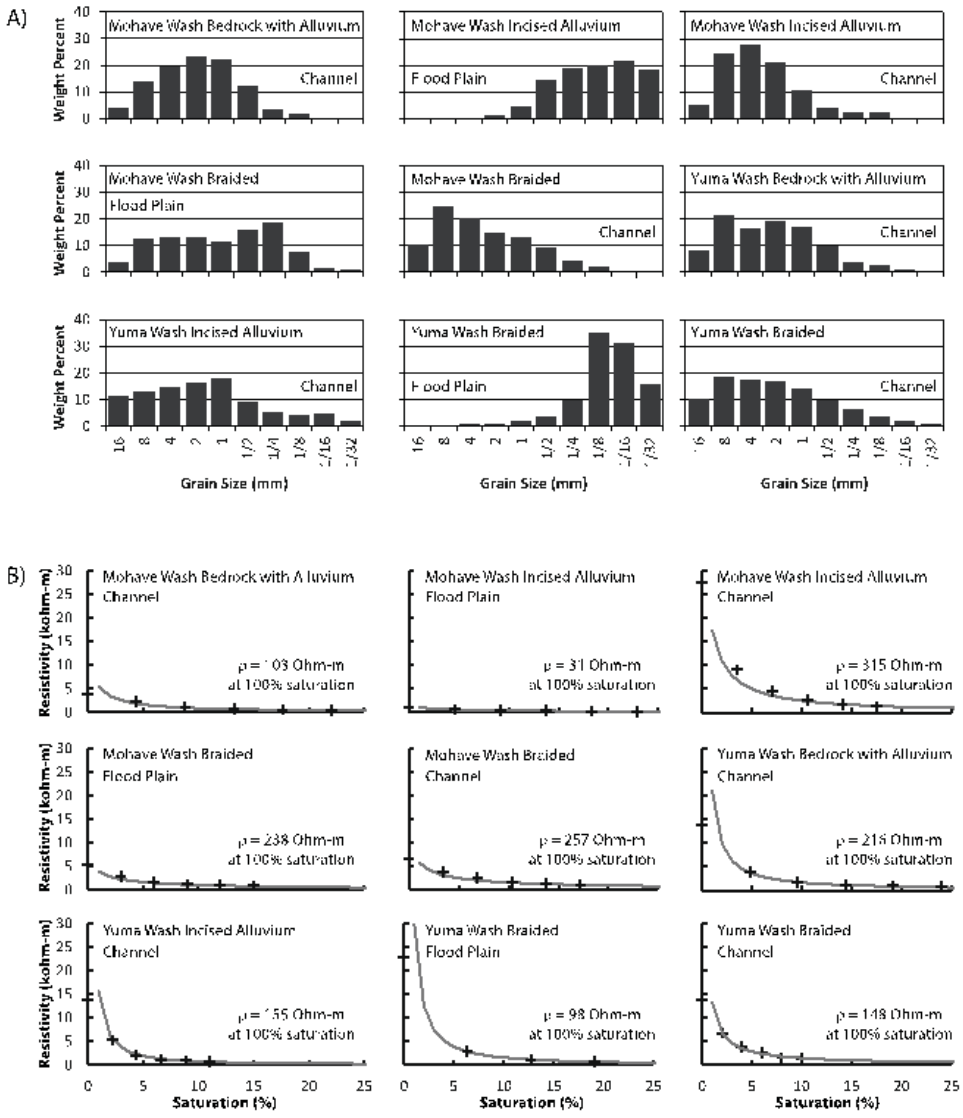

Figure 2-2. A) Grain size distribution in sediment samples from YPG stream sites. B) Resistivity as a function of volumetric pore water saturation. Solid lines indicate best-fit curve from Archie's Law.

the facies in the bedrock with alluvium sites. Radar facies RF3 is characterized by weak or absent reflections in the AGC data (Fig. 2-3b). The distinctive decrease in AGC reflection amplitude at the interface between facies RF3 and RF2 is designated radar horizon RH2. At the bedrock with alluvium channel sites, an abrupt downward decrease in reflection amplitude is the sole identifying characteristic of RH2. At the incised alluvium and braided channel sites, the abrupt loss of amplitude at RH2 is accompanied in many areas by an overlying relatively long period, high amplitude reflector that is continuous over distances of 2 to 10 m, referred to as reflection RH2r. Horizon RH2 lies at depths ranging from 1.7 to 2.8 m, with the depth varying between drainages and within individual drainages.

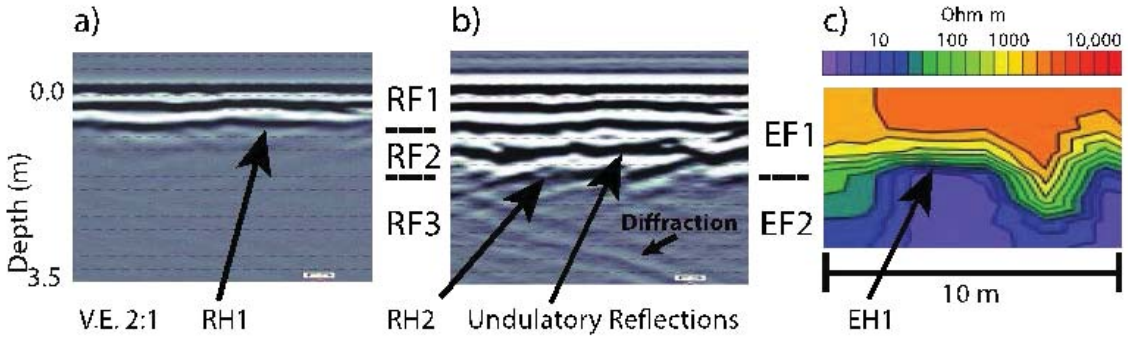

Figure 2-3. Radar facies and electrofacies identification. Images are from the Mohave Wash incised alluvium site, but are typical of all sites. A) GPR profile with spherical divergence and exponential attenuation gain correction (SEC) applied. B) The same GPR profile with Automatic Gain Control correction (AGC) applied. C) Electrical resistivity tomography (ERT) image from the same section.

Table 2-1. Soil porosity and Archie's Law parameters

Sample Location	Porosity	B	n
Mohave Wash Bedrock w/ Alluvium	0.41	10.75	1.06
Mohave Wash Incised Alluvium	0.40	1.60	0.64
Mohave Wash Braided Stream	0.50	6.38	0.76
Yuma Wash Bedrock w/ Alluvium	0.39	20.21	1.10
Yuma Wash Incised Alluvium	0.58	14.20	1.30
Yuma Wash Braided Stream	0.60	12.83	0.96

Two distinctive electrofacies are recognized at all of the stream sites (Fig. 2-3c). The surficial facies, EF1, is similar at all sites and is characterized by relatively high resistivity, ranging from 250 to 2500 ohm-m. Electrofacies EF1 encompasses radar facies RF1 and RF2. The deeper electrofacies, EF2, has resistivity ranging from 5 to 500 ohm-m. A moderate to sharp resistivity gradient at depths ranging from 1.5 to 3.5 m (electrohorizon EH1) separates EF2 from the overlying facies EF1, with the depth of electrohorizon EH1 coinciding with radar horizon RH2 in most places.

Subsurface Interpretation

Braided Channels

The braided stream sites are located within relatively straight 300 to 500 m wide washes that encompass a series of individual braided channels (Fig. 2-4). The individual channels are bound on either side by low, poorly defined banks incised into modern floodplain surfaces. The composite channel systems, which span the width of the washes, are confined by vertical banks up to 6 m high incised into partially-consolidated alluvial fill in the surrounding piedmont.

Geophysical Characteristics

Radar facies RF1 extends from the surface to 0.5-1.0 m depth, and consists of high amplitude conformable and nearly horizontal reflections that are continuous over the length and width of the survey area (Fig. 2-5). Radar horizon RH1, at the base of facies RF1, is marked by an abrupt decrease in reflection amplitude. The underlying facies RF2 appears reflection-free in the SEC profiles. In the AGC profiles, facies RF2 is characterized by a 0.5 to 1.8 m thick interval of high amplitude sub-horizontal reflections that are distinguishable from RF1 by their larger dominant period. Reflections in RF1 conformably overlie parallel to sub-parallel reflections in facies RF2 in most

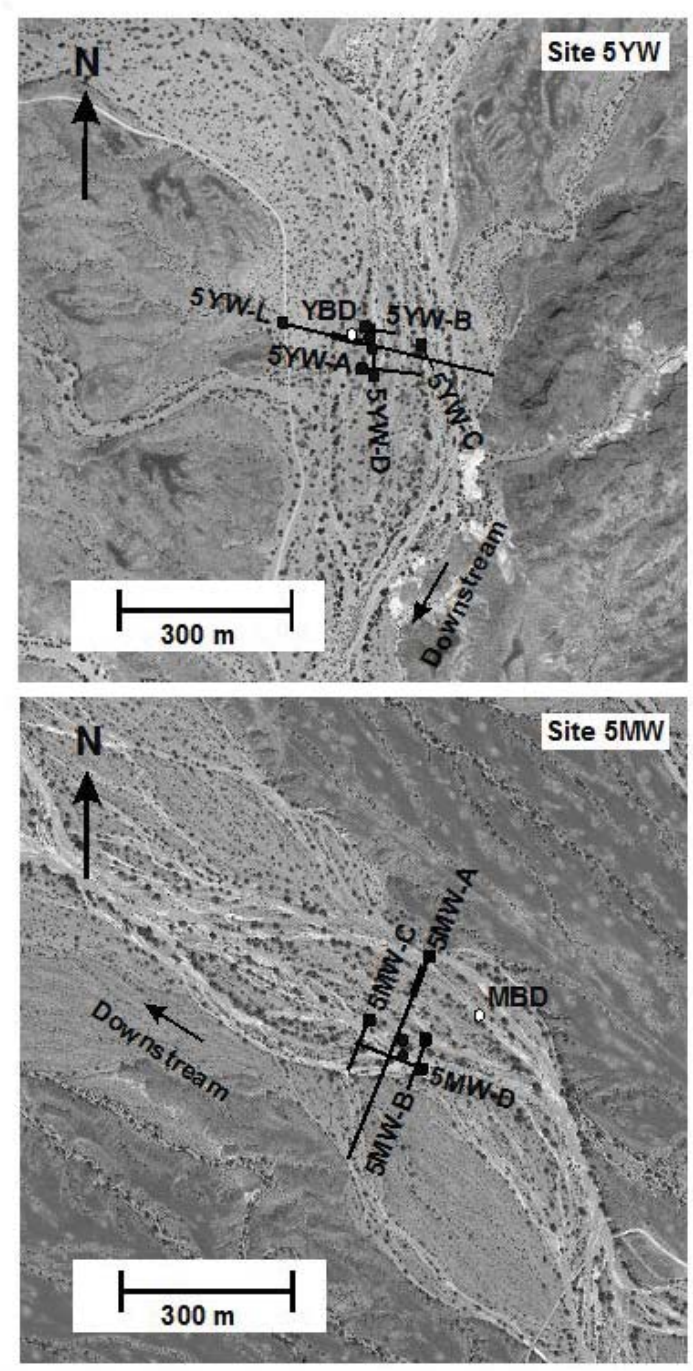

Figure 2-4. Aerial photographs of braided channel sites. A) Yuma Wash. B) Mohave Wash. Solid lines indicate GPR and ERT profiles, with squares at the beginning of each profile. Solid circles indicate locations of common midpoint (CMP) radar surveys. Open circles indicate trench locations.

areas, inter-fingering in the downstream direction and occasionally onlapping and burying mounded low relief features (< 0.25 m amplitude) at the top of facies RF2. Reflections in the middle and lower part of radar facies RF2 are undulatory and laterally continuous for distances of a few tens of meters, with gently dipping downlapping downstream and cross-stream reflections that onlap and merge upstream with the sub-horizontal reflections in the upper part of the facies. Concave upward scour marks, filled with side-lapping and downlapping sub-horizontal

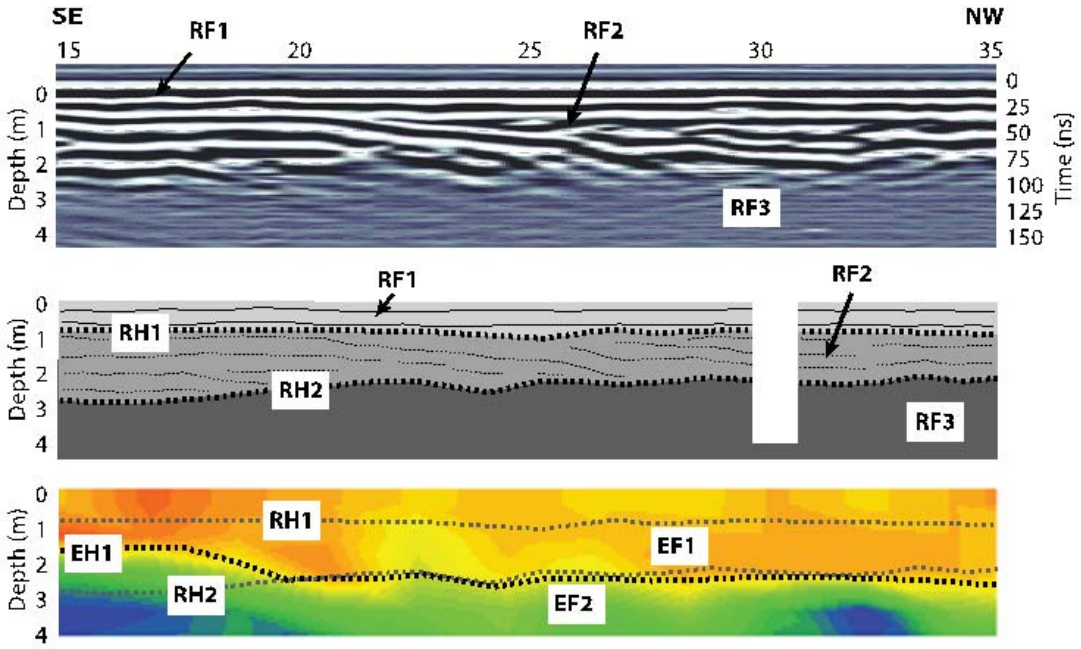

Figure 2-5. GPR and ERT data for representative sections of geophysical profiles at the braided stream sites. A) Yuma Wash. B) Mohave Wash. For each wash, a section of the AGC GPR profile (top), radar stratigraphy (middle) and ERT profile (bottom) are shown.

reflections, are common within RF2, as are bidirectional dips, prograding stacking patterns, and inter-fingering of reflections. Diffractions are common in the lower part of the facies. Radar horizon RH2, marking the base of facies RF2, is characterized by a gradational loss of reflection amplitude in the AGC sections over a 0.50 to 0.75 m thick interval. A distinctive high amplitude low frequency undulatory reflection (RH2r) coincides with RH2 in some areas, and is absent or weakly developed in others, with its character persisting over horizontal distances of a few tens of meters. Where RH2r is strong, the loss in AGC amplitude with depth is much more abrupt than in areas where the reflection is absent or less well developed. Below horizon RH2, radar facies RF3 is distinguished from facies RF2 primarily by a lack of diffractions and a loss of AGC amplitude. The upper part of RF3 contains weak reflections with geometries and dominant periods that are similar to those in RF2.

Both braided channel sites have a well-developed two-layer resistivity structure. The upper layer, electrofacies EF1, is a relatively homogeneous high resistivity layer extending from the surface to 1.5-2.7 m depth. EF1 encompasses radar facies RF1 and RF2. Resistivity in EF1 ranges from 200 to 700 ohm-m at the Yuma Wash site, increasing systematically downstream. Resistivity in EF1 ranges from 400 to 1000 ohm-m at the Mojave Wash site, with the lowest values being concentrated within 50 m of the center of the wash, and higher resistivity toward the wash sides. The base of EF1 is marked by a relatively sharp vertical resistivity gradient (electrohorizon EH1) that roughly centers on the 250 ohm-m resistivity contour. In most places EH1 is nearly flat, approximately 2.0 m deep, and correlates closely with the position of radar horizon RH2. The resistivity gradient is steepest where reflection RH2r is strongest, and the decrease in AGC radar amplitude at horizon RH2 is sharpest. In areas where the change in radar amplitude is more gradational, the resistivity gradient at horizon EH1 is less sharp. In these areas electrofacies EF1 extends as deep as 2.7 m. Electrofacies EF2 is a relatively homogeneous layer beneath horizon EH1 that correlates with radar facies RF3, and has a distinctively lower resistivity than facies EF1, ranging from 50 to 200 ohm-m at the Yuma Wash site and 50 to 300 ohm-m at the Mohave Wash site.

In summary, the braided channel sites both have radar reflection patterns indicative of two depositional layers. The upper layer, RF1, extends from the surface to approximately 1 m depth and is dominated by relatively uniform, horizontal beds extending the length and width of the reach. The second layer, RF2, consists of lower-frequency undulatory reflections with common downlapping and onlapping reflection terminations and abundant diffractions emanating from the lower part of the layer. The boundary between facies RF1 and RF2 coincides with an abrupt loss of SEC-gained reflection amplitude. The base of facies RF2 is marked by a gradational loss of AGC-gained reflection amplitude at horizon RH2 that in places coincides with a distinctive low-frequency reflection (RH2r). AGC reflection amplitude loss below RH2 is most abrupt where RH2r is best developed. Radar facies RF1 and RF2 are indistinguishable on the basis of the electrical resistivity, both occurring within low resistivity electrofacies EF1. A relatively steep resistivity gradient separates these facies from underlying electrofacies EF2, which has distinctively lower resistivity. The resistivity gradient separating electrofacies EF1 and EF2 is sharpest in areas where radar reflection RH2r is best developed and the downward loss in AGC-gained reflection amplitude is most abrupt.

Trench Correlation, Moisture Content, and Geomorphic and Hydrostratigraphic Interpretation

The radar and electrical facies at the braided stream profiles correlate well with hydrostratigraphy revealed in trenches that were dug after the geophysical profiles were collected (Figs. 2-4 and 2-5). Radar facies RF1 correlates with a 0.8-1.5 m thick surficial layer composed of poorly sorted gravel and cobble with a sandy matrix that is interpreted to be active channel deposits. In the trenches, this layer consists of weakly sub-horizontally stratified beds a few decimeters thick, similar to the GPR reflection character of RF1. Within individual beds, sediments contain trough cross beds on the millimeter scale, which is below the GPR resolution. The lateral continuity and near horizontal attitudes of the GPR reflections in facies RF1 and correlative strata in the trenches suggest that these sediments were deposited primarily under upper-regime flow conditions that we infer to have occurred during periodic large floods, when plane bed depositional conditions prevail. Cross bedding within individual layers are interpreted to indicate sediment re-working by dune and longitudinal bar migration during flood recession. Archie's Law, calibrated to the laboratory resistivity measurements, indicates volumetric pore saturation at the time of the geophysical surveys ranged from 12 to 42% in this facies at Mohave Wash, and varies as much as 20% across the wash. At the Yuma Wash site, volumetric pore saturation is estimated to have ranged from 7 to 54% in this facies, with the higher values occurring nearer the center of the channel.

An abrupt change in stratigraphy occurs 0.8-1.5 m below the surface in the trenches. Here, the sub-horizontal strata of facies RF1 unconformably overly gently dipping weakly to moderately lithified strata consisting of redish, poorly sorted sand to cobble deposits with weakly developed cross-beds on the decimeter scale. The unconformable contact at the base of the active alluvium correlates with radar horizon RH1 and the underlying partially lithified strata correlate with radar facies RF2. The strata exposed in this interval in the trenches is inferred to be Plio-Pleistocene valley fill deposits that outcrop nearby based on similarity of bedding attitude, degree of cementation, clastic composition, and the distinctive red color of the matrix. The GPR profiles indicate that the Plio-Pleistocene alluvium underlays the active channel deposits throughout the braided stream sites. The complex onlapping, downlapping, and truncating reflections in RF2 are similar in scale and dip attitude to the cross bedding observed in the Plio-Pliestocene strata in the trenches. These sedimentary structures are indicative of lower energy depositional environments with shifting flow direction associated with lateral and longitudinal accretion and migration of channel bars. The difference in bedding structures, degree of lithification, and reddening due to oxidation of clay minerals between radar facies RF1 and RF2 suggests substantially different hydroclimatic regimes during deposition of the Plio-Pliestocene strata and the modern channel sediments. No difference in moisture content was noted between the active alluvium and Plio-Pleistocene strata in the trenches. We therefore attribute the abrupt loss in radar amplitude in the SEC data below RH1 to a change in electrical properties between the unconsolidated active alluvium and underlying partially cemented and oxidized Pleistocene deposits rather than to a change in moisture content.

Gravel and cobbles are more abundant and the strata were visually wetter at depths greater than 2.0-2.5 m below the surface in the trenches. The top of the coarser, wetter strata correlates with geophysical horizons RH2/EH1, and the strata below correlates with geophysical facies RF3/EH2. The strata below 2.0-2.5 m in the Yuma trenches are similar in color, friability, and bedforms to the drier, slightly finer grained layer above, leading us to infer that this is a coarser unit of the Pleistocene valley fill. This is consistent with the similarity in all but amplitude of the

reflections in facies RF2 and those at the top of facies RF3. Cobbles are more abundant in the lower part of this unit in the trenches, consistent with the common presence of diffractions near the base of RF2. The change in AGC radar amplitude and electrical resistivity below horizons RH2/EH1 are attributed to an increase in sediment moisture content, which was observed in the trenches. Electrofacies EF1 encompasses the dry upper part of the strata at the braided stream sites, which includes the upper part of the Pleistocene alluvium and the overlying modern channel deposits. Electrofacies EF2 encompasses the wetter and coarser part of the Pleistocene alluvium.

At the Mohave braided site, the contact between the drier and wetter strata is in some places associated with a distinctive, partially lithified siltstone bed that is at least 1.0 m thick. Based on unit descriptions and nearby exposures [Metzger, 1968; Youberg et al., unpublished], we interpret this siltstone bed to be part of the underlying Bouse Formation. The depth to the top of the siltstone bed encountered in the trenches varies across the fluvial corridor, ranging from 2.6-3.0 m near the middle of the wash to 1.1 m near the wash margin and outcropping in the lower 1,0-1.5 m of the cutbanks that bound the wash. The top of this siltstone bed correlates with radar reflection RH2r, which appears intermittently at the top of radar facies RF3 on the GPR profiles from the Mohave Wash braided channel site. The differences in the depth to the siltstone bed in trenches spanning the wash and the intermittent character of reflection RH2r suggests that several meters of relief have been eroded onto the top of the Bouse Formation. Where radar reflection RH2r is present, the gradients in AGC radar amplitude and resistivity that mark horizons RH2 and EH1 are relatively sharp, which is consistent with the sharp nature of the lithologic contact at the top of the siltstone bed and the abrupt downward increase in moisture at this contact in the trenches. In these areas, horizons RH2/EH1 are interpreted to coincide with the top of the Bouse Formation, which is inferred to be associated with an abrupt moisture interface. In areas where reflection RH2r is absent, we interpret the Bouse Formation to be more deeply eroded. In these areas, the decreases in radar amplitude and resistivity below horizons RH2 and EH1 are gradational over a 50 cm thick interval, and are similar to appearance to horizons RH2 and EH1 at the Yuma Wash braided channel site. We interpret this gradational change in electrical properties to be a result of a gradational change in moisture content in areas where the sharp lithological contact associated with the siltstone bed at the top of the Bouse Formation is absent. In these areas, we interpret horizons RH2/EH1 to primarily be a gradational moisture interface within the Plio-Pleistocene alluvium that underlies the active channel deposits.

Incised Alluvium Channels

The incised alluvium study sites are located within straight channels, immediately downstream of minor tributary confluences (Fig. 2-6). At both sites, the channels are incised > 2 m into partially consolidated alluvium, and exhibit well-developed lateral and point bars. The Yuma Wash incised alluvium channel is approximately 20 m wide and contains a 0.3 m high inset floodplain (3 to 5 m wide) along the southern margin. The incised alluvium reach at Mohave Wash ranges from 40 to 50 m wide, and is bordered by a 1.0 m high, laterally extensive floodplain along the eastern margin.

Geophysical Characteristics

The incised alluvium channels have a two layer geophysical structure similar to the braided channel sites. Radar facies RF1 consists of high amplitude conformable and nearly horizontal reflections that are laterally continuous for tens of meters (Fig. 2-7). The base of facies RF1 is marked by an abrupt decrease in SEC reflection amplitude at depths between 0.8 and 1.0 m. Facies RF2 is a 0.8-1.0 m thick interval of high amplitude sub-horizontal reflections in the AGC gained profiles, approximately 0.5 m thinner on average than facies RF2 at the braided channel sites. Stratal relations between facies RF1 and RF2 at the incised alluvium and braided channel sites are similar. Reflections in RF1 conformably overlay parallel reflections of facies RF2 in most areas, occasionally onlapping and burying low relief features (< 0.25 m amplitude) on horizon RH1. In some areas, reflections in radar facies RF2 are undulatory and continuous over distances of 2 to 5 m, with gently dipping onlapping and downlapping reflection patterns. However, in most places RF2 reflections are sub-horizontal and laterally continuous for several tens of meters. Diffractions are common in the lower part of facies RF2 at the Yuma Wash incised alluvium site, but are sparse at the Mohave Wash site. Radar horizon RH2 is in all places characterized by a sharp downward decrease in reflection amplitude over a 0.5-0.7 m thick interval in the AGC profiles. In many areas at the Mohave Wash incised alluvium site RH2 is also marked by a distinctive low frequency high amplitude reflection, RH2r, similar to the Mohave Wash braided channel site. As at the braided channel site, the downward decrease in AGC reflection

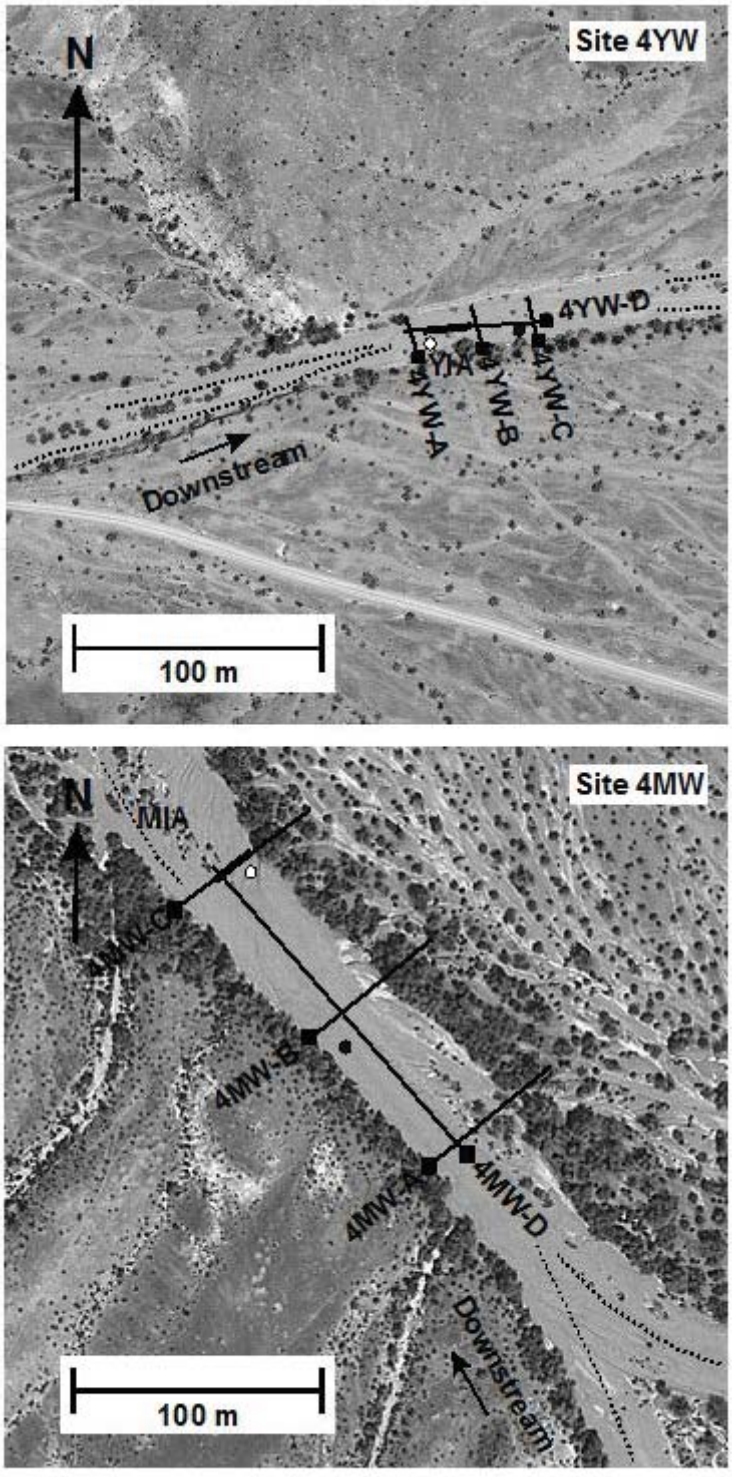

Figure 2-6. Aerial photographs of incised alluvium sites. A) TOP - Yuma Wash. B) BOTTOM - Mohave Wash. Solid lines indicate GPR and ERT profiles, with squares at the beginning of each profile. Solid circles indicate locations of common midpoint (CMP) radar surveys. Open circles indicate trench locations.

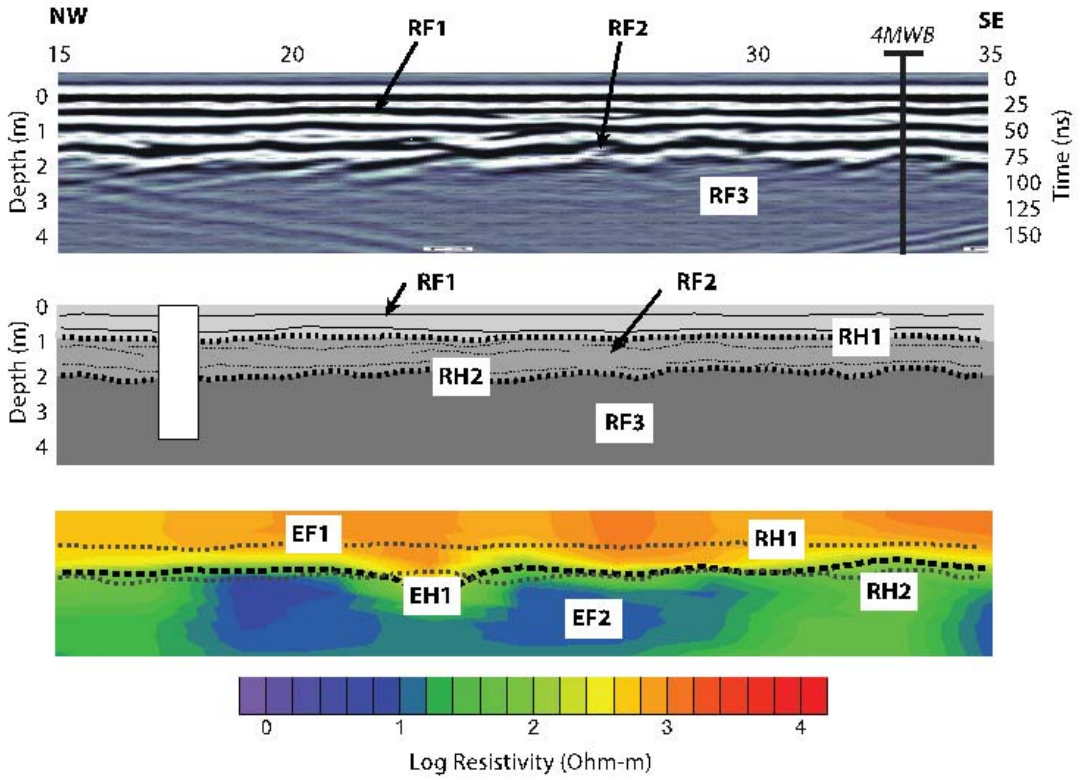

Figure 2-7. GPR and ERT data for representative sections of geophysical profiles at the incised alluvium channel sites. A) Yuma Wash. B) Mohave Wash. For each wash, a section of the AGC GPR profile (top), radar stratigraphy (middle) and ERT profile (bottom) are shown.

amplitude is more abrupt in areas where RH2r is present than in areas where the reflection is absent. Radar facies RF3, underlying horizon RH2, is distinguished from facies RF2 primarily by its lower AGC amplitude. As at the braided stream sites, the upper part of RF3 contains weak reflections with geometries and dominant periods that are similar to those in RF2.

Electrofacies EF1 at the incised alluvium sites extends from the surface to depths ranging from 2 to 3 m, encompassing radar facies RF1 and RF2. EF1 is relatively homogeneous, with resistivity ranging from 300 to 700 ohm-m at the Yuma Wash site, decreasing downstream. Resistivity in EF1 ranges from 250 to 1500 ohm-m at the Mojave Wash site, again decreasing downstream. Electrohorizon EH1, at the base of facies EF1, is marked by a moderately steep vertical resistivity gradient that corresponds roughly to the 200 ohm-m resistivity contour, similar to horizon EH1 at the braided channel sites. Horizon EH1 lies at an average depth of about 2.1 m and in most areas correlates closely with the position of radar horizon RH2. EH1 and RH2 diverge in isolated areas where electrohorizon EH1 extends downward to form either narrow concave upward depressions of about 1 m in width or broad flat bottomed depressions about 10 m in width, both with amplitude of 1.0 to 1.5 m. Electrofacies EF2, beneath horizon EH1, has a distinctively lower resistivity than facies EF1, ranging from 5 to 50 ohm-m at the Yuma Wash site and 15 to 150 ohm-m at the Mohave Wash site.

In summary, the incised alluvium channel sites both have two-layer radar reflection patterns and resistivity structures that are broadly similar to the braided channel sites. The upper layer, RF1, is virtually identical in character and thickness to the braided channel sites, extending from the surface to approximately 1 m depth and dominated by horizontal laminar deposits extending for distances of several tens of meters. The second layer, RF2, consists of lower-frequency reflections with downlapping and onlapping reflection terminations, similar to RF2 at the braided channel sites. Abundant diffractions emanating from the base of RF2, as observed at both braided channel sites, are present at the Yuma Wash incised alluvium site but are sparse at the Mohave Wash incised

alluvium site. At the braided channel and incised alluvium sites at both washes, the boundary between facies RF1 and RF2 coincides with an abrupt loss of SEC reflection amplitude. The base of facies RF2 is marked by a gradational loss of AGC reflection amplitude over a 0.5 to 1.5 thick interval. Radar facies RF1 and RF2 are indistinguishable on the basis of electrical resistivity, both laying within low resistivity electrofacies EF1. Resistivity in electrofacies EF1 is generally higher at the incised alluvium sites than at the braided channel sites, and the steep resistivity gradient marking electrohorizon EH1 at the base of facies EF1 is sharper and more continuous at the incised alluvium sites. Electrofacies EF2 has a distinctively lower resistivity than facies EF1, and is also lower on average by about 100 ohm-m than at the braided channel sites.

Trench Correlation, Moisture Content, and Geomorphic and Hydrostratigraphic Interpretation

The radar and electrical facies at the incised alluvium sites correlate well with hydrostratigraphy revealed in trenches dug after the geophysical profiles were collected (Figs. 2-6 and 2-7). The strata exposed in the trenches and the geophysical correlations are similar to those at the braided channel sites. Radar facies RF1 correlates with a ~0.8 m thick surficial layer composed of weakly stratified, horizontal to sub-horizontal parallel beds of poorly sorted sand, gravel, and cobble interpreted to be active channel sediments. The lateral continuity and near horizontal attitudes of the GPR reflections in facies RF1 suggest that these strata are primarily plane bed sedimentary features deposited during large flood events. An abrupt change from the laminar structure of RF1 to more complex bedding characteristics occurs approximately 0.8 m below the surface in the trenches, at a depth corresponding to radar horizon RH1. Here, the nearly horizontal strata of facies RF1 unconformably overlie weakly lithified, low-angle cross-stratified beds of poorly sorted gravel and cobbles in a sandy matrix. Based on reddening from oxidized clay minerals, the degree of lithification, and comparison to outcrops bordering the braided channel sites, we interpret this unit to be Plio-Pleistocene alluvium. This stratigraphic interval correlates with radar facies RF2, which underlays the active channel deposits on the GPR profiles throughout the incised alluvium survey sites. As at the braided stream sites, we attribute the loss in SEC radar amplitude below radar horizon RH1 to result from a change in electrical properties associated with the differences in composition, grain size, and cementation between radar facies RF1 and RF2, with the Pleistocene deposits in facies RF2 being the more attenuating of the two facies.

The strata below 2 m in the trenches at the Mohave Wash incised alluvium site is markedly better consolidated than the shallower sediments and consist of well consolidated poorly sorted gravel and sand similar to the Bouse Formation encountered in the trenches at the braided channel sites. A ca. 10 cm thick siltstone bed similar to the siltstone marking the top of the Bouse Formation at the Mohave Wash braided channel site was encountered in a trench located near Profile C at the downstream end of the Mohave Wash incised alluvium survey area (Fig. 2-6b). This siltstone is absent in trenches located 20 m upstream. At the Yuma Wash incised alluvium site, the consolidated sediments below 2 m in the trenches contain more angular clasts than the overlying strata and the consolidated strata at the other washes. These strata resemble those in a Miocene fanglomerate that outcrops nearby, and are thus interpreted to be part of the same deposit. At both the Mohave Wash and Yuma Wash incised alluvium sites, the top of the better consolidated strata correlates with horizons EH1 and RH2 in geophysical profiles close to the trenches, and the underlying consolidated strata correlate with electrofacies EF2 and radar facies RF3. The change in AGC radar amplitude and electrical resistivity below horizons RH2/EH1 at both sites is attributed to increased cementation in the older deposits, and does not require a change in water content.

Electrofacies EF1 at the incised alluvium sites encompasses the modern channel deposits and the upper part of the underlying Plio-Pleistocene alluvium. Laboratory calibrated resistivity measurements indicate that moisture content in electrofacies EF1 at the time of the geophysical surveys ranged from 4 to 20% over most of the Yuma Wash site, rising to as much as 39% at the downstream end of the survey. Estimated pore saturation in this facies at the Mohave Wash site ranges from less than 2% to as much as 20% over most of the survey, but exceeds 50% in localized (< 3 m wide) areas. Electrofacies EF2 encompasses partially lithified Miocene fanglomerate at the Yuma Wash site and the upper Bouse Formation at the Mohave Wash site.

Bedrock with Alluvium Channels

The bedrock with alluvium sites at Mohave and Yuma Washes are located in approximately 50 m long straight reaches bounded by meanders upstream and downstream (Fig. 2-8). The channels range from 3 to 18 m wide and are confined by 1 to 2 m high sub-vertical bedrock banks capped with thin colluvium. Profiles at the Yuma Wash site

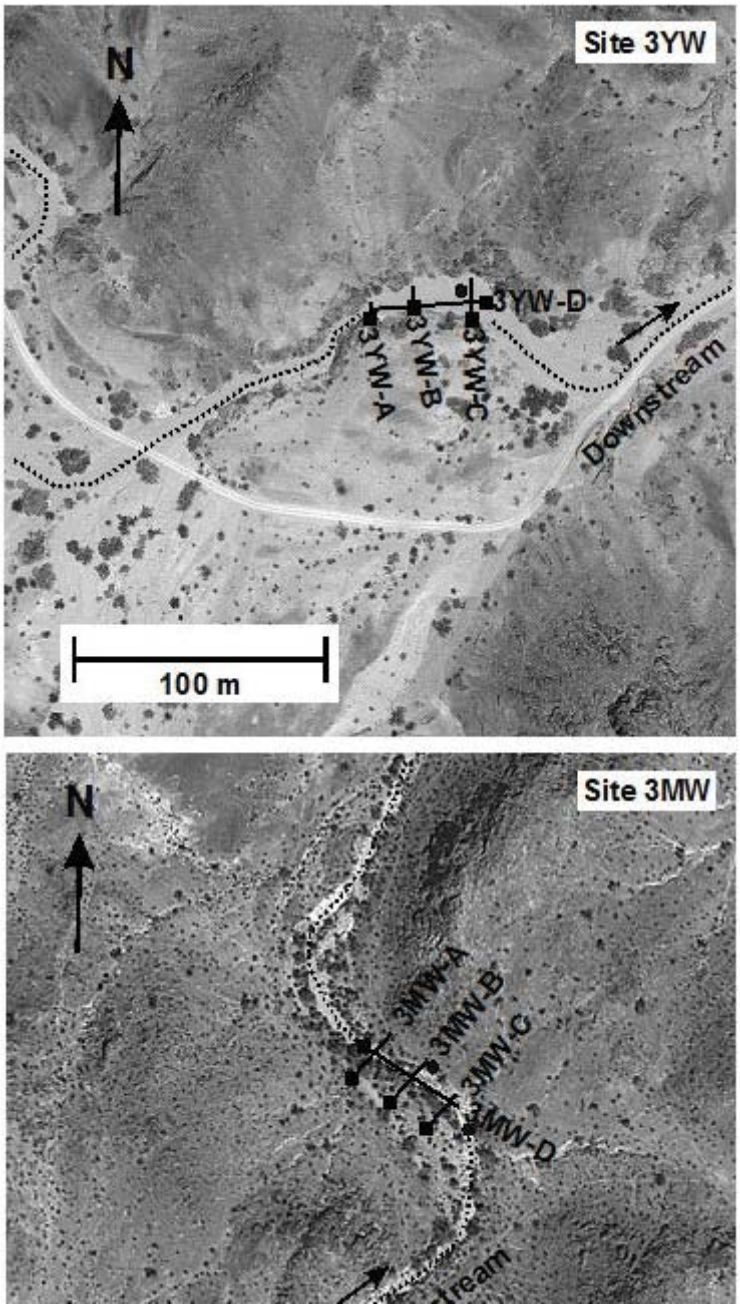

Figure 2-8. Aerial photographs of bedrock with alluvium sites. A) Yuma Wash. B) Mohave Wash. Solid lines indicate GPR and ERT profiles, with squares at the beginning of each profile. Solid circles indicate locations of common midpoint (CMP) radar surveys. Open circles indicate trench locations.

were located immediately downstream of a 4 m wide bedrock constriction, where channel width increased from 10 to 18 m as it enters a meander bend (Fig. 2-8a). The Mohave Wash bedrock with alluvium channel ranges from 3 to 7 m wide, with an abandoned alluvial terrace (< 1.0 m thick) overlying the bedrock along the western channel margin (Fig. 2-8b). Highly fractured rhyolite is exposed along the banks in the upper half of this study reach, whereas colluvium covers the banks in the lower half.

Geophysical Characteristics

The bedrock with alluvium channels have a 0.5-1.1 m thick upper layer, radar facies RF1, similar to but on average slightly thinner than facies RF1 at the incised alluvium and braided channel sites. At the bedrock with alluvium channel sites, RF1 consists of high amplitude relatively high frequency sub-horizontal reflections that span the width of the channels and are continuous downstream for distances of 5 to 10 m (Figs. 2-9 and 2-10). Vertical relief of up to 0.5 m, interpreted as erosional scours on the basis of overlaying infilling and sidelapping stratal relationships, is common on radar horizon RH1, which marks the base of facies RF1. As at the incised alluvium and braided channel sites, horizon RH1 is marked by an abrupt downward decrease in SEC reflection amplitudes and frequency. The vertical relief on RH1 is filled and onlapped by weakly hummocky reflections in the lower half of facies RF1, with the hummocky reflections in turn covered by sheet-like reflection geometries in the upper part of facies RF1. As at the incised alluvium and braided channel sites, facies RF2 is characterized by lower frequency content than facies RF1, less reflection continuity (continuous for distances of less than 3 m), and common downlapping reflection terminations at depths ranging from 0.5-1.0 m (the base of RF1) to 1.7-2.4 m. Facies RF2 at the bedrock with alluvium sites differs markedly from RF2 at the incised alluvium and braided channel sites in that the downlapping patterns can be grouped into coherently dipping reflection packages with internally conformable downlapping, and in the opposite direction toplapping, sets of reflection terminations. These reflections form distinct packages prograding across the width of the channel from either side. At Yuma Wash three stacked prograding packages are recognized (Fig. 2-9). At Mohave Wash, the prograding facies are cut by a series of low angle thrust detachments that verge toward the center of the channel and sole into a common decollement just above horizon RH2 at about 2 m depth (Fig. 2-10). The thrust detachments are recognizable by offset reflection patterns and by weak reflections from the detachment surface. Horizon RH2 has up to 1.5 m of relief. The underlying facies, RF3, is characterized by markedly lower AGC reflection amplitudes and abundant diffractions emanating from within the facies. Weak reflections, such as those observed at the incised alluvium and braided channel sites, are not evident within facies RF2 at either of the bedrock with alluvium sites.

Electrofacies EF1 at the bedrock with alluvium sites extends from the surface to average depths of 1.8 to 2.2 m, encompassing radar facies RF1 and RF2. EF1 is laterally heterogeneous at both sites, with resistivity ranging from 300 to 2500 ohm-m at the Yuma Wash site and 100 to 1500 ohm-m at the Mojave Wash site. No systematic downstream variations in resistivity are observed at either site, but cross-stream heterogeneity is pronounced, with differences of several hundred ohm-m between the GPR reflection packages described above. Electrofacies EF1 encompasses radar horizons RF1 and RF2. Lateral changes in resistivity in EF1 appear to be stratigraphically controlled, with abrupt changes in resistivity occurring between the prograding stratigraphic packages at Yuma Wash and between detachment bounded packages at Mohave Wash. The base of facies EF1 at the Mohave Wash bedrock with alluvium site is approximately 1.8 m deep and is marked by a sharp vertical resistivity gradient that corresponds in most places to the position of radar horizon RH2. Electrofacies EF2 at Mohave Wash has a distinctively lower resistivity than facies EF1 in most places, ranging from 10 to 250 ohm-m (although resistivity greater than 100 ohm-m in facies EF1 is confined mostly to the centers of the channels). At the Yuma Wash bedrock with alluvium site electrohorizon EH1 is poorly developed, and is marked by a gradational downward decrease in resistivity at depths ranging from 2.0 to 3.5 m rather than a sharp resistivity gradient. Electrofacies EF2 at this site has much higher resistivity than at the other sites, ranging from 50 to 500 ohm-m.

In summary, the bedrock with alluvium sites are broadly similar to the incised alluvium and braided channel sites in that all sites have layered radar reflection and resistivity structures. The sheet like reflection geometry of radar facies RF1 is similar at all sites, although thinner at the bedrock with alluvium sites. Radar facies RF2 at the bedrock with alluvium sites is similar to that of the other sites in its lower frequency content, lower continuity, and downlapping reflection terminations. However, at the bedrock with alluvium sites facies RF2 can be grouped into distinct sedimentary packages that prograde across the channel and, at the Mohave Wash site, show evidence of slumping into the channel. Such prograding reflection patterns are absent in facies RF2 at the incised alluvium and braided channel sites. As at the incised alluvium and braided channel sites, radar facies RF1 and RF2 at the bedrock with alluvium sites are indistinguishable on the basis of the electrical resistivity, both laying within low resistivity electrofacies EF1. Resistivity in electrofacies EF1 at the bedrock with alluvium sites is generally higher than at the incised alluvium and braided channel sites, with lateral heterogeneity that correlates with stratigraphic package boundaries and detachment surfaces. Electrohorizon EH1 and electrofacies EF2 differ between the Mohave Wash

Fig. 9

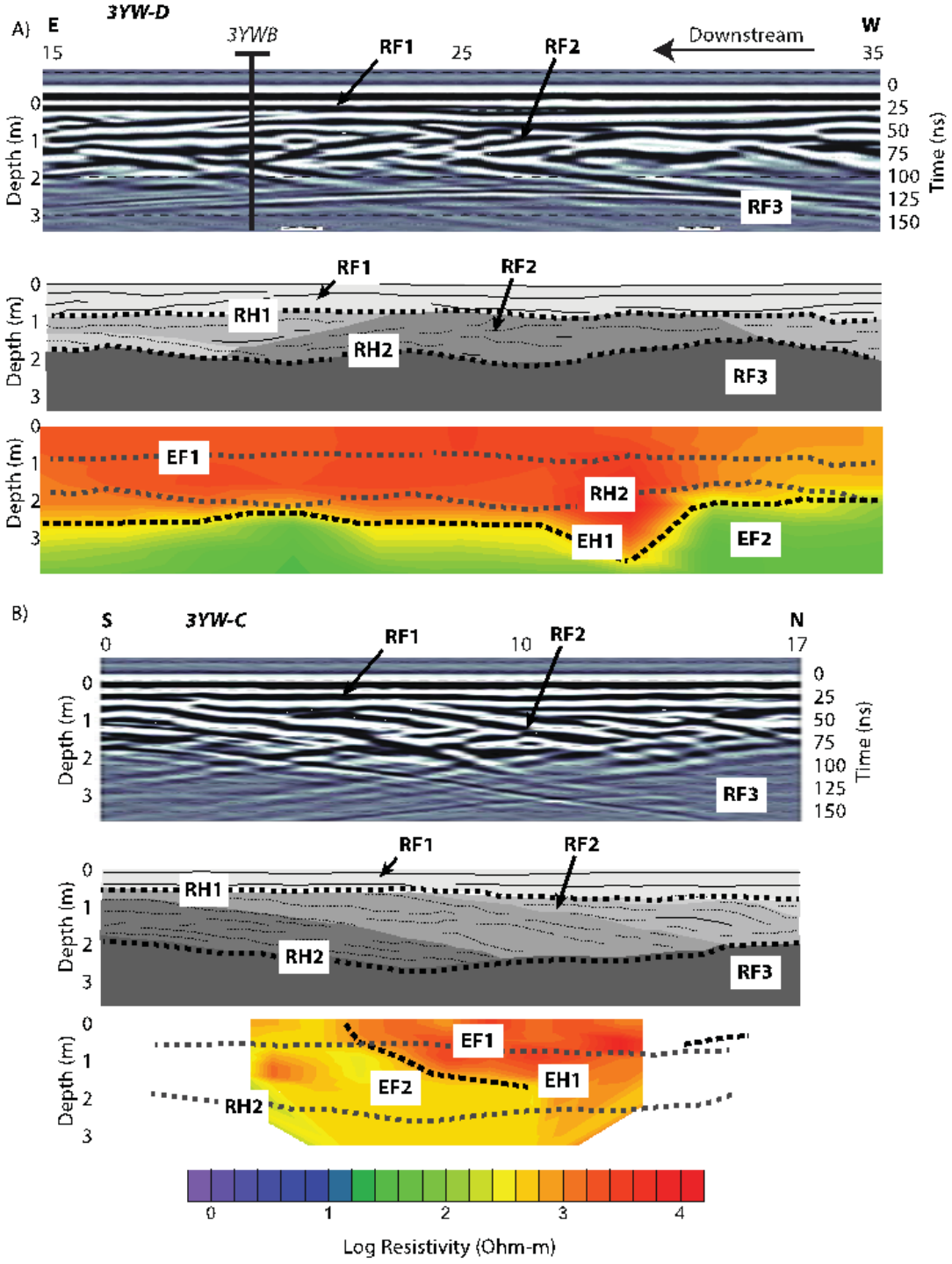

Figure 2-9. GPR and ERT data for representative sections of geophysical profiles at the Yuma Wash bedrock with alluvium sites. A) Longitudinal profile. B) Cross-stream profile. A portion of the AGC GPR profile (top), radar stratigraphy (middle) and ERT profile (bottom) are shown for each section.

Fig. 6

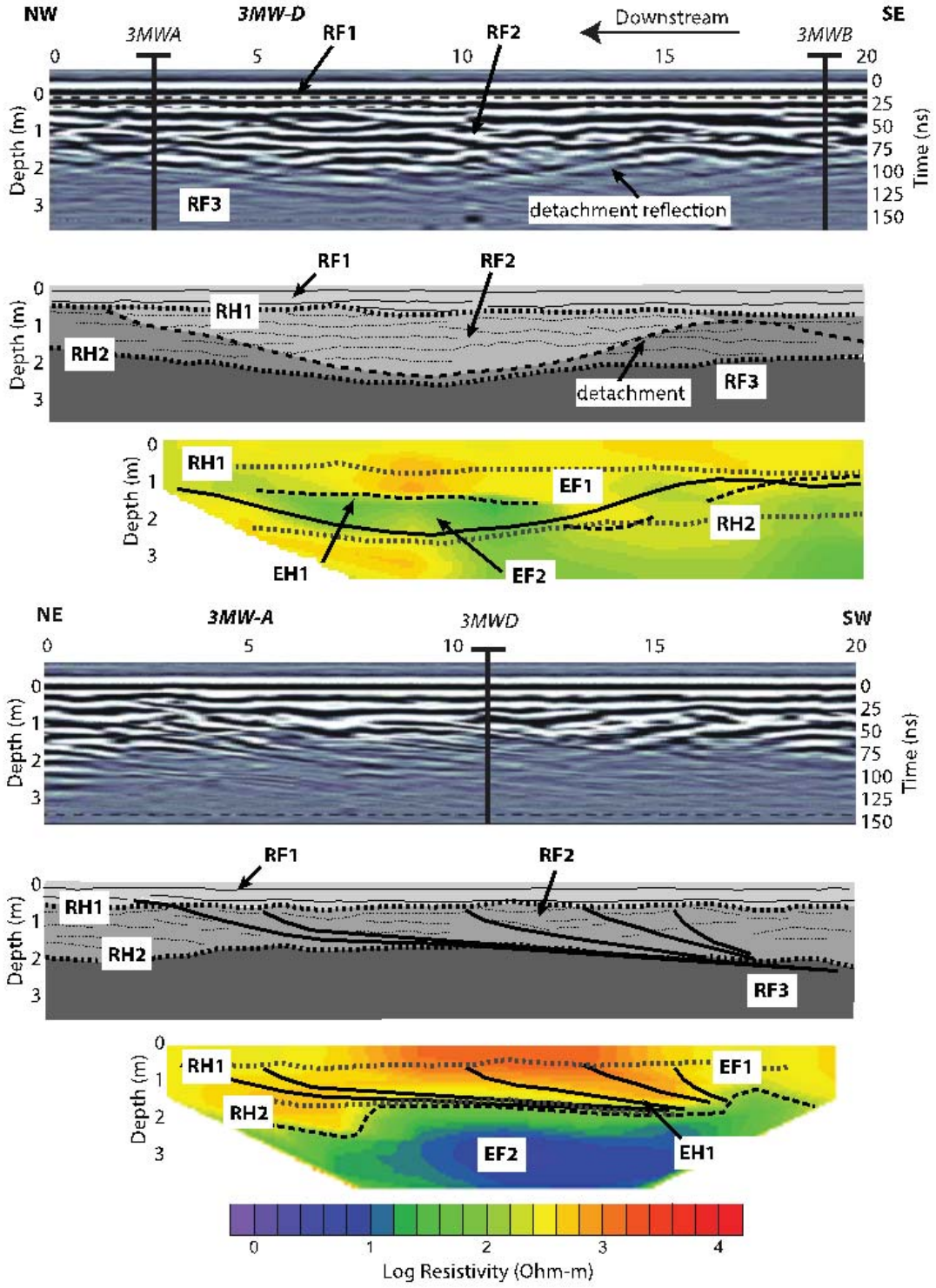

Figure 2-10. GPR and ERT data for representative sections of geophysical profiles at the Mohave Wash bedrock with alluvium sites. A) Longitudinal profile. B) Cross-stream profile. A portion of the AGC GPR profile (top), radar stratigraphy (middle) and ERT profile (bottom) are shown for each section.

and Yuma Wash bedrock with alluvium sites. At the Mohave Wash site, EH1 and EF2 resemble their counterparts at the incised alluvium and braided stream sites, with EH1 being marked by a relatively sharp resistivity gradient and EF2 characterized by a relatively low average resistivity of less than 300 ohm-m. At Yuma Wash, EH1 is marked by a more gradual downward decrease in resistivity, and EF2 has markedly higher resistivity (50-500 ohm-m) than at the other sites.

Moisture Content and Geomorphic and Hydrostratigraphic Interpretation

Radar facies RF1 at the bedrock with alluvium sites, although thinner, is otherwise identical to facies RF1 at the other sites, and is interpreted similarly to be sheet-like modern channel deposits reworked during periodic floods. The overlapping and inclined parallel structures in radar facies RF2 appear to reflect periodic lateral sediment inputs associated with mass wasting events from steep convergent hillslopes along each study reach (Fig. 2-8). Facies RF1 and RF2 have similar electrical resistivity, so horizon RH1 (represented by a loss of SEC reflection amplitude at the interface between RF1 and RF2) is attributed to a lithology change rather than a moisture change. Lateral variations in resistivity within facies RF2 are interpreted to result from minor variations in moisture content, with stratigraphic packaging partitioning moisture on scales of 2-5 m. This is particularly evident in the Yuma Wash downstream profile, where low resistivity in the lower half of facies RF2 manifests a shape similar to that expected by moisture ponding above downwarps in the detachment surface. Laboratory resistivity measurements compared to the ERT data indicate moisture content of the channel fill ranges from 5 to 30% at the Yuma Wash site and 8 to 35% at the Mohave Wash site, with the variation in resistivity occurring primarily between electrically homogeneous depositional packages. The variation in moisture content in facies RF2 at each site is attributed to differences in grain size, sorting, and stratigraphic structure between individual mass-wasting deposits.

Facies RF3 at the bedrock with alluvium sites coincides with electrofacies EF2, but differs from similar radar and electrofacies at the other sites. Relief on the interfaces between facies RF2/EF1 and RF3/EF2 at the bedrock with alluvium sites is much more pronounced than at the incised alluvium and braided channel sites. Strong diffractions emanating from within facies RF3 are common at the bedrock with alluvium sites but are rare and relatively weak at the other sites. Electrofacies EF2 at the bedrock with alluvium sites is more homogeneous and has distinctively lower resistivity than at the incised alluvium and braided channel sites. The resistivity of facies EF2 (10-500 ohm-m) is within the range expected for fractured, wet intermediate to silicic composition igneous rocks [Telford et al., 1990], which confine the channels at both bedrock with alluvium sites. The bedrock outcrop is highly fractured, which is consistent with the presence of abundant radar diffractions in RF3, and has erosional relief similar to that observed on horizons RH2/EH1. For these reasons, facies RF3/EF2 at the incised bedrock with alluvium sites is interpreted to be igneous bedrock, and the abrupt loss of AGC signal is attributed to the lithology change and to the absence of bedding within the bedrock.

Discussion

Implications for Geomorphic and Sedimentological Processes

The active alluvium deposits are generally similar at all of the study sites, suggesting similar modern geomorphic processes shape the channels in braided, incised alluvium, and bedrock with alluvium channel types throughout the study area. The active surficial deposits in all of the streams consist of poorly sorted gravel to cobble with sand matrix that form horizontal to sub-horizontal beds on the 10 cm scale. The bedding is characteristic of plane bed morphologies formed during upper-regime flow conditions [Picard and High, 1973; Simons et al., 1965]. Similar planar deposits are ubiquitous in sandy ephemeral streams in other arid regions experiencing high-energy floods [Frostick and Reid, 1977; Stear, 1985; Tunbridge, 1981]. Consequently, the active alluvium deposits found in the streams studied here are interpreted to be sediments deposited during large episodic floods. Millimeter scale trough cross beds within the horizontally layered strata comprising the active alluvium are interpreted to indicate reworking of surficial sediments by dune and bar migration during the waning stages of major floods, or during smaller flow events. Preservation of these upper-regime sedimentary structures reflects rapid flood recession, which is consistent with stream stage records from 18 reaches in the area (Faulconer et al., in prep). The stream stage records and the prevalence of plane bed morphologies in alluvial channels throughout the study area [Sutfin et al., 2014] indicate that rapid cessation of geomorphically effective discharges is prevalent during flooding in streams throughout the region. This is also consistent with limited surficial evidence of low-flow regime sedimentary structures, which were

observed in the field to occur only in sparse patches of 1 to 5 m^2 area where surficial ripples are superimposed on transverse bars and low dunes, and in low areas between bars where 0.1 to 1 cm thick lenses of fine silt accumulate.

The average thickness of the active alluvium differs between stream types, progressively increasing downstream in the watershed from bedrock with alluvium (highly variable, but averaging 0.6 m thick), to incised alluvium channels (averaging 0.9 m thick), and braided channels (nearly uniform 1 m thick). Similar downstream increases in Holocene alluvial storage occur within streams of the semi-arid Colorado Plateau, both at the multi-century and decadal time scales [Graf, 1987]. We therefore interpret our data to reflect systematic longitudinal variation in the storage of modern alluvium.

The active alluvium in all of the channels surveyed is underlain by sedimentary strata with distinctly different bedding attitudes, which is inferred to indicate different geomorphic processes in the past. At the incised alluvium and braided reaches, the surficial alluvium overlies and in some places inter-fingers with partially consolidated Plio-Pleistocene alluvium. These older strata contain gently dipping beds on scales of meters to tens of meters, with occasional scour and fill structures and multiple bidirectional downlapping and onlapping relationships. The bedding attitude becomes more planar and horizontal upward in the section, and in places beds become conformable with and interfinger with the overlaying active alluvium. The trenches show that the Plio-Pleistocene strata at the braided and incised alluvium channel sites contain low-angle cross bedding that we interpret to be formed by a combination of dune and longitudinal bar migration and lateral channel movement [Miall, 1977; Picard and High, 1973]. Preservation of these lower-regime sedimentary structures, and the greater degree of sediment sorting, suggest that the Plio-Pleistocene depositional environment in braided and incised alluvium sites had a higher ratio of sediment supply to transport capacity than is apparent in modern deposits [Bull, 1991; Melton, 1965]. Relative to late Holocene conditions, the Plio-Pleistocene likely exhibited more attenuated streamflow regimes and higher rates of fine sediment generation from hillslopes [Bull and Schick, 1979; Bull, 1991]. In contrast, the active alluvium at the bedrock with alluvium sites onlaps and overlays dipping strata of unknown age and composition that form distinct stacked stratigraphic packages comprised of internally coherently dipping strata bedded on the 10 cm scale that prograde into and in some areas across the washes. At Mohave Wash, detachment surfaces show evidence of slumping into the channel. The orientation and lobate structure of these older deposits are indicative of lateral sediment inputs from hillslope mass wasting events, which were subsequently buried by the more recent alluvium. These large hillslope sediment pulses likely occurred during the period of widespread colluvial stripping associated with increasing aridity at the Pleistocene-Holocene transition [Bull and Schick, 1979; Bull, 1991].

Consistent differences in the stratigraphic structure of RF2 between the bedrock with alluvium sites and the incised alluvium and braided sites reflect distinctive geomorphic process domains among the two primary ‘lithotopo units’ (sensu [Montgomery, 1999]) within the region: crystalline mountain blocks and lowland alluvial valleys. In the mountainous terrain, lateral sediment inputs from periodic mass wasting events on adjacent hillslopes appear to have produced the distinctive stratigraphic structures beneath the active alluvium of the bedrock with alluvium sites. In the piedmont and alluvial valley settings, longitudinal sediment fluxes dominated Plio-Pleistocene deposition at the incised alluvium and braided reaches, where reduced lateral confinement and lower-gradient adjacent upland surfaces minimized lateral sediment inputs. The distinction between colluvial inputs in montane channels and fluvial inputs in lowland channels that characterizes the Plio-Pleistocene deposits does not occur in the modern alluvium. Instead, the broadly similar stratigraphic structure of surficial alluvial deposits at all sites suggests that landscape-scale topographic effects are attenuated under modern hydroclimatic conditions and sediment supply. In other words, modern fluvial deposition in montane and lowland settings of the study area reflect a greater similarity in geomorphic processes than is apparent in older deposits.

In all of the streams studied, the alluvial sedimentary strata unconformably overlay bedrock, which consists of crystalline igneous basement in the bedrock with alluvium channels and, except for the Yuma Wash incised alluvium site, the Pliocene Bouse Formation in the incised alluvium and braided channels. At the Yuma Wash incised alluvium site, bedrock beneath the channel consists of Miocene fanglomerate that outcrops and the edges of the wash (Tosdal, unpublished map). These unconformities have locally rugged relief of 1 to 3 m over wavelengths of 3 to 10 m, and form the bedrock channel at the bedrock with alluvium stream sites. At the braided channel sites and the Mohave Wash incised alluvium site, the top of the Bouse Formation exhibits similarly rugged vertical relief, forming a surface capped in places by siltstone and in others incised up to 3 meters into underlying sand and gravel

deposits. At the Yuma Wash incised alluvium site the unconformity incises into poorly sorted sand, gravel, and conglomerates of the Miocene fanglomerate. We interpret the unconformities at the bedrock with alluvium, incised alluvium, and braided channel sites to be correlative and to represent a period of low base level during early Pliocene, at which time the primary drainage networks in the area were established [Bull, 1991; Eberly and Stanley, 1978].

Implications for Moisture Regimes and Riparian Ecology

The high (> 250 ohm-m) resistivity in the active alluvium and upper portions of underlying older alluvial deposits (electrofacies EF1) suggests that moisture content in the shallow (< 2 m) subsurface beneath the streams was low (less than 35% in most areas) . The low spatial variation in resistivity values of this facies within and among all sites indicates a rather uniformly low long-term storage capacity in the shallow alluvium throughout the study area. Such low spatial variation in resistivity suggests that shallow subsurface water content is controlled primarily by evapotranspirational demand, rather than variations in substrate infiltration and retention capacities. At the incised alluvium and braided reaches, localized variability on the 1 to 5 m scale in the near surface in resistivity, and by inference moisture content, is likely associated with canopy shading and hydraulic redistribution of moisture by large woody vegetation.

At depths greater than about 2 m, stratigraphic boundaries influence moisture storage, giving rise to a sharp vertical resistivity gradient that separates nearly dry strata from underlying wetter strata that store moisture for periods of a least several months. This conclusion is supported by relatively stable water content below 2 m depth measured over a two year period at the incised alluvium and braided sites (Kampf et al., in prep.). At the bedrock with alluvium sites, the strata underlying the active alluvium show well-developed stratigraphic structures that correlate with the resistivity structure. We interpret this to indicate an increase in moisture storage in the older undated deposits immediately below the active alluvium, with strong local (meter scale) vertical and lateral partitioning of moisture controlled by the stratigraphic boundaries and, in slumps, detachment surfaces. Complex subsurface structural and textural variations in the sediments, as well as irregularities in the underlying bedrock surface, control the storage and redistribution of moisture between hydrologic pulses in these montane streams.

Although our observations were limited to a rainless period during winter, differences in alluvial depth and subsurface structure suggest divergent hydrologic responses among stream types over longer timescales. Because the amplitude of seasonal and annual moisture variation in arid environments decreases with greater sediment depth [McAuliffe, 1994], we expect temporal variability to be highest in bedrock with alluvium reaches, and progressively lower in incised alluvium and braided reaches. The thinner channel fill in bedrock with alluvium reaches would likely approach saturation more frequently, both from winter frontal storms and summer convective storms, whereas upstream transmission losses and greater moisture storage capacity at incised alluvium and braided reaches might limit saturated conditions to infrequent summer floods occurring once every one or two years. During droughts, moisture content in the thinner alluvial profiles of the bedrock with alluvium reaches may be significantly depleted by evapotranspiration, but moisture content within deeper facies of the larger alluvial reaches could remain stable over multiple years. A similar temporal pattern in the frequency and extent of saturated zones as a function of alluvial depth occurs beneath ephemeral streams of the semi-arid Colorado Plateau [Shaw and Cooper, 2008].

These findings provide insights into the ecohydrological mechanisms of plant community organization in ephemeral stream networks of the Lower Colorado River Valley. Strong seasonal variability in moisture content of shallow sediments favors drought deciduous, succulent, and herbaceous species capable of exploiting periodic resource pulses, while the more stable moisture supply in deeper substrate facilitates evergreen species [Gibson, 1996; McAuliffe, 1994; Shmida and Burgess, 1988]. Extreme seasonal resource limitation may also select for functional trait convergence, whereas resource stability provides opportunities for niche partitioning and functional diversification [Mitchell et al., 2008]. In deserts around the world, the stature and longevity of woody plants from a range of functional types increases with sediment depth and access to stable moisture [Mitchell et al., 2008; Shaw and Cooper, 2008; Shmida and Burgess, 1988; Shreve and Wiggins, 1964]. Therefore, we expect bedrock with alluvium reaches to be dominated by drought deciduous shrubs and herbaceous species. Greater spatial heterogeneity in moisture content due to stratigraphic complexity in these channels may also result in patchier vegetation. Incised alluvium and braided reaches would likely exhibit higher potential species and functional diversity, with a greater proportion of trees and evergreen woody plants. Canopy shading and hydraulic

redistribution by large woody vegetation in these lowland streams could also create favorable microsites for diverse herbaceous and understory species. The observed similarity in alluvial structure of incised alluvium and braided sites suggests that vegetation differences between these two stream types may be largely driven by flood disturbance dynamics.

Implications for Climate and Channel Evolution in the Lower Colorado River Valley

Stratigraphic differences between radar facies RF1 and RF2, which form the alluvium underlying the channels beneath all the stream sites, indicate regional temporal hydroclimatic variations. Periods of prolonged valley floor and bajada aggradation followed Pliocene and Pleistocene glacial epochs, when cool and moist conditions promoted extensive chemical weathering of the crystalline mountain blocks [Bull, 1991; Eberly and Stanley, 1978; Melton, 1965]. These aggradational deposits consist primarily of well sorted and cross-bedded gravel in a clayey sand matrix, formed by persistent streamflow capable of greater sediment sorting than occurs in more recent deposits [Bull, 1991]. Preservation of these structures indicates gradual flood recession or sustained baseflow [Frostick and Reid, 1977; Miall, 1977; Simons et al., 1965], suggesting that intermittent or perennial streamflow regimes prevailed among tributaries in the Lower Colorado River Valley following the Pleistocene stadials. In contrast, mid- to late-Holocene alluvium consists of coarser and poorly sorted sediments exhibiting greater downstream fining, reflecting episodic transport associated with flashier ephemeral streamflow [Bull, 1991].

Since the Pinedale stadial, climate-mediated changes in sediment supply and base level fluctuations have caused channel incision throughout the Lower Colorado River Valley [Bull, 1991; Eberly and Stanley, 1978; Melton, 1965]. Increasing aridity and vegetation contraction initiated widespread stripping of colluvium, resulting in depositional pulses preserved as inset channel terraces between 11 and 6 ka [Bull and Schick, 1979]{Bull, 1991 #2249}. The reduced caliber and volume of sediment generated from exposed bedrock since the mid-Holocene has led to a lowered critical stream power threshold, promoting bed material export and channel degradation [Bull and Schick, 1979; Bull, 1991; Clapp et al., 2000; Melton, 1965]. Quaternary incision of the Colorado River lowered the regional base level by approximately 100 m, but climatic influences on sediment production have caused significant lags in tributary adjustment [Anders et al., 2005; Bull, 1991].

Summary

All of the sites surveyed contain two distinct lithostratigraphic facies that are distinguished on the basis of GPR reflection wavelengths, continuity, dip, and amplitude. The upper facies, RF1, contains reflectors with sheet-like geometries that span the width of the drainage and extend downstream for the length of the survey profiles (30-300 m). This facies is interpreted to be active channel plane bed deposits that are re-worked during floods. The underlying facies, RF2, is characterized by less continuous bi-directional dipping reflection patterns with abundant downlap and onlap patterns are indicative of rapid aggradation, channel incision and infilling, and cross stream sediment transport that is typical of a lower energy depositional environment. Because the distinction between the two lithofacies persists across both the Mohave and Yuma Wash drainages and between channel sizes, it seems most likely that the change between depositional processes in facies RF2 and RF1 is associated with regional climatic changes. Lack of geochronological data to constrain the age of facies RF2 prevents assessment of the timing of this climate change.

The spatial distribution of water content and controlling processes are found here to vary substantially with stream type, watershed size, and landscape position. In the smaller bedrock with alluvium streams, water content is influenced by stratigraphic architecture, with the surficial ebb-flood deposits retaining little moisture (< 35%). Deeper colluvial deposits in these montane washes show increased water storage capacity, with stratal dip and fault surfaces apparently controlling the distribution of subsurface moisture. Faults at the base of slumps appear to play a major role, acting as barriers to moisture transport and sequestering moisture in the footwall of stacked thrust sheets at shallow depths (< 1.5 m) and in synclinal folds above faults at greater depths (>2.5 m). The influence of stratigraphic architecture on subsurface moisture retention and transport diminishes with increasing draining size, as streams traverse alluvial valleys. At the incised alluvium stream sites, a sharp increase in water content occurs at the stratigraphic interface between facies RF2 and RF3, and is likely the cause of the rapid decrease in radar reflection amplitudes. Lobate regions of anomalously low moisture content dip in directions conformable with the stratal dip, suggesting that moisture transport occurs parallel to stratal interfaces and strata boundaries act as boundaries for

moisture transport. At the braided stream sites, there is no strong relationship between stratal dips and moisture distribution, and the alluvium is generally drier at all depths images (< 3.5 m) than at the smaller streams.

Chapter 3. Thresholds for Runoff Generation in Ephemeral Streams with Varying Morphology In The Sonoran Desert In Arizona, USA

Abstract

In ephemeral streams, infrequent surface flow can be the main source of moisture that sustains plants throughout long dry periods. The objectives of this research are to determine (1) whether or not runoff occurrence in ephemeral channels can be predicted by a rain threshold, and (2) identify the rain intensity thresholds that cause runoff in different ephemeral stream types. Two watersheds on the Yuma Proving Grounds (YPG) in the Sonoran Desert near Yuma, Arizona were instrumented with eight tipping bucket rain gauges to monitor precipitation. To measure runoff, 18 pressure transducers were placed in the channel beds of five different channel types with contributing areas ranging from 0.002 km^2 to 225 km^2. Precipitation event intensities and magnitudes were compared to the record of runoff events to determine possible thresholds in rainfall intensity and depth for runoff generation in the different channel types. Over approximately two years of data collection, between 11-48 rain events were recorded at the rain gauge sites. Stream types with bedrock channels and small watershed areas between 0.005 km^2 and 0.015 km^2 produced runoff during rain events where the peak 60-minute precipitation intensities (I60) exceeded precipitation thresholds between 4-6 mm hr^{-1}. Of the precipitation events recorded at these sites, 17-25 percent of the events produced flow. Tributary streams formed on mid-Pleistocene piedmont surfaces covered by desert pavement with contributing areas of 0.021-0.061 km^2 produced runoff when rain events had values of I60 exceeding 5-9 mm hr^{-1}. Flow was produced during 31-36 percent of rain events at these sites. Streams incised into bedrock with some alluvium fill produced runoff when the I60 during a rain event was greater than 13-18 mm hr^{-1}. Contributing areas for these sites were 0.8 km^2 to 2.2 km^2, and up to 10 percent of precipitation events at these sites produced flow. Precipitation thresholds for runoff generation in streams with contributing areas >3 km^2 were not clearly defined due to the influences of variable precipitation in upstream tributaries and transmission losses of streamflow through channel bed alluvium. Rain intensity thresholds increase with the log of catchment area for watersheds with <3km^2, and as a result flow frequency is greatest in channels with small catchment areas.

Introduction

Arid and semi-arid regions make up 41% of the earth's land area, and in 2005 more than 2 billion people out of the 6.5 billion world human inhabitants lived in these regions (Millennium Ecosystem Assessment 2005). Climate change is increasing the amount of area classified as arid, and anthropogenic land use continues to degrade lands and increase areas of desertification. The majority of biodiversity in arid regions is found in the riparian regions (Shaw and Cooper, 2008; Levick, 2008) since inter-channel arid soils have limited moisture from precipitation and often low infiltration values (Hogan et al. 2004).

Runoff in ephemeral stream channels is typically caused by high intensity precipitation that produces infiltration excess overland flow on the inter-channel soils and bedrock. Channel transmission losses can be substantial in ephemeral streams, and some studies report that these losses increase with increased catchment area due to transmission losses through the channel network (Simanton and Osborn, 1983; Goodrich et al., 1997). These losses along the channel make it difficult to predict when and where ephemeral channels will flow, and a better understanding is needed of how runoff occurrence relates to varying channel morphology and contributing area size.

In ephemeral streams, infrequent surface flow can be the main source of water that sustains plants throughout long dry periods, so an understanding of the runoff processes and precipitation characteristics that lead to flow is important to understanding these ecosystems. Prior research suggests that runoff generation in arid ephemeral streams is a threshold-like process, with runoff occurring only during storms above a threshold precipitation intensity (Kidron and Pick, 2000; Yair and Lavee, 1985). This research aims to: (1) explore seasonality of rainfall runoff in different channel types; (2) examine how runoff thresholds vary by channel type. Understanding the runoff-producing rainfall thresholds will allow researchers to better understand how changes in precipitation will affect runoff, and the water contributed by flow events to the ecosystem of arid environments.

Background

Storms that produce runoff in arid regions are usually highly localized, short duration, high intensity convective storms (Osborn, 1964). The scarcity of rainfall and limited rainfall depth in short storms generally preclude subsurface flow and the development of saturated areas, so saturation overland flow is not common in arid regions (Yair and Lavee, 1985). High rainfall intensity leads to more runoff generation through infiltration excess overland flow (Wilcox et al., 1997), and as a result prior research has found that precipitation intensity is more correlated with runoff production than precipitation depth or duration for runoff production in arid regions (Osborn, 1964; Osborn and Lane 1969; Simanton and Osborn, 1983; Yair and Lavee, 1985; Syed et al., 2003). Convective storms with high intensity precipitation have high spatial variability, and the location of the storm core within a watershed affects the amount of runoff production (Syed et al., 2003).

Development of infiltration excess overland flow on desert land surfaces also relates to the land cover types such as bedrock and desert pavement that have low permeability (Springer, 1958; Yair and Lavee, 1985). In the inter-channel areas of the western United States, desert pavement is widely distributed (Turk and Graham, 2011). Desert pavement consists of a one or two-particle thick layer of closely packed, angular to sub-rounded, darkly varnished cobble surface overlaying a horizon layer of eolian fines a few centimeters deep with low permeability (Springer, 1958; McFadden et al., 1987). In the Sonoran Desert this horizon has been reported to have a very low infiltration rate of less than 1 cm hr^{-1} (McDonald et al., 2004). This horizon can be a critical regulator of infiltration (Springer, 1958; Turk and Graham, 2011; Young et al., 2004).

In contrast to the bedrock and desert pavement surfaces, ephemeral stream channels are composed of unconsolidated alluvium with high permeability (Yair and Lavee, 1985). Once runoff reaches the channel network, transmission losses of surface flow to the underlying alluvium are common. Transmission loss in ephemeral channels can reduce the flow volume and peak discharge downstream (Osborn and Lane, 1969; Simanton and Osborn, 1983; Yair and Lavee, 1985). Osborn and Lane (1969) reported that runoff from small watersheds is much greater per unit area than runoff from larger complex watersheds. This is the result of larger watersheds having more channel transmission losses due to the greater channel area, particularly in downstream reaches (Simanton and Osborn, 1983; Goodrich et al., 1997). Spatial and temporal connectivity of the drainage network is rare except in the most extreme runoff events (Jaeger and Olden, 2012) because of both partial area storm coverage and transmission losses (Goodrich et al., 1997). Flow discontinuity increases in large watersheds due to increased channel widths and depth of alluvium (Yair and Lavee, 1985). Convective cells can move 100 times greater than flow velocities, thus preventing runoff generation from occurring simultaneously over the entire area covered by rain (Yair and Lavee, 1985).

Because of the short duration of runoff-producing convective storms, Osborn (1964) concluded that durations of 15, 30, and 60 minutes are needed when comparing rain to runoff. On average 66% of a convective storm's rain falls in the first 15 minutes, 90% in 30 minutes, and 100% in an hour. Other studies have identified 5-minute (Schreiber and Kincaid, 1967) and 15-minute rainfall intensities (Osborn and Lane, 1969) to be the dominant variables for determining runoff volume and peak flow. Ranges of runoff-producing rainfall thresholds have been identified in prior studies in arid and semi-arid environments. Yair and Lavee (1985) determined that rain intensities of 9 mm hr^{-1} produced runoff in 45 minutes and 12 mm hr^{-1} produced runoff in 30 minutes. Goodrich et al. (1997) and Syed et al. (2003) used 10-minute intensities of greater than 25 mm hr^{-1} as their designation of a storm core because they determined that it was a conservative estimate for producing runoff. This study expands on these prior studies by examining how precipitation thresholds for runoff generation are affected by stream morphology and contributing area size.

Study area

The study location is in the Northern Sonoran Desert on the United States Army Yuma Proving Grounds (YPG) in the southwest corner of Arizona in the Southwest United States (Figure 3-1). This region of the Sonoran Desert has a mean aridity index of 0.047, which makes it hyper-arid (Howe 2013). YPG's mean annual precipitation from 1958-2010 was 90 mm (Western Regional Climate Center, 2013), and this precipitation falls primarily during two seasons. During the winter months of November to March frontal systems from the Pacific Ocean bring low intensity, long duration rains that cover a large area (Hallack-Alegria and Watkins, 2007). During the summer

months of July to September, the North American monsoon (NAM) causes short duration, high intensity convective thunderstorms covering no more than a few tens of square kilometers (Hallack-Alegria and Watkins, 2007). Pacific Ocean tropical storms can also bring rain during the summer.

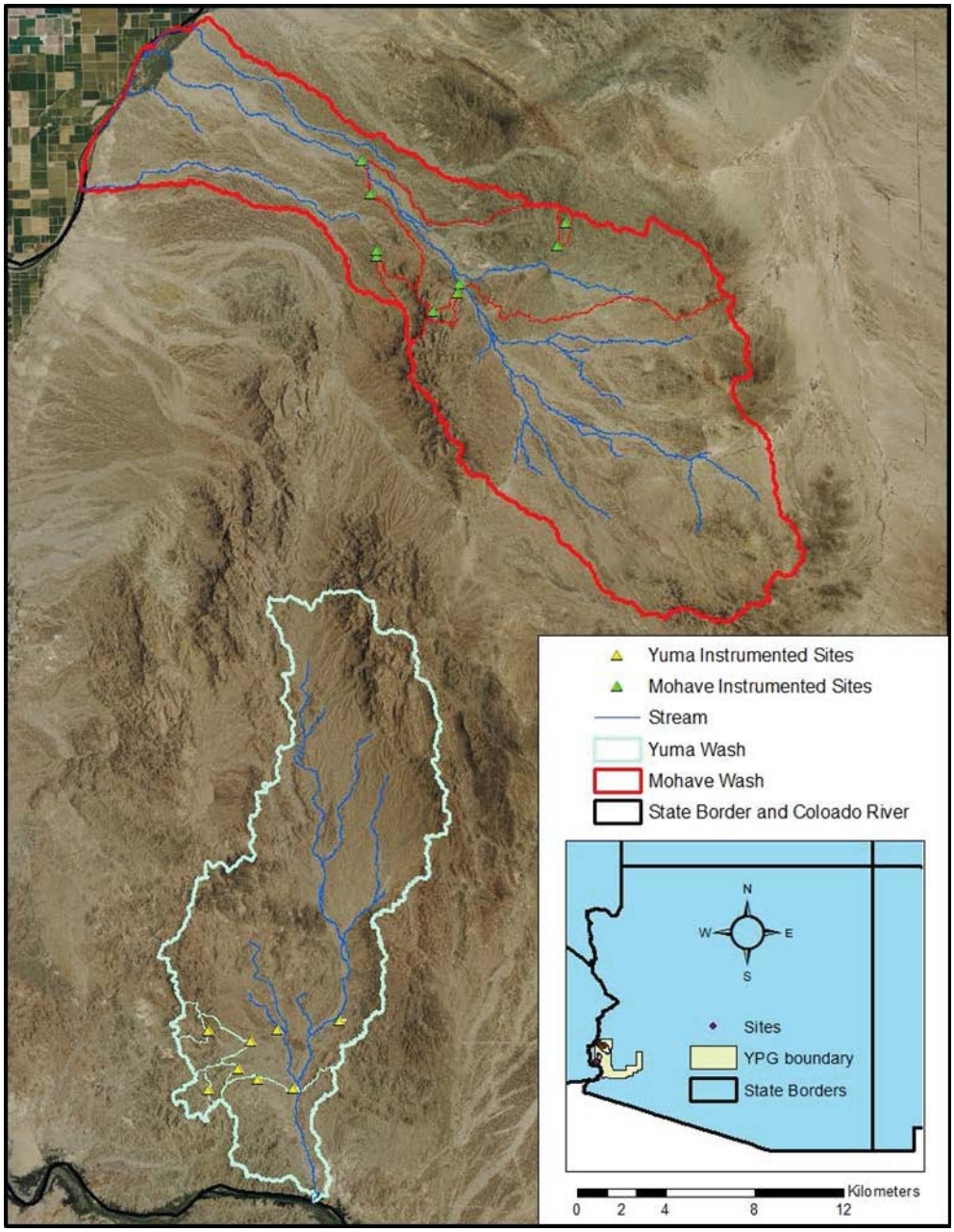

Figure 3-1. Map of study area with the outline of the two study watersheds and locations of instrumented sites.

The two study watersheds are Yuma Wash and Mohave Wash (Figure 3-1), which drain into the Colorado River. Yuma Wash drains to the south, and Mohave Wash drains to the northwest. Yuma Wash is 28 km long and has a drainage area of 188 km^2. Mohave Wash is 37 km long with a total drainage area of 323 km^2. Bedrock in the study area is mostly intrusive and extrusive igneous with some marine layers. Most of the bedrock in Yuma Wash is rhyolite (47% of total watershed area), with 12% sandstone 7% granite, and 4% amphibolite. The remaining 30% of the area is covered by alluvium, determined by a geology map from the Arizona Geological Survey (AGS) (2000). In Mohave Wash rhyolite covers only 20% of the watershed area; granite and sandstone cover 10% and 2% of the watershed area, respectively, and the remaining 68% is alluvium. Bedrock is exposed mainly in the jagged

mountains of the study watersheds, with the lowland valleys filled with alluvium. Gently sloping Pleistocene alluvial fans covered in desert pavement fill in most of the areas between the exposed bedrock and lowland alluvium. These areas are termed piedmont surfaces in this study.

Desert pavement areas have limited vegetation, with the exception of creosote bush and cactus, including ocotillo, *Carnegiea* (saguaro), and *Opuntia* (cholla). Vegetation is more abundant and diverse in the riparian zone, with species types including *Cercidium* spp. (palo verde), *Olneya tesota* (iron wood), *Prosopis* spp. (mesquite), *Lerraea tridentada* (creosote bush), *Ambrosia dumosa* (white bursage), *Pleuraphis rigida* (big galleta grass), *Fouquieria splendens* (ocotillo), and *Krameria grayi* (white ratany), with most of the biomass as ironwood, palo verde, and creosote bush (McDonald et al., 2004; Sutfin, 2014).

Stream classification

The geomorphic stream classification presented in Sutfin et al. (2014) was used in this research to select instrumentation sites. The stream classification divides the fluvial system into five morphologically distinct stream types: Piedmont Headwater, Bedrock, Bedrock with Alluvium, Incised Alluvium, and Braided (Table 3-1). The channel types represent a downstream progression from the headwaters in the mountains and piedmont surfaces to the valley bottoms. Piedmont surfaces are mid-Pleistocene alluvial fans and other old, near mountain, depositional surfaces that are stable and have formed desert pavement. The upper piedmont is the area at the base of the present day mountains. Headwater channels have incised into either bedrock or piedmont surfaces. Further downstream, stream channels have gravel- to cobble-sized material in the channel beds, and these channels have incised into the sand to cobble-sized Pleistocene alluvium in valley bottoms of the study area. The width and depth of alluvium in the channel beds tends to increase downstream. All of the channel types are ephemeral, with flow only after rain events.

Sites

In Table 3-2, stream stage sites monitored in this study are grouped by channel geomorphic type following Sutfin et al. (2014) with the exception of MIA1, which was grouped with the Braided channels. Although MIA1 is a single threaded Incised Alluvium channel at the study reach, it has a braided reach upstream, and its basin area size is closer to the Braided channel types. The M or Y preceding the channel type abbreviation from Table 3-2 indicates if the site is located in Mohave Wash (M) or Yuma Wash (Y). Section 4.2 describes the methods for determining contributing areas and channel lengths for each site listed in Table 3-2. Piedmont Headwater (PH) channel types have the smallest contributing areas and shortest stream lengths. PH sites have contributing areas ranging from 0.002 km^2 to 0.049 km^2 and contributing stream lengths ranging from 0.01 km to 1.16 km (Table 3-2). Bedrock (BK) channel sites have the next smallest contributing areas and stream lengths, with overlapping size ranges with the PH sites, with contributing area sizes ranging from 0.005 km^2 to 0.093 km^2, and stream length sizes ranging from 0.04 km to 1.62 km. Bedrock with Alluvium (BA) sites have contributing areas ranging from 0.8 km^2 to 2.2 km^2 and stream lengths of 16.3 km to 35.6 km. The contributing area range for the Incised Alluvium (IA) sites is 3.0 km^2 to 5.7 km^2, and the stream length range is 60.3 km to 99.8 km. The Braided (BD) channels, including MIA1, range from 170 km^2 to 225 km^2, with stream lengths from 3079 km to 4211 km.

Table 3-1. Channel types, locations, descriptions, and corresponding abbreviations for each study watershed defined by Sutfin (2013).

Channel Type	Location	Description	Abbreviation
Piedmont Headwaters	Piedmont	Small channels incised into the desert pavement. Confined by unconsolidated alluvium.	PH
Bedrock	Headwaters in the mountains	Cut into exposed bedrock. Void of persistent alluvium.	BK
Bedrock with Alluvium	Upper piedmont	Partially confined by bedrock. Enough persistent alluvium to create bedforms.	BA
Incised Alluvium	Piedmont	Incised into the piedmont's unconsolidated alluvial material.	IA
Braided	Alluvial basins between mountain ranges	Large, multithreaded channels.	BD

Table 3-2. Stream stage measurement sites with contributing area, stream length, channel width, and site elevation. If the site is in Yuma Wash the channel type abbreviation is preceded by a Y and is preceded by an M if the site is in Mohave Wash.

Site	Area (km^2)	Stream Length (km)	Channel Width (m)	Site elevation (m)
Piedmont Headwaters				
YPH1	0.021	0.37	1.9	156
YPH2	0.002	0.01	1.4	154
MPH1	0.061	1.16	no data	226
MPH2	0.049	1.02	3.0	242
Bedrock				
YBK1	0.005	0.04	no data	225
YBK2	0.013	0.32	1.7	166
MBK1	0.093	1.62	2.9	464
MBK2	0.015	0.40	1.4	384
Bedrock with Alluvium				
YBA1	2.2	35.6	10.1	211
YBA2	1.7	30.9	7.7	207
MBA1	0.9	18.4	7.1	279
MBA2	0.8	16.3	4.1	328
Incised Alluvium				
YIA1	3.6	60.3	21.9	176
YIA2	5.7	99.8	22.8	162
MIA2	3.0	63.6	9.7	249
Braided				
MIA1	170	3190	38.7	270
YBD1	170	3079	124.1	116
MBD1	225	4211	113.8	201

Figures 3-3 to 3-6 show examples of the different types of channels and contributing areas. Piedmont Headwater and Bedrock channels are narrow, between 1.4 m to 3 m, and have little to no alluvium within channels (Table 3-2, Figures 3-3, 3-4). Most of the vegetation on the piedmont grows in Piedmont Headwater channels, where the desert pavement is eroded exposing the Pleistocene alluvium. Bedrock with alluvium channels are typically wider (4 m to 10 m) with alluvium filling the base of the channel from bank to bank (Figures 3-4). Incised Alluvium channels are wider (10 m to 23 m) with vegetation typically near or on the banks, and they may have some vegetation within the channel (Figures 3-5, 3-6). YIA1 has a piedmont headwater channel contributing directly upstream and on the same side of the IA channel as the YIA1 pressure transducer (Figure 3-6). Braided channels are multi-threaded channels that span widths up to 124 m, with vegetation growing between active channel threads (Figure 3-2).

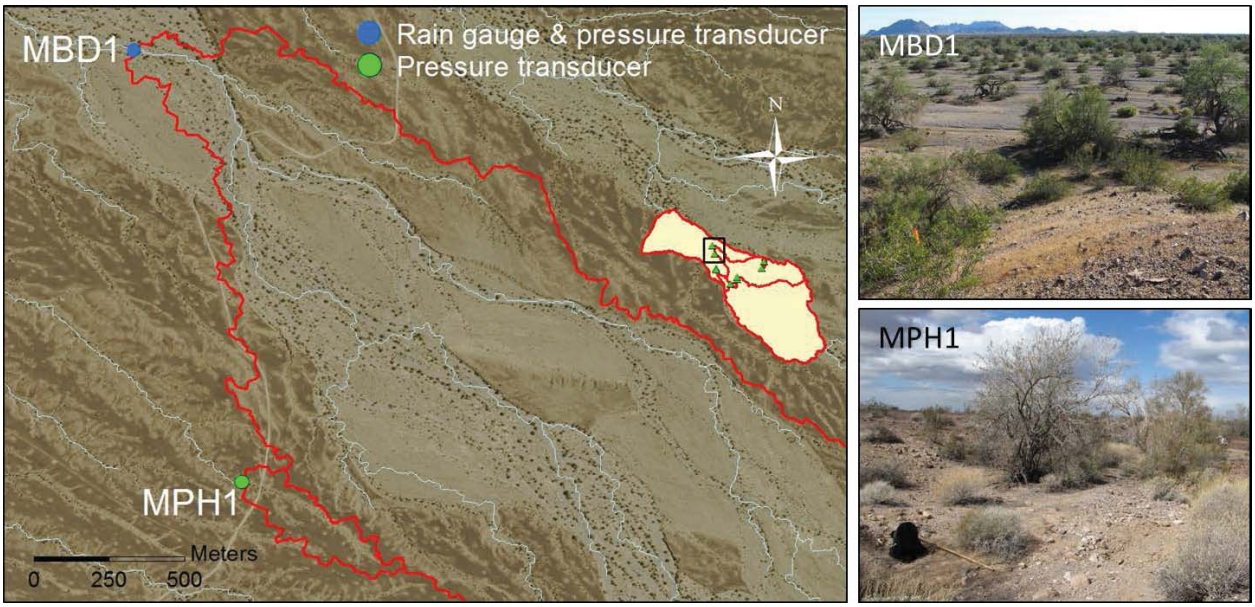

Figure 3-2. Site location, contributing area boundaries, and photographs for MBD1 and MPH1.

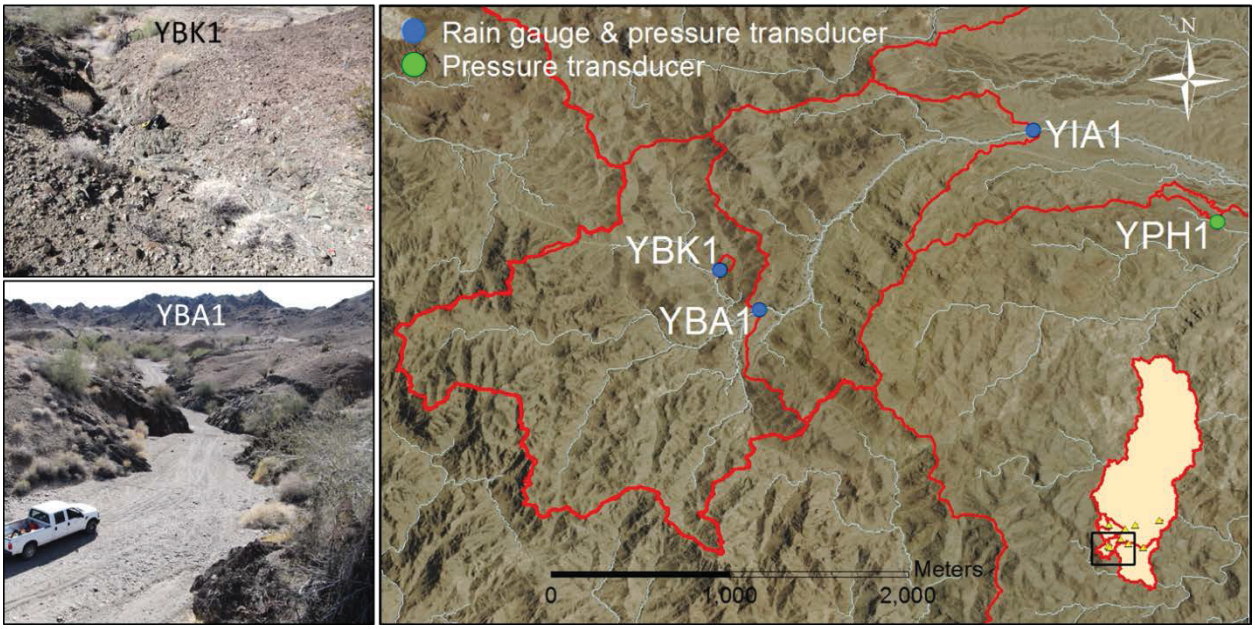

Figure 3-3. Site location and contributing area boundaries for YPH1, YBK1, YBA1, and YIA1. Photographs of YBK1 and YBA1.

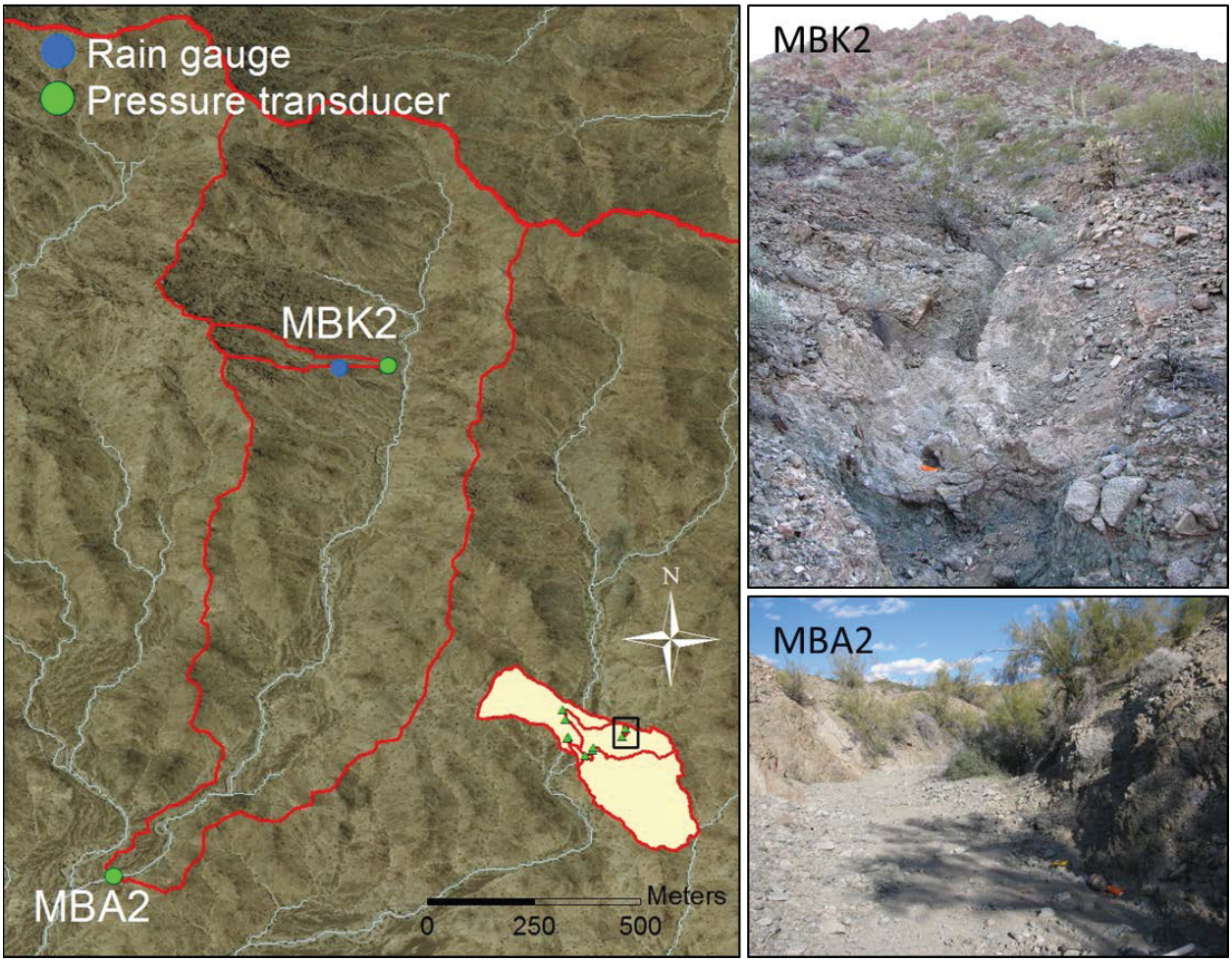

Figure 3-4. Site location, contributing area boundaries, and photos for MBK2 and MBA2.

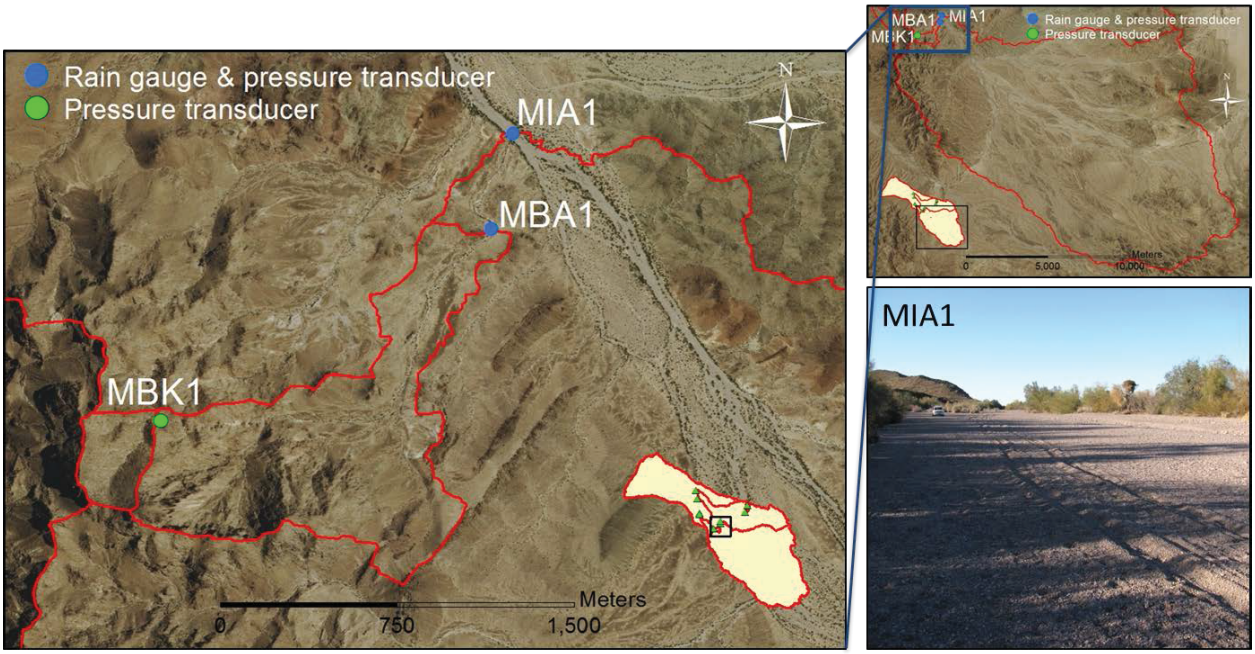

Figure 3-5. Site location and contributing area boundaries for MBK1, MBA1, and MIA1. Photo of MIA1.

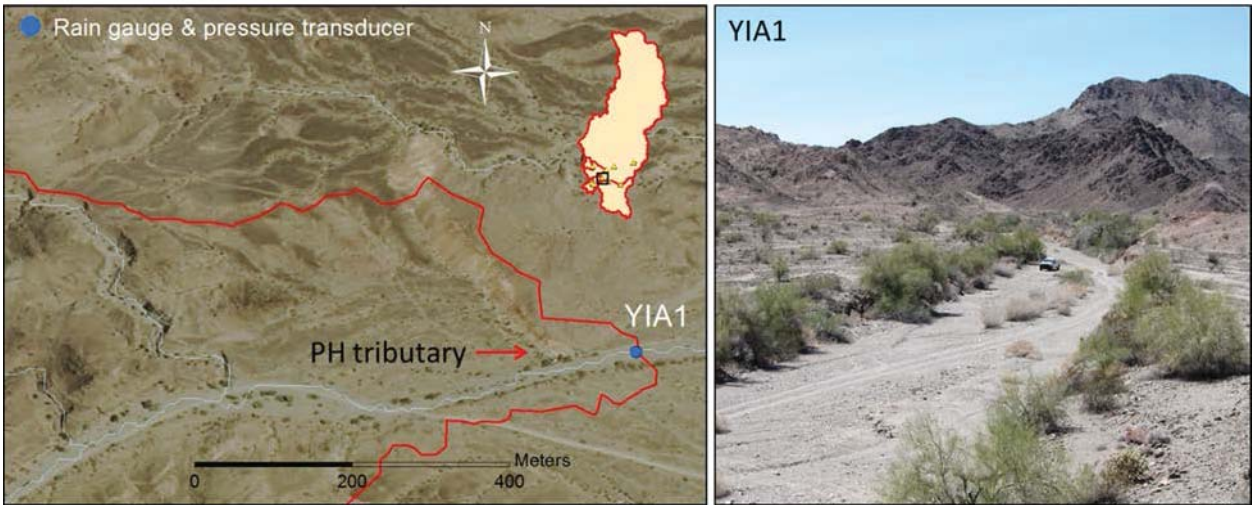

Figure 3-6. Site location and picture of YIA1. Upstream PH tributary shown on map.

Methods

Data collection

To examine precipitation thresholds for runoff generation in channels with different morphologies, a network of precipitation and stream stage measurements was installed in the two watersheds (Figure 3-7). Each watershed has four rain gauges and nine pressure transducers for monitoring stream stage. Precipitation was monitored with either RG3-M tipping-bucket rain gauges, which measured 0.2 mm per tip, and recorded with Onset HOBO Pendant Event loggers (Figure 3-8.A) or TE525 and TB4 tipping bucket rain gauges that measured 0.254 mm per tip and logged by Campbell dataloggers. At sites with Campbell dataloggers other measurements were recorded, including subsurface water content. In-Situ Inc. Rugged TROLL 100 pressure transducers were installed in channel beds at two locations for each type of channel in both watersheds, except braided (BD) channels, which only have pressure transducers in one location per watershed. Braided channels only had one monitoring location because each watershed has only one main stem braided channel. Flow depths were also difficult to measure in these channel types since they are wide multi-thread channels where flow events do not consistently pass through the same section of channel. The pressure transducers at each site were placed inside vented PVC pipe for protection and bolted into bedrock or trees to keep them in place during flow events (Figure 3-8.B). The Rugged TROLL 100 pressure transducers must be used in conjunction with a barometric pressure logger (barologger) in order to subtract out the barometric fluctuations from the water level changes. An In-Situ Inc. Rugged BaroTROLL was placed at the braided site in both watersheds. Point values were continuously logged in 15-minute time steps.

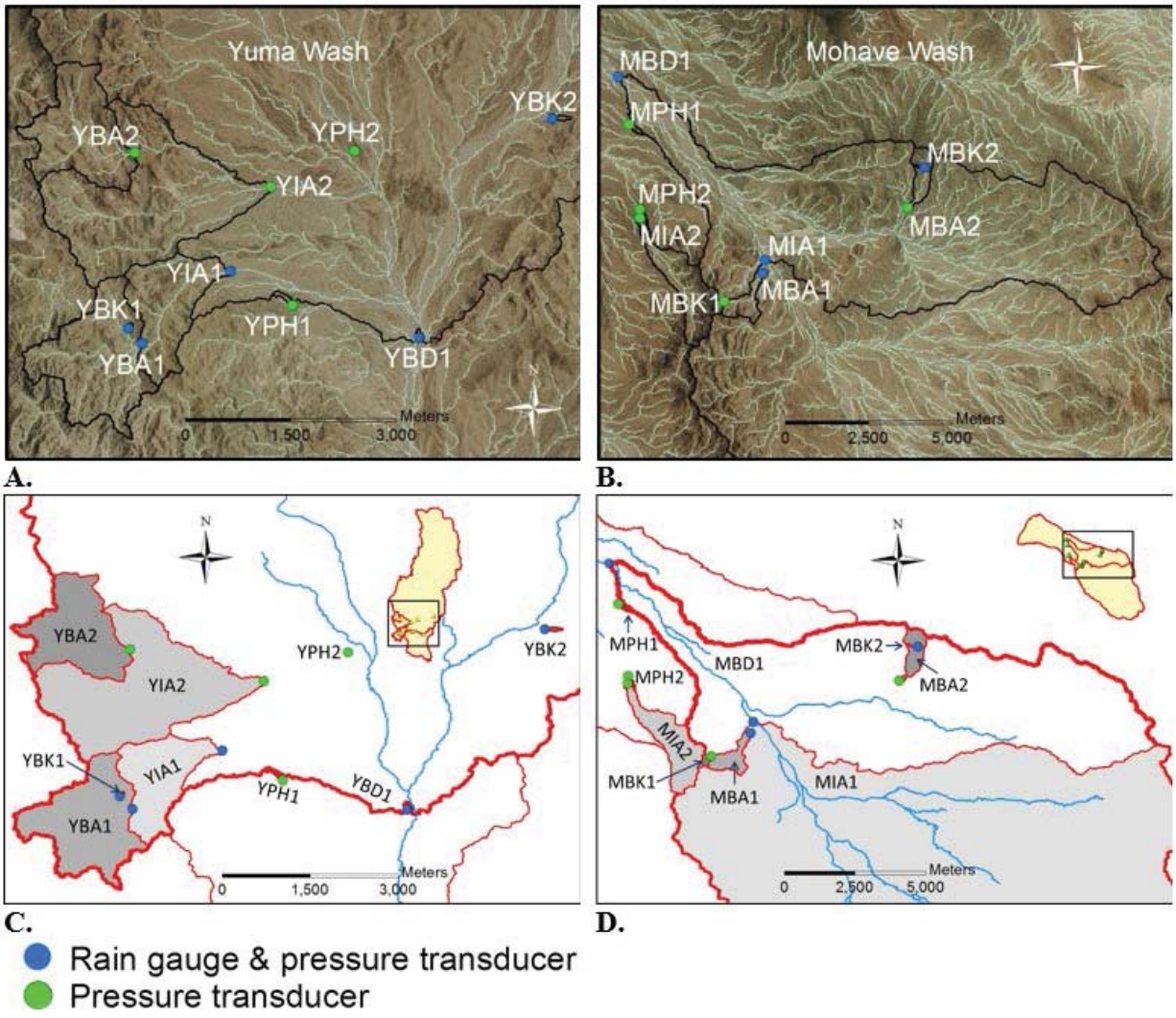

Figure 3-7. Yuma Wash (A and C) and Mohave Wash (B and D) instrument locations. Images A and B are ortho-photographs with black contributing area boundary lines and the names of the instrumented locations. Maps B and D show the contributing areas shaded in grey scale with the site names within each contributing area above a pressure transducer monitoring site. Blue dots are sites with rain gauges and pressure transducers. Green dots are sites with just pressure transducers.

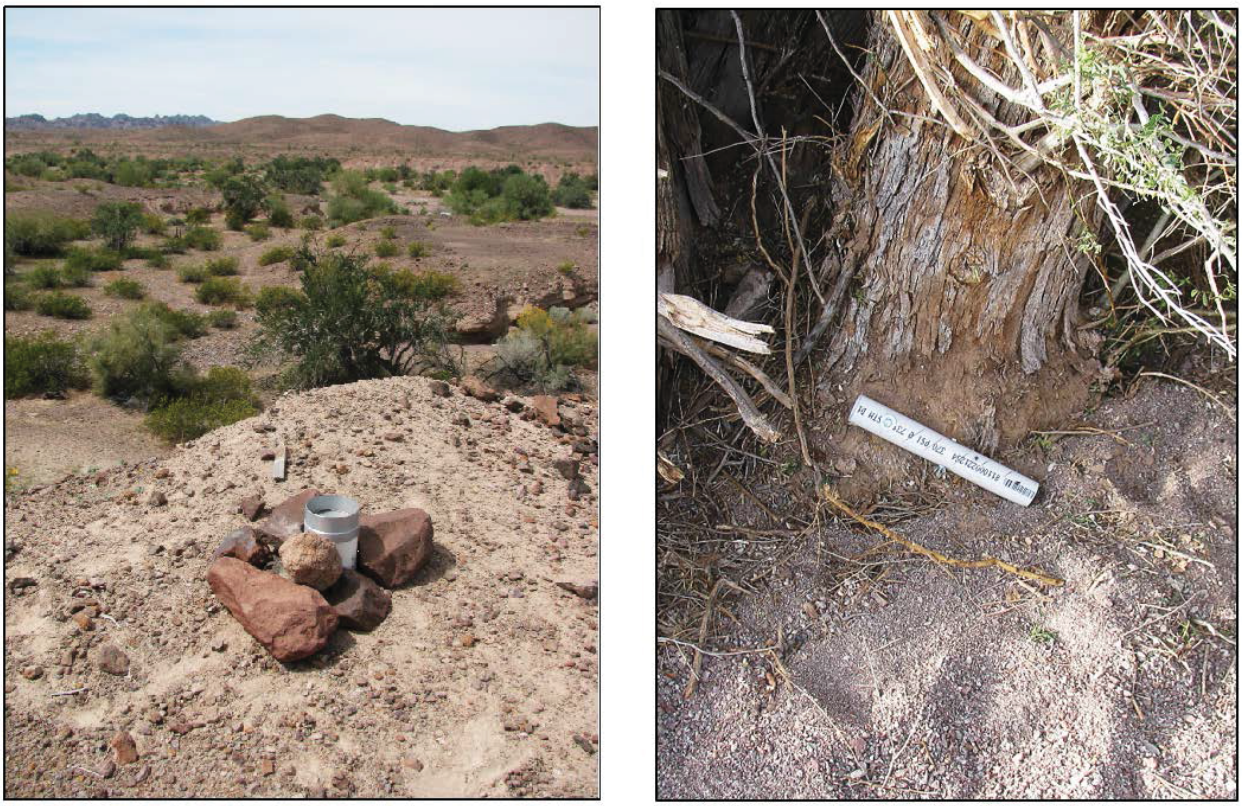

Figure 3-8. Photographs of (A) the RG3-M stand-alone tipping bucket rain gauge with Onset HOBO Pendent Event logger at YBK2 and (B) pressure transducer inside PVC pipe anchored to an Ironwood at YIA2.

Drainage area characteristics

The contributing area to each study location was delineated using the D8 flow direction algorithm in ArcGIS's hydrology tools with 3.6 meter DTMs (Digital Terrain Models) made available from YPG. The length of channel that could potentially lead to infiltration losses was also calculated. Using the DTM in ArcGIS, a flow accumulation raster was created. A threshold of 100 cells was selected as the contributing area threshold for channel initiation. This threshold was selected by iteratively testing thresholds of flow accumulation to determine which best corresponded to visually distinguishable channels in ortho-photographs obtained from the United States Department of Agriculture's Farm Service Agency's National Agriculture Imagery Program (NAIP imagery obtained from the Aerial Photography Field Office, June 9, 2013). The stream length was estimated by counting the number of cells above this threshold and multiplying the count by the length of a cell edge.

Data analysis

To link runoff events with precipitation characteristics, the precipitation record was divided into events. Storm events were defined based on the precipitation minimum inter-event time (MIT), which is the minimum time between tips of a rain gauge that separates rain events. An MIT of 7 hours was selected based on the data and literature. The longest flow duration at a site recorded during this study, 6.5 hours, was used to determine an appropriate MIT. Dunkerley (2008) noted that an MIT of 6-8 hours is widely used in studies. Over a quarter of the 26 published articles reviewed by Dunkerley (2008) use MITs in this range. To test the influence of MIT on study results, analyses were also computed using alternate MITs. Rain events of two tips or less of the rain gauge tipping bucket were excluded from the analyses. The time of flow beginning, peak, and end was identified for each rain event, and four precipitation metrics were calculated for each event at each site: total event magnitude (Depth) and 15, 30, and 60-minute peak intensities (I15, I30, I60).

Table 3-3. Stream stage measurement sites with the site location, distance, and elevation difference of the closest rain gauge. Some sites were not used for threshold analysis because of data problems, rain gauge distance, or elevation difference. PT stands for pressure transducer.

Site	Rain gauge	Distance to rain gauge (km)	Elevation difference: PT and rain gauge (m)	Used in threshold analysis
Piedmont Headwaters				
YPH1	YIA	1	-19	Yes
YPH2	YIA	2.5	-21	No[1]
MPH1	MBD	1.5	19	Yes
MPH2	MBA	4.2	-38	No[1]
Bedrock				
YBK1	On site until 2/10/2013 then YBA	0.3	16	Yes
YBK2	On site	0	-3	Yes
MBK1	MBA	1.4	184	No[2]
MBK2	On site	0	-36	Yes
Bedrock with Alluvium				
YBA1	On site	0	1	Yes
YBA2	YIA	2.2	31	No[1]
MBA1	On site	0	-1	Yes
MBA2	MBK5	1.3	-92	Yes
Incised Alluvium				
YIA1	On site	0	0	Yes
YIA2	YIA	1.4	-14	Yes
MIA2	MBA	4	-31	No[1]
Braided				
MIA1	On site	0	-1	Yes
YBD1	On site	0	1	Yes
MBD1	On site	0	-6	Yes

1. Rain gauge >1.5 km away
2. Elevation change to rain gauge too great

Pressure transducer stream stage data were analyzed to identify flow events. Most flow events were easily distinguished from background noise after correcting for barometric pressure, and converting the pressure transducer data to depth. However, residual noise in the data made it difficult to discern small flow events. To distinguish potential flow events from background noise, cumulative distribution functions (CDFs) were created from the stage data at each site. The CDFs were intended to bring out the highest values based on relative amounts of time to indicate potential flows. Stage depths greater than the 99.5 were pulled out of the data. These values were graphed and visually analyzed for hydrograph features, and the dates and times were compared to the rainfall data to determine whether the high stage values were runoff events or noise. Once flow events were identified, the start time, peak, and end of each hydrograph were determined for each flow event.

The stream hydrographs from each site were compared to the nearest rain gauge (Table 3-3) to determine precipitation event characteristics for each flow occurrence at each site. If a rain gauge was not located on the site with the pressure transducer then the closest working rain gauge was used. The lag time between peak precipitation and peak flow was determined. Preliminary data analysis showed poor correspondence between precipitation and flow event records for stream channels that did not have rain gauges within 1.5 km, so YPH2, MPH2, YBA2, and MIA2 were excluded from the threshold analysis. The correlation between MBK1 flow and the nearest rain gauge (MBA1, 1.4 km) was also poor, with flows produced during low intensity rains and high intensity rains not producing flow. This may be due to the 184 meters difference in elevation between the stream stage site and corresponding rain gauge, so this site also was excluded from threshold analysis. Both equipment failure and installation timing led to a few cases where the closest rain gauge did not have data for a runoff event. If the closest rain gauge was not recording during the time of the flow, than the next closest rain gauge was used if it was within 1.5 km. If no rain gauge within that distance was recording during a flow event, the flow event was excluded from further analysis. Two runoff events at MPH (9/6/2013 and 9/2/13) and one runoff event (8/17/12) at YBD were taken out due to no rain gauges in the 1.5 km radius recording. One runoff producing rain event on 12/13/2012 was not recorded for an unknown reason at YBK, so the rain gauge at YBA was used. Only the rain events recorded during the time of an actively working pressure transducer were used in the analysis of a particular site.

For each site, all precipitation events were assigned a binary value for flow or no flow. Precipitation event metrics (Depth, I15, I30, I60) were then sorted from highest to lowest for each metric to determine which of the metrics best indicated precipitation thresholds for runoff production. A threshold would was defined when the majority of the values above a given magnitude produced runoff, and the majority of values below that magnitude did not. Based on this analysis, the metric best suited for defining runoff thresholds was selected, and precipitation thresholds for runoff generation were compared between geomorphic groupings of channel types. The fraction of rain events producing runoff was also calculated for the total period of record and by season and compared between channel types.

Results

Seasonality of rain

For this study, the year is broken-up into two seasons: winter (November thru April) and summer (May thru October). This division separates the convective systems that characterize warm-season precipitation from the frontal systems that supply cold season precipitation (Hallack-Alegria and Watkins, 2007). The seasonal patterns of precipitation are summarized in Table 3-4 and 3-5; data used for this analysis have some gaps due to data loss, and the values listed in the tables represent recorded values only. As mentioned in the Methods section, rain events were the rain gauge or pressure transducer were not working at a particular site have been removed from that site's data. Therefore this analysis does not try to accurately surmise climate variations. In this study area, most sites had more rain events and greater total rain depth during the summer than during the winter months (Table 3-4). The average of all sites' total rain depth for the three winters was between 26-41 mm and between 43-114 mm for the two summers (Table 3-5). The range of winter rain event depths at all sites was between 1 mm and 31 mm, and the range of depth for the summer storms was from 1 mm to 87 mm. The range of event depths during the summer was wider than the range during the winter, due to individual high depth summer storms. However, the average event depths for winter and summer are similar, with the summer averages ranging from 7-13 mm, and the winter averages ranging from 4-14 mm. The winter of November 2011 – April 2012 was the driest winter, with an average site total depth of 26 mm and an average event depth of 4 mm. The following summer, May 2012 – October 2012, was the wettest season during the study with an average site total depth of 114 mm and an average event depth of 13 mm. Although there were more rain events and more rain accumulation in the summer, winters tended to have longer event durations. The average durations of the winter rain events were between 3.25-17 hours, whereas the average summer rain events lasted 2.25-3.5 hours. The range of winter storm duration was between 0.25 hours and 41.75 hours, and the range of summer rain duration was from 0.25 hours to 10.75 hours. At most sites the total duration of rain during the summer was shorter than the winter (Table 3-4). YBK1 was the only site where the summer rain duration was longer, 2.8 times longer, than winter rain duration. At most sites the average I60 of summer storms was greater than the average I60 of winter storms, ranging from 1.08 to 2.26 times greater. YBK1 and YBA1 had average I60s of winter storms greater than summer storms. The average I60 of winter storms was 3-4 mm hr^{-1}, and summer storms

average I60 was 5 and 11 mm hr^{-1} (Table 3-5). The range of winter storms' I60 was between 1 mm hr^{-1} and 24 mm hr^{-1}, and the range of summer I60s was up to 70 mm hr^{-1}.

Table 3-4. Seasonality of rain at each site, with differences between summer and winter total recorded precipitation depth, total duration, and storm average I60 for Nov 2012 – Oct 2013. YPH1 is not included because the majority of the PT data between 9/23/2012 – 12/6/13 was not usable. YBK2, MBK2, MBA2, and YIA2 are not included because they were installed in February or March of 2013.

Site	Number of winter rain events	Number of summer rain events	Depth during year (mm)	% total depth occurred in winter	% of total depth occurred in summer	Duration ratio Summer/ Winter	Average I60 ratio Summer/ Winter
Piedmont Headwaters							
MPH1	5	3	81	63.4	36.6	0.26	2.26
Bedrock							
YBK1	3	10	61	38.8	61.2	2.80	0.48
Bedrock with Alluvium							
YBA1	5	10	87	56.7	43.3	0.93	0.55
MBA1	4	9	157	35.3	64.7	0.98	1.53
Incised Alluvium							
YIA1	5	8	87	49.7	50.3	0.80	1.09
Braided							
MIA1	4	5	91	59.4	40.6	0.57	1.12
YBD1	3	7	98	44.7	55.3	0.94	1.08
MBD1	5	3	81	63.4	36.6	0.26	2.26

Table 3-5. Seasonality of rain for sites with continuous measurements during three winters (Nov-Apr) and two summers (May-Oct). Sites used: YPH1, MPH1, YBK1, YBA1, MBA1, YIA1, MIA1, YBD1, and MBD1.

	Average total depth (mm)	Average event depth (mm)	Range of event depth (mm)	Average total duration (hrs)	Average event duration (hrs)	Range of event duration (hrs)	Average event I60 (mm hr^{-1})	Range of event I60 (mm hr^{-1})
Winter								
Winter 11-12	26	4	1 - 24	19	3.25	0.25 - 15.5	3	1 - 24
Winter 12-13	41	11	1 - 25	27.25	7.25	0.5 - 20.75	4	1 - 12
Winter 13-14	27	14	1 - 31	34	17	0.5 - 41.75	3	1 - 6
Summer								
Summer 12	114	13	1 - 87	20.25	2.25	0.25 - 12	11	1 - 70
Summer 13	43	7	1 - 53	21.25	3.5	0.25 - 10.75	5	0 - 28

Rainfall-runoff events

The sites experienced between 11 and 48 rain events from November 2011 to May 2014 that caused between 0 to 9 runoff events (Table 3-6). Most of the runoff-producing rain events affected the entire study area, though the storm total depth and maximum intensity varied across the watersheds (Figure 3-9). Because of this variance, most of the flows were localized to only one or two sites, but there was one flow recorded throughout both watersheds on 7/13/12 (Figure 3-11). With the exception of 11 runoff-producing storms of 9 hours or more, most precipitation event durations were between 1 and 4 hours.

Table 3-6. Time period analyzed for each site, total precipitation measured at the site, and total number of rainfall and runoff events by site.

Site Name	Start date	Last download	Total Precip (mm)	Total rain events	Total runoff events	% rain causing runoff
Piedmont Headwaters						
YPH1	3/14/2012	5/12/2014	151	11	4	36
MPH1	11/12/2011	5/11/2014	231	29	9	31
Bedrock						
YBK1	11/12/2011	5/12/2014	276	30	7	23
YBK2	3/20/2013	5/13/2014	83	12	2	17
MBK2	2/9/2013	5/15/2014	80	12	3	25
Bedrock with Alluvium						
YBA1	11/13/2011	5/12/2014	310	31	3	10
MBA1	11/13/2011	5/11/2014	299	22	2	9
MBA2	2/9/2013	5/15/2014	80	12	0	0
Incised Alluvium						
YIA1	11/13/2011	5/12/2014	255	25	5	20
YIA2	3/20/2013	5/13/2014	74	11	0	0
Braided						
MIA1	11/13/2011	5/14/2014	325	48	2	4
YBD1	2/17/2012	5/13/2014	206	19	1	5
MBD1	4/1/2012	5/14/2014	205	26	1	4

The storm in Yuma Wash on 8/22/2013 is a good example of the spatial variability of storm intensity and depth (Figure 3-9). The storm produced more rain depth at a higher intensity lower in the watershed at YBD1 and YIA1, than it did higher in the watershed at YBA1 and YBK2. Due to this spatial variability of the storm, the rain intensity and depth were only great enough to produce flow at YIA1 and YPH1 (Figure 3-11). These sites are 1 km apart, and the rain gauge at YIA1 is used for YPH1 (Table 3-3). The storm's largest I60, 28 mm hr^{-1}, and largest depth, 29 mm, occurred at YBD1. The I60 and depth dropped to 15 mm hr^{-1} and 16 mm 2.8 km east of YBD1 at YIA1. At YBA1, only 1.6 km southeast of YIA1, the storm had its lowest intensity of 2 mm hr^{-1} and a depth of 2 mm (Figure 3-9). At YBK2, the furthest site from YBD1, 3.6 km, and the furthest northern site, the I60 of the storm was 5 mm hr^{-1}, and the depth was 5 mm, which is higher than the intensity and depth at YBA1.

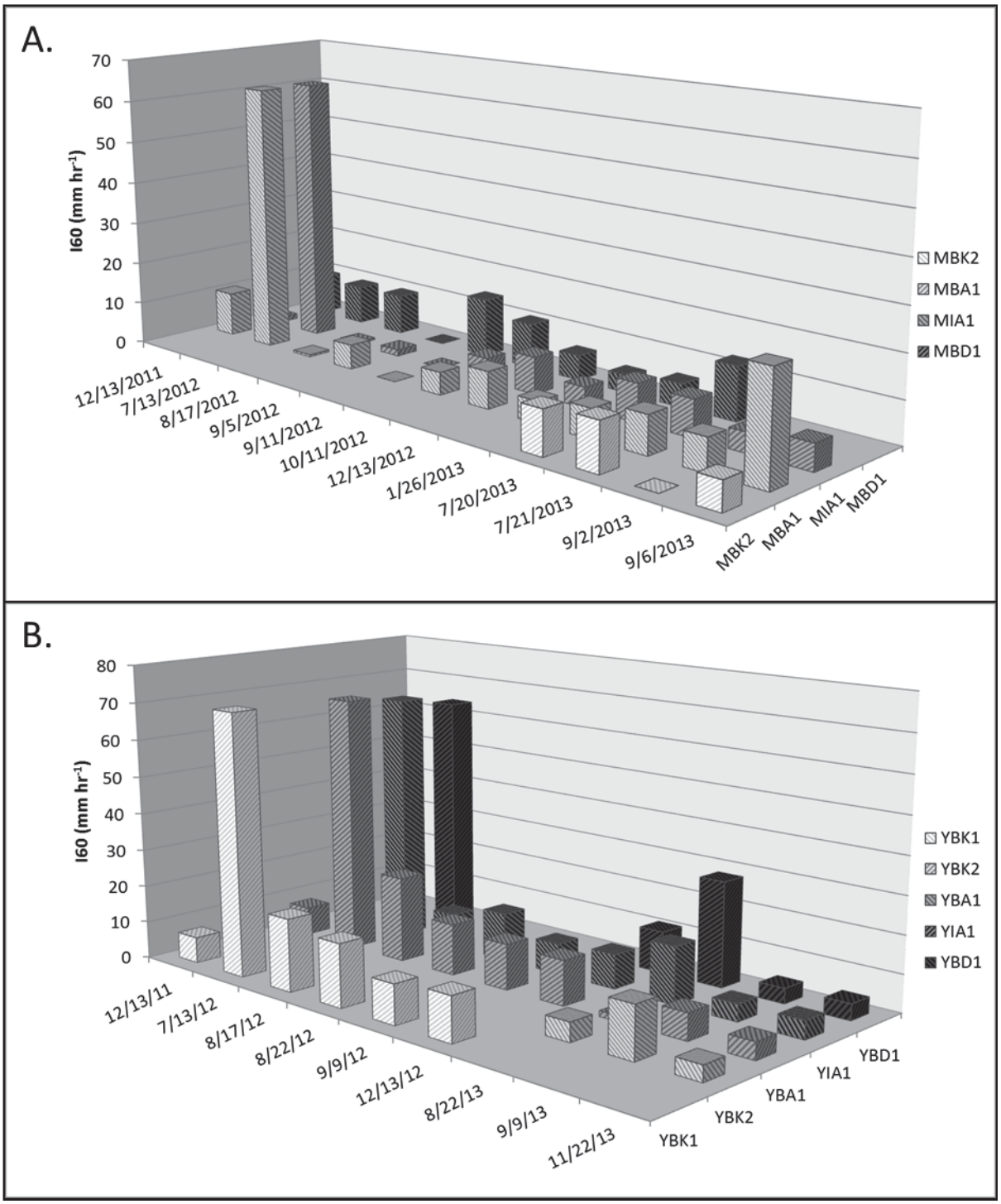

Figure 3-9. Spatial variability of peak I60 for rain events that produced runoff at one or more monitoring locations. Periods lacking rain are illustrated by flat boxes, and no boxes indicate equipment was not recording during this time. (A) rain gauges in Mohave Wash, (B) rain gauges in Yuma Wash.

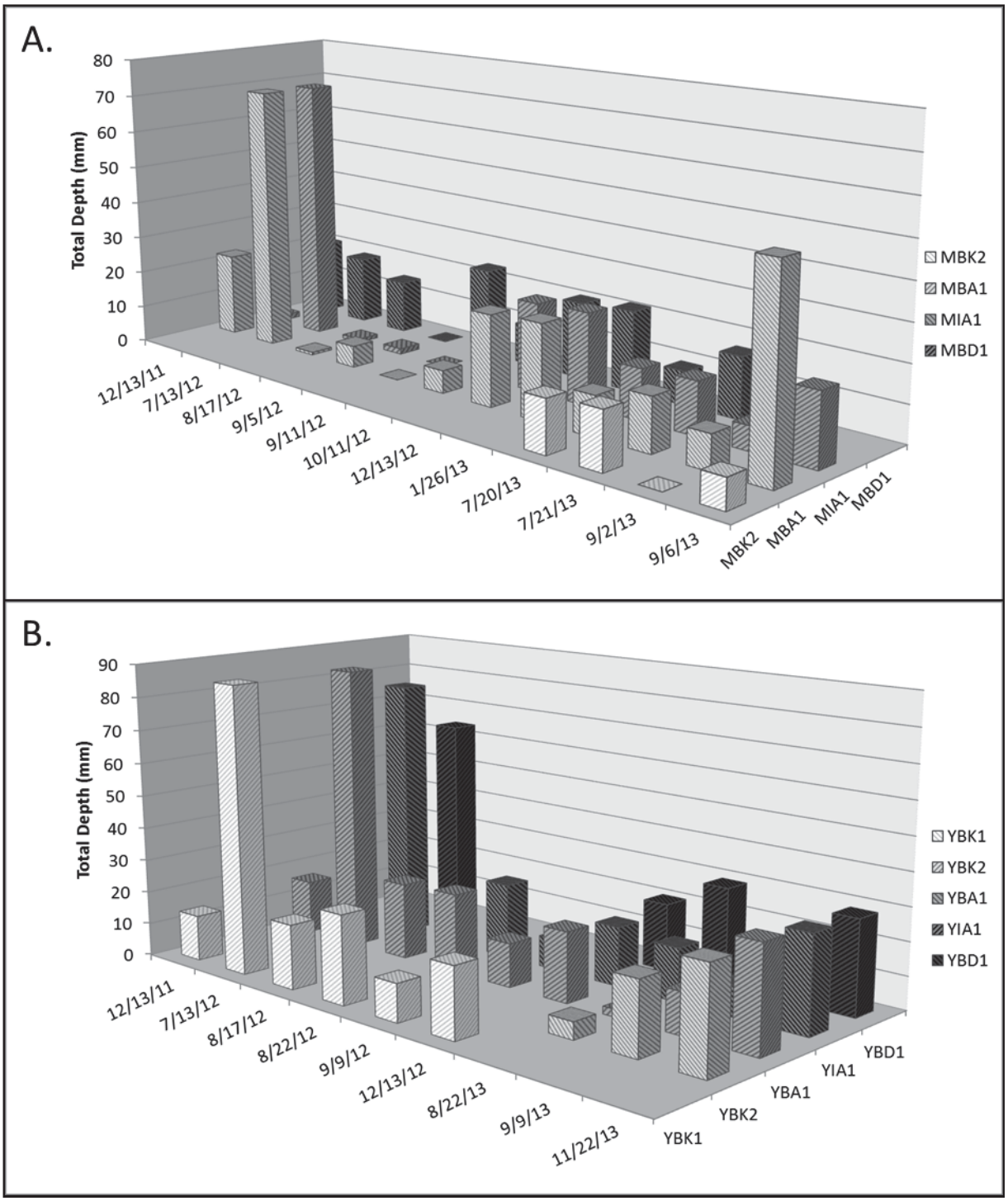

Figure 3-10. Spatial variability of total storm depth for rain events that produced runoff at one or more monitoring locations. Periods lacking rain are illustrated by flat boxes, and no boxes indicate equipment was not recording during this time. (A) rain gauges in Mohave Wash, (B) rain gauges in Yuma Wash.

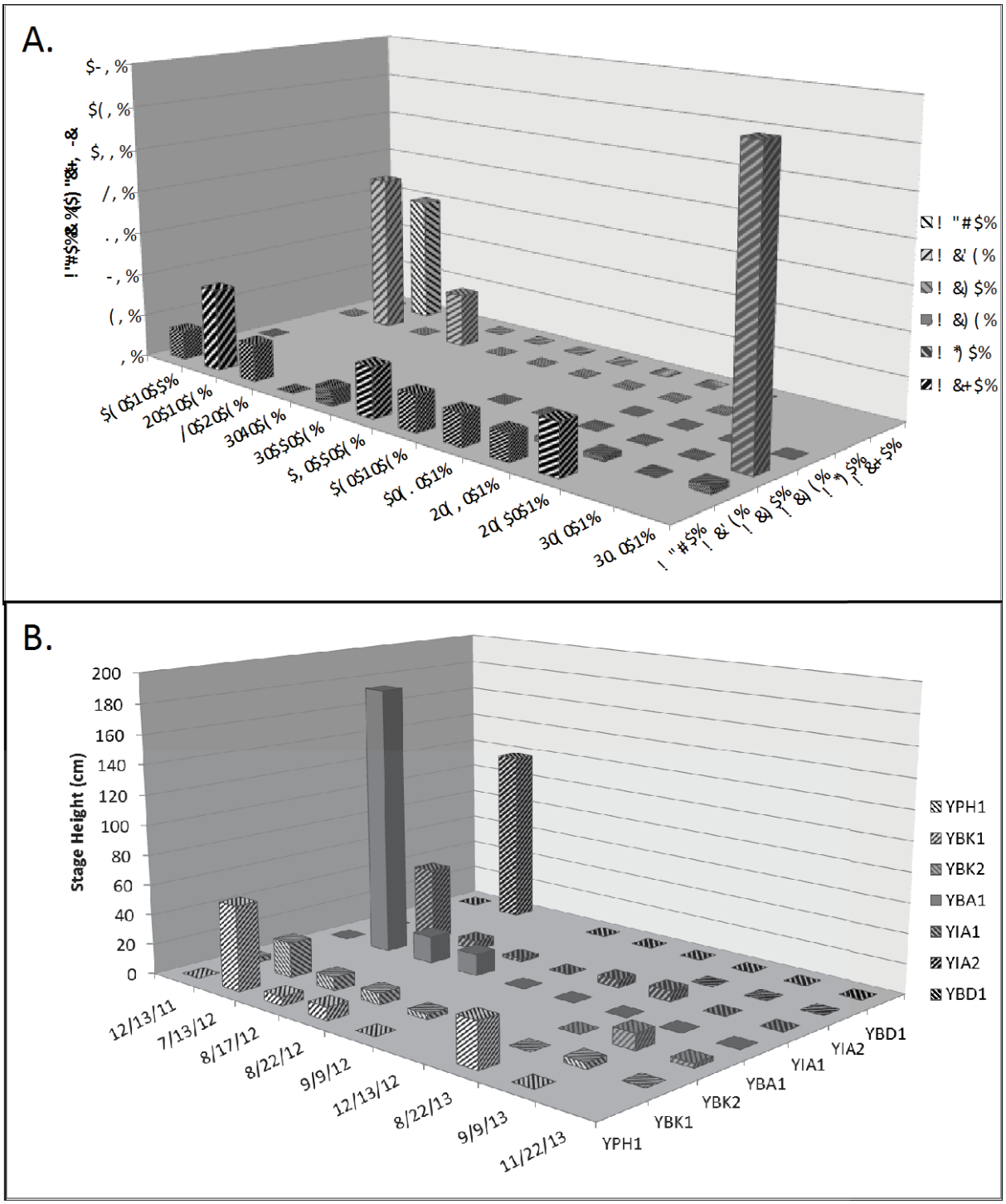

Figure 3-11 Spatial variability of flow occurrence for rain events that produced runoff at one or more monitoring locations. Periods without flow are illustrated by flat boxes, and no boxes indicate equipment was not recording during this time. (A) pressure transducers in Mohave Wash, (B) pressure transducers in Yuma Wash.

The largest runoff event recorded in both watersheds during this study occurred on 7/13/12 (Figure 3-11). The storm that produced this runoff generally had the most rain and highest I60 (Figure 9-5.2). The I60 of most sites fell in the range of 63 mm hr^{-1} – 70 mm hr^{-1}, with the highest intensity of 70 mm hr^{-1} recorded at YBK1 (Figure 3-9). Most

sites received between 64 mm and 87 mm at YBK1 (Figure 3-10). The lowest recorded I60 and depth for this event was at MBD1, which was 9 mm hr^{-1} and 18 mm.

Runoff was recorded in each site that was operational at during the 7/13/12 rain event. The pressure transducer at MBA1 was washed away and lost during this flow, so no stage data were recorded there, although flow occurrence at MBA1 during this event is used later in the threshold analysis. The lowest peak stage height was 23 cm at YBK1, and the flow lasted 2 hours here (Figure 3-11). YBA1 had the highest recorded peak stage of 180 cm though the flow only lasted 1.25 hours with a sharp rise and fall of the hydrograph. YIA1's flow had a peak stage of 50 cm, and YPH's flow peaked at 57 cm. The flows at both sites lasted 2.75 hours. YBD1, which is 124 m wide (Table 3-2), had a peak stage of 118 cm, and the flow lasted for 4.5 hours. The longest duration flow was 6.25 hours at MIA1 and had a peak stage of 75 cm. The MPH1 had two flows; the first flow peaked at 38cm and lasted 2.25 hours, and the second lasted over 2.5 hours and had a lower peak stage of 31 cm. MBD1 had the shortest flow duration of 1 hour with a quickly rising and falling hydrograph peaking at 60 cm.

Only four sites recorded flow during the winter: MPH1, YBK1, YBK2, and YIA1 (Table 3-7). With the exception of the one winter flow at YIA1, the remaining winter flows occurred at the small bedrock and piedmont headwater channels. MPH1 experienced the most runoff-producing rains (9, Table 3-6), and the most winter flows (3; Table 3-7). YIA1 had 20 percent of runoff producing rains occurring in winter, which was the lowest percentage out of the sites that experienced winter runoff. Fifty percent of the runoff at YBK2 occurred during winter, but there were only two flows, one in summer and one in winter.

Table 3-8 summarizes the lag time between the peak of a runoff-producing rain event and the peak of the runoff event. In some cases the peak flow occurred at the monitoring site before the rain gauge measured the peak rain. This is shown in Table 3-8 as negative lag times. The average lag times at each site were less than half an hour, and with the exception of two events, the lag times for individual events were less than an hour. The piedmont headwater sites have the greatest distances between pressure transducers and rain gauges and have the largest range of lag times. Excluding incised alluvium and braided sites, flow-monitoring sites with rain gauges on site had small ranges in lag times, no greater than half an hour. The one flow event at MBD1 had a lag time of -2.5 hours, which reflects flow responding to precipitation upstream in the watershed, before peak precipitation at the MBD1 site.

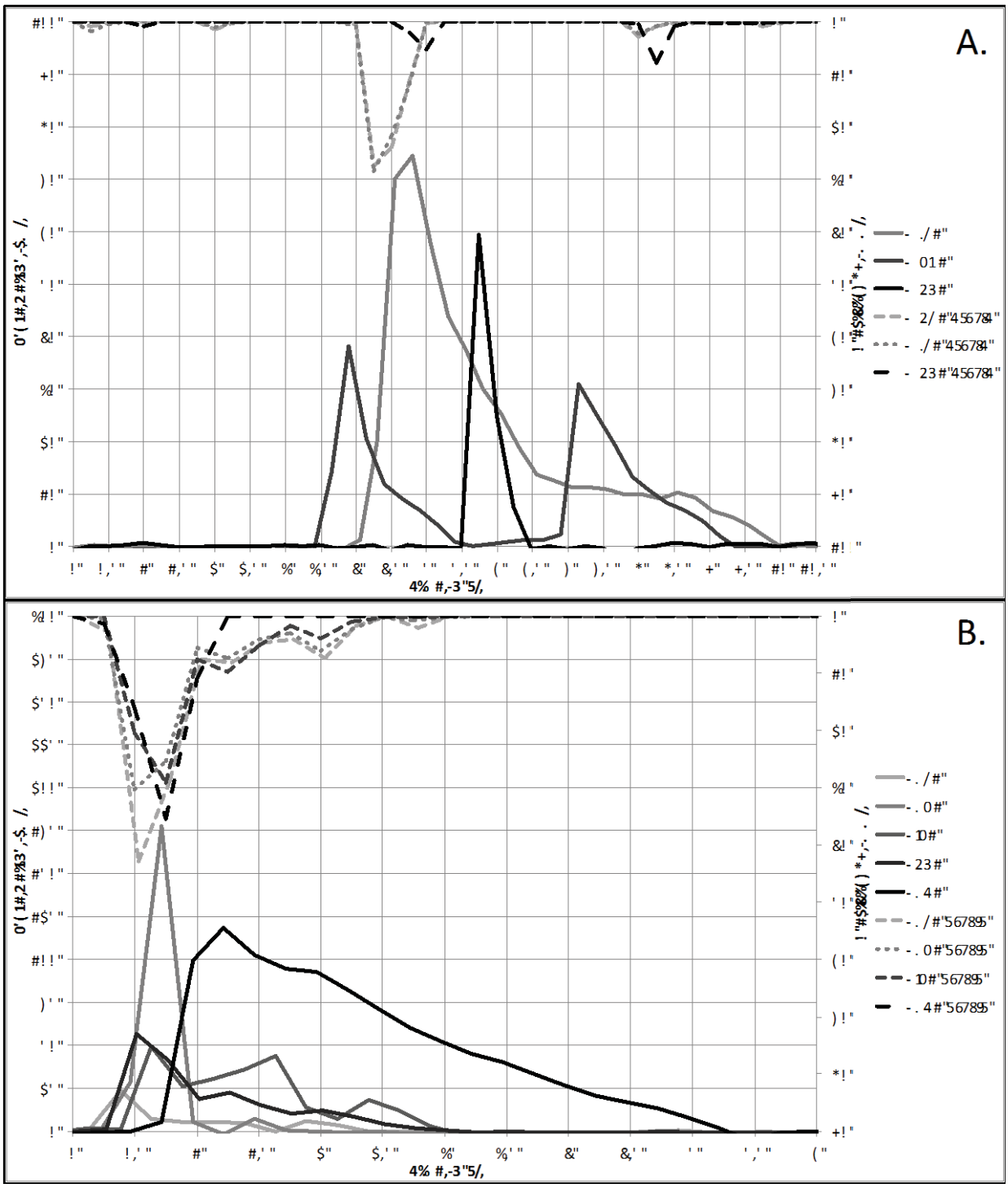

Figure 3-12. Hydrographs of the 7/13/12 flow event at both watersheds. Sites in the order of upstream to downstream. (A) Mohave Wash, (B) Yuma Wash.

Table 3-7. Seasonality of runoff-producing rain events.

Site Name	Winter rain events that caused flow	Summer rain events that caused flow	% runoff producing rains that occurred during winter	% runoff producing rains that occurred during summer
Piedmont Headwaters				
YPH1	0	4	0	100
MPH1	3	6	33	67
Bedrock				
YBK1	2	5	29	71
YBK2	1	1	50	50
MBK2	0	3	0	100
Bedrock with Alluvium				
YBA1	0	3	0	100
MBA1	0	2	0	100
MBA2	0	0	0	0
Incised Alluvium				
YIA1	1	4	20	80
YIA2	0	0	0	0
Braided				
MIA1	0	2	0	100
YBD1	0	1	0	100
MBD1	0	1	0	100

Table 3-8. Summary statistics for rainfall-runoff event timing. Lag times for runoff events are expressed as lag time between peak 15-minute precipitation and peak 15-minute stream stage. Positive values of lag time indicate precipitation peaked before stream stage; negative values indicate stream stage peaked before precipitation.

Site	Distance to rain gauge (km)	Average flow duration (hrs)	Range of flow duration (hrs)	Average rain duration (hrs)	Range of rain duration (hrs)	Average lag time (hrs)	Range of lag times (hrs)	Average peak stage (cm)	Range of peak stage (cm)
Piedmont Headwaters									
YPH1	1.0	1.25	0.5 to 3	2.25	1 to 3.25	0.25	0 to 0.75	25	6 to 57
MPH1	1.5	3.50	2.25 to 4.75	7.50	2 to 18.25	-0.50	-0.25 to -1.25	15	0.3 to 23
Bedrock									
YBK1	0.3	1.00	0.5 to 2.25	4.75	1.25 to 13	0.25	0 - 0.5	8	4 to 23
YBK2	0.0	0.75	0.5 to 0.75	19.25	10.25 to 28.25	0.50	0.25 to 0.5	7	3 to 11
MBK2	0.0	2.00	1.5 to 2.5	4.00	3.25 to 4.25	0.00	0 to 0.25	2	2 to 3
Bedrock with Alluvium									
YBA1	0.0	1.25	0.5 to 2.0	2.50	1.25 to 3	0.25	0 to 0.5	71	14 to 181
MBA1	0.0	34.75	30 to 45	7.25	4.5 to 10	0.00	0 to 0.25	133	133
MBA2	1.3	No Flow							
Incised Alluvium									
YIA1	0.0	2.25	0.25 to 4.25	3.00	1 to 6	0.25	0 to 0.75	14	2 to 49
YIA2	1.4	No Flow							
Braided									
MIA1	0.0	4.00	1.5 to 6.5	6.25	0.5 to 12	0.75	0.25 to 0.75	50	25 to 75
YBD1	0.0	4.75	4.75 to 5.0	1.00	1 to 1.25	0.50	0.25 to 0.5	118	118
MBD1	0.0	1.25	1 to 1.25	9.00	9 to 9.15	-2.50	-2.5 to -2.75	60	60

Selection of rain event metrics for threshold analysis

Table 3-9 compares the four precipitation metrics (Depth, I15, I30, I60) at each site to identify how well the metric did at sorting flow producing rain events above a threshold. For each metric the number of no-flow producing rain events over the threshold (false positive) and the number of flow producing rain events under the threshold (false negative) out of the total number of flows were identified. The metrics that had the lowest total number of false positives and false negatives were then identified and noted in the final column.

Table 3-9. Selection of precipitation metrics for runoff threshold analysis. FP (false positive) is no-flow rain events above the threshold, and FN (false negatives) is flow-producing rain events below the threshold. The final column shows the percent of rain events correctly classified as flow or no-flow by the best threshold metric.

		Total depth		15 min		30 min		60 min		Best	
Site	# rain events	FP	FN	FP	FN	FP	FN	FP	FN		% correctly identified
Piedmont Headwaters											
YPH1	11	1	0	1	0	1	0	0	0	60	100
MPH1	29	1	0	0	3	1	1	1	1	Depth	97
Bedrock											
YBK1	30	1	0	1	0	0	0	0	0	30, 60	100
YBK2	12	0	0	3	0	2	0	1	0	Depth	100
MBK2	12	1	0	0	0	0	0	0	0	15, 30, 60	100
Bedrock with Alluvium											
YBA1	31	1	0	1	0	0	0	0	0	30, 60	100
MBA1	22	0	0	0	0	0	0	0	0	Depth, 15, 30, 60	100
MBA2	12	No Flow	No Flow	No Flow	No Flow	No Flow	No Flow	No Flow	No Flow		No Flow
Incised Alluvium											
YIA1	25	2	1	1	0	1	0	0	0	60	100
YIA2	11	No Flow	No Flow	No Flow	No Flow	No Flow	No Flow	No Flow	No Flow		No Flow
Braided											
MIA1	48	0	1	0	1	0	1	0	1	Depth, 15, 30, 60	98
YBD1	19	0	0	0	0	0	0	0	0	Depth, 15, 30, 60	100
MBD1	26	4	0	1	0	2	0	4	0	15	96

Table 3-10 compares how the four metrics did at organizing the runoff producing events above a threshold. I60 was found to produce the best indication of a precipitation threshold for runoff, with precipitation events sorted with decreasing I60s having the majority of corresponding flow events at the top of the list. The I60 metric was one of the best-performing threshold metrics for 8 out of the 11 sites with 97.2% overall accuracy. The I30 metric was the next best with an accuracy of 96.9%, followed by I15 with an accuracy of 95.8%, and then depth with an accuracy of 95.5%. All four metrics could be used to create thresholds for the different sites with an accuracy of 95.5% and greater. I60 had an overall percent accuracy only 1.7% greater than the worst metric, but it predicted 7 sites with 100% accuracy, whereas the other metrics only predicted 3 to 5 sites with 100% accuracy (Table 3-9). Because I60 was overall the best metric for identifying runoff thresholds, this metric was used in subsequent threshold analysis.

Table 3-10. Summary of site-based threshold analysis in Table 3-9, indicating the number of sites for which each metric was or was not among the best metrics for identifying runoff thresholds.

Metric	Overall % accuracy	# of sites metric was among the best choices	# of sites metric was not among the best choices
Depth	95.5	5	6
I15	95.8	5	6
I30	96.9	6	5
I60	97.2	8	3

Runoff thresholds by channel type

The precipitation thresholds for runoff generation vary between channel types. Pressure transducers at two Piedmont Headwater sites, YPH1 and MPH1, were used in the threshold analysis for piedmont headwater channels. Table 3-11 and Figure 3-13 shows the total depth and I60 threshold range and mean for each site. Precipitation values are reported to the nearest 0.1 mm to illustrate differences, but the precision of the rain gauges is 0.25 mm per tip. The lower end of the threshold range is the highest total storm depth and I60 that did not produce runoff, excluding false negatives, and the upper end of the threshold range is the lowest total storm depth and I60 that created runoff, excluding false positives. The mean of the threshold range in Table 3-11 is the mean of the lower and upper threshold limits. Figure 3-14 shows I60 plotted against the total storm depth for the rain gauges at MBD1 and YIA1 with the corresponding flow events at MPH1 and YPH1.

The range of the total depth threshold at YPH1 is between 4.8-8.9 mm (Table 3-11, Figure 3-14). This gives a mean total depth threshold of 6.9 mm at YPH1. YPH1 has an I60 threshold range of 8.1-8.9 mm hr^{-1}, giving it a mean threshold of 8.5 mm hr^{-1}. There were no false positives or false negatives for YPH1's I60 threshold. MPH1 has a total depth threshold range between 5.8-8.9 mm, with a threshold mean of 7.4 mm. The I60 threshold for MPH1 is between 4.6-5.3 mm hr^{-1}. The mean of this threshold range is 5.0 mm hr^{-1}. Rain events around the I60 threshold at YPH1 have a recurrence interval of one year, and at MPH1 the recurrence interval for the threshold is less than one year (Bonnin et al., 2011).

At MPH1 there was one rain event over the I60 threshold that did not produce flow, and one high magnitude winter rain event that produced runoff under the I60 threshold (Figure 3-14). This winter event occurred on January 26, 2013 and had a high total depth of 21 mm and an I60 of 4 mm hr^{-1} (Figure 3-9). The total depth metric worked the best at defining a runoff threshold at this site (Table 3-9). The storm total depth threshold separates flow and no flow events independent of storm intensity.

Table 3-11. Depth and I60 precipitation thresholds by site. 'Below threshold' indicates the highest value of the precipitation metric (depth or I60) with no flow, excluding FN, and 'above threshold' indicates the lowest value of the precipitation metric with flow, excluding FP. Mean threshold values are the mean of the precipitation values below and above the threshold.

Site Name	Depth below threshold (mm)	Depth above threshold (mm)	Mean of depth threshold range (mm)	I60 below threshold (mm hr^{-1})	I60 above threshold (mm hr^{-1})	Mean of threshold I60 range (mm hr^{-1})
Piedmont Headwaters						
YPH1	4.8	8.9	6.9	8.1	8.9	8.5
MPH1	5.8	8.9	7.4	4.6	5.3	5.0
Bedrock						
YBK1	7.9	11.4	9.6	4.6	7.0	5.8
YBK2	7.8	21.8	14.8	3.9	4.2	4.0
MBK2	4.8	7.8	6.3	6.1	6.6	6.4
Bedrock Alluvium						
YBA1	21.1	23.1	22.1	12.2	13.7	13.0
MBA1	31.0	52.6	41.8	10.4	25.2	17.8
MBA2	24.6	no flow	no flow	11.3	no flow	no flow
Incised Alluvium						
YIA1	9.4	16.0	12.7	8.1	8.9	8.5
YIA2	29.0	no flow	no flow	15.2	no flow	no flow
Braided						
MIA1	30.7	70.9	50.8	23.9	62.7	43.3
YBD1	29.2	63.8	46.5	28.2	63.8	46.0
MBD1	16.3	18.3	17.3	5.8	9.1	7.5

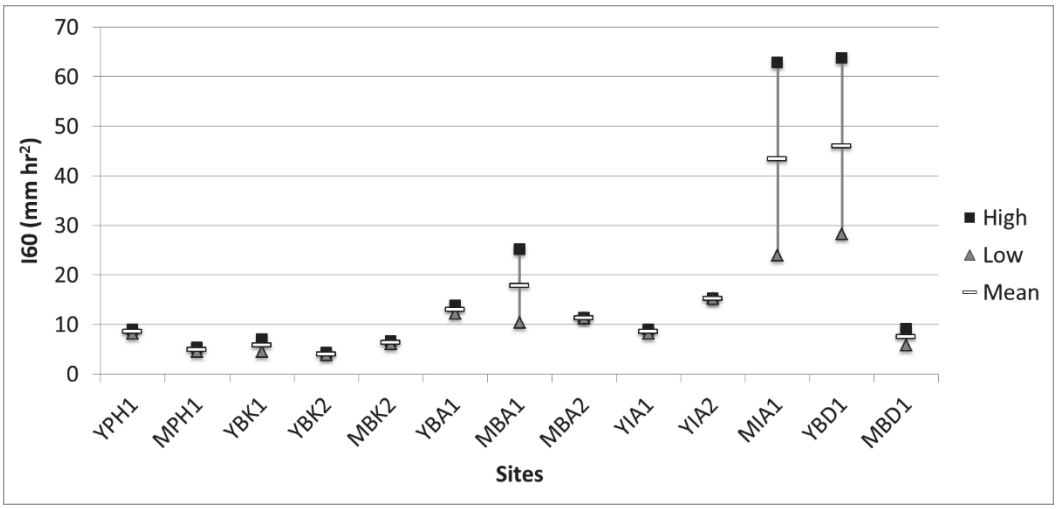

Figure 3-13. Range of I60 thresholds by site. For each site the lowest value is the highest I60 that did not produce runoff, excluding FN; the highest value is the lowest I60 that produced runoff, excluding FP; and the mean of the upper and lower ends of the threshold is shown as a horizontal line. MBA2 and YIA2 did not have flow, so the mean horizontal line is the highest I60 recorded at that site.

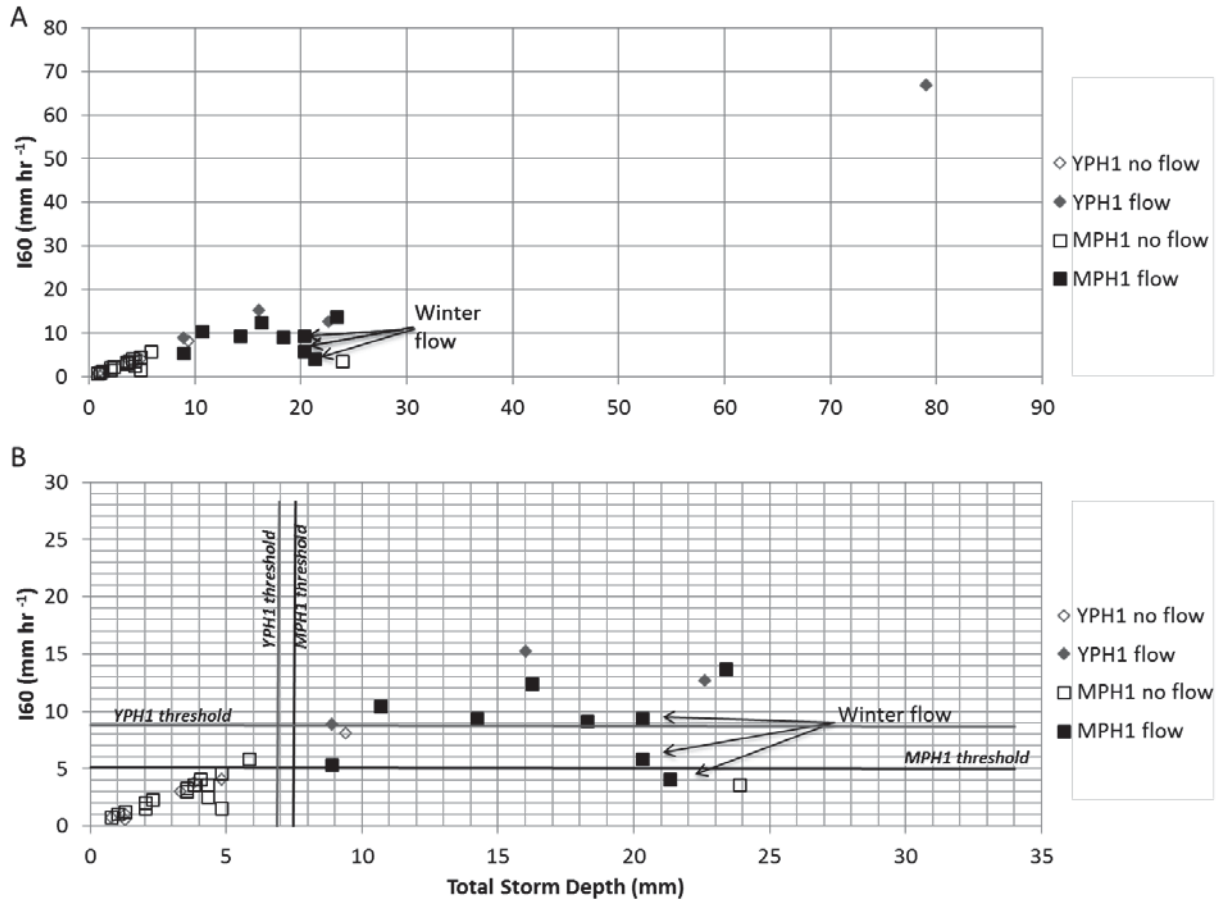

Figure 3-14. Piedmont Headwaters I60 vs. total storm depth of all storm events. Diamonds represent rain events at YPH1, and squares represent MPH1. Open symbols represent rain events that did not produce runoff, and solid symbols represent rain events that produced runoff at that site. (A) all rain events and (B) close-up around threshold.

The bedrock channel types had thresholds in a similar range as those in the piedmont headwater sites. Figure 3-15 shows the precipitation events at the bedrock channels and whether or not there was flow associated with the event. YBK1 had a rain gauge on site until February 10, 2013; after this date the rain data came from YBA1, which is 0.3 km away (Table 3-3). YBK's threshold range for total depth is between 7.9-11.4 mm, which gives it a mean threshold of 9.6 mm (Table 3-11). YBK1 shows a clear runoff-producing I60 threshold between the highest I60 rain event that did not produce runoff, with an I60 of 4.6 mm hr^{-1}, and the lowest I60 rain event that did produce runoff, with an I60 of 7.0 mm hr^{-1} (Figure 3-15). This gives an estimated I60 threshold of 5.8 mm hr^{-1} (Table 3-11). There were no no-flow rain events above this threshold, and no flow events below it. YBK2 has a total depth range between 7.8-21.8 mm. This is a large range, and the mean threshold of 14.8 mm is higher than the other sites. YBK2 has an I60 threshold range of 3.9-4.2 mm hr^{-1}. This gives an estimated I60 threshold of 4.0 mm hr^{-1}. There was one no-flow rain event above this threshold. MBK2's total depth threshold range is between 4.8-7.8 mm with a mean of 6.3 mm. The MBK2 site's range for the I60 runoff producing threshold is from 6.1-6.6 mm hr^{-1}, and has an estimated threshold of 6.4 mm hr^{-1}. No flows occurred under this threshold, and no no-flow rain events occurred above it. The estimated I60 thresholds at YBK1, YBK2, and MBK2 have a recurrence interval of less than one year (Bonnin et al., 2011).

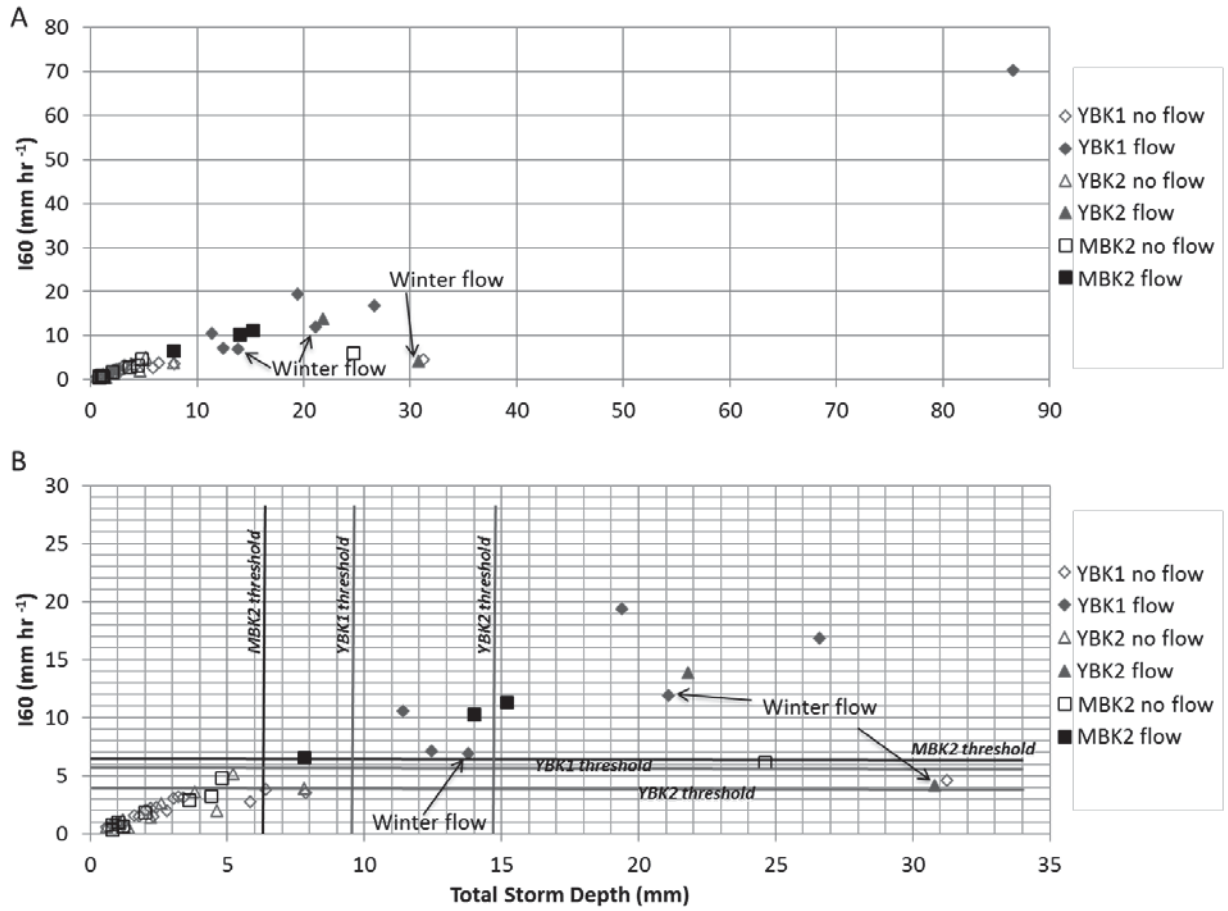

Figure 3-15. Bedrock channels I60 vs. total storm depth of all storm events. Diamonds represent rain events at YBK1, triangles represent YBK2, and squares represent MBK2. Open symbols represent rain events that did not produce runoff, and solid symbols represent rain events that produced runoff at that site. (A) all rain events and (B) close-up around threshold.

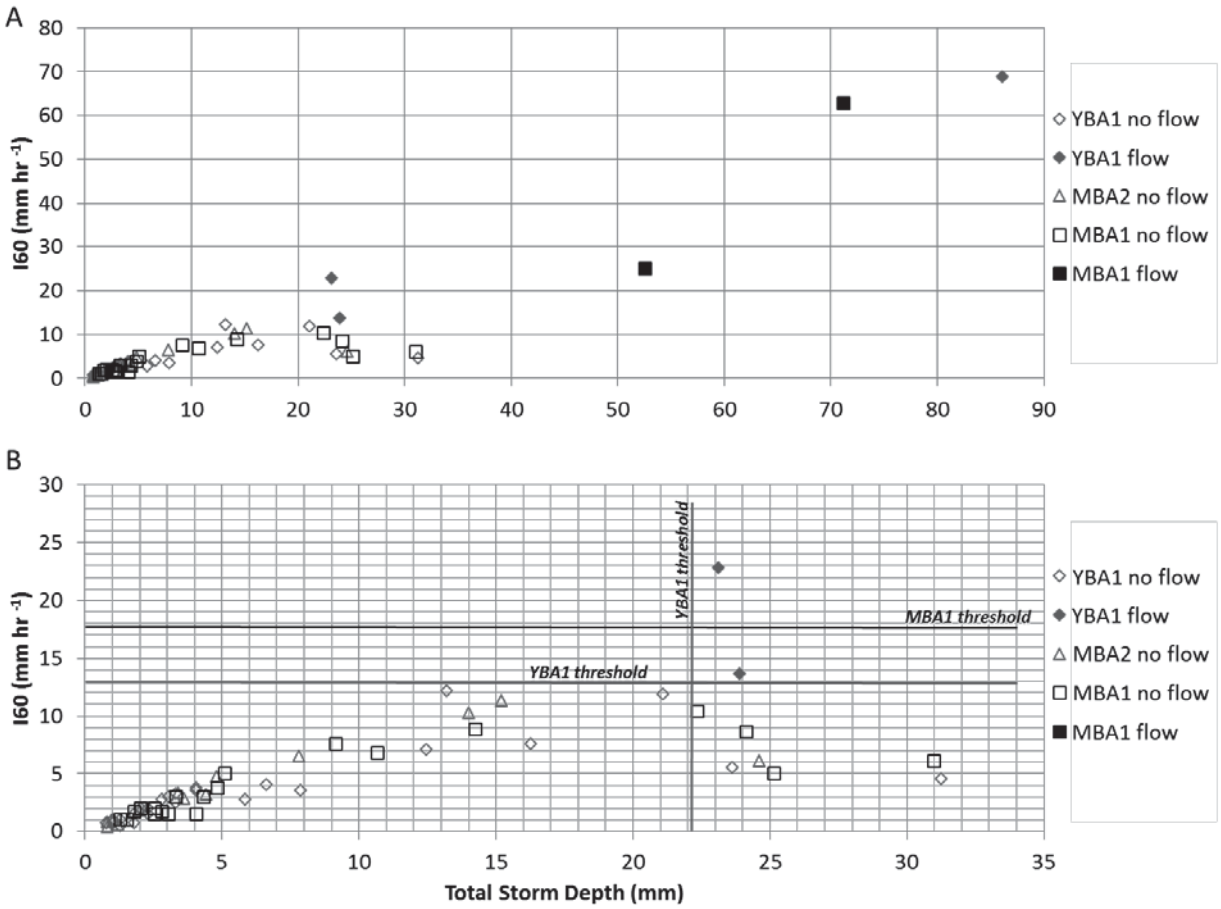

Figure 3-16. Bedrock with Alluvium channel I60 vs. total storm depth of all storm events. Diamonds represent rain events at YBA1, triangles represent MBA2, and squares represent MBA1. Open symbols represent rain events that did not produce runoff, and solid symbols represent rain events that produced runoff at that site. (A) all rain events and (B) close-up around threshold.

Bedrock with alluvium channel types had larger precipitation thresholds than the PH and BK channel types. The range of the total depth threshold at YBA1 is between the total depth of the largest no-flow producing rain event below the threshold, which is 21.1 mm, and the smallest total depth of the runoff producing rain event directly above the threshold of 23.1 mm (Table 3-11 and Figure 3-16). This gives a mean total depth threshold of 22.1 mm at YBA1. The YBA1 site has an I60 runoff-producing threshold between 12.2-13.7 mm hr^{-1} (Figure 3-13, 5.7). This produces an estimated threshold around 13.0 mm hr^{-1}, with no rain events producing runoff below it and no no-runoff rain events above it. MBA1 has a total depth threshold range between 31.0 mm and 52.6 mm, with a mean threshold of 41.8 mm. The I60 runoff-producing threshold at MBA1 is between 10.4-25.2 mm hr^{-1}. This is a large range, with the average between these rain events at 17.8 mm hr^{-1}, which correctly predicted no-flow and flow rain events. MBA2 did not have flow during the time of its operation. The highest total depth recorded during a rain event was 24.6 mm, and the most intense rain event recorded at MBA2 had an I60 of 11.3 mm hr^{-1}. The highest I60 rain event is shown as the lower end of the threshold in Figure 13. The recurrence interval for the estimated I60 threshold at YBA1 is 2 years, and between 2 and 5 years for the estimated I60 threshold at MBA1.

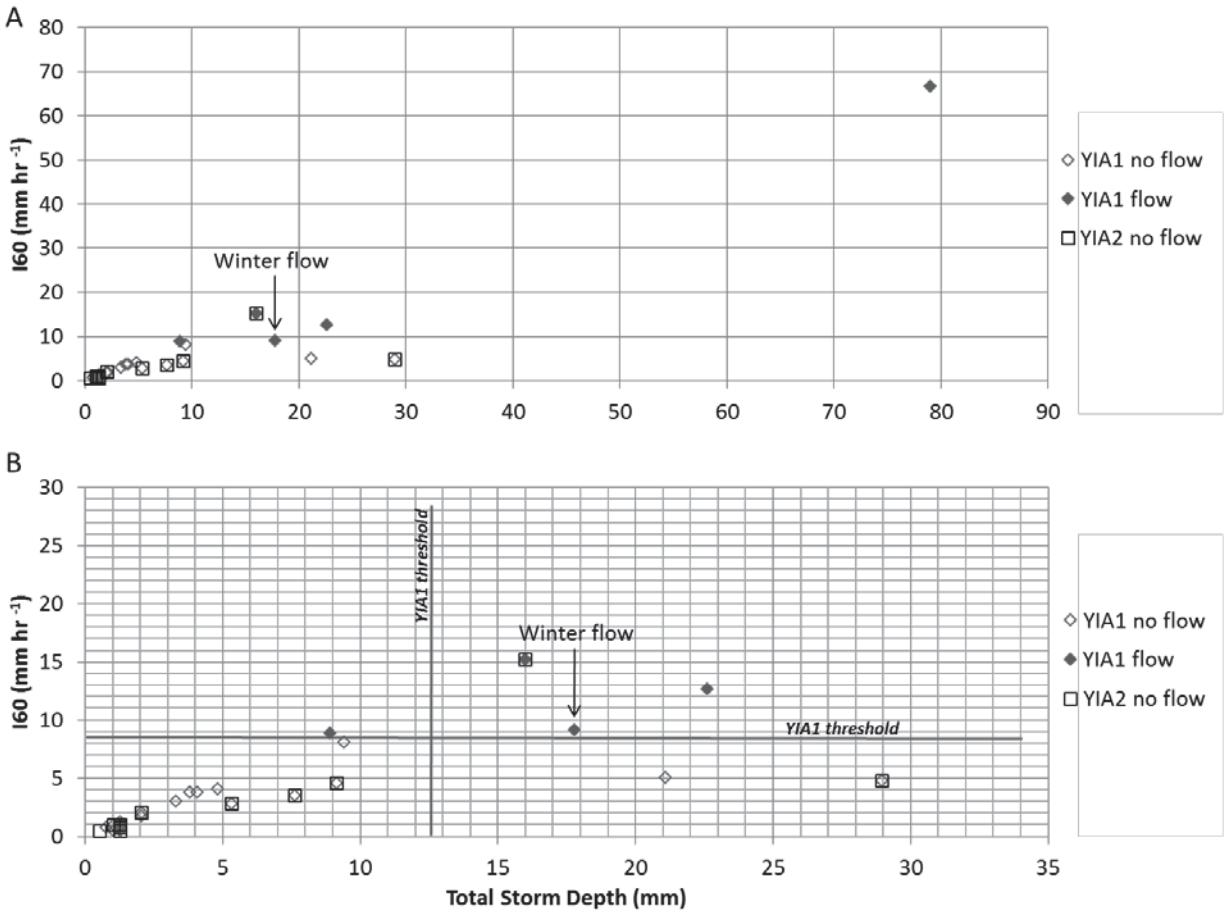

Figure 3-17. Incised Alluvium channels I60 vs. total storm depth of all storm events. Diamonds represent rain events at YIA1 and squares represent YIA2. Open symbols represent rain events that did not produce runoff, and solid symbols represent rain events that produced runoff at that site. (A) all rain events and (B) close-up around threshold.

Data for threshold analysis at incised alluvium channel types were more limited, with only one site analyzed producing flow. At this site, YIA1, the mean of the runoff producing, total depth threshold is 12.7 mm and the range is between 9.4-16.0 mm (Table 3-11 and Figure 3-17). The highest I60 of a no-flow producing rain event at YIA1 was 8.1 mm hr^{-1}, and the lowest I60 of a runoff producing rain event was 8.9 mm hr^{-1}, so the I60 runoff threshold at this site is estimated to be 8.5 mm hr^{-1} (Figure 3-13). This threshold accounts for all no-flow and flow events. This is the same threshold range as listed for YPH1, which used the YIA1 rain gauge in the threshold analysis.

YIA2 did not record flow. The largest total storm depth recorded was 29.0 mm, and the highest I60 recorded during a rain event was 15.2 mm hr^{-1}, which has a 2-year recurrence interval (Table 3-11). Both values are above the depth and I60 thresholds that would have produced flow at YIA1, so YIA2's threshold is different than that of YIA1. Figure 3-13 only shows the lower end of the threshold range for YIA2.

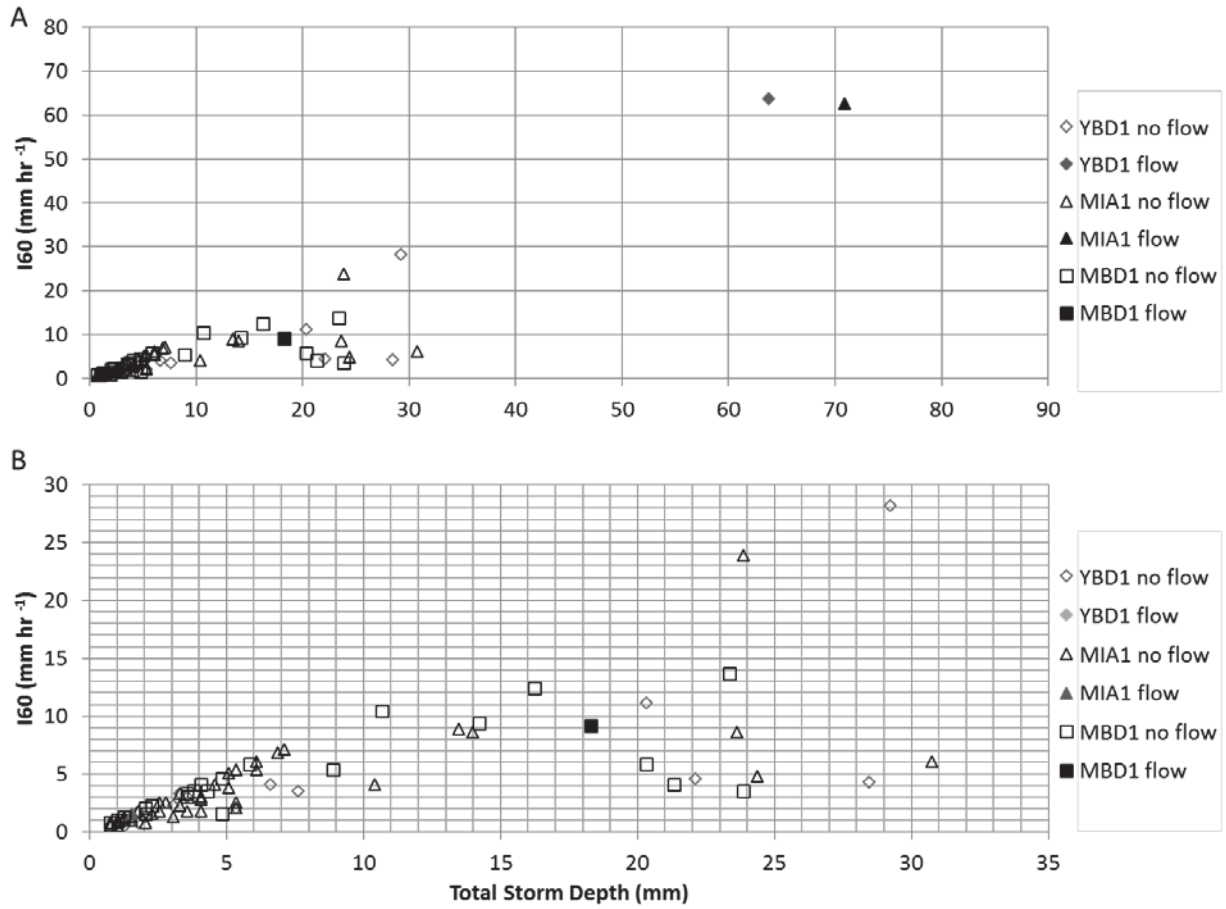

Figure 3-18. Braided channels I60 vs. total storm depth of all storm events. Diamonds represent rain events at YBD1, triangles represent MIA1, and squares represent MBD1. Open symbols represent rain events that did not produce runoff, and solid symbols represent rain events that produced runoff at that site. (A) all rain events and (B) close-up around threshold.

YBD1 and MBD1 only had one runoff event each in this analysis, and it occurred during the same rain event on 7/13/12 (Figure 3-11). The total storm depth at YBD1 during this storm was 63.8 mm, and the no-flow rain event with the next largest total depth rained 29.2 mm, creating the large and high range for the YBD1 total depth threshold (Table 3-11 and Figure 3-18). The mean of this depth threshold is 46.5 mm. At YBD1 the I60 runoff threshold mean, between the flow event with an I60 of 63.8 mm hr^{-1} and the highest no-flow rain event with an I60 of 28.2 mm hr^{-1}, is 46.0 mm hr^{-1}, which has a 50-year recurrence interval according to the NOAA atlas for Yuma Proving Ground station, site ID: 02-9654. At MBD1 the total depth runoff threshold is from the runoff-producing rain event with a total depth of 18.3 mm and the 16.3 mm total depth of the no-flow event. The mean of this total depth runoff threshold range is 17.3 mm. The I60 runoff threshold mean is 7.5 mm hr^{-1}, which has a recurrence interval of less than one year, and is between the flow producing event with an I60 of 9.1 mm hr^{-1} and the no-flow event with an I60 of 5.8 mm hr^{-1} (Table 3-11 and Figure 3-13). There were two flows at MIA1, and one of them was also during the large rain event on 7/13/12. The total depth runoff threshold range at MIA1 is between the large rain event's total depth of 70.9 mm and the next highest magnitude of a no-flow producing event with a total depth of 30.7 mm. The mean depth threshold is 50.8 mm. The I60 threshold range is between the large rain event's I60 of 62.7 mm hr^{-1}, which has a 100-200-year recurrence interval, and 23.9 mm hr^{-1}. The mean of the I60 threshold is 43.3 mm hr^{-1}, with a 50-year recurrence interval. The other flow event at MIA1 is below this threshold. The depth and I60 of that rain event at MIA1 were 1.5 mm and 1.5 mm hr^{-1}, respectively.

Discussion

Runoff thresholds

The range and mean of the five channel types' basin area size and the range and mean of the mean I60 threshold for each site is illustrated in Figure 3-19A and B, respectively. The overall trend of these plots shows that the mean I60 of a rain event to cause runoff increases with increased basin area for PH, BK, and BA channel types. The channel length increases with increased catchment area (Table 3-2), so this trend applies to channel length for these three channel types as well.

The range of basin area sizes for each channel type is narrow (Table 3-2 and Figure 3-19A). Both PH and BK channel types have small catchment areas, and the mean I60 of the runoff threshold range for these two channel types are similar. The range of I60 thresholds at each PH and BK sites are small, which increases the certainty that a rain event with an I60 above the threshold mean will produce runoff (Table 3-11 and Figure 3-13). BA sites are larger and have a higher I60 runoff threshold (Figure 3-19). The range for the I60 threshold at MBA1 is larger than the range at the PH and BK channels and at YBA1 (Table 3-11 and Figure 3-13). This is due to the lack of recorded rain events near the threshold at MBA1, which increases the uncertainty of the I60 threshold at this site (Figure 3-16). MBA2 did not have any flow events during the recording period. MBA2 is excluded from Figure 3-19B.

Even with the uncertainty of the threshold at MBA1 and no flow events at MBA2, the I60 thresholds increase with the log of catchment areas for the PH, BK, and BA channel types, but this relationship breaks down for catchments >3 km^2 (Figure 3-20).

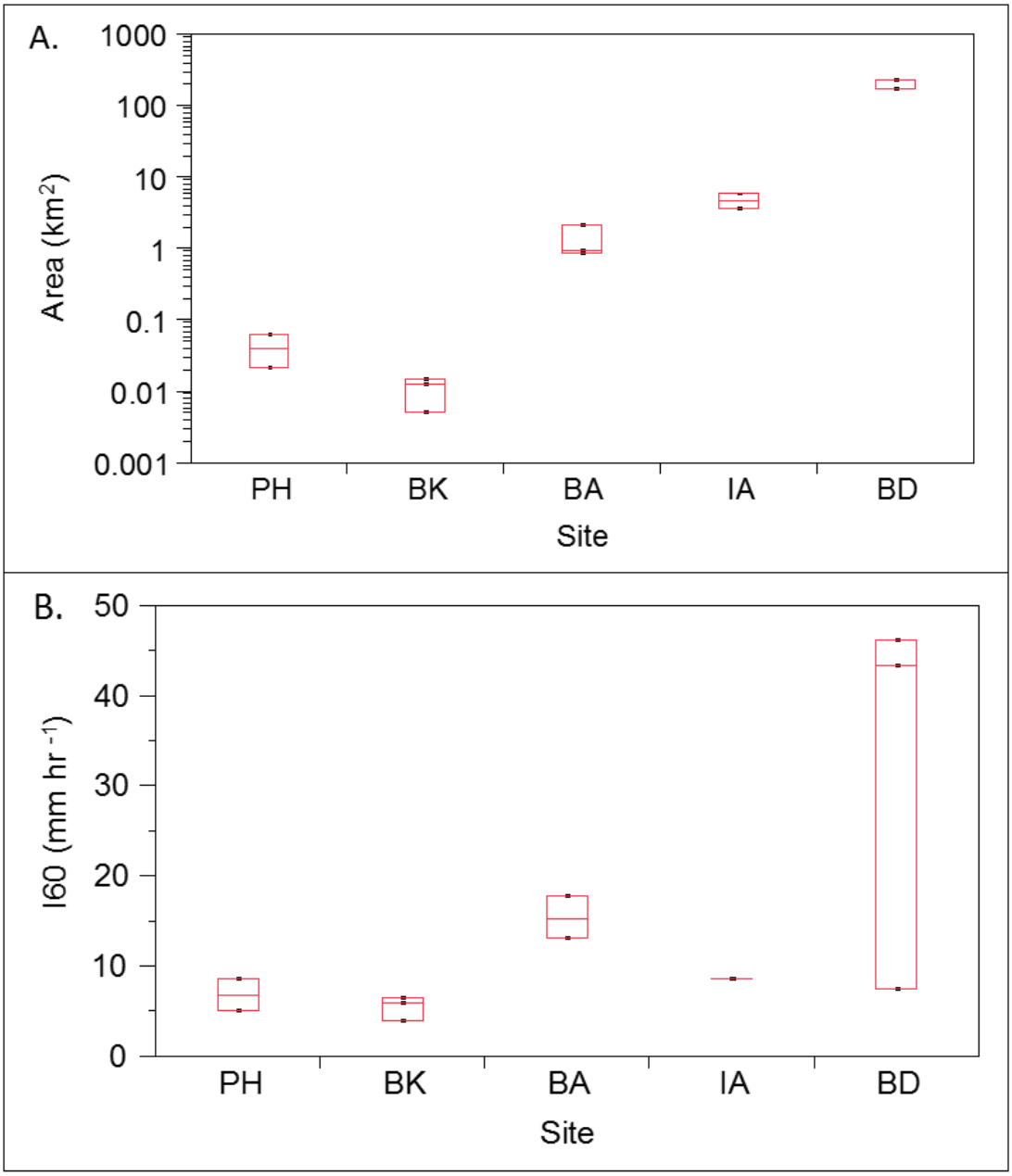

Figure 3-19. Box plots with data points of (A) basin area (y-axis in log scale) and (B) the mean of the I60 threshold range for all the sites analyzed in each stream type. There was only one IA channel site that experienced flow, so there is only one data point.

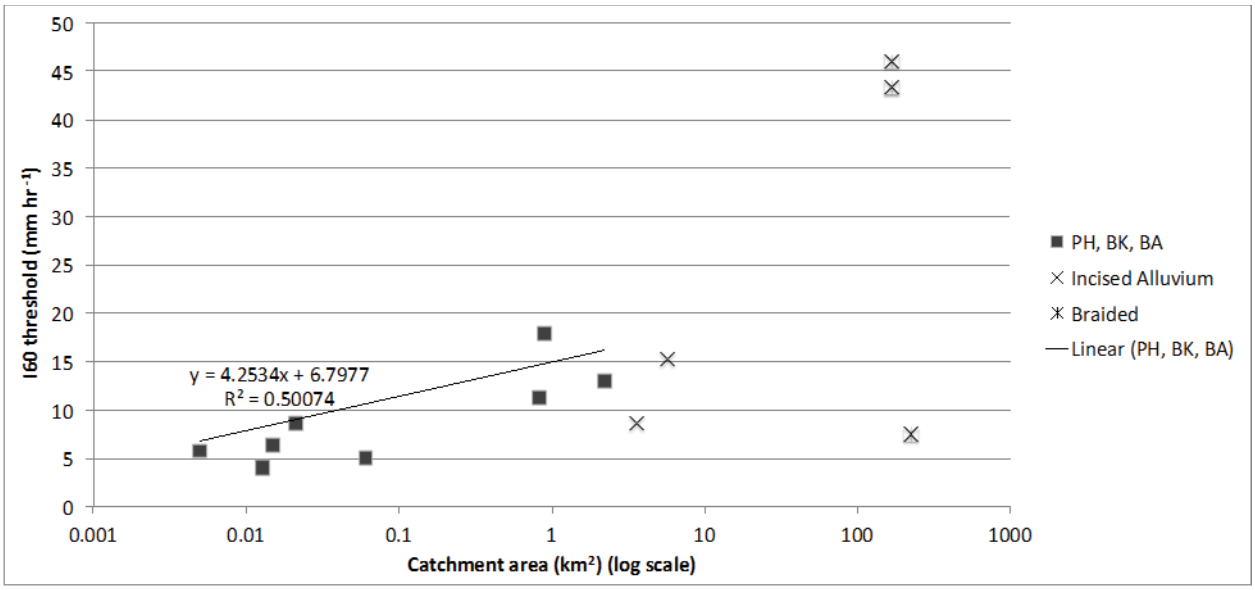

Figure 3-20. The I60 threshold mean of each site plotted against the site's catchment area. The X-axis is in log scale. PH, BK, and BA sites are plotted as one group (solid boxes) with a linear trend line illustrating the linear increase of the I60 threshold with a log increase of the catchment area for these channel types. IA (Xs) and BD (stars) channel types are plotted as separate groups.

Only one IA site, YIA1, had runoff, so there is only one data point in Figure 3-19.B for the IA channels. The other IA site, YIA2, did not have flow. The lowest I60 rain event at YIA1 to cause flow was much lower than expected for a channel type with this size of basin area if there is a linear runoff response relationship between catchment area and I60. The rain event with the lowest I60 to cause flow at YIA1 occurred on 8/17/12 and had an I60 of 9 mm hr^{-1} and a depth of 9 mm at YIA1. At the two upstream sites, YBK1 and YBA1, the I60 was larger and above the BK and BA I60 runoff threshold, and flow was recorded at both sites (Figure 3-11). The rain event had an I60 of 23 mm hr^{-1} and a depth of 23 mm at YBA1, which is 1.63 km away from YIA1, and at YBK1, 1.67 km away from YIA1, the rain event had an I60 of 19 mm hr^{-1} and a depth of 19 mm. YPH1, 1 km away, which uses the same rain gauge, also had flow, though it does not contribute to YIA1. Downstream at YBD1, there was also flow, though the rain gauge was not working, so this event is excluded from the runoff threshold analysis. The flow at YIA1 and YBD1 is probably due to inputs from upstream, where the rain event had a higher I60 and depth, and at YIA1 the inputs were probably also from surrounding piedmont surfaces that contributed more localized flows.

YIA1 has a PH tributary that contributes flow directly upstream of and on the same side of the channel as the pressure transducer (Figure 3-6). There were two flow producing rain events at YIA1 that did not produce flow 1.6 km upstream at YBA1. These events, which occurred on 12/13/12 and 8/22/13, had I60s of 9 and 15 mm hr^{-1} at YIA1, and I60s at YBA1 of 12 and 2 mm hr^{-1}, respectively. The I60s of the rain events at YIA1 were over the runoff threshold for the PH channels, and the 12/13/12 event was under the BA thresholds. YPH1, 1 km away, had flow during the 8/22/13 event, but the pressure transducer was not recording during the 12/13/12 event. YIA1 and YPH1 have the same I60 threshold (Table 3-11). Therefore the localized flow observed at YIA1 was more than likely produced on the piedmont surfaces and input directly to YIA1, making the threshold at YIA1 more representative of a PH threshold than an IA threshold.

The highest I60 rain event recorded at the YIA2 site was 15 mm hr^{-1}, and no flow was recorded at that site. A threshold at this site greater than 15 mm hr^{-1} would be consistent with the increasing I60 thresholds for this site's catchment area of 5.7 km^2. YIA2 does not have a PH channel contributing directly to the site, so its flow contributions are from further upstream at YBK2 and YBA2 sites and would be subject to transmission losses as flow moves downstream to this site. It is possible that catchment area differences, such as a different basin area, different permeability of bedrock types, different percentages of desert pavement, or vicinity to desert pavement

could be the reason there was no flow at YIA2, and the threshold is higher than at YIA1. The reason for no flow could also be that the rain gauge 1.4 km away did not record the correct precipitation characteristics for the YIA2 site. A rain gauge distance of 1.4 km may be too far away to give accurate information on precipitation within the contributing area.

The large threshold at YBD1 suggests that it takes a large rain event with a high I60 and depth in the watershed to produce flow this far downstream. The only recorded flow at YBD1 on 7/13/12 was produced by a rain event that had a high I60 and depth at all monitoring sites. The largest I60 and depth of this rain event was recorded at YBK1, which had an I60 of 70 mm hr^{-1} and a depth of 87 mm, and YBD1 recorded the lowest I60 and depth with an I60 of 64 mm hr^{-1} and a depth of 64 mm. There was flow at all monitoring sites during the recorded 7/13/12 runoff event and the runoff event on 8/17/12 when the rain gauge was not recording (discussed above), which suggest that in order for there to be flow at YBD1 the majority of the basin area needs a large enough rainfall to produce runoff that contributes to YBD1.

There was only one recorded flow at MBD1 on 7/13/12 (Figure 3-11). The rain event that produced the flow had an I60 of 9.1 mm hr^{-1} and a depth of 18.3 mm at MBD1. This rain event also produced flow in all the other monitoring sites that were working at the time. The I60 and depth was much greater at other sites. At MBA1 and MIA1 the I60 was 63 mm hr^{-1} and the depth was 71 mm. The low rainfall at MBD1 compared with the high intensity and depth in a large part of the contributing area illustrates the importance of rainfall in the contributing area for runoff production at this site.

MIA1, which is grouped with braided channels based on contributing area, had two flow events. One was the event on 7/13/12, and the other was on 9/5/12 (Figure 3-11). The I60 and depth for the 9/5/12 rain event at MIA1 was only 1.5 mm hr^{-1} and 1.5 mm (Figure 3-9). There was no pressure transducer at MBA1 (it had not been replaced from washing away during the 7/13/12 flow event), and the I60 and rainfall depth was only 5.8 mm hr^{-1} and 5.8 mm respectively, but subsurface water content data suggest that there was flow at MBA1. The MBA1 site is in a small tributary to MIA1, 0.4 km away from the MIA1 site (Figure 3-5). MIA1 has a large contributing area, and most of the basin is not instrumented with rain gauges. Because the flow contributed from MBA1 is unknown, and the rain at MIA1 was not enough to produce runoff on the piedmont, it is likely that the majority of flow was produced in the ungauged part of the basin. There was no flow and no rain at MBD1, so whatever runoff passed through MIA1 on 9/5/12 had infiltrated before reaching MBD1.

The BD channels have the largest basin area size and the largest runoff threshold range. This large range indicates a large uncertainty in the threshold, if it exists. Only a limited number of flow events were recorded at these sites, but from those recorded, it is clear that the flow does not respond solely to a local precipitation threshold. Occurrence of flow in both IA and BD sites depend largely on upstream inputs. With a larger record of flow events recorded by a dense network of rain gauges and pressure transducers, it may be possible to examine precipitation to define thresholds based on contributing area for larger contributing area channels if partial area coverage of storms are also considered in threshold analysis. Distribution of this study's rain gauges was not sufficient to do that, nor was there enough flow events to establish a threshold.

Runoff frequency

Runoff frequency logically should go up with smaller I60 thresholds, because the chance of a rain event with an I60 above a small threshold increases. This does seem to be the case, as there is a steady decrease in runoff frequency from PH to BK to BA. PH and BK sites have very similar thresholds, with PH sites having slightly larger catchment areas and higher thresholds. Higher I60 thresholds at PH sites should correspond with lower runoff frequency than at BK sites, but this pattern is not evident in Figure 3-6. It is possible that there are systematic differences in rain intensity characteristics between sites, as the bedrock sites tend to be at higher elevations. Another reason for the difference in frequency could be the time period that each site was active. YPH1 experienced the most data lose due to equipment failure, and a large percentage of data from 9/21/12 to 12/6/13 was lost. Also, YBK2 and MBK2 were installed in 3/30/13 and 2/9/13, respectively, compared to 11/12/11 for YBK1 and MPH1, and 3/14/12 for YPH1. YPH1 was active for a good portion of 2012 monsoon season but missed a large portion of 2013 monsoon season. YBK2 and MBK2 were active for the 2013 monsoon season but not the 2012 monsoon season. In Yuma Wash, there were four recorded flow producing rain events during the 2012 monsoon season, and only two during the 2013

monsoon season (Figure 3-9). In Mohave Wash, there were five flow producing rain events during the 2012 summer, and four during the summer of 2013. Therefore, PH sites having a larger runoff frequency than the BK sites could be due to the 2012 monsoon season having slightly more runoff producing rain events than the 2013 monsoon season, and two BK sites were active only during the 2013 monsoon season and one PH site was only active during the 2012 monsoon season.

The time that MPH1 and YBK1 were active does not explain why the PH sites had larger runoff frequencies than the BK sites, because they were both working most of the time between their installation until the end of the study, and they recorded roughly the same amount of rain events (Table 3-6). MPH1 had a higher runoff percentage than YBK1 due to two more flow events. The difference could be due to location. Mohave Wash, with a total of 12 flow producing rain events during the study period, had more flow producing rain events than Yuma Wash, which had nine (Figure 3-9).

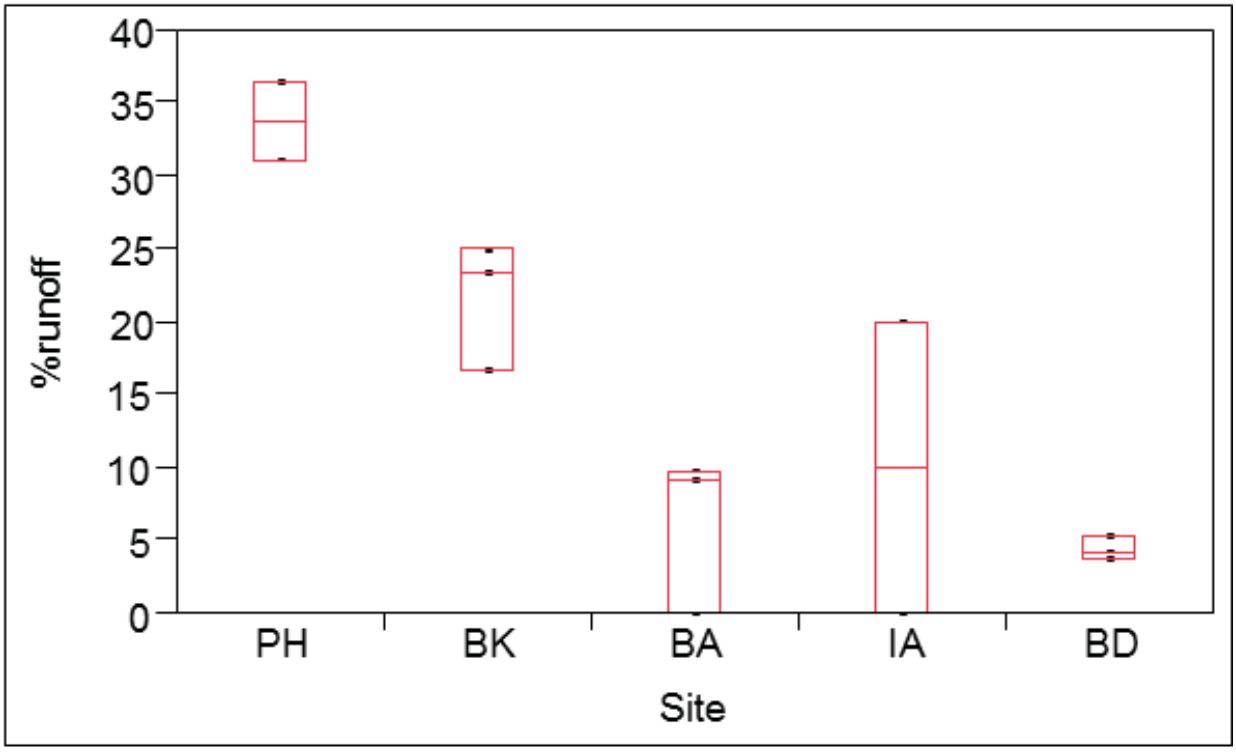

Figure 3-21. Box plots of percentage of rain events that produced runoff for each site grouped in the five channel types.

The BA sites had less frequent flows than PH and BK sites, and one BA site produced no flow (Figure 3-21). This lower frequency is to be expected because as the catchment area increases, stream length and channel width increases, which increases the amount of channel alluvium. The I60 threshold for runoff also increases. The increased amount of channel alluvium increases transmission losses by infiltration of stream flow. The decreased frequency is due to increased transmission loss with the increased channel length and width in increasingly larger catchment areas (Goodrich et al 1997; Simanton and Osborn, 1983). The increased I60 threshold is a reflection of this transmission loss, as well as a reason for the reduced runoff frequency. Due to the increased channel alluvium and channel width, the size of a storm in the headwaters must be larger to produce enough runoff to overcome the transmission losses accrued with the increased stream length on the way to the BA sites. The need for a larger storm reduces the potential frequency of runoff events in larger catchments.

The lack of flow at YIA2 and the decreased frequency at the BD channels are also due to the increased transmission loss of in channel flow. The large frequency range for the IA channels in Figure 6.3 is due to YIA1 having a 20% runoff frequency. This larger than expected frequency for an IA channel is due to the flow contributions from the

previously mentioned tributary PH channel upstream of the pressure transducer. The three BD channels have a low runoff frequency and a small frequency range.

Uncertainty

Minimum Inter-event Times (MIT)

Different minimum inter-event times (MIT) were tried in the rain event separations before 7 hours was selected for the final analysis. Increasing the MIT can lump multiple storms and reduce the number of rain events. The effects of MIT choice are most evident for small watersheds, where flow responds quickly to rain. At MPH1 a total of 35 rain events were recorded with an MIT of 2 hours, resulting in 229 mm depth of rain and 11 flow events. This gave a 31% flow frequency for the recorded time period. When the MIT was changed to 7 hours the total depth of rain increased to 231 mm because discarded rain events less than 0.5 mm with an MIT of 2 hours were lumped with other rain events when the MIT changed to 7 hours. With the increase in MIT the total rain events decreased to 29 due to the lumping. The number of runoff events decreased to 9 because there were 2 rain events over 2 hours apart, but less than 7 hours apart on 7/13/2012 and 9/11/2012. These 2 rain events caused 2 distinct runoff events on both dates at MPH1. However, with the 7-hour MIT the rain events were lumped, and therefore the 2 runoff events were connected to one rain event. The percentage of runoff to rain events remained the same because one rain event and one runoff event were lost to the analysis. The depth threshold changed with an MIT of 2 hours because the lowest depth to produce flow was 7.4 mm with an MIT of 2 hours and went up to 8.9 mm when the MIT was increased to 7 hours. The lowest I60 to produce flow was 4.1 mm hr^{-1}, which did not change with a change in MIT. Since winter storms are usually long duration, low intensity storms, longer MITs can change the number of winter storms. It is possible that there should be a shorter MIT for the summer than for the winter, since these storms are so different in duration and intensity.

The percentage of runoff events to rain events can slightly change with a change in MIT. At YBK1 an MIT of 2 hours gave 32 rain events, and with an MIT of 7 hours there were 30 rain events. There were 7 runoff events regardless of MIT, which produced a runoff to rain event percentage of 21.9% for an MIT of 2 hours and 23.3% for an MIT of 7 hours.

Winter storm effects

Winter storms produced runoff at MPH1, YBK1, YBK2, and YIA1 (Table 3-7). BA and BD sites did not have winter flow, and with the exception of the one winter flow at YIA1, which was from local contributions to the channel from the surrounding piedmont surfaces, all other winter flows occurred in the headwater channel types. MPH1 and YBK2 had the highest percentage of winter storms causing runoff events, and these two sites are the only sites for which the precipitation depth metric was the only best choice for the runoff threshold (Table 3-9). The depth metric better accounts for the large total depth and low intensity rains of the winter months and is a better metric for runoff thresholds in winter storms in headwater channels.

While winter rain events help determine the threshold range at some headwater channels, they create false positives and false negatives in threshold analysis as well. The large depth of winter storms decreases the I60 necessary for runoff production at headwater sites. In some cases this can cause a runoff-producing winter storm to create a false negative in an intensity threshold analysis. Determining an intensity threshold can be complicated by winter storms if the intensity of a runoff producing winter storm is just below a no-flow monsoonal storm near the intensity threshold. Using the winter storm's I60 for the threshold causes the monsoon storm to be a false positive, but using the monsoon event's I60 causes the winter storm to create a false negative. Though the depth metric was better for winter storms, it is possible that no-flow winter storms can cause false negatives because of their large depth when compared with low depth, runoff-producing monsoon storms. In headwater channels seasonal metrics could help identify more accurate precipitation thresholds.

Lag times

The lag between the rain event peak and the flow peak is due to multiple factors, including the distance between pressure transducer and rain gauge, the speed and direction of rain events, the speed of the flow downstream, and the runoff response time to precipitation. The flow response to water inputs at BK and PH channels is rapid, since overland flow develops quickly on the low permeable bedrock and piedmont surfaces. The headwater sites' flow response to the rain event on 7/13/12 (Figure 3-12) is a good example of how the combined movement of storm cells and runoff can affect interpretations of runoff responses. YBK1, which had a rain gauge on-site, had the smallest lag time, around 10 minutes, showing the quick runoff response at headwater channels. Both flows at MPH1 occurred around an hour before it rained at the closest rain gauge 1.5 km away at MBD1. The flow at YPH1 peaked around 15 minutes before the peak rain at its rain gauge at YIA1, only 1 km away. The flow occurring at these two PH sites before it rained at their nearest rain gauge shows the importance of having a rain gauge on-site in order to measure runoff response times. The lag times for these sites (Table 3-8) is a combination of the actual runoff response time, the speed and direction of the storm cell, and the distance to the rain gauge. Also, since the response time at these headwater sites can be less than 15-minutes, a temporal resolution greater than 15-minutes is necessary to determine actual lag times.

The lag times for flow events at sites with large catchment areas do not clearly illustrate the time it takes for runoff from a rain event to produce flow in that location. Storm speed and direction and channel flow speed contribute to the recorded lag time. The 7/13/12 flow event at MBD1 and YBD1 are examples of this. The peak flow moved faster than the storm at MBD1, and at YBD1 the storm core moved faster than the flow (Figure 3-12). The rain gauge and pressure transducer network in this study is not dense enough to decipherer the lag time caused from the accumulation of runoff verses the travel time of the storm, so it's not possible to determine if the two watersheds have a fundamentally different lag time behavior. To understand lag time at the sites with larger catchment areas it is necessary to have high spatial resolution of both rain and runoff.

Conclusions

Precipitation thresholds for runoff generation are best defined for watersheds <3 km^2, where rain intensity thresholds increase with the log of the catchment area. For larger catchments, spatial variability of storms in the contributing area means that thresholds are not well defined. Wide channels with large catchment areas can still experience small flows from low intensity rains if a headwater tributary contributes water directly into the channel near an observation location. However, this flow may not fill the whole width of the channel, and may not travel very far down stream due to channel bed transmission loss. Besides some uncertainty with PH and BK runoff frequency, flow frequency increases with smaller I60 thresholds and decreased catchment area.

Although storm depth and intensity varied across the watershed, and rain event durations were short, usually between one and four hours, runoff-producing rain events usually affected the entire study area. Only one of these runoff-producing rain events led to runoff throughout the study channels; all other runoff events were localized, only in one or two sites.

All four precipitation metrics – depth, I15, I30, and I60 – had an accuracy of at least 95.5% at identifying a runoff threshold. Overall, I60 was found to be the best metric at predicting runoff. However, winter storm runoff thresholds were not always represented accurately with the I60 metric. At headwater channels, where runoff can be produced by winter storms, the depth metric, which does better with the long duration, low intensity winter storms, sometimes worked better. For small headwater channels, identifying runoff-producing events for precipitation thresholds may require different metrics for the two seasons: depth metric for winter rain events and I60 for summer rain events. The event definition used can also affect the threshold depth and flow frequency in small watersheds. Winter and summer rain events are so different that using a shorter minimum inter-event time (MIT) in the summer and a longer MIT in the winter might be more appropriate.

To accurately understand the connection between rain events and runoff events, a dense network of rain gauges and flow monitoring devices with high temporal resolution are needed. Rain gauges on-site reduced uncertainty in lag times and showed that lag times at sites with small watersheds were short, less than half an hour. Rain gauges are necessary at channel types with small watersheds in order to understand lag times. Understanding lag times in larger channels is difficult because of the storms movement and channel flow. Densely spaced rain gauges, greater than

one gauge per 1.5 km used in this study, and more with elevation change, are needed to capture storm movement. Without densely spaced gauges, it becomes problematic to identify precipitation characteristics associated with channel flow in small channels and to distinguish how flow responses in large channels relate to spatial variability of rain versus speed of flow through channel. Because of the rapid response, fine temporal resolution is needed for recording both precipitation and stage. The 15-minute resolution in this study was too coarse to capture the dynamics of these events.

While precipitation thresholds do not indicate runoff magnitude in ephemeral channels, they can be important tools for predicting flow in these systems, where measurements of stream discharge are rare and difficult to obtain. Advances in radar observations of rain patterns can be linked with runoff thresholds to identify when and where flash floods are likely to occur. The thresholds can also help to understand how flow frequency will be affected by changes of storm intensities due to climate change. This in turn can help predict the change in water regimes and plant available water in these ecosystems.

Chapter 4. Subsurface moisture dynamics beneath ephemeral stream channels

Abstract

In arid regions, ephemeral stream channels are important sources of groundwater recharge and moisture for riparian vegetation. This study examines the moisture regime in the alluvium of ephemeral stream channels in the Sonoran Desert, Arizona, USA. Moisture measurements were collected over a three-year time period in the alluvium below six channels with varying precipitation and depths of alluvium. All of the channels are filled with coarse alluvium composed primarily of sands and larger particles, with some locations also having localized layers of fine sediment at 2-3 m depth. Changes in moisture were greatest during infrequent summer flow events, which led to pulses of saturation that percolated rapidly through the channel alluvium. Saturation persisted in the alluvium for less than two days, except where fine sediment layers led to a perched water table that persisted for up to a month after flow. Rain events with >10 mm depth were almost all associated with a moisture response even if there was no channel flow, but moisture responses to rain events were not detected at depths greater than 1 m, whereas channel flow percolated beyond 3 m depth within hours after flow. After rain and flow events, moisture subsided rapidly due to low water retention in the alluvium, followed by a more gradual drying when volumetric water contents dropped below around 0.1. These rates of drying were higher in summer than in winter, leading to a subtle seasonal difference in average moisture, with summers drier than the previous winter. Throughout the three years of study, the sites experienced a gradual wetting trend, as a dry summer the first year was followed by two wet summers. The study sites each had different precipitation and alluvium depths, but because of the rapid percolation of water during flow and low water retention of the alluvium, the moisture conditions appeared unrelated to these broad site characteristics. Instead, site to site differences in moisture regime are limited, except where layers of fine sediments impede deep percolation.

Introduction

Ephemeral stream channels in arid regions are important sources of groundwater recharge (Renard et al. 1964), and they are hot spots of biodiversity relative to surrounding uplands (need reference). Both direct rain on the normally dry channel beds and episodic flow events can contribute moisture to the subsurface along ephemeral stream corridors. Hydrologic research in these types of streams have focused on how the streams transmit water during flow, quantifying infiltration rates into channel bed sediments (Blasch et al. 2006), groundwater recharge rates (Izbicki et al. 2000; Stonestrom et al. 2004), and transmission losses as flood waves travel through the channels (Knighton and Nanson 1994; Costelloe et al. 2003). Fewer studies have addressed the long-term dynamics of subsurface moisture in ephemeral channel beds between flow events. Rain falling on surfaces outside of channel corridors in arid regions may never recharge groundwater (Small 2005 and articles cited), and a result plants in arid uplands may rely primarily or exclusively on shallow soil moisture, with the timing and type of rain event affecting plant response (Reynolds et al. 2004). This research aims to study the dynamics of moisture in the alluvium of ephemeral channels during episodic flow events, rain events that do not generate channel flow, and drying periods between rain events as a means of characterizing controls on the moisture regime within these systems.

Study site

The study area is in southern Arizona, USA in the Sonoran Desert. The mean annual precipitation in this area is only 94 mm at the Yuma Proving Ground weather station, making it hyper-arid. Precipitation tends to fall either during the winter (November – February) during frontal or cutoff low pressure systems or in the summer during the North American monsoon (June – September), with dissipating tropical cyclones also sometimes contributing precipitation in September – October (Pool 2005). At the Yuma Proving Ground weather station, the months of highest precipitation on average are December-February and August-September.

Study sites are nested within two watersheds, Mohave Wash and Yuma Wash (Figure 4-1). Six channel sections were selected for subsurface moisture monitoring based on the geomorphic channel classification of Sutfin et al. (2014), who identified five channel types in this region. Headwater channels were classified as either bedrock or piedmont headwater channels, which do not have alluvium stored in the channel bed. Higher order ephemeral channels all contain stored alluvium in the channel bed, and these are the channel types examined in the subsurface moisture study. The smallest of these channel types is bedrock with alluvium (BA), which is bounded on either side by bedrock but has alluvium within the channel bed. Further downstream channels incised into old alluvium are

called incised alluvium (IA) channels. The largest main channels in each study watershed are braided (BD) channels.

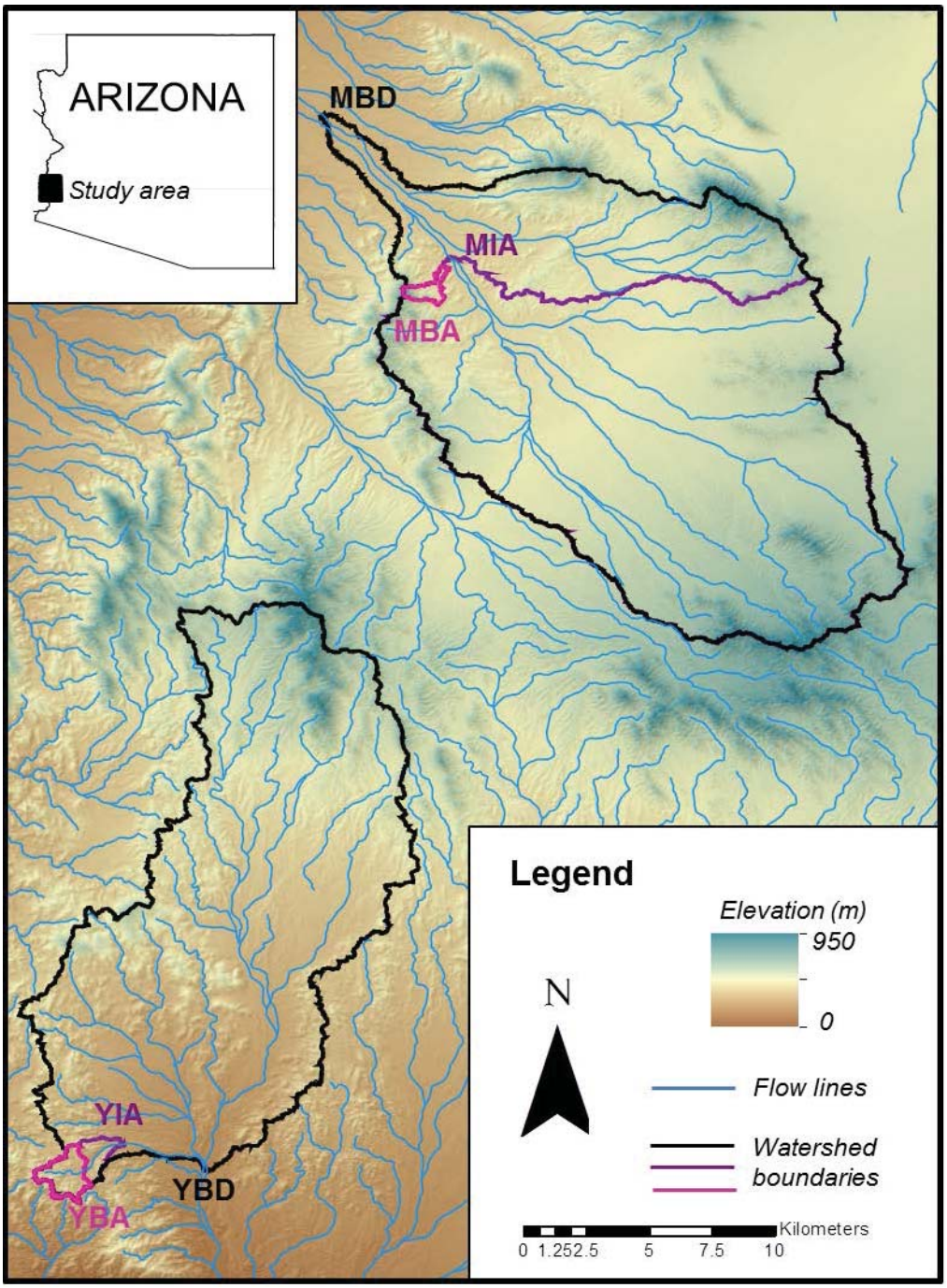

Figure 4-1. Location of study watersheds within Arizona. Watershed boundaries are shown in black for braided sites (MBD, YBD), purple for incised alluvium sites (MIA, YIA), and pink for bedrock with alluvium sites (MBA, YBA).

Methods

Instrumentation and site characterization

To examine how rain events, flow events, and drying between events affects moisture dynamics in these different types of ephemeral streams, we set up a network of precipitation, stream stage, and subsurface moisture sensors in BA, IA, and BD channel types in both Mohave (M) and Yuma (Y) Wash for a total of six channel locations (Figure 4-2). Most sensors except those in the deep subsurface (Table 1) were installed in early 2011 and remained in place until May 2014, giving approximately 3 years of record. Each monitoring location ahad a Texas Electronics TE525 tipping bucket rain gauge for recording precipitation and an In-Situ Inc. Rugged TROLL 100 pressure transducer for recording streamflow stage. The pressure transducers were un-vented and had to be corrected for barometric pressure fluctuations using In-Situ BaroTROLL loggers installed in each watershed.

To track shallow subsurface moisture responses to rain and channel flow, Delta-T Devices Ltd. SM300 soil moisture and temperature sensors were installed in hand-dug pits at depths of 10, 20, and 50 cm in all study sites. At IA and BD sites, deeper trenches were also dug with a backhoe, and sensors were installed at greater depths (Table 3-1). For all sites except YBA, which is bounded entirely by bedrock, additional SM300 or SM150 soil moisture sensors were installed in the vegetated floodplain outside the main channel at depths of 10, 20, and/or 50 cm. Sensors were installed horizontally into an undisturbed face of the pit or trench, and the holes were then backfilled with the excavated material. Standard calibration equations for SM300 and SM150 volumetric water contents (VWC) produced negative VWC values in dry conditions for many of the sensor locations. Therefore, a 5-gallon sample of alluvium was also used to develop calibrations for the SM300 and SM150 VWCs. Beginning with initially dry samples, raw readings were recorded for the sensor, and the VWC was determined by oven-drying a known volume sub-sample of the material. Water was added to the sample gradually, each time attempting to mix the added water throughout the sample. At each incremental addition of water another moisture reading was collected, and VWC was determined through oven-drying. This process continued until the samples were fully saturated, and the resulting sensor – VWC data were used to create a calibration curve.

To characterize the texture of the alluvium at the monitoring locations, we collected samples from trenches at approximately 50 cm depth increments. These samples were sorted in sieve shakers to derive particle size distributions.

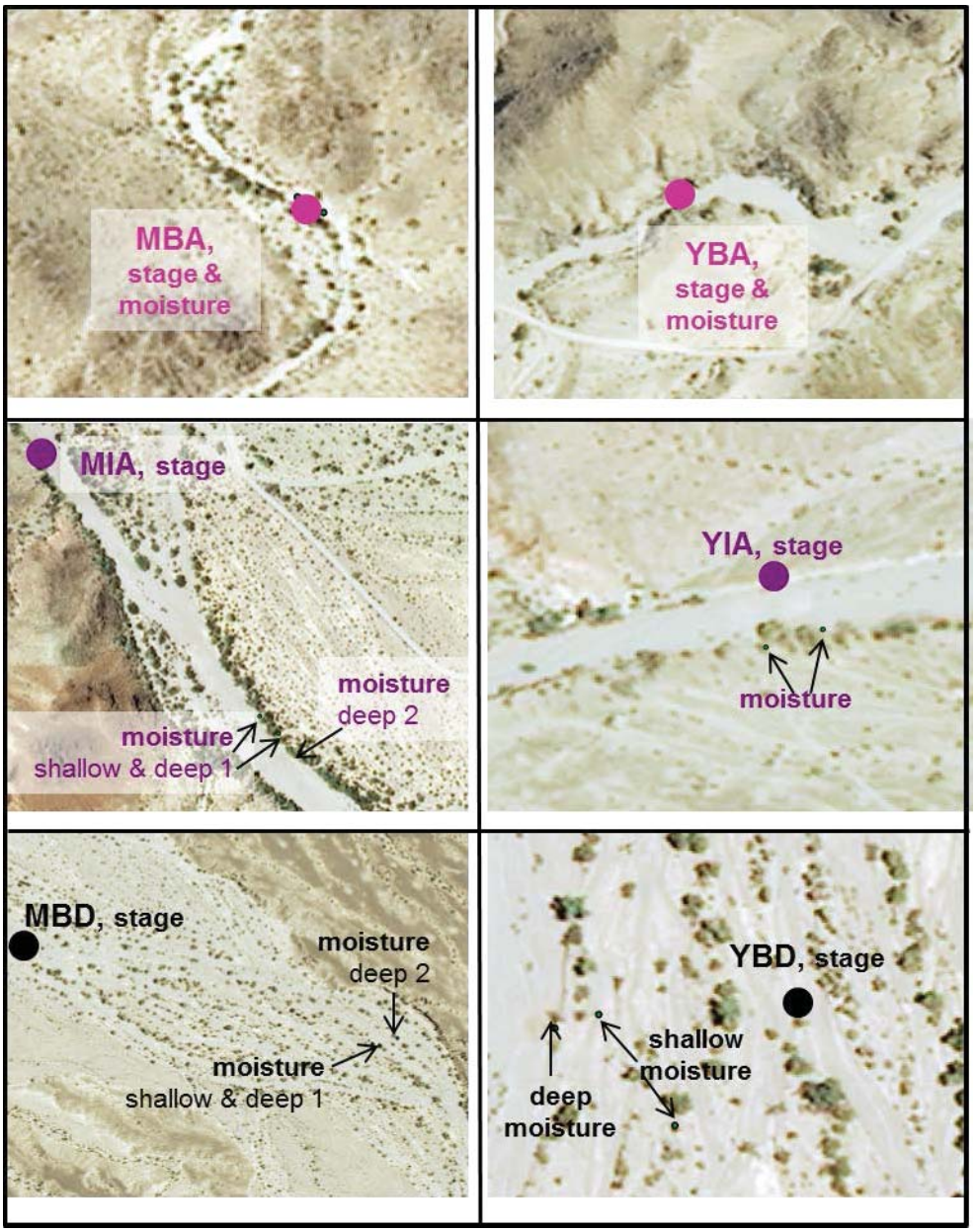

Figure 4-2. Aerial images of study sites from NAIP (give details) showing locations of pressure transducers (stage) and soil moisture sensors. The moisture sites labeled "shallow" have sensors in the top 50 cm of alluvium; the deep locations have moisture sensors installed in trenches dug either in winter 2011-2012 (deep 1) or May 2013 (deep 2).

Table 4-1. Depths (cm) of SM300 sensors installed at each study location. For deep channel locations, date of installation also indicated

Site	Channel, shallow	Channel, deep	Floodplain
MBA	10, 20, 50		10. 20
MIA	10, 20, 50	80, 195, Jan 2012 85, 200, May 2013	10, 20, 50
MBD	10, 20, 50	70, 180, 300, Jan 2012 100, May 2013	10, 20, 50
YBA	10, 20, 50		
YIA	10. 20. 50	110, 280, Nov 2011 100, 200, May 2013	20, 50
YBD	10, 20, 50	100, 200, 300, May 2013	10, 20, 50

Analysis

To examine moisture response to rain events, flow events, and to drying between events, we evaluated the data over both seasonal and event time scales. Precipitation totals were calculated by season for each rain gauge and for the Yuma Proving Ground long-term weather station (National Climatic Data Center). Following Hallack-Alegria and Watkins (2006) and Faulconer et al. (in prep), the record was divided into winter and summer seasons, with winter lasting from November-April and summer from May-October. For days with data loss at a rain gauge, missing precipitation values were estimated as the average of the precipitation at the two stations closest in elevation. We also divided precipitation records into rain events using the Rainfall Intensity Summarization Tool (RIST) developed by the United States Department of Agriculture Agricultural Research Service. Separate rain events were separated by a minimum inter-event time of 7 hours. To ensure that each event analyzed was a precipitation event and not spurious tips of the rain gauge, only events with more than two tips (>0.5 mm) were considered in data analysis.

To determine whether rain events were also associated with flow, we used pressure transducer records. Pressure transducer values after barometric pressure correction were noisy, and the reference values during no-flow conditions were not consistently at a pressure level of 0. Generally any changes in stage values that were less than 1 cm relative to the reference value were indistinguishable from noise. Therefore, to identify flow events, we calculated cumulative frequency distributions of stage values to identify the highest stages recorded. These high stage values were examined for hydrograph features and for correspondence with rain events to verify whether or not they represented channel flow. Once flow events were identified, the pre-event stage was set to zero, and stages during flow were adjusted relative to the reset base stage. For each flow event identified, we documented the start time of flow, lag from peak precipitation to peak flow, total flow duration, and peak stage.

Next, to examine moisture patterns during events and between seasons, we screened the moisture data to remove errors. Soil moisture readings would sometimes drift, possibly when the sensors lost good contact with the alluvium. Periods of drift in a sensor were identified where the VWC values of the sensor diverged from those of other sensors. We removed any time periods where a sensor drifted or had other evident data errors from the record. With the remaining data, we examined VWC values for each rain event and documented the presence or absence of a moisture response at each measurement depth. Similarly for each rain event, we noted the presence or absence of flow in the stream channel, as determined from pressure transducer data. Where pressure transducer data were missing, some events were classified as potential flow events if they produced saturation in the channel alluvium. For any flow events that led to saturation in the channel alluvium, we recorded the time of saturation onset and total duration of saturation.

To evaluate seasonal moisture pattern, we produced two moisture datasets, the first including all measurements remaining after screening for errors and the second including only moisture values during dry time periods. The dry time period dataset excluded days with rain and the subsequent two days. For both complete and dry period datasets,

we then compared both average VWC values and ranges of VWC values between measurement sites, depths, seasons, and position beneath channel or floodplain.

Results

Site characteristics

All study channels contain coarse alluvial sediments, and at most locations more than half of the sediment by mass is gravel size or larger (> 2mm diameter; Figure 4-3). Field interpretations during trench digging at each site suggest that the upper 0.5-0.8 m of sediment is active alluvium that is reworked during flow events. Active alluvium is loose and uncemented, whereas deeper alluvium shows varying degrees of cementation. Bedding patterns are also different for active and older alluvium.

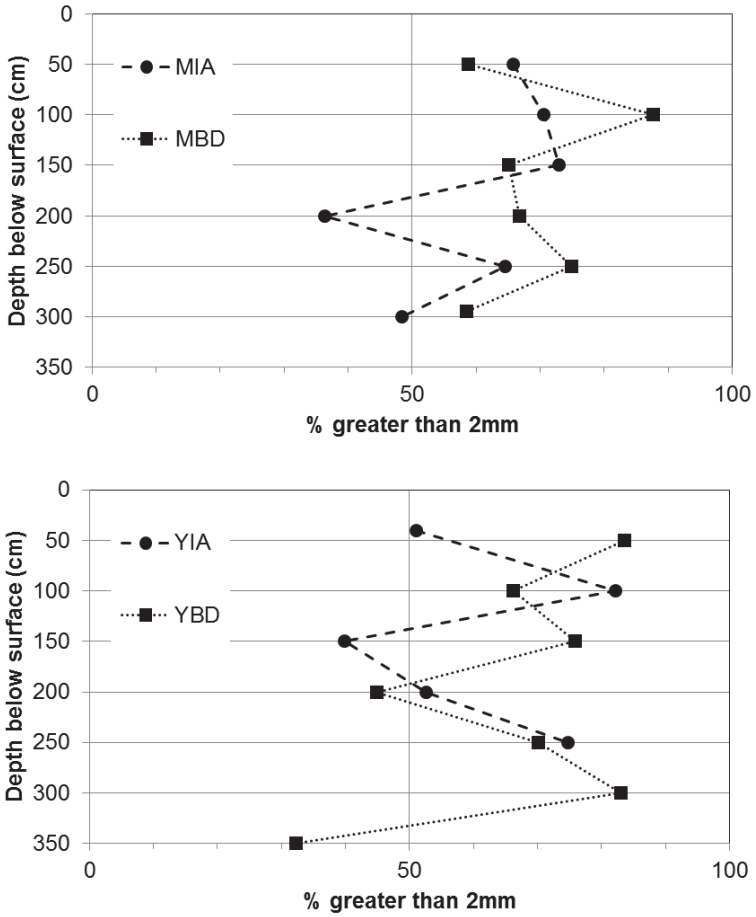

Figure 4-3. Depth distribution of alluvium texture for samples collected from trenches dug in May 2013.

The incised alluvium (IA) sites have deeper alluvium, with an estimated depth of XX at MIA and XX at YIA. In both watersheds, the alluvium is mostly coarse-textured (Figure 4-3), but field interpretations during trench digging highlighted a layer of finer compacted sediments at around 200 cm depth at the MIA site. This layer was present in the January 2012 trench (Figure 4-4), another adjacent trench dug in October 2012 trench, but not in a trench approximately 30 m upstream that was dug in May 2013, suggesting that the fine materials deposited at depth in this channel are not continuous along the channel. While there are variations in alluvium texture at the YIA site (Figure 4-3), no sharp texture break was noted in field interpretations of trench stratigraphy for that site.
The braided (BD) sites likely have the deepest alluvium, estimated at XX. At MBD, a layer of fine compacted sediments similar to the layer identified at MIA was identified at approximately 250-300 cm depth in the January 2012, October 2012, and May 2013 trenches, which were all dug adjacent to one another, but in the May 2013

trench, the layer was only evident on the northern side of the trench, not the southern side. A separate trench dug in May 2013 in a separate branch of the braided channel about 50 m north of the other trenches encountered a fine layer of sediments at 110 cm depth, again showing heterogeneity in fine sediment layers across the channel. At YBD, no sharp texture break was noted in field interpretations, with all layers representing coarse alluvium.

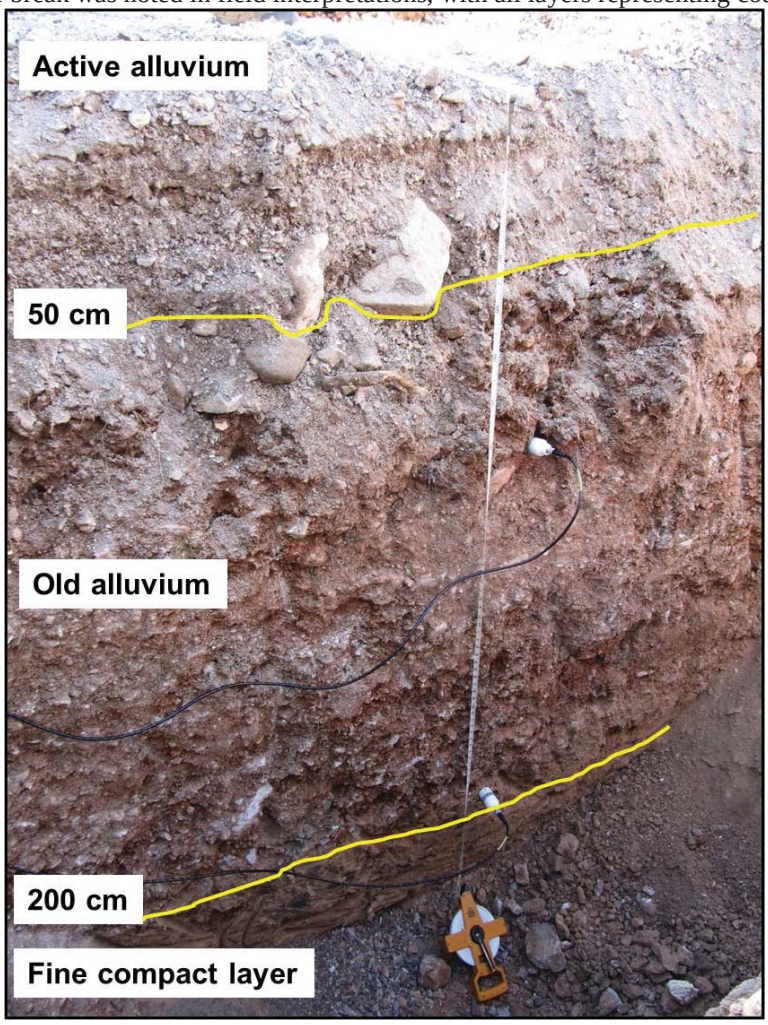

Figure 4-4. Upstream face of trench at MIA site dug in January 2012. SM300 sensors are shown at 80 and 195 cm depth, with the deeper sensor just above a finer, more compact layer of sediments.

Precipitation

The three years of study had below average precipitation at the Yuma Proving Ground meteorological station (Table 4-1), where annual average precipitation is 94 mm, with 40 mm on average during summer (May-Oct) and 54 mm in winter (Nov-Apr) (wrcc, 1958-2010). The first summer (2011) was exceptionally dry, with only 8-18 mm of precipitation, but the second summer (2012) was wetter in the study watersheds, with around three times normal precipitation, 113-139 mm on average. Mohave wash tended to have higher precipitation than Yuma wash as a result of higher elevations overall. Precipitation totals increase with elevation from a minimum at the YBD site at 115 m elevation to a maximum at the MBA site at 280 m elevation (Figure 4-5). Missing data for the first summer and winter seasons at YBD site lead to greater uncertainty in precipitation totals at that location.

Table 4-2. Average precipitation by watershed during study time period compared to the Yuma Proving Ground (YPG) weather station at 99 m elevation.

Season	YPG P (mm)	Mohave P (mm)	Yuma P (mm)
Summer 2011	17	18	8
Winter 2011-2012	41	58	42
Summer 2012	27	113	135
Winter 2012-2013	29	54	47
Summer 2013	38	79	46
Winter 2013-2014	31	36	33

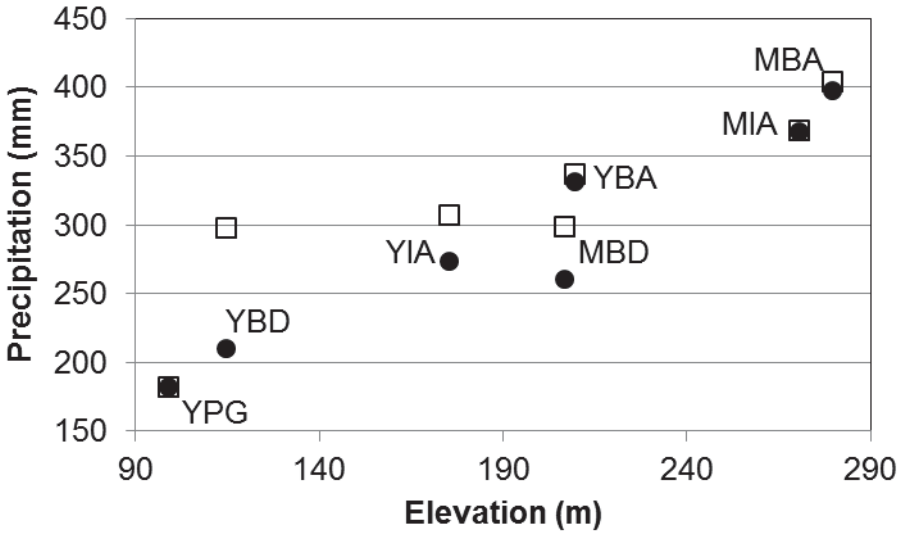

Figure 4-5. Total May 2011 – April 2014 precipitation vs. rain gauge elevation. Filled circles are raw precipitation totals for each station, and open squares are gap-filled precipitation totals, with gaps for each station filled using the average precipitation from the two other stations closest in elevation.

Over the three-year time period, the six sites reported between 21-54 rain events with >0.5 mm total depth. The largest event at all sites except MBD was on July 13, 2012, when the sites received between 18-86 mm of rain. The minimum rain during this event was at MBD, and all other sites had >60 mm of rain. According to the NOAA atlas precipitation frequency tables for the Yuma Proving Ground weather station, events with 24-hour magnitudes between 60-86 mm have a recurrence interval of 10-50 years.

Moisture patterns

All events

Subsurface moisture responded to fewer than half of the rain events analyzed. Sensors at 10 cm depth were the most responsive, with 43% of all rain events leading to a moisture increase. Deeper sensors responded to fewer events (Figure 4-6) both within the channels and the floodplains. A greater fraction of events reached 20-50 cm in the channel than in the floodplain, where only 10% of all rain events reached 50 cm depth. Of the events recorded, only 11% were associated with to channel flow. During flow events, moisture response tended to reach deeper below the subsurface, with a moisture response recorded at all sensors in the top 110 cm of soil for all but one flow event (89% of flow events). This one flow event was recorded in the pressure transducer at YIA on 8/22/13, with a peak stage of 12 cm. The moisture response at shallow depths during this event was minimal, suggesting that the flow may not have passed over the location of the moisture sensors. Where flow events were in channels with deeper sensors, moisture reached the 180-200 cm depth range for all flow events recorded and reached the 280-300 depth range for

75% of the flow events recorded. In contrast, no rain events without channel flow had a moisture response at 180 cm or greater, with only 3% of these no-flow rain events reaching the 70-110 cm depth range.

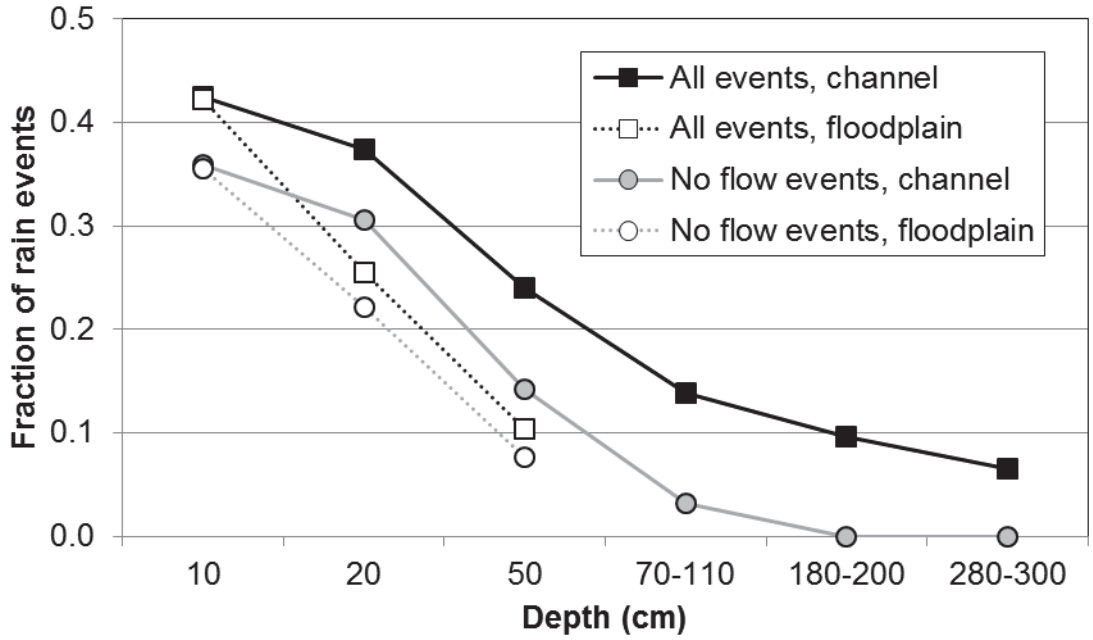

Figure 4-6. Fraction of rain events leading to an increase in moisture at each depth or depth range for moisture sensors below the active channel bed and sensors in the floodplain. Rain events are all events > 2 tips, or 0.5 mm.

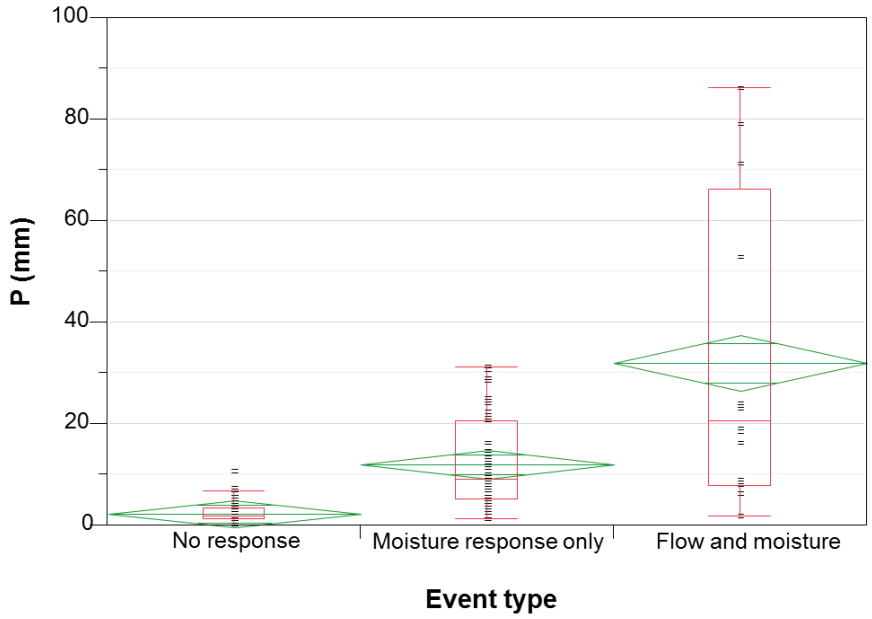

Figure 4-7. Box plot of precipitation magnitudes for all precipitation events > 2 tips (0.5 mm) that either produced no evident moisture response, just a moisture response without channel flow, or both a moisture response and channel flow response. Green triangles show the mean and 95% confidence interval.

Flow events

Flow events recorded by pressure transducers at the study sites ranged in duration from less than 15 minutes up to 33 hours, after a long duration (>4 hour) storm on September 6, 2013 at the MBA site (Table 4-3). Excluding this

one long duration event, the average flow duration was 2 hours. The lag time between peak precipitation and peak stream stage averaged 0.75 hours, ranging from less than 15 minutes up to 14 hours at the YIA site during the large 7/13/12 event. Peak flow stage ranged from 2-177 cm for the events recorded. The 7/13/12 event had the highest stage for all sites where the pressure transducer was not lost during this event. This event swept away the pressure transducer at MBA, and at YBD it both swept away the pressure transducer and damaged the data loggers and sensors recording precipitation and moisture.

Most flow events produced saturated conditions within the channel alluvium, as indicated by steady VWC values. Saturated conditions typically began within two hours after peak precipitation and persisted for several hours after flow stopped, with the duration of saturation persistence tending to increase with depth below the channel bed. At some sites, the saturation persistence was similar in length to flow duration (MBA, YIA, Table 4-3). The YBA site had the most limited range of saturation durations between 5-8 hours, and these periods of saturation were substantially longer than the short flow durations at this site. At MIA, saturation durations were usually much longer than at the other sites, with saturated conditions persisting for up to a month at 195 cm depth. The only event recorded at MBD did not lead to saturated conditions at any depth. No flow events are listed in Table 3 for YBD because no flow pulses were evident in the pressure transducer data. However, there was one event on 8/22/13 that was not detected by the pressure transducer but led to saturated conditions at 100 and 200 cm depth.

Table 4-3. Summary of flow event statistics for each study site. Times are reported to the nearest 15 minute increment. Lags to peak stage and saturation are reported as time elapsed since peak precipitation. No flow events were recorded in the pressure transducer for YBD.

Site	Flow events	Flow duration (hr)	Lag to peak flow (hr)	Peak stage (cm)	Lag to saturation (hr)	Saturation duration (hr)	Saturation / flow duration
MBA	7/13/12 9/5/12 10/11/12 9/6/13	33[1]	<0.25[1]	133[1]	0-0.75	3-34	1[1]
MIA	7/13/12 9/5/12 9/2/13 9/6/13	1-6[2]	0.5-1[2]	25-75[2]	0-3.75	4-734	45-136[2]
MBD	7/13/12	0.5	-2.5	60	No saturation	No saturation	No saturation
YBA	7/13/12 8/16/12 8/22/12	0.25-1	<0.25	14-177	0-0.5	5.75-7.75	7-31
YIA	7/13/12 8/17/12 8/22/12 8/22/13	1-4	0.75-13.75	2-49	0.25-3.25	0.75-8.75	0.7-2

[1]Missing flow data for all events but 9/6/13
[2]Missing flow data for 2013 events

Flow and moisture patterns for the large 7/13/12 event illustrate some of the common patterns of moisture response to flow (Figures 4-8,4-9). Precipitation was high at both MBA and MIA sites, with 71 mm total reported for the event at both rain gauges. The flow lasted for around 6 hours at MIA, but the pressure transducer was lost for MBA. At MBD, precipitation was considerably lower (18 mm), and the flow recorded lasted only about a half hour. This flow appeared to be a delayed response to the precipitation recorded at higher elevations, as precipitation peaked at MBD after the flow pulse had already passed.

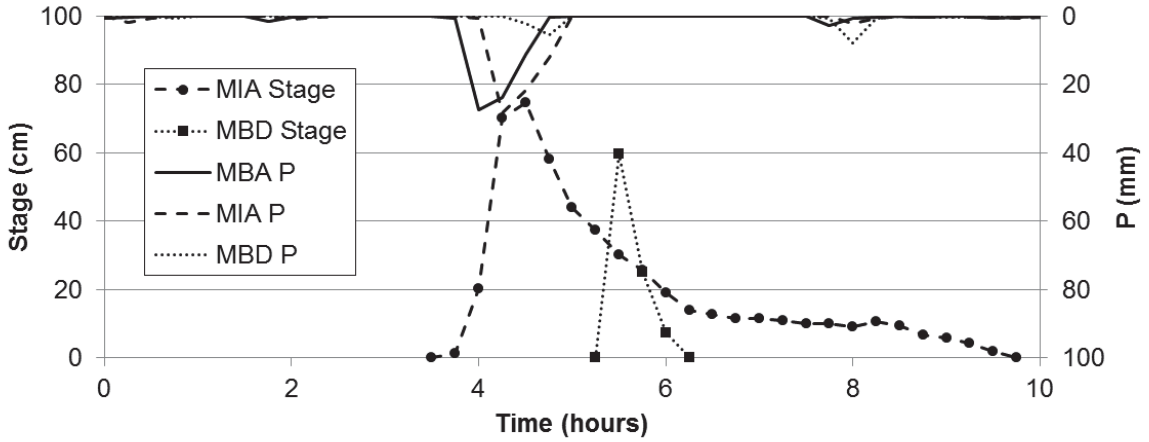

Figure 4-8. Precipitation and stream stage in Mohave Wash sites for the 7/13/12 event, starting at the onset of precipitation at 11:30. The pressure transducer for MBA was lost during this event.

Moisture responses to this flow event are shown on a separate time scale in Figure 4-9, as the duration of moisture response was much longer than the duration of flow. At MBA, all three measurement depths were saturated within 15 minutes of peak precipitation, with saturation indicated by a constant VWC. Reworking of sediments near the surface of the channel bed may have contributed to the oscillation of moisture contents during the saturated time period at 10 cm, which lasted 17.5 hours. Saturation lasted 23 hours at 20 cm depth and 34 hours at 50 cm depth. All three moisture sensors recorded a steep drop in water contents after saturation, returning to near constant water contents. MIA sensors had a similar pattern of a rapid rise to saturation at all depths, but saturation persisted longer than at MBA. At the 10 cm sensor, saturation lasted for 26 hours; at 50 cm, saturation persisted for 5 days; at 80 cm for 6 days, and at 195 cm, saturation lasted for a month. Except at 195 cm, declines in VWC after saturation were rapid.

The MBD site had only a short pulse of flow (Figure 4-8), and that flow pulse appeared to affect some of the deep sensors (70, 180 cm) but not the shallow sensors (10, 20, 50 cm). At this site, the shallow sensors were not in the main channel bed, so their response likely reflects just the input of precipitation at the site. The deeper sensors were installed later in a nearby location in the main channel corridor. While the 70 and 180 cm sensors reached VWC values close to saturation (0.35), no steady water contents were recorded at either site. A moisture pulse did reach 300 cm depth, but it only raised the VWC by around 0.05. At almost all sites and depths, VWC changes were rapid during wetting and drying as the moisture from channel flow moved through the alluvium, and after the pulse of moisture passed through, each sensor location returned to a relatively steady moisture value that was higher than the VWC prior to the event.

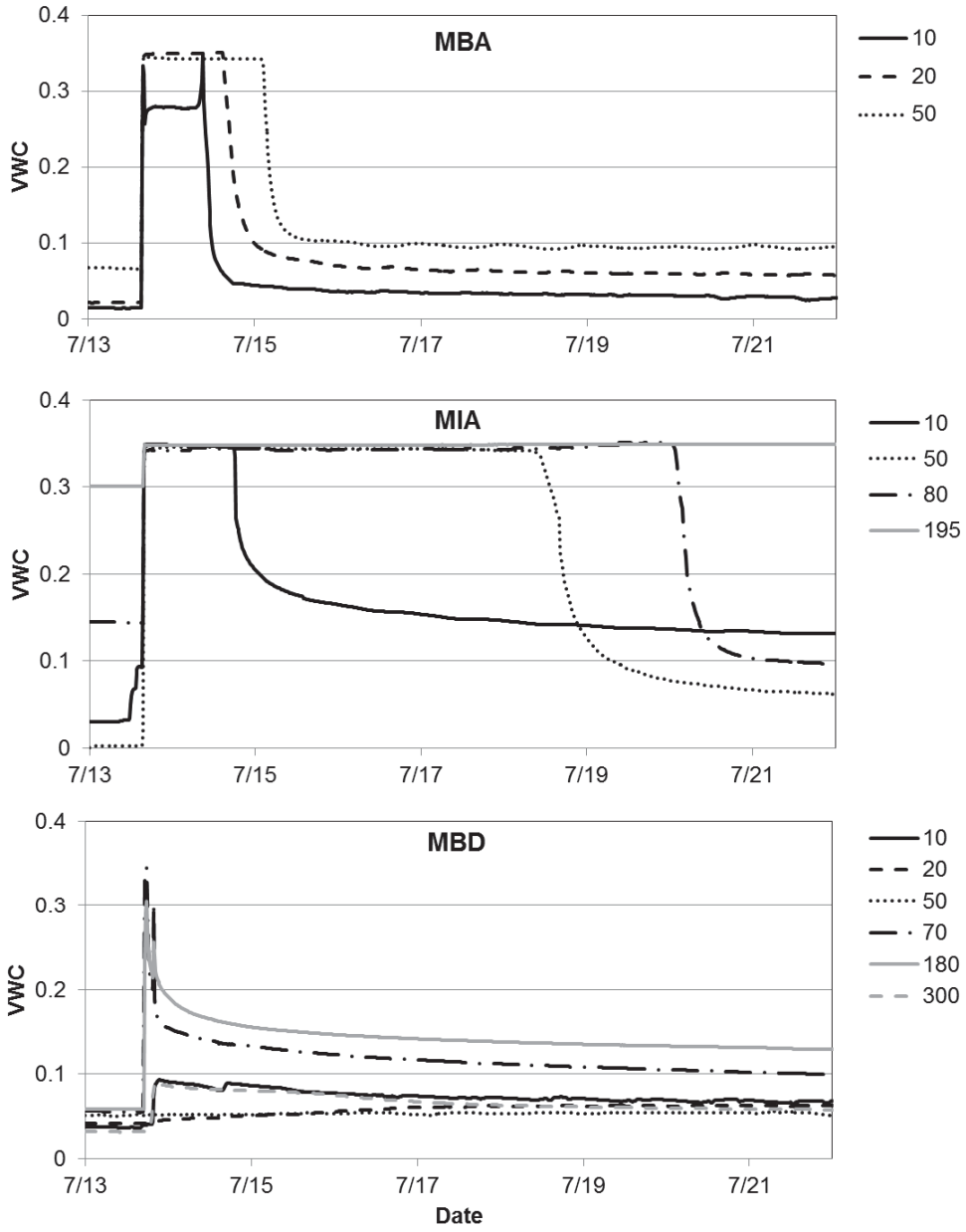

Figure 4-9. Moisture (VWC) responses to the 7/13/12 event in Mohave Wash. Series labels indicate depth in cm below the channel bed surface at the time of sensor installation. Deep (>50 cm) sensors for MIA and MBD were in the trenches dug in January 2012.

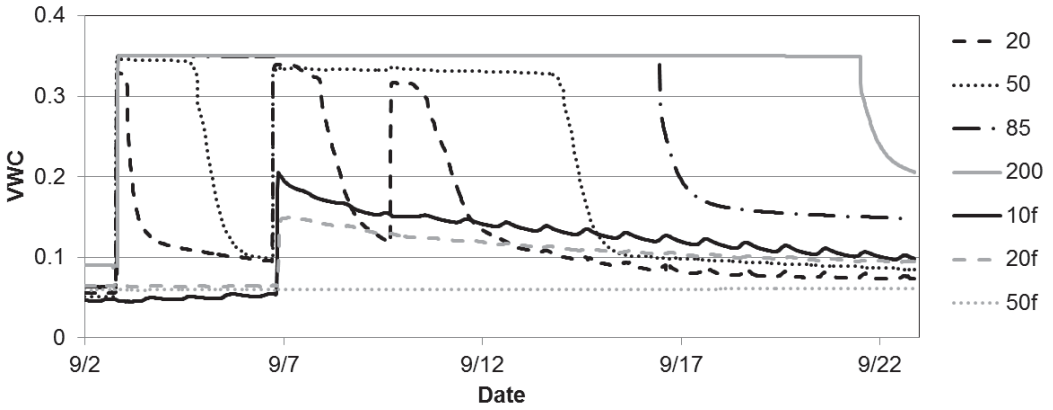

Figure 4-10. Moisture responses to a sequence of events in September 2013 at MIA. Series labels indicate depth in cm below the channel bed or floodplain (f). Deep (>50 cm) sensors were in the trench dug in May 2013. The 10 cm sensor for the channel was not in place for this time period.

Flow events usually led to saturation below the channel bed but not in the floodplain, and shown in Figure 4-10. In this example, a sequence of three flow events led to repeated saturation at 20 cm depth, two pulses of saturation at 50 cm depth, and saturation that persisted for all three events at 85 and 200 cm depth. In contrast, the floodplain sensors only recorded a response to one precipitation event, which did not produce saturation. The finer sediments in the floodplain led to a more gradual decline in moisture after the rain event than the decline in channel bed sediments after the flow event. Precipitation records for this time period showed a 9 mm event on 9/2, a 53 mm event on 9/6 that likely produced the pulse of floodplain moisture, and a 3 mm event on 9/9. Magnitudes of the first and last event were low to produce flow pulses, and pressure transducer data were not available for these events to verify whether or not there were three distinct flow pulses. Possibly offsite precipitation contributed to these pulses of flow.

Site and seasonal differences

Comparisons of long-term moisture patterns between sites are challenged by the differences in period of record for each sensor location. All locations had intermittent periods of data loss, but these periods varied by sensor and by location. To remove some of the bias introduced in moisture values for different periods of record, average VWC values for dry periods are shown in Figure 4-11. Average moisture values including days with precipitation are higher than the values shown, but in all cases the increase in average VWC including rain periods is <0.01 . Average moisture during the study time period increased with depth in the top 50 cm at most locations. In this depth range, all channel sensors had average VWC <0.1, with the BA the driest sites for both watersheds at VWC values of 0.05 or less. The MIA site had the highest average VWC for rain-free periods across all study locations, with the sensor above the layer of fine sediments at 200 cm depth from the January 2012 trench (Figure 4-4) staying at or near saturation much of the time. The second set of deep moisture measurements (May 2013 trench) for MIA were installed in a pit where this fine layer was not present, and VWC values were lower, on average 0.11-0.14. The YIA site was substantially drier, with average VWC < 0.1 at all depths. Moisture at braided sites increased with depth to 100-200 cm then declined again at 300 cm. The MBD site had average VWC < 0.1 at all depths, with peak VWC at 100 cm in the second trench (May 2013), where the moisture sensor was installed above a layer of fine sediments. The YBD site was wetter, with average VWC peaking at 0.16 at 200 cm depth in the May 2013 trench.

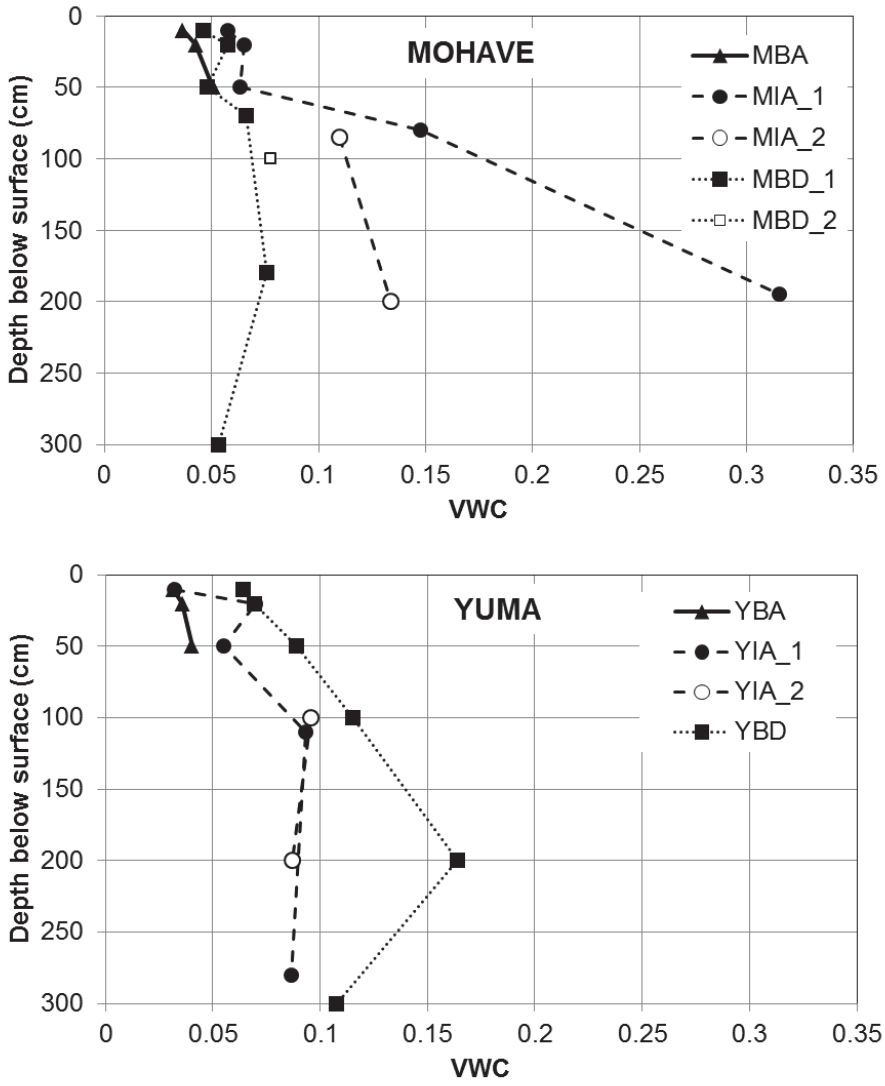

Figure 4-11. Average volumetric water content for all days of measurement from May 1, 2011 – April 30, 2014, excluding days with rain and the subsequent two days after rain. MIA_1, MBD_1, and YIA_1 are the near-surface (50 cm or less) sensors installed in 2011 and the January 2012 deep sensors; MIA_2 and MBD_2 are the deep sensors installed in May 2013. YBD includes the near-surface sensors installed in 2011 and the deep sensors installed in May 2013.

To evaluate moisture patterns by season, we used 20 cm depth measurements, as these had the least data loss of any depth range. Moisture at 20 cm had a wider range beneath the channel bed than on the floodplain, but the means differed by less than the measurement precision, at 0.055 beneath the channel and 0.053 beneath the floodplain. Therefore, we grouped all 20 cm sensors together for the seasonal analysis. Overall, the sites experienced a gradual increase in moisture at 20 cm, from a mean of 0.03 in Summer 2011 to a mean of 0.07 in Winter 2014 (Figure 4-12). Winter average VWC was always higher than the previous summer even though summer precipitation totals were higher than winter totals in both watersheds (Table 4-2). This overall wetting pattern through the three years of study was evident in all sites except YBA.

As an example of the wetting and drying patterns, Figure 13 illustrates how the sequence of wetting and drying from the end of summer 2011 to winter 2013 affected VWC at the MBA site. After the dry summer 2011, moisture values were all low and steady. Pulses of rain increased moisture in the winter, and VWC values declined gradually (at a rate of 0.0003-0.0006 per day) throughout winter 2012 and early summer 2012, not quite returning to the low

baseline values observed at the end of summer 2011. The flow events on 7/13 and 9/5/12 led to elevated moisture after the event pulse had subsided, particularly at 20 and 50 cm depth, and as a result moisture levels were higher going into winter 2013. The longest interval of drying in summer 2012 was after the 9/5 flow event and before another rain event on 10/10. During this interval, once the response to flow had subsided, the rate of drying was higher than during the winter drying periods, at a rate of 0.0013 per day.

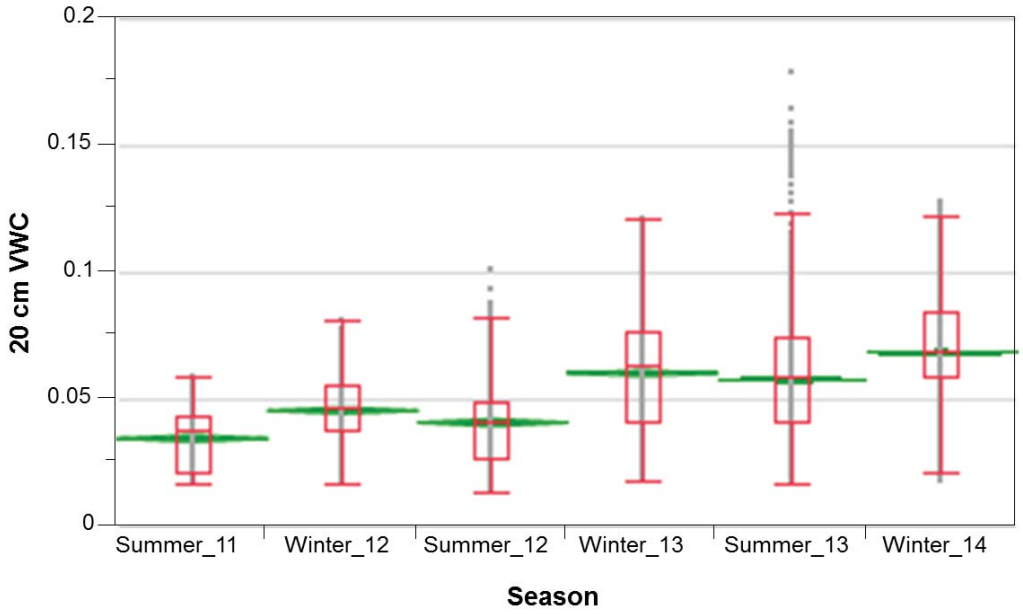

Figure 4-12. Box plot of seasonal 20 cm VWC values across all sites, excluding days with rain and the subsequent two days after rain. Green triangles show the mean and 95% confidence interval.

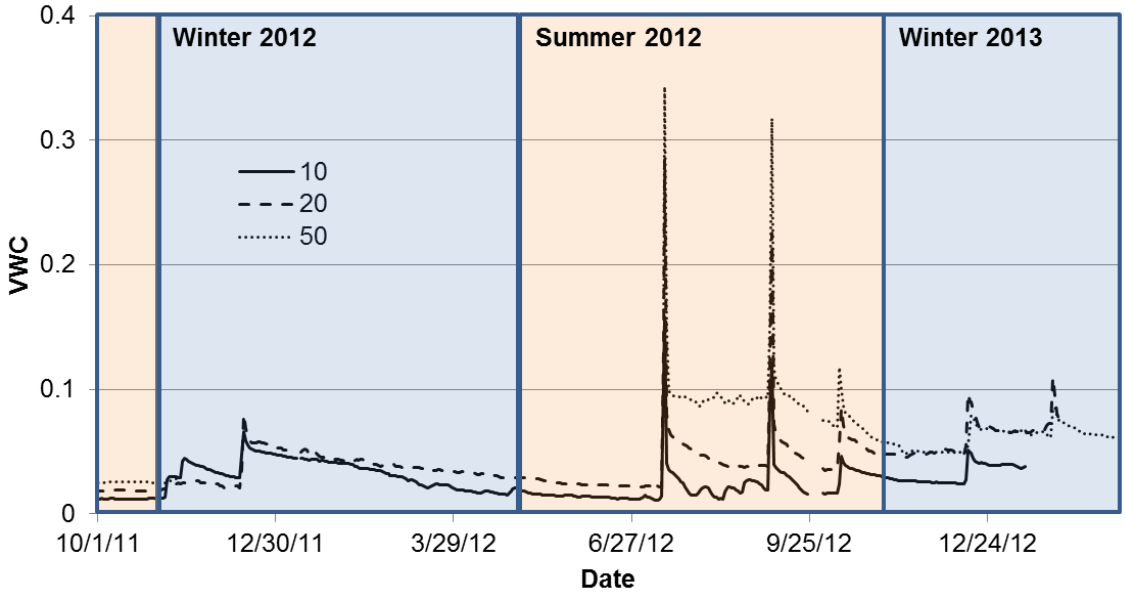

Figure 4-13. Time series of VWC at the MBA site illustrating steady low VWC at the end of summer 2011 and increases in moisture base level after rain events in winter and summer 2012.

Discussion

Moisture in the alluvium of ephemeral stream channels varies both seasonally and in response to flow events, with the largest changes in moisture observed during brief, infrequent flow events. This discussion addresses the factors that impact both the event and the longer-term seasonal moisture dynamics.

Event response

In the absence of flow events, moisture responses to rain were not detected at depths greater than 1 m, which was the maximum depth that a rain response was detected in the absence of flow. This deep rain response was at YBD during a multi-day storm with 28 mm total precipitation; the next deepest rain response was also during a long duration winter storm at MBD, where a response was detected at 70 cm after 21 mm of rain. The dominance of rain response in the shallow subsurface except during long winter rains is consistent with the modeling results of Reynolds et al. (2004) and Scott et al. (2000) (check out Andraski 1997 also), who simulated soil moisture recharge in response to rain events for different soil textures in southwestern U.S. deserts (need to check study domain). Reynolds et al. (2004) concluded that rain recharge below 80 cm is uncommon but more likely in coarser texture soils than finer texture soils, and Scott et al. (2000) (and studies they cite) concluded that less intense winter rains were more likely to reach deeper in the subsurface than high intensity summer rains.

Because rain responses were not detected below 1 m depth in the channel bed alluvium, flow events appear to be the dominant source of water to the deep subsurface. Channel flow typically produces pulses of wetting that travel rapidly through the alluvium and lead to transient saturation beneath the channel bed. The patterns of transient saturation we observed in the study channels are similar to those reported for Rillito Creek, also in the Sonoran Desert (Hoffmann et al. 2003; Blasch et al. 2006), where water contents rise to saturation, and durations of saturation increase with depth below the surface. As a consequence, understanding of the conditions that produce flow in these ephemeral stream channels is essential for predicting the likelihood of deep percolation and groundwater recharge. In an accompanying study, Faulconer et al. (in prep) analyzed a broader range of channel types in this study area, including smaller bedrock and piedmont headwater channels that do not have alluvium stored in the base of the channel. Particularly for the smaller channels, Faulconer et al. (in prep) found that thresholds of rain intensity were strong predictors of whether or not a channel would experience flow, with the rain intensity threshold increasing linearly with the log of catchment area up to an area of around 3 km^2. BA channels in this study are below the maximum contributing area where precipitation thresholds for runoff can be defined (YBA = 2.2 km^2; MBA = 0.9 km^2), but IA and BD channels are all larger (3.6-225 km^2).

With the possible exception of one winter event at YIA where flow was detected in the pressure transducer but not in the shallow soil moisture sensors, the study channels only experienced flow during summer storms, which are typically convective storms that can have higher intensities than winter frontal storms, thus making channel flow more likely. Convective storms are often highly localized, so point precipitation measurements may not adequately represent the precipitation contributing to flow in a channel with large contributing area. This may explain why some flow events were detected in the study channels even for relatively low precipitation magnitudes (Figure 4-7) and means that accurate prediction of flow requires detailed spatial information on precipitation patterns. There is some indication that upstream channels have greater likelihood of flow than downstream channels due to transmission loss, as predicted in other studies (Morin et al. 2009), but this difference is most evident in the braided channels, whereas the upstream (BA and IA) channels experienced similar numbers of flow events. The widening of channels in braided channels (Figure 4-2) may lead to greater transmission losses during flow relative to the more confined BA and IA channels. Braided channels also have lower precipitation than the upstream channels in each watershed (Figure 4-3), and in the one definite flow event observed at MBD, precipitation higher in the contributing area was responsible for the flow observed in the braided reach.

At most study sites, the coarse alluvium has low water retention, so saturation in the alluvium persisted for only a few hours after flow events. At BA sites, the alluvium sits directly on top of fractured bedrock, so the saturated zone that builds up in the alluvium during flow events may decline either through downslope flow along the bedrock contact or percolation into the fractured bedrock. At YBA, the channel gradient is relatively shallow, and the duration of saturation after a flow event has little variation with depth and with event (5-8 hours), suggesting that the water percolates vertically at a rate set by the hydraulic conductivity of the bedrock. At MBA, the channel gradient is steeper, and the duration of saturation is typically longer (>11 hours), with longer persistence of saturation at greater depths. Either lower permeability bedrock or lateral flow may contribute to the longer periods of saturation

at this location. The one flow event without data loss at this location had an extended long recession that was unique compared to any other flow events, indicating that the storage capacity of the alluvium may have been completely filled during the flow event. In the Walnut Gulch watershed, Renard et al. (1964) reported instances where the water table reached the surface as well after flow events; in our study watersheds, water tables reaching the surface probably occurred only at MBA, which has the shallowest alluvium of all the sites.

The only site where saturated conditions persisted for more than 2 days after flow was the MIA site, where the 2 m layer of fine sediment proved to be an effective barrier to deeper infiltration, leading to a perched water table that lasted as long as a month after the large flow event on 7/13/12. Even in the second trench location where the fine sediment layer was not encountered, saturation still persisted at 2 m depth for days after flow events at depths greater than 50 cm (Figure 4-10), an indication that the saturated zone perching above the fine sediment layer has a lateral influence that extends beyond the boundaries of that layer. Other ephemeral channel studies have also identified likely lateral flow along fine sediment layers or into finer floodplain sediments (Renard et al. 1964; Izbicki et al. 2000). In the YIA channel, where there was no fine sediment layer to extend the period of transient saturation after flow, durations of saturation were only a few hours.

While there were fine sediment layers detected at the MBD site, these layers did not have the evident influence on moisture patterns observed at MIA. This may have been because of the low flow occurrence, with only one event recorded at MBD during the large 7/13/12 storm. One event at YBD (8/22/13) did produce saturation in deep sensors, but no flow event was recorded in the pressure transducer for this time period, and moisture pulses were inconsistent across measurement locations. Because braided channels are so wide, large laterally extensive flow events would be needed to saturate the alluvium extensively below these channels. This combined with the infrequent flow in these channels means that pulses of moisture reaching deep into the alluvium are infrequent relative to the other channel types, and the influence of fine sediment layers is less evident than in channel types with more frequent flow.

Seasonal-annual response

Seasonal patterns of moisture in the alluvium reflect the interaction of rain and flow inputs with drying. The low water retention of most of the channel alluvium means that moisture declines very rapidly at the end of saturated pulses from both rain and flow events (Figures 4-9, 4-10, 4-13), and except near the fine sediment layers in MIA, the high VWC values during events have little effect on long-term average moisture because the pulses of moisture typically subside within 2 days after an event. But both rain events and rain+flow events typically lead to elevated base levels of moisture after the initial rapid decline. The moisture at this elevated base level still gradually declines, but at a much lower rate (Figure 4-13). There is some indication that this gradual decline is greater during summer than during winter, suggesting greater evapotranspiration in summer, but the rates of decline are on the order of 0.0001-0.001 per day. Such rates are so slight that they are within the precision of the moisture sensors, and noise in the VWC values at low water contents makes the rates difficult to quantify precisely. However, a decline in water contents each summer relative to the previous winter (Figure 4-12) does suggest that rates of drying are higher in summer, even at very low water contents. Other studies in this region have suggested that drying rates are greater in summer than in winter (Renard et al. 1964; Phillips et al. 2004; Reynolds et al. 2004), but quantifying these differences in drying rates at such low water contents in our study area will require further data analysis to separate signal from noise.

The small seasonal signal evident in Figure 4-12 is superimposed on an overall wetting trend throughout the study time period, which may reflect the patterns of summer precipitation. Average precipitation over the study area during the first summer 2011 was only 35% of normal at the YPG station, whereas precipitation during the next two summers were 307 and 154% of the long-term average at the YPG station. While the summers produce a net drying relative to the previous winter, frequent pulses of rain and particularly pulses of flow during summer lead to elevated baseline moisture going into the winter. While previous studies have emphasized the importance of winter precipitation for recharge of soil water (studies cited in Pool 2005; Phillips et al. 2004), in our study area the dominance of flow events in the summer means that summer storms are critical for deep groundwater recharge, even if they have drier near-surface moisture than winters.

Comparing average moisture conditions across study sites, the local differences in texture and depth to an impeding layer appear to be stronger controls on the moisture regime than differences in precipitation and flow. BA sites in each watershed had higher precipitation (Figure 4-3) and frequent flow, yet they were the driest sites in the top 50

cm of soil (Figure 4-11), likely due to very coarse textures of alluvium. The Yuma braided channel, which had the lowest precipitation of all sites and no flow detected by the pressure transducer, had the highest average moisture of the Yuma channels. This higher moisture content may reflect the time period of measurement, as this site was not functioning during the dry summer 2011. Deeper water contents at this site were from sensors installed in May 2013, and thus the long-term averages shown in Figure 4-11 reflect a time period with higher moisture overall (Figure 4-12). The only site with persistent high water contents was the MIA site where the layer of fine sediment led to development of a perched water table after flow events. Water contents were high when sensors were initially installed in the deep trenches at this site in January 2012, with a steady water content of 0.3 at 195 cm, indicating that even after the dry period at the start of the measurement record, this site still retained high moisture. These examples highlight the critical role of alluvium stratigraphy in the long-term moisture regime.

Challenges and uncertainties

Collecting reliable long-term measurements in this extreme environment posed several challenges. Attempts to access the deep subsurface with drilling were unsuccessful due to the presence of large boulders in unconsolidated material. Trenches dug with a backhoe allowed us to install the deeper sensors in the alluvium, but the maximum depth of these trenches was limited by safety and stability of side slopes in the unconsolidated material. As a result, we do not have information about the fate of water percolating into the deeper alluvium.

Moisture sensors installed within the alluvium in many cases did not give continuous reliable data. It is not clear why this was the case, but drifts in sensor measurements tended to happen during drying periods, suggesting that the sensor lost good contact with the alluvium. In some cases, a sensor that had drifted would start recording reasonable values again after a flow event. Because the alluvial materials are so coarse, it is possible that fine sediments moved downward in the profile during flow events, which may lead to variable water retention properties over time. This possibility of fine sediment infilling has been noted in other studies (Hoffman et al. 2003) as a potential cause of declining hydraulic conductivity in alluvium during a flow event. Further the near-surface alluvium is mobilized during flow events, and flows in these channels may lead to either aggradation or incision of alluvium. In some cases after flow events with evident alluvium depth changes, the sensors had to be removed and reinstalled. Any changes in the depth of alluvium affect the depth of sensors relative to the channel bed.

Finally, particularly in the braided channels, the large width and multiple possible pathways of flow mean that an extensive number of both stage and moisture sensors are needed across the channel to ensure that connections between flow pulses and stage are measured adequately. In several cases, we detected possible flow pulses in the moisture sensors that were not evident in the pressure transducers or flow pulses in the pressure transducers that were not associated with a large moisture response. The unvented pressure transducers we installed were for the most part able to withstand the extreme conditions of these sites, although it can be difficult to install them securely enough that they will not get swept away by large flows.

Conclusions

The ephemeral channels in our study site exhibited short-term responses to infrequent pulses of flow and longer-term wetting and drying trends. The short-term flow pulses produced the largest changes in moisture and were the only events where increased moisture was detected past the top 1 m of alluvium. While we do not have information on where a regional water table is located beneath the channel alluvium, pulses of saturation reached as deep as three meters in less than four hours and persisted in the alluvium for less than two days, indicating that the water continued to percolate into the deeper subsurface.

This rapid percolation of water from flow events combined with low water retention of the alluvial materials means that most of the time the alluvium is dry (VWC <0.1) except where fine sediment layers allow a perched water table to develop after flow. Fine sediment layers are rare in this high energy flow environment, so in most of the study area limited moisture was stored in the channel bed alluvium. Between flow events, moisture dynamics in the channel bed alluvium become similar to those in upland environments, with changes in moisture affected by the interaction of rain pulses with seasonally variable evapotranspiration and little to no percolation of moisture past the top meter of alluvium.

Chapter 5. Ecological Significance of a Hydrogeomorphic Stream Classification: Riparian Plant Community Composition

Abstract

We evaluated the ecological significance of an ephemeral stream hydrogeomorphic classification by testing for compositional differences among stream types in the relative cover and density of plant species and functional groups. Bedrock, piedmont headwater, and braided streams support distinctive riparian communities. Vegetation along incised alluvium and bedrock with alluvium streams, while different from the other stream types, was distinguishable only on the basis of species density. Within the northern Sonoran Desert of Arizona, USA, compositional differences among stream types is largely due to differing canopy coverage and density of the most common species and plant functional groups. Spatial patterns in riparian community composition were best explained variation in channel gradient, bankfull width:depth, and stream reach elevation. We discuss the global applicability of this stream classification, and its implications for the study, management, and restoration of dryland ephemeral streams.

Introduction

Stream channel classifications have been widely employed in geomorphology (Naimen et al. 1992, Montgomery and Buffington 1998, Montgomery 1999) and aquatic ecology (Newson and Newson 2000, Thorp et al. 2006), but riparian ecologists have been slow to adopt this approach. Instead, riparian studies have focused largely on the roles of lateral and longitudinal physical gradients in shaping biotic patterns. While these abiotic gradients undoubtedly form the habitat templates that constrain ecological dynamics, incorporating generalizable channel types into riparian ecology would provide context by identifying which portions of riverine continuums are described, simplify the design of controlled comparisons, and aid in isolating specific portions of gradients for examining finer-scale dynamics.

Existing channel classifications have been developed almost exclusively from observations of perennial rivers in temperate regions. Much of the focus has been on stream networks draining forested mountainous terrain, with lesser attention to lowland rivers (Naimen et al. 1992). Dryland ephemeral streams are the most common, but least studied fluvial environment (Bull and Kirkby 2002, Nanson et al. 2002), and only recently has an ephemeral stream channel classification been proposed (Sutfin et al. 2014). Increased focus on dryland riparian ecology in recent years has led to a growing global data set, but a broader understanding has been hampered by a lack of cohesive conceptual framework for interpreting these data.

Stream networks may be divided into stream types (also known as functional process zones or process domains), which exhibit similar hydrogeomorphic processes and patterns (Montgomery and Buffington 1998, Montgomery 1999, Thorp et al. 2006). The abundance and spatial arrangement of stream types within watersheds are determined by geologic discontinuities and network structure (Montgomery 1999, Benda et al. 2004, Thorp et al. 2006, Poole 2010). Differences in the magnitude, frequency, and duration of sediment and water fluxes among reach types produce fluvial environments with distinctive landforms, hydraulics, and alluvial characteristics (Montgomery and Buffington 1998, Montgomery 1999, Benda et al. 2004). These properties in turn affect the frequency and duration of hydrologic connections, which ultimately determine nutrient cycling dynamics, erosion and deposition of geomorphic surfaces, and subsurface moisture regime (Gregory et al. 1991, Fisher et al. 2007, Poole 2010, Larned et al. 2011).

Ecological patterns and processes within dryland stream networks are shaped by the spatial and temporal distributions of hydrologic fluxes (Fisher et al. 2007, Larned et al. 2010) and geomorphic disturbance (Gregory et al. 1991, Montgomery 1999, Benda et al. 2004). Hydrologic connections govern the availability of water and nutrients, thereby determining the distribution of resources for plant growth (Poole 2010, Larned et al. 2010). Geomorphic disturbances produce habitat heterogeneity, drive plant community succession, and modify population dynamics (Gregory et al. 1991, Thorp et al. 2006, Larned et al. 2010). Spatial distributions of riparian plants within stream networks reflect differing tolerances along gradients of water availability and geomorphic disturbance, in addition to the diffusive effects of biotic interactions (Hupp and Osterkamp 1996, Bendix and Hupp 2000). Compositional shifts in relation to these abiotic drivers lead to distinctive community types associated with particular hydrogeomorphic settings (Bendix 1994, Shaw and Cooper 2008, Angiolini et al. 2011). Therefore, the characteristic physical and

chemical environments of each stream type are expected to produce distinctive ecological dynamics (Thorp et al. 2006).

While species are the fundamental units in ecology, analysis with respect to functional traits can provide greater insight into ecological processes and yield more broadly applicable relationships (Shmida and Burgess 1988, Merritt et al. 2010). When plant functional groups relate to the acquisition and processing of carbon, water and nutrients, they provide insight into ecosystem functions such as production, decomposition, and nutrient cycling (Diaz and Cabido 2001, Naeem and Wright 2003). Plant growth forms (e.g. tree, shrub, grass) characterize broad differences in woodiness, canopy architecture, and root distributions that relate to patterns of spatial resource partitioning (Shmida and Burgess 1988, Stromberg 2013). Differences in rooting depth and lateral spread among growth forms (Canadell et al. 1996, Schenk and Jackson 2002) correspond to distinctive patterns of water use (Davis and Mooney 1986, Shmida and Burgess 1988). Such morphological groupings also exhibit differences in flood disturbance tolerance (Sandercock and Hooke 2010), and distinctive regeneration niches (Cornelissen et al. 1996, Flores et al. 2004, Butterfield and Briggs 2011). Subdivisions of growth forms based on photosynthetic habit and leaf phenology (e.g. evergreen, winter deciduous, drought deciduous) reflect differences in physiological rates and responses to variation in resource availability that relate primarily to temporal partitioning of niches (Chabot and Hicks 1982, Smith et al. 1997, Sperry and Hacke 2002).

In an age of rapidly changing climate and land use, understanding the distributions of biodiversity, ecosystem functions, and patterns of sensitivity and resilience to environmental alteration are critical needs. Identifying the hydrogeomorphic drivers of plant community characteristics among stream types at the reach scale will clarify these ecological patterns and processes at the watershed and landscape scales (Newson and Newson 2000, Thorp et al. 2006), and framing these relationships in terms of plant functional groups can enhance their utility (Shmida and Burgess 1988, Merritt et al. 2010). To this end, we address the following questions: (1) Does reach scale species and functional group composition of perennial riparian plant communities differ among the proposed hydrogeomorphic stream types? (2) What geomorphic characteristics drive variation in ephemeral stream riparian community composition at the reach scale?

Methods

The composition of perennial riparian plant communities was measured in variably-sized plots within 86 stream reaches at US Army Yuma Proving Ground (YPG) and 15 reaches at US Air Force Barry M. Goldwater Range (BMGR) (Figure 1-1). Study reaches were selected to maximize geographic distribution and to represent the range of geomorphic conditions within accessible areas, without regard to vegetation characteristics. Reach lengths were scaled to four channel widths in braided streams and twelve channel widths in all others. The entire active fluvial corridor of smaller reaches was surveyed, while 10 m wide belt transects spanning the fluvial corridor were surveyed along two to four cross sections within larger reaches, resulting in surveyed areas ranging from 50 m^2 to 1700 m^2. Variably-sized plots were necessary to adequately sample plant communities in proportion to plant density and physiognomy. In small bedrock or piedmont headwater reaches, fluvial corridor widths were as small as 2 m, while channel characteristics and stream type often changed over distances of <50 m. Conversely, patchy vegetation and variable landforms within large braided reaches were not adequately characterized in plots sized for headwater reaches (<100 m^2). In alluvial streams, the active fluvial corridor consisted of channel and floodplain surfaces below relict terraces. Active fluvial corridors of streams incised into bedrock or piedmont surfaces were delineated by the elevation of fluvial landforms, desert pavement, or staining on bedrock canyon walls.

Individuals of all perennial plant species were counted on each active fluvial surface (bed, bank, floodplain/overbank), and the percentage of total canopy coverage by species was obtained by averaging visual estimates from two independent observers. To standardize errors in counting rhizomatous grasses and shrubs, plants were considered to be individuals when separated by at least 1 m for discrete patches of grass and shrubs and 3 m for trees, unless connecting lateral roots or prostrate stems indicated otherwise. Abundances (density) were derived by dividing counts by sampled area. Vegetation surveys were conducted during spring months (March-May) in 2011 and 2012. Voucher specimens (excluding Cactaceae) are housed at the University of Arizona Herbarium (ARIZ).

We derived 18 *a priori* plant functional groups consisting of major growth forms subdivided on the basis of photosynthetic habit and leaf phenology (Table 5-1), similar to those of Shreve and Wiggins (1964), Lavorel et al. (1997) and Scholes et al. (1997). These groupings comprise functional trait combinations affecting resource acquisition and use, and should therefore exhibit distinctive responses to disturbance and resource availability (Petchey and Gaston 2006). Functional groups were assigned based on published species accounts and field observations over two years (Appendix A-2).

Table 5-1. A priori plant functional groups. Functional groupings for each species and associated references are in Appendix A-2.

Functional Group	Species	Examples
Evergreen Trees	4	*Olneya tesota*; *Condalia globosa*
Photosynthetic Stem Trees	3	*Parkinsonia* spp.; *Psorothamnus spinosus*
Winter Deciduous Trees	2	*Prosopis* spp.; *Chilopsis linearis*
Columnar Cacti	1	*Carnegiea gigantea*
Evergreen Shrubs	6	*Larrea tridentata*; *Simmondsia chinensis*
Drought Deciduous Shrubs	13	*Lycium* spp.; *Fouquieria splendens*
Photosynthetic Stem Shrubs	6	*Krameria* spp.; *Ephedra aspera*
Winter Deciduous Shrubs	4	*Acacia* spp.; *Colubrina californica*
Shrubby Cacti	5	*Cylindropuntia* spp.; *Opuntia* spp.
Evergreen Subshrubs	2	*Ambrosia ambrosiodes*; *Tiquilia canescens*
Drought Deciduous Subshrubs	19	*Encelia farinosa*; *Ambrosia dumosa*
Photosynthetic Stem Subshrubs	2	*Carlowrightia arizonica*; *Porophyllum gracile*
Winter Deciduous Subshrubs	1	*Ayenia microphylla*
Low Cacti	5	*Mammillaria* spp.; *Opuntia basilaris*
Vines	2	*Sarcostemma cynanchoides*; *Cottsia gracilis*
Herbaceous	7	*Sphaeralcea ambigua*; *Eriogonum inflatum*
Grasses	6	*Hilaria rigida*; *Aristida purpurea*
Epiphytic Parasites	1	*Phoradendron californicum*

Geomorphic and hydraulic characteristics were derived from topographic surveys along four equally-spaced cross sections in each study reach (Sutfin et al. 2014). Variables included channel gradient and entrenchment ratio (Rosgen 1994), as well as bankfull measures of width:depth, boundary shear stress, and stream power. Mean elevation was derived from 30-m DEMs, and Solar Analyst in ArcMap was used to estimate total annual insolation (Fu and Rich 1999).

Differences in community composition among stream types were assessed using nonparametric permutational MANOVA (PerMANOVA) and distance-based tests of homogeneity of multivariate dispersion (PermDISP) from group centroids (Anderson 2001, 2006). These tests were performed on Bray-Curtis similarity matrices relativized by sample unit totals for both cover and abundances of species and functional groups. Prior to calculating distance matrices, relative cover and density values were arcsine-square root transformed, and rare species occurring in less than 5% of sites were omitted (McCune and Grace 2002). Nonmetric Multidimensional Scaling was used to visualize multivariate differences in location and dispersion among reach types (Kruskal and Wish 1978). Species

and functional groups responsible for compositional dissimilarity among stream types, and compositional similarity within stream types, were identified with the SIMPER procedure (Clarke 1993).

Abiotic drivers of compositional differences among stream types were identified as the subset of variables from the environmental similarity matrix that optimized the Spearman rank correlation with biotic matrices (Clarke and Ainsworth 1993). The environmental matrix was calculated from Euclidean distances on $\log_{10}$ transformed and normalized abiotic variables. Environmental gradients were illustrated as vectors on ordinations, scaled proportionally to correlations with axis scores.

Results

A total of 88 perennial plant species were observed in study reaches at YPG and BMGR. The 86 study reaches at YPG contained 72 species, while 60 species were found in the 15 reaches at BMGR. We observed only one exotic species, *Tamarix aphylla* (L.) Karst., in our study reaches, consisting of one individual each in two braided reaches. Twenty-three species occurred in less than 5% of study reaches, and were omitted from further analysis.

Species Cover

The composition and variability of species relative cover differed significantly among the reach types (Table 5-2; Figure 5-1A). Bedrock, piedmont headwater, and braided streams exhibited distinctive composition, while incised alluvium and bedrock with alluvium streams were similar (Table 5-3). Beta diversity was highest in bedrock streams and lowest in braided streams. Bedrock with alluvium, incised alluvium and piedmont headwater streams exhibited similar dispersion (Table 5-4).

Table 5-2. Tests for global differences among stream types in riparian plant community composition (PerMANOVA) and compositional variance (PermDISP).

Source	PerMANOVA			PermDISP	
	R^2	F	P	F	P
Species Cover	0.239	6.27	<0.001	12.0	<0.001
Species Density	0.230	5.96	<0.001	7.84	<0.001
Functional Group Cover	0.252	6.73	<0.001	13.8	<0.001
Functional Group Density	0.284	7.94	<0.001	5.85	0.002

Differences in the relative cover of *O. tesota*, *P. microphylla*, *E. farinosa*, *L. tridentata*, and *A. dumosa* led to the most compositional dissimilarity among stream types (Figure 5-2A). *Lycium torreyi*, *Hyptis emoryi*, and *Acacia greggii* exerted moderate influence on dissimilarity between stream types. Although they did not substantially contribute to dissimilarity between other stream types, *P. florida* and *Ambrosia salsola* were useful in distinguishing braided streams. Similarities within stream types were largely due to the relative cover of *P. microphylla*, *E. farinosa*, *L. tridentata*, *O. tesota*, and *A. dumosa*, although *A. greggii* was also important in braided streams (Figure 5-2B).

Differences in species cover among stream types occurred primarily along a covarying gradient of channel slope and width:depth (Figure 5-1A). Piedmont headwater, incised alluvium, and bedrock with alluvium streams occupied similar portions of this gradient, but the distinctive composition in piedmont headwater streams was associated with lower stream power and elevation. Differences in species cover among stream types was best explained by channel slope and reach elevation (Table 5-5).

Species Density

The composition and dispersion of species relative density differed between stream types (Table 5-2; Figure 5-1B). Each stream type exhibited a unique species composition (Table 5-3), and bedrock streams had significantly greater variability than other stream types (Table 5-4). Relative density of *E. farinosa* drove compositional dissimilarity among stream types, followed by *L. tridentata*, *A. dumosa*, *Fagonia laevis*, and *L. torreyi* (Figure 5-3A). Densities

Table 5-3. Pairwise comparisons for differences in riparian plant community composition (PerMANOVA) among stream types. Bold P-values are significant at $\alpha = 0.05$.

	Species Cover		Species Density		Functional Group Cover		Functional Group Density	
Comparison	**t**	**P**	**t**	**P**	**t**	**P**	**t**	**P**
Bedrock vs Bedrock with Alluvium	1.75	**0.004**	1.55	**0.024**	2.13	**<0.001**	1.53	0.064
Bedrock vs Incised Alluvium	2.43	**<0.001**	2.07	**0.001**	2.82	**<0.001**	2.27	**0.004**
Bedrock vs Piedmont Headwater	2.50	**<0.001**	2.35	**<0.001**	2.14	**0.002**	1.59	**0.041**
Bedrock vs Braided	3.41	**<0.001**	3.22	**<0.001**	3.71	**<0.001**	4.20	**<0.001**
Bedrock with Alluvium vs Incised Alluvium	1.40	0.079	1.44	**0.033**	1.42	0.087	1.41	0.092
Bedrock with Alluvium vs Piedmont Headwater	2.48	**<0.001**	2.53	**<0.001**	2.01	**0.002**	1.88	**0.007**
Bedrock with Alluvium vs Braided	2.81	**<0.001**	2.91	**<0.001**	2.45	**<0.001**	3.87	**<0.001**
Incised Alluvium vs Piedmont Headwater	2.22	**<0.001**	2.26	**0.001**	2.56	**<0.001**	2.58	**<0.001**
Incised Alluvium vs Braided	2.32	**0.002**	2.34	**<0.001**	2.34	**<0.001**	3.04	**<0.001**
Piedmont Headwater vs Braided	3.67	**<0.001**	3.73	**<0.001**	4.07	**<0.001**	5.22	**<0.001**

Table 5-4. Pairwise comparisons for differences in riparian plant community compositional variance (PermDISP) among stream types. Bold P-values are significant at $\alpha = 0.05$.

	Species Cover		Species Density		Functional Group Cover		Functional Group Density	
Comparison	**t**	**P**	**t**	**P**	**t**	**P**	**t**	**P**
Bedrock vs Bedrock with Alluvium	2.72	**0.021**	2.08	**0.049**	2.71	**0.023**	2.31	**0.043**
Bedrock vs Incised Alluvium	4.54	**0.001**	3.43	**0.001**	5.10	**<0.001**	3.30	**0.004**
Bedrock vs Piedmont Headwater	4.17	**0.002**	4.21	**0.001**	3.46	**0.008**	3.58	**0.002**
Bedrock vs Braided	7.44	**<0.001**	5.50	**<0.001**	7.98	**<0.001**	4.89	**<0.001**
Bedrock with Alluvium vs Incised Alluvium	1.80	0.11	1.30	0.25	1.88	0.087	0.851	0.42
Bedrock with Alluvium vs Piedmont Headwater	1.66	0.14	2.12	0.052	0.619	0.59	1.06	0.31
Bedrock with Alluvium vs Braided	4.55	**<0.001**	3.16	**0.005**	4.56	**<0.001**	2.17	**0.035**
Incised Alluvium vs Piedmont Headwater	0.007	0.99	0.849	0.45	1.25	0.27	0.192	0.86
Incised Alluvium vs Braided	2.71	**0.016**	1.86	0.084	3.70	**0.002**	1.39	0.21
Piedmont Headwater vs Braided	2.30	0.051	0.933	0.40	4.10	**0.002**	1.22	0.27

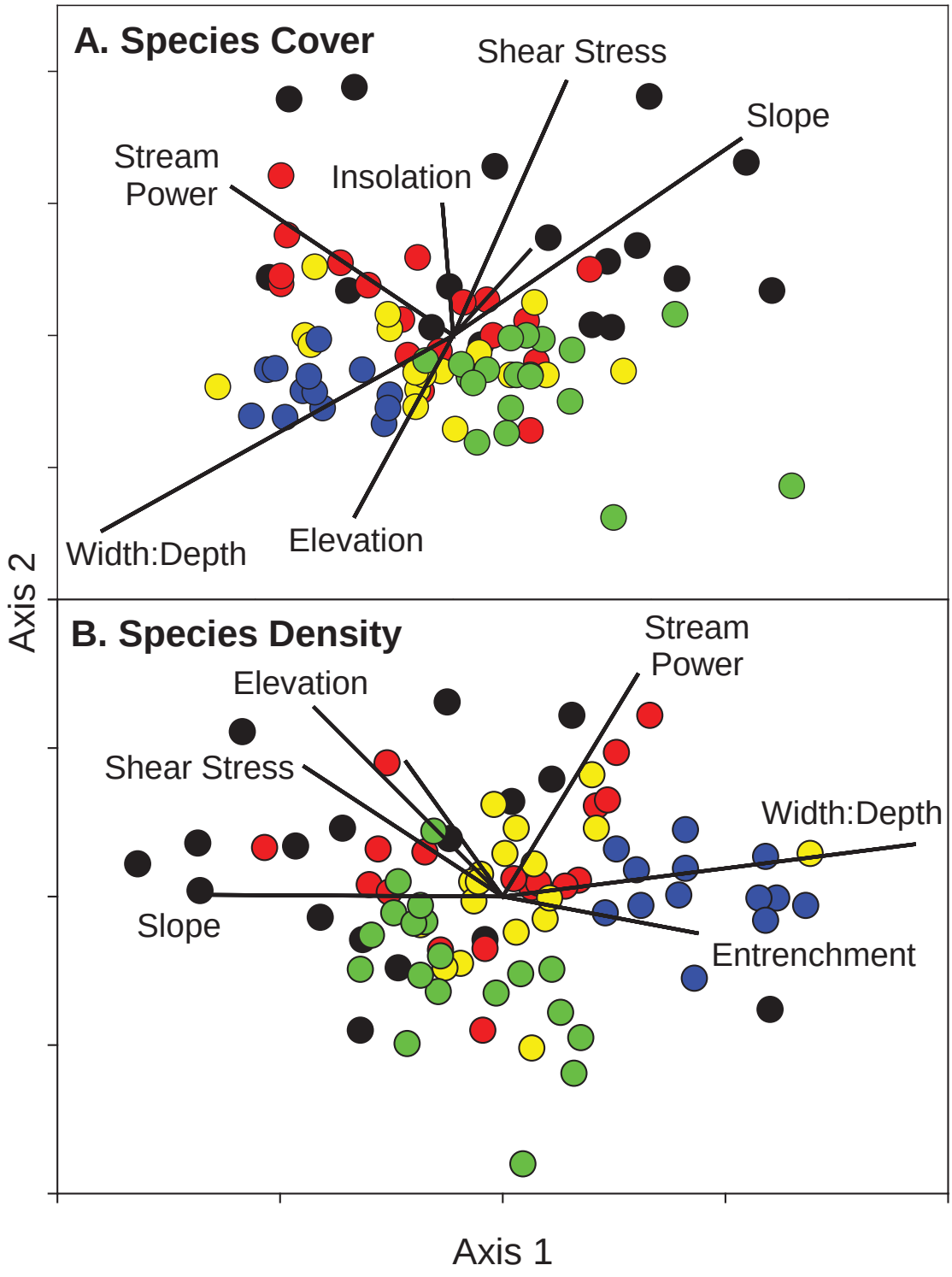

Figure 5-1. Nonmetric Multidimensional Scaling ordination of (A) species relative cover (stress = 0.145), and (B) species relative density (stress = 0.169). Symbol colors: black = bedrock; red = bedrock with alluvium; yellow = incised alluvium; green = piedmont headwater; blue = braided.

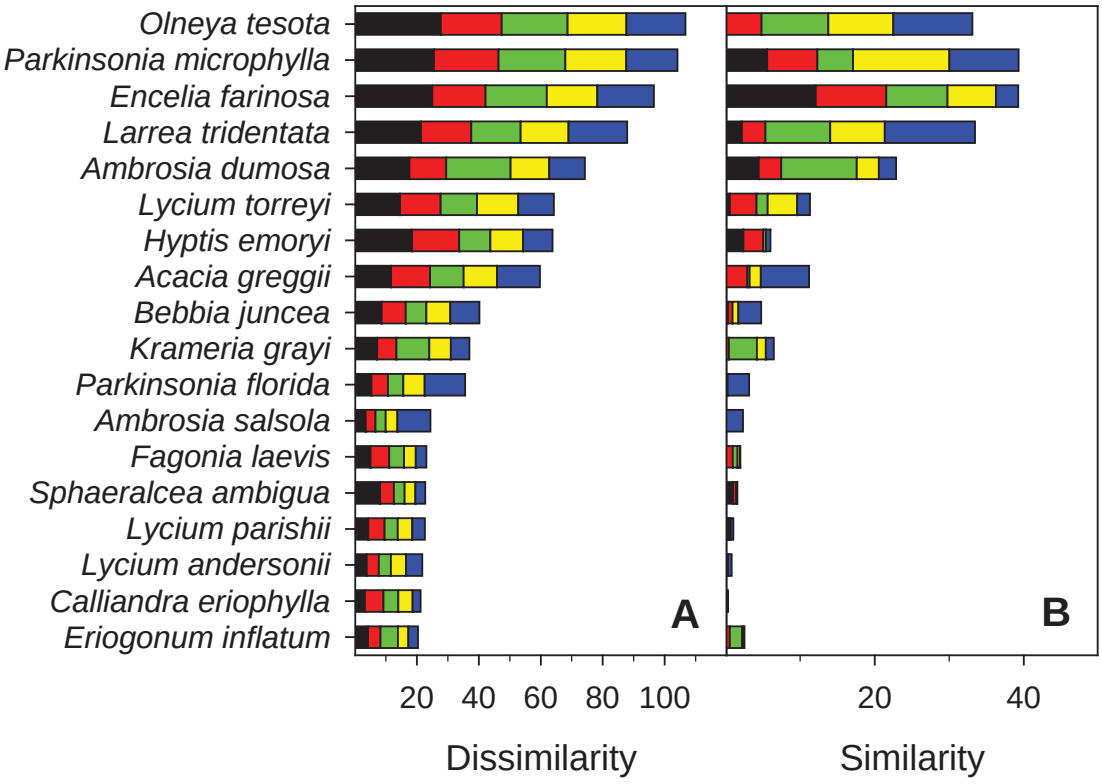

Figure 5-2. Ranked contribution of species relative cover to average Bray-Curtis dissimilarities between stream types (A), and similarity within stream types (B). Only the 18 highest-ranked species are shown. See Figure 5-2 caption for symbol colors.

of *Bebbia juncea* and *Ambrosia salsola* helped to distinguish braided streams, while *Fagonia pachyacantha, P. microphylla,* and *Sphaeralcea ambigua* separated bedrock streams from others. Similarity within stream types was overwhelmingly due to varying densities of *E. farinosa*, with lesser contributions from *A. dumosa, L. tridentata,* and *P. microphylla* (Figure 5-3B).

As with species cover, differences in species density among stream types occurred mainly along gradients of channel slope and width:depth, while piedmont headwater streams were separated from incised alluvium and bedrock with alluvium streams along a gradient of stream power and elevation (Figure 5-1B). The most parsimonious subset of abiotic variables explaining differences in species density among stream types consisted of channel slope, width:depth, and elevation (Table 5-5). The inclusion of stream power or shear stress yielded negligible effects on correlations among matrices.

Functional Group Cover

Plant communities defined by the relative cover of functional groups differed among stream types (Table 5-2; Figure 5-4A). Bedrock with alluvium and incised alluvium streams were not significantly different, but all other streams exhibited unique composition (Table 5-3). Beta diversity was highest in bedrock streams and lowest in braided streams, but was similar among all other stream types (Table 5-3).

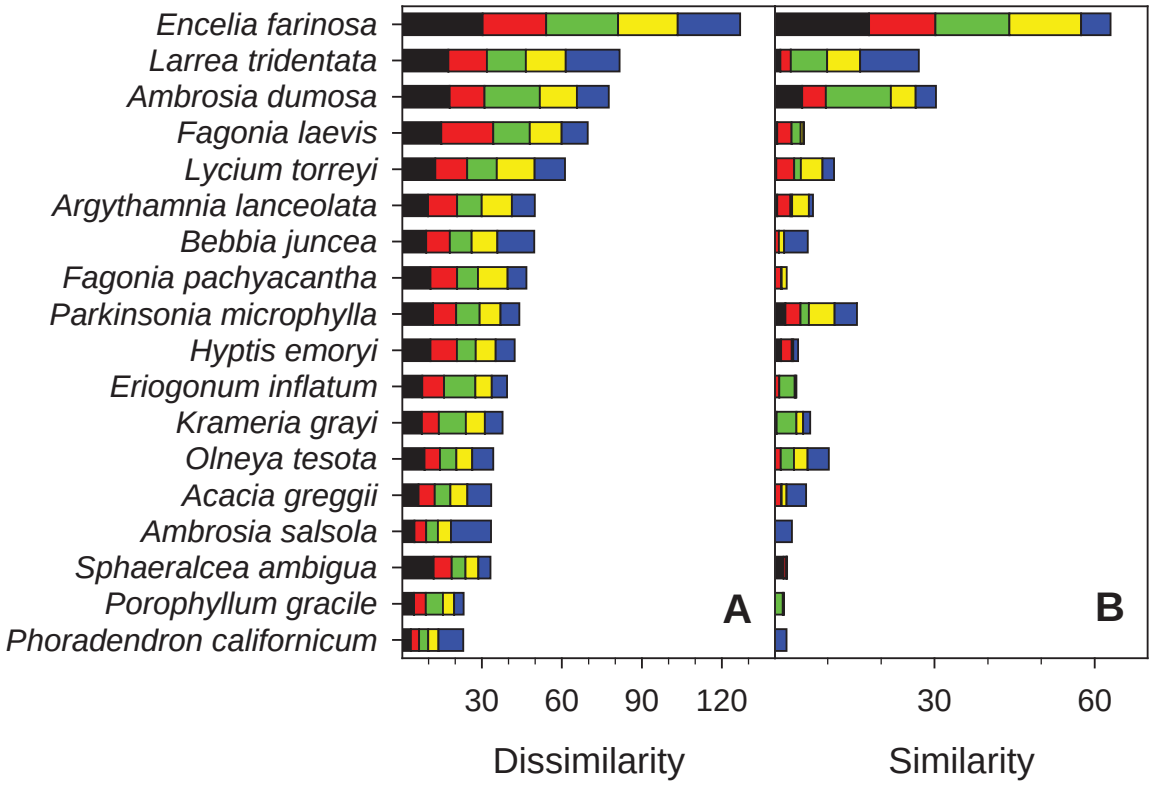

Figure 5-3. Ranked contribution of species relative density to average Bray-Curtis dissimilarities between stream types (A), and similarity within stream types (B). Only the 18 highest-ranked species are shown. See Figure 5-2 caption for symbol colors.

Table 5-5. Ranked subsets of reach scale abiotic variables that correspond to differences in riparian plant community characteristics among stream types. R_s = Spearman rank correlation.

	Variable Subset	r_s
Species Cover	Slope, Elevation	0.505
	Slope, Shear Stress, Elevation	0.504
	Slope, Stream Power, Elevation	0.504
	Slope, Shear Stress, Stream Power, Elevation	0.501
	Slope, Width:Depth, Shear Stress, Elevation	0.501
Species Density	Slope, Width:Depth, Stream Power, Elevation	0.485
	Slope, Width:Depth, Elevation	0.482
	Slope, Width:Depth, Shear Stress, Elevation	0.474
	Slope, Width:Depth, Shear Stress, Stream Power, Elevation	0.468
	Width:Depth, Shear Stress, Elevation	0.455
Functional Group Cover	Slope, Shear Stress	0.461
	Slope, Shear Stress, Elevation	0.460
	Slope	0.460
	Slope, Shear Stress, Stream Power, Elevation	0.451
	Slope, Elevation	0.444
Functional Group Density	Slope, Width:Depth	0.468
	Slope, Width:Depth, Stream Power	0.458
	Slope, Width:Depth, Shear Stress	0.445
	Slope, Width:Depth, Stream Power, Elevation	0.443
	Slope, Width:Depth, Elevation	0.442

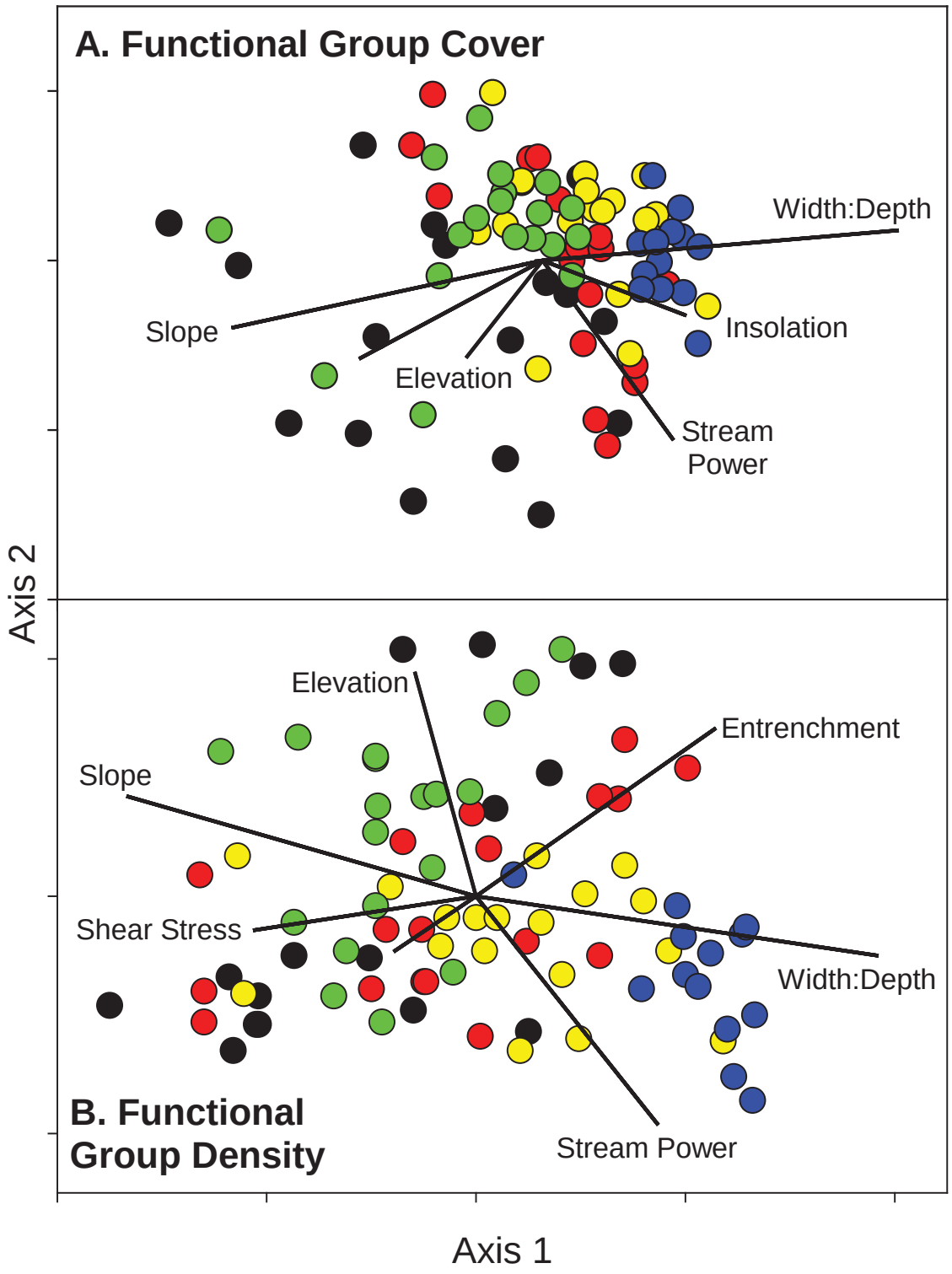

Figure 5-4. Nonmetric Multidimensional Scaling ordination of (A) functional group relative cover (stress = 0.132), and (B) functional group relative density (stress = 0.111). See Figure 5-2 caption for symbol colors.

The relative cover of evergreen and photosynthetic stem trees, and drought deciduous subshrubs, contributed the most to differences among stream types (Figure 5-5A). Evergreen, drought deciduous, and winter deciduous shrubs were also important dissimilarity components. Relative cover of drought deciduous subshrubs provided the most compositional similarity within stream types, followed by evergreen shrubs, photosynthetic stem trees, and drought deciduous shrubs (Figure 5-5B). Coverage of evergreen trees was also important to compositional similarity among all stream types except bedrock streams, where they did not occur.

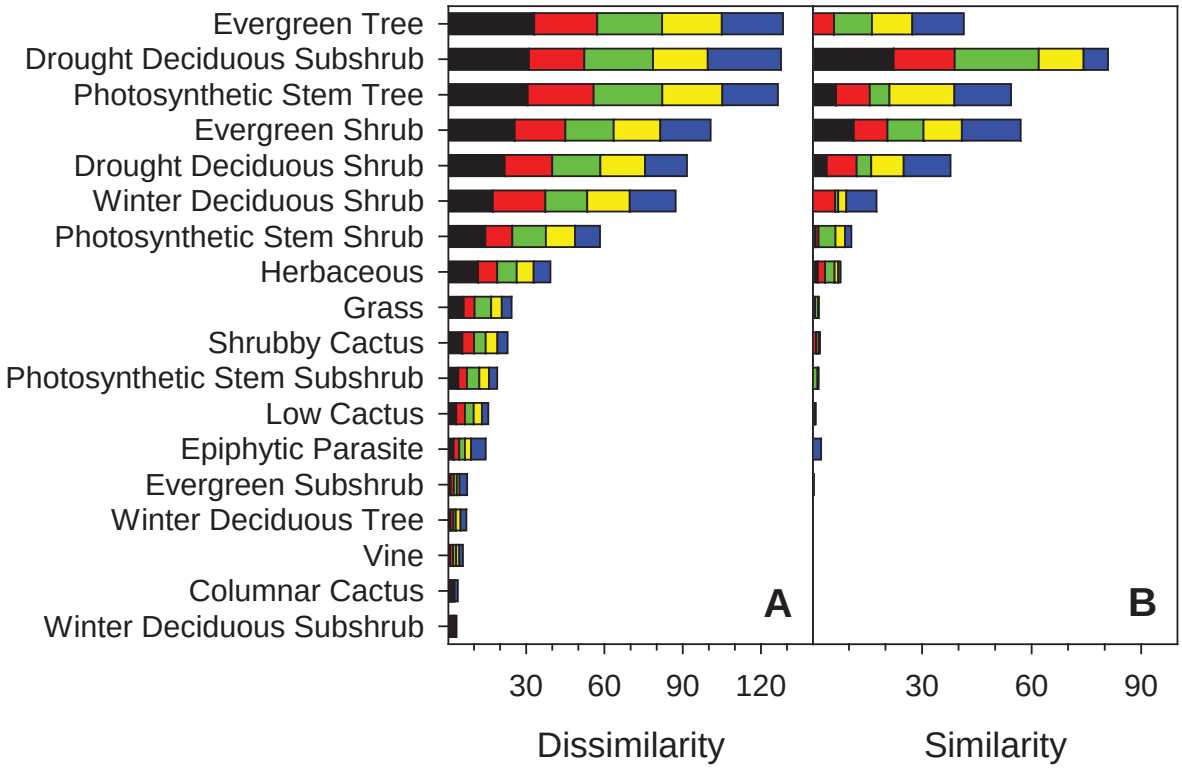

Figure 5-5. Ranked contribution of functional group relative cover to average Bray-Curtis dissimilarities between stream types (A), and similarity within stream types (B). See Figure 5-2 caption for symbol colors.

Similar to species composition, the relative cover of functional groups in stream types differed primarily along the covarying gradient of channel slope and width:depth (Figure 5-4A). Compositional differences between piedmont headwater and incised alluvium riparian communities were associated with lower stream power in piedmont headwater streams. Channel slope provided the most parsimonious explanation of differences in functional group cover among stream types (Table 5-5). The inclusion of shear stress and elevation did not improve correlations between abiotic and compositional distance matrices.

Functional Group Density

Stream types were significantly different in the composition and dispersion of functional group densities (Table 5-2; Figure 5-4B). Relative densities of functional groups in bedrock with alluvium streams was similar to that of bedrock and incised alluvium streams, but all other pairwise comparisons were significantly different (Table 5-3). Beta diversity was similar among all stream types, except for bedrock streams, which had the greatest dispersion (Table 5-4).

Functional group dissimilarity among stream types was most heavily influenced by the density of drought deciduous subshrubs (Figure 5-6A). Relative densities of drought deciduous shrubs, evergreen shrubs, herbaceous plants, and photosynthetic stem trees provided much of the remaining dissimilarity among stream types. Similarity within

stream types arose primarily from the density of drought deciduous subshrubs (Figure 5-6B). Similarity within braided streams was also influenced by density of drought deciduous shrubs and evergreen shrubs.

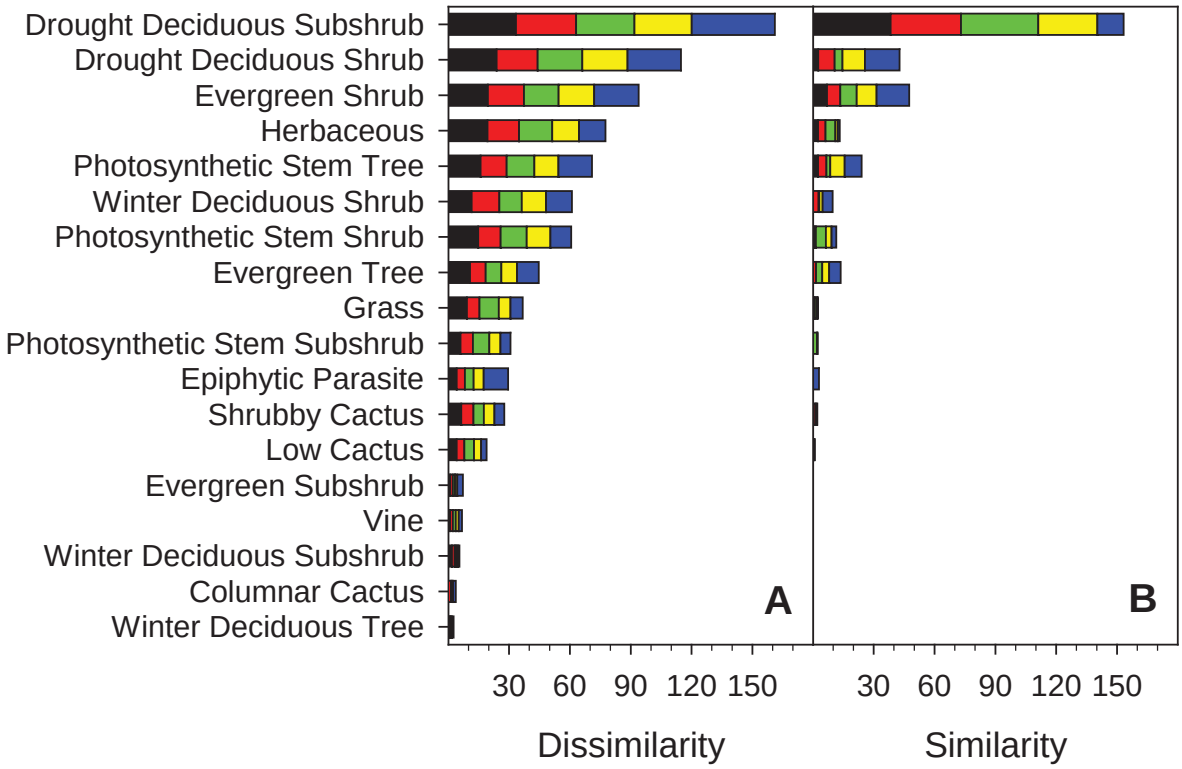

Figure 5-6. Ranked contribution of functional group relative density to average Bray-Curtis dissimilarities between stream types (A), and similarity within stream types (B). See Figure 5-2 caption for symbol colors.

Variation in channel slope and width:depth corresponded to differences in functional group densities among stream types (Figure 5-4B). Distinctive composition in piedmont headwater streams was associated with lower stream power and higher elevation. Channel slope and width:depth best explained differences in functional group densities among stream types (Table 5-5).

Discussion

The hydrogeomorphic stream types exhibited distinctive riparian plant community composition with respect to the relative cover and density of species and functional groups. Each of these compositional aspects differed substantially between braided, bedrock, and piedmont headwater streams. Incised alluvium and bedrock with alluvium streams, while different from other channel types, exhibited similar plant communities that were distinguishable only by species density. Comparison of channel geometry and hydraulic variables showed a similar pattern, with distinctive physical environments occurring in braided, bedrock, and piedmont headwater streams, while incised alluvium and bedrock with alluvium streams were poorly distinguished (Sutfin et al. 2014).

Distinctiveness in the physical environments and perennial plant communities of braided, bedrock, and piedmont headwater streams correspond to their placement as end-members along the fluvial continuum of ephemeral watersheds of the Sonoran Desert. Braided streams occur in the flat lowland portions of our study region, resulting in wide and low-gradient channels that have low erosive potential (Sutfin et al. 2014). Bedrock streams represent the

opposite end of the continuum, with steep, narrow and confined channels draining mountainous uplands. Piedmont headwater streams exhibit moderate gradients that reflect the topography of mountain pediments, but small discharges in these headwater segments generate low stream power and sediment transport capacity. Similarities in the physical environments and plant communities between incised alluvium and bedrock with alluvium streams arise from their shared occurrence within the middle portions of stream networks. These two channel types are often interspersed along the transition zone from mountainous uplands to lowland valleys.

Despite general similarities among bedrock with alluvium and incised alluvium channels, fundamental differences in boundary materials imply differing sensitivities to disturbance, processes of geomorphic adjustment, and ecohydrological dynamics that warrant separate treatment. With the exception of bed aggradation from reduced streamflow or increased sediment loads, vertical and lateral adjustment of bedrock with alluvium streams is largely constrained by resistant channel boundaries over typical management timescales (<100 yr). In contrast, disturbances such as large floods, as well as more gradual changes in sediment and streamflow regimes, could result in bed incision, channel widening, and avulsion within incised alluvium streams. The thickness of active alluvial deposits within bedrock with alluvium streams is typically less than those of incised alluvium channels (Harry et al. *in prep*), likely giving rise to differential rates of streamflow transmission losses (Goodrich et al. 1997) and subsurface moisture dynamics (Shaw and Cooper 2008, Kampf et al. *in prep*.). The resulting disparity in the magnitude and frequency of streamflow, and patterns of root zone water availability, are expected to produce differences in the timing and extent of plant establishment and mortality, water stress and gas exchange. Finally, we recognize that aggregation of abiotic and biotic characteristics across the reach scale may preclude detection of geomorphic and ecological differences among these stream types that occur at finer scales.

Species Composition

Compositional differences between reach types within our study area is driven by the most common species in the regional flora. *Ambrosia dumosa, E. farinosa,* and *L. tridentata* dominate landscapes throughout the northern Sonoran Desert (Shreve and Wiggins 1964, Turner et al. 1995), and were the most influential components of variation between riparian communities of all stream types. *Encelia farinosa* commonly occurs on rocky slopes (Parker 1988, Smith et al. 1997), and its tolerance for the low water availability typical of coarse thin sediments allows it to attain the greatest relative cover in bedrock streams. In contrast, *A. dumosa* and *L. tridentata* occupy sandier soils and alluvial sediments (Shreve and Wiggins 1964), resulting in their higher abundance in piedmont headwater, and braided and incised alluvium streams, respectively. *Olneya tesota* and *P. microphylla* are the most abundant and widespread trees in xeroriparian communities of the Lower Colorado Valley, and commonly occur on upland surfaces in wetter portions the northern Sonoran Desert (Shreve and Wiggins 1964, Turner et al. 1995). Their ubiquity throughout the studied watersheds reflect the ability to inhabit a wide range of substrates and geomorphic settings (Parker 1988), but their scarcity in bedrock streams is likely due to lower moisture availability during dry seasons. Although occurring at lower densities than other species, the larger stature of these trees heavily impacted relative cover in all stream types.

Secondary differences among stream types arise from more localized species occurrences, according to their affinity for specific substrates and facilitative interactions. Species typical of braided and incised alluvium streams such as *B. juncea, A. salsola, P. florida* and *P. spinosus* are found on thick unconsolidated sediments and active alluvium throughout their ranges (Campbell and Green 1968, Turner et al. 1995, Baldwin et al. 2002). *Phoradendron californicum,* a common epiphytic parasite of Fabaceae trees throughout the region (Shreve and Wiggins 1964), unsurprisingly attains its greatest cover and abundance in braided and incised alluvium streams, where tree density is highest. Similarly, shaded microsites under trees and large shrubs supported uncommon species such as *Trixis californica*, several *Lycium* spp, and *Mirabilis laevis* in braided, incised alluvium, and piedmont headwater streams respectively.

Functional Group Composition

Dominant plant functional groups have the largest competitive advantage in utilizing available soil moisture, allowing for the coexistence with others from more specialized niches (Noy-Meir 1973). The dominance of drought deciduous subshrubs throughout ephemeral watersheds of the northern Sonoran Desert, particularly in the more xeric bedrock and piedmont headwater streams, results from the ability to rapidly utilize brief moisture pulses and minimize water demands during drought periods by shedding photosynthetic tissue (Shreve and Wiggins 1964, Smith et al. 1997). A similar strategy for coping with environmental fluctuations in herbaceous perennials is reflected by a comparable spatial pattern of relative abundance. While larger drought deciduous shrubs follow the same temporal pattern of resource acquisition as their subshrub counterparts, they were most abundant in downstream alluvial portions of stream networks, suggesting that greater rooting depth enables them to access moisture in deeper strata (Davis and Mooney 1986, Shmida and Burgess 1988). Gas exchange and growth rates of evergreen and photosynthetic stem plants are lower than those of drought deciduous growth forms, but they require more persistent soil moisture to meet the metabolic demands of maintaining photosynthetic tissue throughout the year (Smith et al. 1997). The greater importance of these functional groups within incised alluvium and braided streams suggests that lower rates of resource acquisition provides a competitive advantage in lower network positions, where infrequent flow events may only recharge deep alluvium once every one or two years. In dryland settings, cacti of all sizes and perennial grasses are most abundant where reliable warm-season moisture occurs (Shmida and Burgess 1988, Smith et al. 1997), which probably explains their relative scarcity within ephemeral watersheds in a region of highly variable monsoon rainfall.

Differences in the frequency and intensity of periodic flood disturbance among the channel types corresponds to variation in the relative density of growth forms. Intense flood disturbance associated with high channel gradient and bankfull shear stress in montane bedrock streams favors the compact and flexible canopies of subshrubs. In contrast, the greater aboveground biomass and rigid stems of arborescent growth forms makes them more susceptible to flood damage, and slower growth rates could limit their ability to recolonize between floods. Although the flexible and multi-stemmed canopies of shrubs are less susceptible than trees to flood disturbance (Sandercock and Hooke 2010), both growth forms exhibited similar spatial distributions. This pattern suggests that access to stable water supplies in deep alluvium exerts greater influence than disturbance regime on the occurrence of larger woody plants in arid watersheds (Shreve and Wiggins 1964, Balding and Cunningham 1974, Shmida and Burgess 1988, Lite and Stromberg 2005).

Reach Scale Geomorphic Drivers of Community Composition

Consistent with findings from more mesic fluvial environments, our analysis demonstrates that channel slope is the dominant reach-scale driver of riparian community composition in dryland ephemeral stream networks. The influence of channel slope on riparian ecological patterns arises from direct effects on disturbance potential, and indirect effects on alluvial storage and subsurface water availability. As the primary determinant of streamflow velocity and sediment transport capacity (Knighton 1998), channel gradient governs channel and floodplain hydraulics, and the associated disturbance regimes that directly shape riparian communities (Hupp 1982, Baker 1989, Bendix 1997). Spatial variation in sediment transport and deposition controls the distribution and character of fluvial landforms, thereby indirectly influencing patterns of flood inundation that are associated with the distributions of plant species and riparian community types (Hupp 1982, 1986, Bendix 1994, Bendix and Hupp 2000). At larger spatial scales, channel slope and related covariates (e.g. stream power, width:depth) determines sediment deposition, and therefore the thickness and extent of alluvial sediments. Sediment thickness limits subsurface moisture storage capacity, and is a fundamental control on desert plant community composition (Kassas and Imam 1954, Shreve and Wiggins 1964, McAuliffe 1999).

Stream reach elevation was consistently identified as a secondary determinant of riparian community composition. Similar patterns have been recognized in mountainous semi-arid watersheds exhibiting higher topographic relief (Baker 1989, Bendix 1994, Sieben et al. 2009), but the limited range of elevations among our study reaches (460 m) is unlikely to create substantial zonation on temperature or rainfall regimes. Instead, elevation likely serves as a proxy for changes in substrate type and other unmeasured physical conditions. Within the study area, bedrocks

streams occur at the highest elevations, piedmont headwaters occur at moderate elevations, and incised alluvium and braided streams are found at the lowest elevations.

Surprisingly, neither entrenchment ratio nor total annual insolation were strongly related to variation in community composition at the reach scale. Insolation or heat load, typically quantified by indices of slope aspect, strongly influences soil moisture dynamics and plant community composition in upland desert environments (Shreve and Wiggins 1964, Noy-Meir 1973, Parker 1988). Our finding that total annual insolation did not covary with riparian composition likely reflects compensation for evapotranspirational losses, due to substantial run-on water subsidies from contributing watersheds and tree canopy shading, that is not typically available in upland sites. Entrenchment ratio quantifies channel confinement, and may be considered an index of flood disturbance potential for floodplain and overbank surfaces (Rosgen 1994). Considering the prominent role of flood disturbance in structuring riparian communities (Hupp and Osterkamp 1996), the lack of correspondence between entrenchment ratio and any measured aspect of community composition in our study area suggests that this geomorphic metric is of limited utility. Aside from potential measurement errors in our data set, the arbitrary elevation at which 'flood prone' width is determined (two times bankfull depth) appears to be an inappropriate datum for shallow and wide ephemeral channels.

Application of the Hydrogeomorphic Stream Classification

Although not previously recognized in terms of the hydrogeomorphic stream types presented here, analogous patterns of species and functional group composition of riparian communities occur in dryland stream networks around the world. Distinctive plant community types in the equivalents of bedrock, incised alluvium, and braided streams have been widely observed in ephemeral watersheds throughout Saudi Arabia (Al Wadie 2002, Alatar et al. 2012, Al-Rowaily et al. 2012, Abdel Khalik et al. 2013, El Ghazali et al. 2013), Egypt (Kassas and Imam 1954, Ali et al. 2000), and Algeria (Benhouhou et al. 2003), as well as along perennial and intermittent rivers in South Africa (Van Coller et al. 1997) and Italy (Angiolini et al. 2011, Nucci et al. 2012). Although bedrock with alluvium and incised alluvium streams in our study area support broadly similar riparian vegetation, compositional differences among the equivalents of these stream types have been recognized in other ephemeral stream networks of the southwestern USA (Shaw and Cooper 2008) and northern Africa (Kassas and Imam 1954, Benhouhou et al. 2003). While specific physical and biological attributes vary with regional climate, geology, and biogeography, considerable evidence indicates that these stream types comprise distinctive hydrogeomorphic and ecological process domains.

Because the ephemeral stream classification described in Sutfin et al. (2014) characterizes spatial patterns of riparian plant communities and physical drivers of ecological dynamics at the stream reach scale, it has many potential applications in research, management, and restoration applications. The classification can be used to select appropriate reference sites for restoration targets, and to identify suitable controls and replicates in manipulative experiments. In observational studies, this stream typology provides a defensible basis for sample stratification, and can be used to identify and isolate specific portions of fluvial gradients for focused process-based investigations. Since these stream types appear to be broadly relevant to dryland fluvial environments around the world, they may facilitate scientific communication as concise and meaningful descriptors of physical and biological process domains. Although the specific attributes of these stream types will vary between climatic, geologic, and biogeographical regions, this typology has potential to provide rich physical and biological information from simple visual inspection of qualitative features. With appropriate spatial data sets, such as DEMs, geologic maps, and aerial imagery, the stream types can further conservation activities such as resource mapping and inventories. Such a tool will enable resource managers to make more informed decisions on the type and locations of land uses in dryland watersheds.

Conclusions

The hydrogeomorphic ephemeral stream types support distinctive riparian plant communities, which were distinguishable on the basis of relative cover and density of species and plant functional groups. Within arid watersheds of the northern Sonoran Desert, spatial variation in riparian community composition is largely driven by distributions of the most common species and functional types in the regional flora. Compositional differences

among stream types correspond primarily to variation in channel gradient and bankfull width:depth, highlighting the role of geomorphic disturbance in spatial shaping patterns of riparian ecological dynamics. Consistent physical and biological attributes of stream types within the study area, and similar general patterns reported from arid regions across the globe, indicate that this ephemeral stream classification is broadly applicable in the study, management, and restoration of dryland ephemeral streams.

Chapter 6. Seasonal Water Sources of Riparian Trees in Arid Ephemeral Stream Networks

Abstract

We examined seasonal use of water sources among four dominant riparian tree species in ephemeral streams of the Sonoran Desert, and tested for differences among hydrogeomorphic stream types across two watersheds. Over the course of two years, all four species relied primarily on water from the upper 50 cm of unsaturated alluvium. Trees preferentially used water from surficial sediments following large storms and streamflow events. During drought periods, all species extracted vadose zone water from both shallow and deep (>50 cm) sources. Deep water sources included fractured bedrock beneath bedrock with alluvium channels, consolidated Pleistocene alluvium underlying piedmont headwater channels, and both unconsolidated and consolidated alluvium within incised alluvium and braided channels. Changes in water source usage were driven by the timing and magnitude of hydrologic pulses, which was highly variable within and among stream types. We conclude that dominant riparian trees in ephemeral streams of the Sonoran Desert occupy similar hydrologic niches despite differences in species distributions, and the preferential use of near-surface waters may maximize nutrient uptake.

Introduction

Key topics in dryland riparian ecohydrology include the identification of water sources for vegetation, how source water usage varies seasonally and during drought, and whether these sources are partitioned among dominant species (Smith et al. 1998). The application of stable isotopes has clarified these issues in many ecosystems (Dawson et al. 2002), but only a few studies have examined riparian trees in ephemeral streams (Kolb et al. 1997, Snyder and Williams 2000, Costelloe et al. 2008). However, these studies focused on groundwater use by phreatophytic trees, and no information is available on seasonal water sources of riparian trees where shallow groundwater does not occur.

Dominant riparian trees in ephemeral stream networks of the Sonoran Desert have photosynthetic stems or evergreen leaves that remain photosynthetically active throughout the year, despite chronic water limitation and intense summer droughts (Szarek and Woodhouse 1977, 1978, Nilsen et al. 1989). Although no data are available on maximum rooting depths for any of these species (Stromberg 2013), it has been assumed that they use deep vadose (Smith et al. 1997) or phreatic water to maintain low xylem water potentials and gas exchange in between precipitation pulses (Nilsen et al. 1984, Gibson 1996).

We compared variation in seasonal water sources among four common riparian tree species in ephemeral watersheds of the Sonoran Desert, across four hydrogeomorphic stream types. Tree species consisted of ironwood (*Olneya tesota*), foothills paloverde (*Parkinsonia microphylla*), blue paloverde (*P. florida*), and smoketree (*Psorothamnus spinosus*). Ironwood, foothills paloverde, and blue paloverde occur throughout the northern Sonoran Desert and occupy upland surfaces within less arid portions of their ranges (Shreve and Wiggins 1964, Turner and Brown 1994, Turner et al. 1995). In contrast, smoketree is an obligate riparian species that occurs only within the arid Lower Colorado Valley of the Sonoran Desert. Differences in the geographic ranges of these species (Turner et al. 1995), and their distributions within ephemeral stream networks of the study area (Shaw and Cooper *in prep.*), suggest that they occupy differing hydrologic niches. We examined water source partitioning by these riparian trees within piedmont headwater, bedrock with alluvium, incised alluvium, and braided streams (Sutfin et al. 2014).

Methods

Plant water sources were determined by comparing $\delta^{18}O$ values of xylem water, alluvial water, and rainfall in two ephemeral tributary watersheds of the lower Colorado River, in the Sonoran Desert of southwestern Arizona, USA. In each of the two watersheds (Yuma Wash and Mohave Wash), plant tissue and shallow alluvium (0-50 cm) samples were collected from one example of each stream type, four times per year in 2012 and 2013. Sampling was timed to characterize seasonal conditions occurring in winter (January), spring (March), summer (June), and fall (September/October). Rainfall, subsurface water content, and streamflow were measured concurrently at each study site (Faulconer et al. *in prep,* Kampf et al. *in prep*.).

During each sampling period, we collected fully suberized terminal shoots (Ehleringer and Osmond 1989) of approximately 2 cm diameter from five individuals of each tree species. Beginning in January 2013, we also sampled 3 to 5 seedlings of each species that had established in the previous year at both braided sites, as availability permitted. The taproot and major lateral roots were collected from small seedlings with unsuberized stems,

otherwise the basal suberized portions of stems were collected. All plant samples were stored in glass vials sealed with Parafilm-wrapped Teflon caps.

Concurrent with plant tissue collection, depth-integrated samples of shallow alluvium were taken from the upper 50 cm of the active channel. Alluvial fill at incised alluvium and braided channels is at least 4 m deep (Harry et al. *in prep.*), and potentially comprises a distinct plant water source. Therefore, we developed $\delta^{18}O$ profiles from trenches dug in January and September 2012, and May 2013. During trenching, depth-integrated alluvium samples were collected at 50 cm intervals, to a maximum depth of 4 m. Alluvium samples were stored in 1 L Nalgene bottles sealed with Parafilm, and all samples were frozen until analysis.

Azeotropic distillation of xylem and alluvial waters was conducted at the EcoCore Stable Isotope Laboratory at Colorado State University, using the distillation apparatus and methods outlined in Revesz and Woods (1990) and Revesz et al. (2012). Since isotopic fractionation likely occurs within photosynthetic tissue beneath the bark of suberized stems in *P. florida* and *P. microphylla*, the bark and cambium of all plant samples were scraped off prior to distillation. Isotopic compositions of extracted waters were determined using a Thermo Scientific Delta V Plus run in continuous mode, connected to a high-temperature conversion elemental analyzer (TCEA) via a Conflo IV. A Thermo AI 1310 autosampler was used to inject three 1 µl aliquots of each sample into the TCEA column, and the resulting measurements were averaged. Measurements were then normalized using a linear equation derived from three laboratory reference materials, and reported as $\delta^{2}H$ and $\delta^{18}O$ relative to V-SMOW (Gonfiantini 1978, Coplen 1988). Long-term 2σ uncertainties for $\delta^{2}H$ and $\delta^{18}O$ using this procedure are ±5.0 ‰ and ±0.8 ‰, respectively. Isotopic analyses were performed at the University of Wyoming Stable Isotope Facility.

At incised alluvium and braided sites, similarity of isotopic compositions at depths >50 cm allowed us to lump alluvium samples below this depth into one water source (Phillips et al. 2005). After sample collection and analysis, we found that xylem waters were at times more enriched than the corresponding depth-integrated shallow alluvial waters, suggesting that plants were deriving water from the upper few cm of sediment. Since our alluvial samples apparently do not represent discrete end-members, we could not apply quantitative mixing models (e.g. Phillips and Gregg 2001) to determine the proportions of various water sources used by plants. Therefore, we restrict our discussion of seasonal plant water sources to qualitative observations. Since there is some evidence that root water uptake by ironwood causes minor $\delta^{2}H$ fractionation (Ellsworth and Williams 2007), we limit our comparisons to $\delta^{18}O$ values.

Results

Aggregated across sites and sample periods, xylem waters from all four riparian tree species exhibited similar slopes when plotted as $\delta^{2}H$ versus $\delta^{18}O$ (Figure 6-1). This patterns demonstrates that evapotranspirational pathways governing the isotopic evolution of xylem waters do not differ appreciably between species. Isotopic composition of deep alluvium samples (>50 cm) from incised alluvium and braided sites showed a slope similar to precipitation samples, suggesting that deeper alluvial waters are recharged by rapid infiltration with minimal evaporation. Shallow alluvial waters (≤50 cm) had much greater variation due to evaporative enrichment following infiltration, which differed across sample periods with varying antecedent rainfall patterns.

Piedmont Headwater

The isotopic composition of water in shallow alluvium exhibited comparable seasonal variation in piedmont headwater sites from both watersheds (Figure 6-2). Mean $\delta^{18}O$ values at the Mohave Wash site ranged from -10 to -12 ‰ during winter, and -1 to 2 ‰ in summer, with the highest value (4 ‰) occurring during fall of 2013 (Figure 6-2A). Similar $\delta^{18}O$ values occurred at the Yuma Wash site during winter 2013 (-11 ‰), but shallow alluvial waters were more enriched during the warmer seasons (Figure 6-2C). Mean $\delta^{18}O$ values ranged from 4 to 7 ‰ from spring to fall in 2012, and increased from -3 to 6 ‰ from spring to fall of 2013.

Relative to the shallow alluvium at each site, plant xylem water isotopic composition showed much less variability, and was similar between species. At Mohave Wash, plant isotopic composition was the same as shallow alluvium during the spring, summer, and fall of 2012 (Figure 6-2B). Xylem waters were more enriched than shallow alluvium samples by 4 and 7 $\delta^{18}O$ ‰ during the winters of 2012 and 2013, respectively, suggesting that the plants were using water from a shallower depth interval than was sampled. In contrast, xylem water had lower $\delta^{18}O$ values than shallow alluvium from spring through fall of 2013, with the difference progressively increasing from 3 to 9 ‰. These differences suggest that the trees were using less enriched water from the consolidated Pleistocene alluvium underlying the channel.

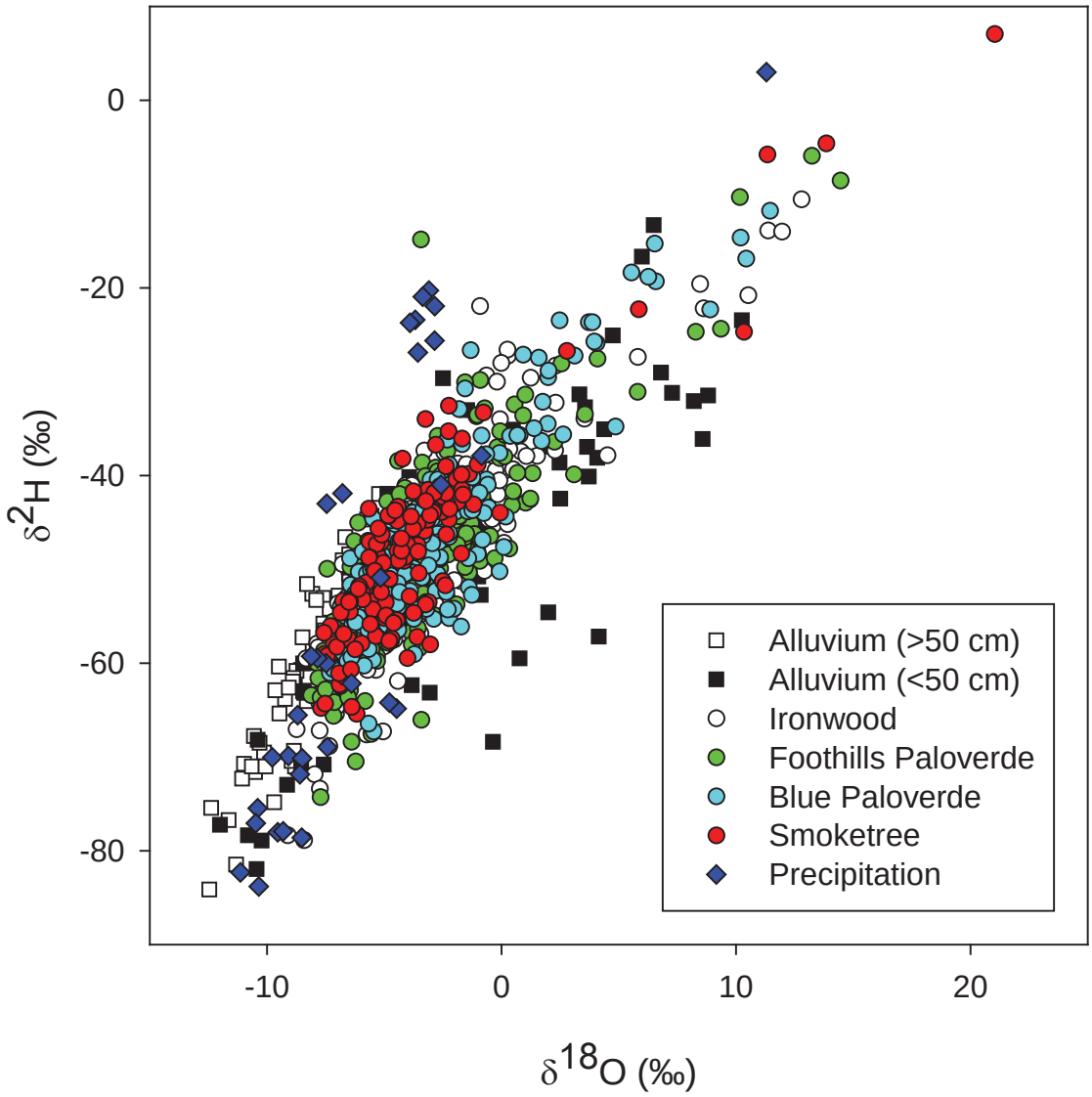

Figure 6-1. Isotopic composition of waters from riparian tree xylem, shallow (<50 cm) and deep (>50 cm) alluvium, and precipitation from all study sites during 2012 and 2013.

Xylem waters at the Yuma Wash piedmont headwater site exhibited a different temporal pattern (Figure 6-2D). In the spring, summer, and fall of both years, xylem $\delta^{18}O$ was lower than shallow alluvium, indicating that the trees were using water from the Pleistocene alluvium throughout the growing season. Xylem was 9 to 12 ‰ lower in 2012, and 3 to 9 ‰ lower in 2013. Similar to the Mohave Wash site, xylem waters at the Yuma Wash piedmont headwater site were about 5 ‰ more enriched in $\delta^{18}O$ than shallow alluvium during the winter of 2013, reflecting a water source in the uppermost portion of the sediment profile. The only samples showing isotopic differences between species were collected during the spring of 2012, when ironwood averaged 8 ‰ higher than foothills paloverde.

Bedrock with Alluvium

Water from shallow alluvium at the Mohave Wash bedrock with alluvium site exhibited less enriched and less variable isotopic composition than at the Yuma Wash site (Figure 6-3A, 6-3C). At Mohave Wash, maximum (1 ‰) and minimum (-9 ‰) $\delta^{18}O$ values both occurred during summer, and all other samples ranged from -4 to -8 ‰. At

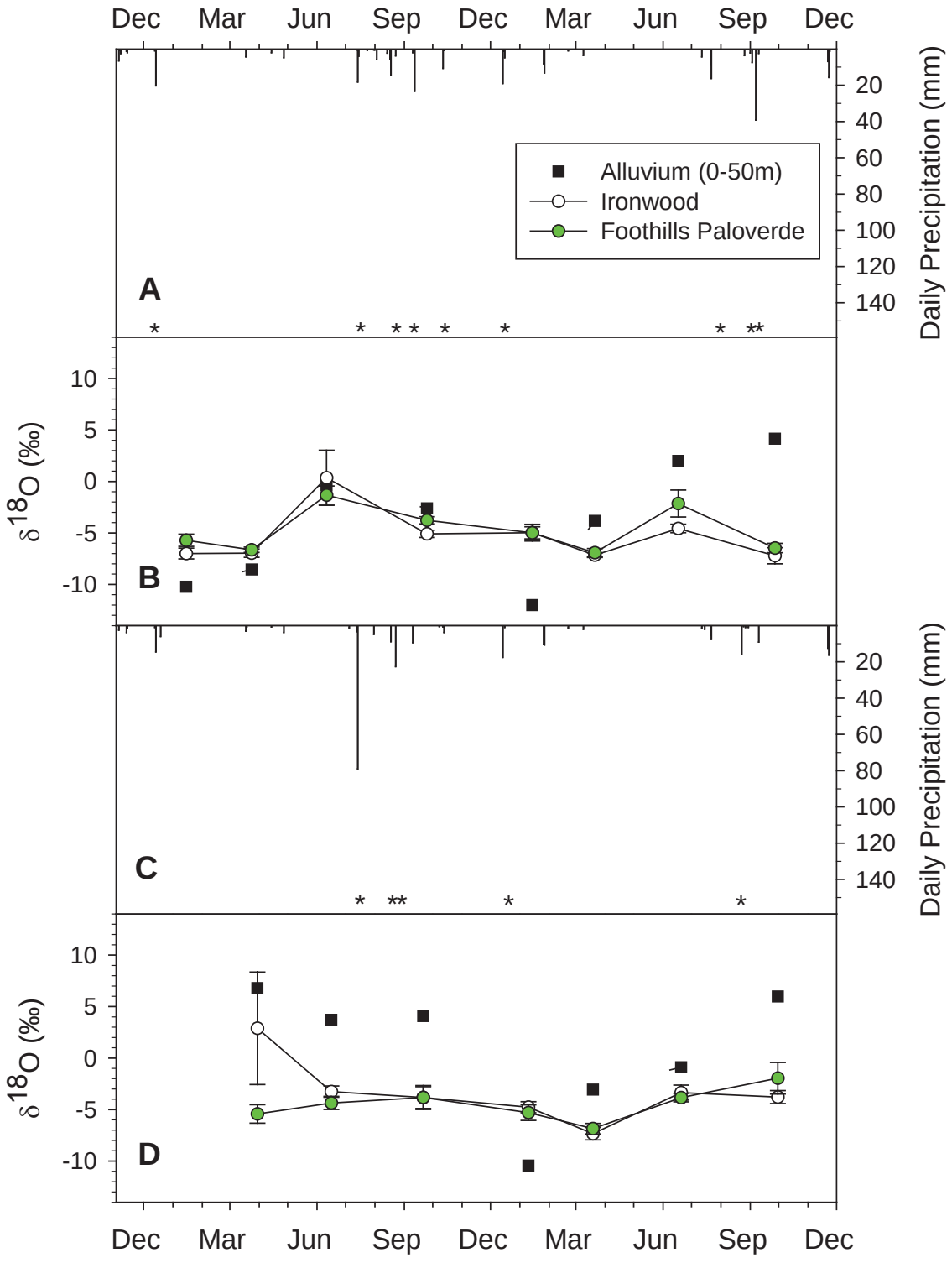

Figure 6-2. Rainfall, streamflow, and $\delta^{18}O$ values of plant xylem and shallow alluvium in piedmont headwater sites. Rainfall and streamflow at Mohave Wash (A); $\delta^{18}O$ values at Mohave Wash (B); rainfall and streamflow at Yuma Wash (C); $\delta^{18}O$ values at Yuma Wash (D). Points are means for each species and error bars are 1 S.E. Asterisks indicate streamflow events.

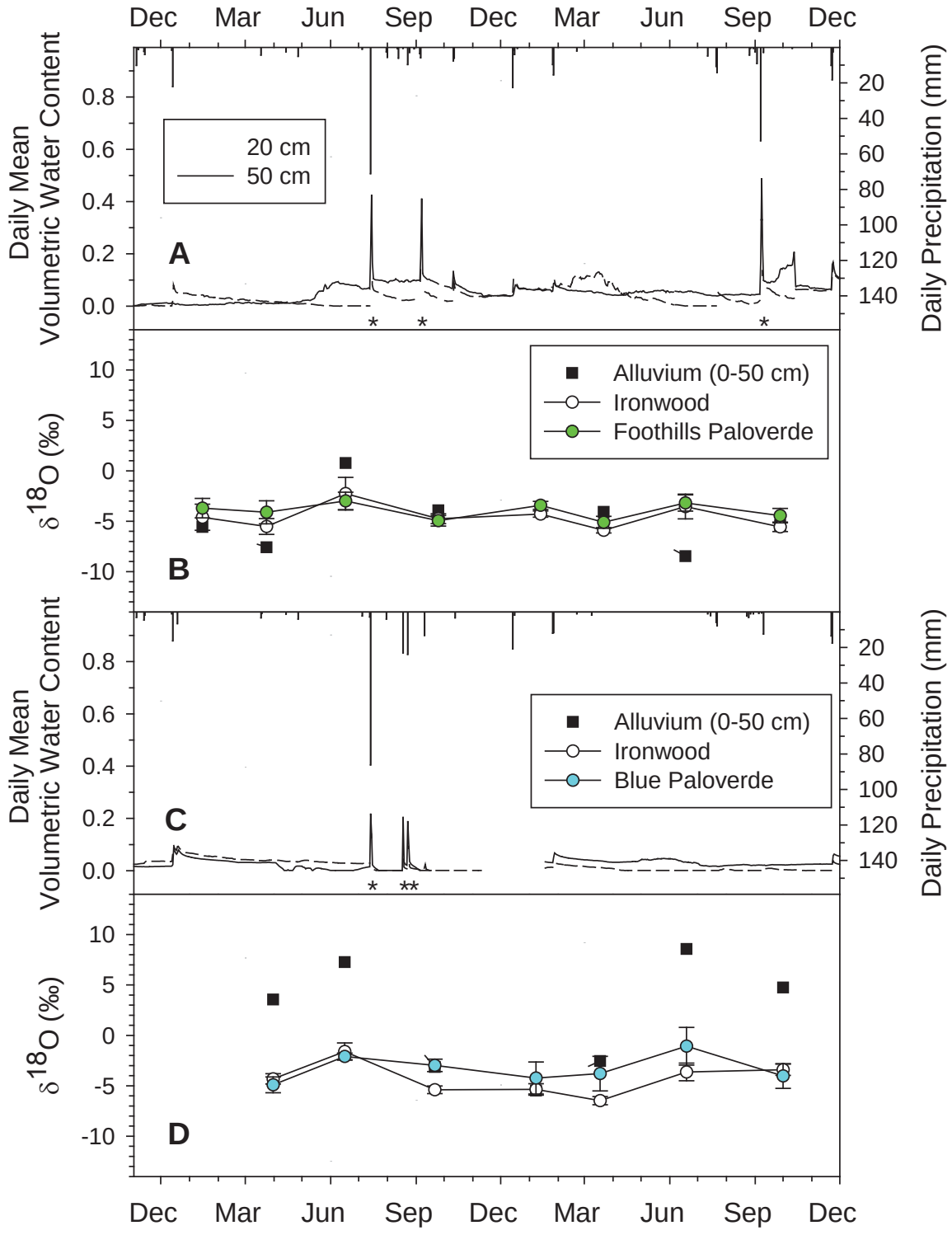

Figure 6-3. Rainfall, streamflow, water content, and $\delta^{18}O$ content of plant xylem and shallow alluvium in bedrock with alluvium sites. Rainfall, streamflow, and water content at Mohave Wash (A); $\delta^{18}O$ values at Mohave Wash (B); rainfall, streamflow, and water content at Yuma Wash (C); $\delta^{18}O$ values at Yuma Wash (D). Points are means for each species and error bars are 1 S.E. Asterisks indicate streamflow events.

Yuma Wash, $\delta^{18}O$ values were 8 to 9 ‰ in summer, but spring and fall samples varied considerably between years, depending on antecedent precipitation and streamflow. Samples collected during spring 2012 and fall 2013 had $\delta^{18}O$ values of 4 ‰ following periods of scant rainfall, whereas streamflow events from three significant monsoon storms resulted in $\delta^{18}O$ values of -3 to -6 ‰ from fall 2012 to spring 2013.

Xylem waters of ironwood and foothills paloverde at the Mohave Wash bedrock with alluvium site were remarkably consistent through time, with $\delta^{18}O$ values averaging -5 ‰ (Figure 6-3B). Throughout most of the study period, xylem isotopic composition of both species closely mirrored that of the shallow alluvium. Slight differences between alluvium and xylem waters were apparent in the spring and summer of 2012. In the spring, mean xylem $\delta^{18}O$ values were 3 to 4 ‰ higher than shallow alluvium, whereas xylem $\delta^{18}O$ values were 3 ‰ lower than shallow alluvium. During the summer of 2013, xylem waters averaged 5 ‰ higher than shallow alluvium, indicating that the trees were using water from surficial sediments.

In contrast to the similarities among plant and alluvium $\delta^{18}O$ values at Mohave Wash, ironwood and blue paloverde isotopic composition at the Yuma Wash bedrock with alluvium site exhibited substantial divergence from shallow alluvium samples (Figure 6-3D). Xylem waters were within 3 ‰ of shallow alluvium values from fall 2012 to spring 2013, but mean $\delta^{18}O$ values of both species were 9 to 13 ‰ lower than shallow alluvium samples at all other times. These significantly lower $\delta^{18}O$ values indicate that both species used water from deeper sediments, or possibly fractured bedrock underlying the alluvium, throughout much of the growing season.

Incised Alluvium

Profiles of $\delta^{18}O$ values in trenches at each incised alluvium site reflected minimal evaporative enrichment below 0.5 to 1 m depth over the study period (Figure 6-4). Isotopic composition of subsurface waters at the Mohave Wash incised alluvium site were showed little variation below 0.5 m, and averaged -7 ‰ (Figure 6-4B). Greater temporal variation was evident at the Yuma Wash incised alluvium site, where $\delta^{18}O$ values below 0.5 m averaged -10 ‰ (Figure 6-4D). Waters from shallow alluvium exhibited significantly greater seasonal variation, with differing patterns between watersheds (Figure 6-5). Summer $\delta^{18}O$ values at Mohave Wash ranged from 0 to 3 ‰ and all other samples were between -3 and -8 ‰ (Figure 6-5A). Shallow alluvium at Yuma Wash was more variable, with seasonal patterns driven by streamflow events (Figure 6-5C). Following a dry period, summer 2012 $\delta^{18}O$ was 10 ‰, but periodic storms resulted in $\delta^{18}O$ values between -5 and -7 ‰ from fall 2012 through the following summer. Only one flow event occurred in the summer of 2013, causing shallow alluvium $\delta^{18}O$ values to rise to 7 ‰.

At the Mohave Wash incised alluvium site, xylem isotopic composition showed considerable variation within and between species during the spring and summer of 2012, but $\delta^{18}O$ values were similar in all other samples (Figure 6-5B). Relative to shallow alluvium, mean $\delta^{18}O$ values of xylem waters were 2-4 ‰ higher in winter and 5-10 ‰ higher in spring 2012, indicating that all species were using water from surficial sediments. During the summer of 2012, $\delta^{18}O$ values of ironwood and both species of paloverde fell between the isotopic composition of shallow and deeper alluvium, but mean xylem $\delta^{18}O$ values of smoketree were similar to shallow alluvium. This pattern suggests that the other species were using water from both shallow and deep alluvium. During the spring and summer of 2013, all species appeared to be using both water sources. Isotopic compositions of xylem and shallow alluvium waters were similar during the other sample periods.

All species at the Yuma Wash incised alluvium site exhibited $\delta^{18}O$ values similar to shallow alluvium from fall 2012 to summer 2013 (Figure 6-5D). During the summer of 2012 and the fall of 2013, all species were using a mixture of shallow and deep alluvium, as shown by intermediate $\delta^{18}O$ values. Both species of paloverde exhibited the same pattern in spring 2012, but mean isotopic composition of ironwood xylem was similar to shallow alluvium.

Braided

Both braided sites showed stable isotopic compositions in subsurface waters below 0.5 m depth (Figure 6-4A, 6-4C). Mean $\delta^{18}O$ values in these deeper strata were -8 ‰ in Mohave Wash, and -10 ‰ in Yuma Wash. As at the other stream types, shallow alluvial water showed greater seasonal variation, with the highest variability occurring in Yuma Wash (Figure 6-6A, 6-6C). The Mohave Wash braided site had $\delta^{18}O$ values of 4 to 8 ‰ during summers, and -5 to 2 ‰ in other seasons. In Yuma Wash, the braided site showed temporal patterns of $\delta^{18}O$ values similar to the incised alluvium site. Following a dry period, shallow alluvium $\delta^{18}O$ values reached 9 ‰ in summer of 2012, but recharge from two late summer floods resulted in $\delta^{18}O$ values between -7 and -11 ‰ through the following spring. In summer and fall of 2013, $\delta^{18}O$ values were -1 and -3 ‰, respectively.

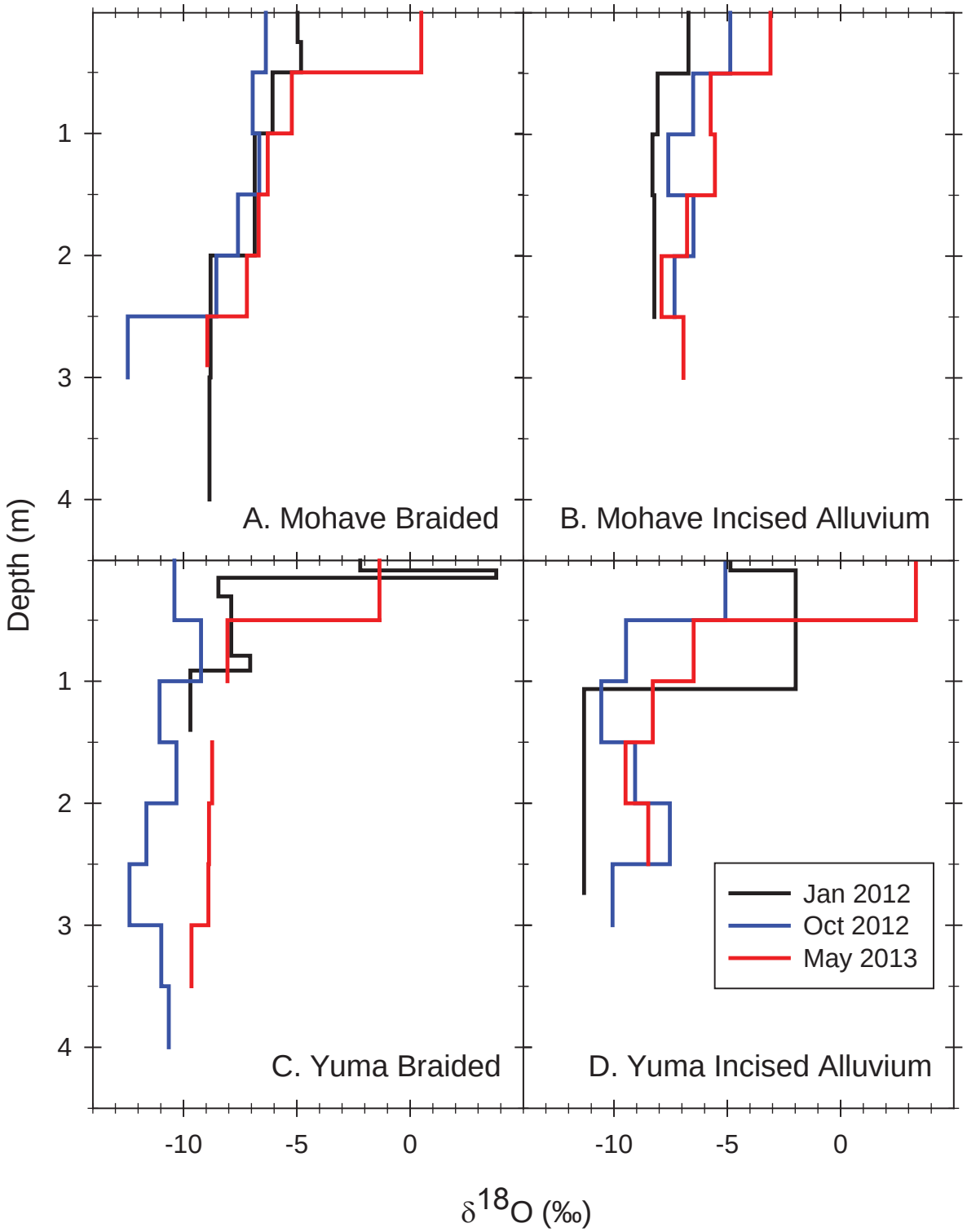

Figure 6-4. $\delta^{18}O$ profiles beneath the active channels of incised alluvium and braided sites.

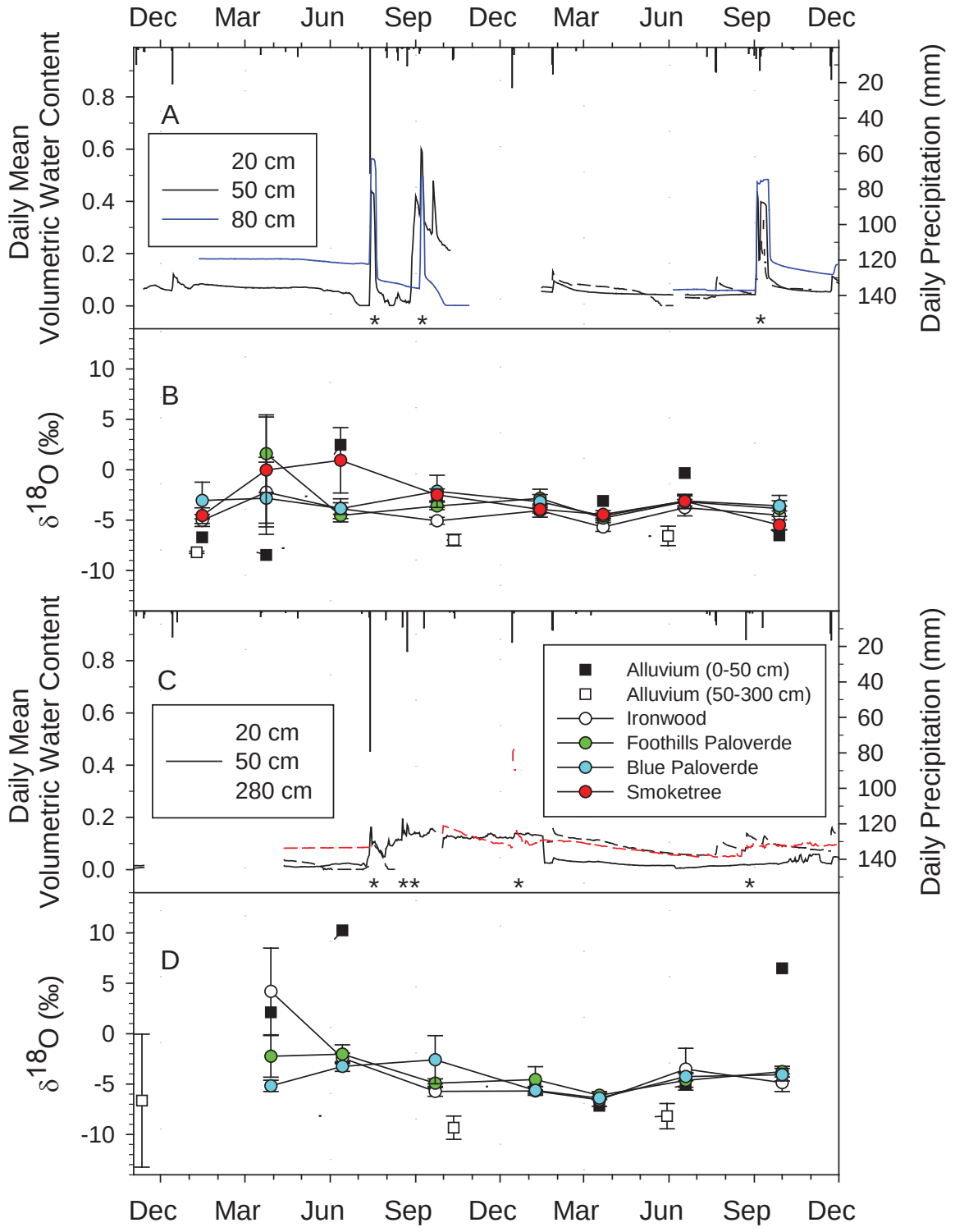

Figure 6-5. Rainfall, streamflow, water content, and $\delta^{18}O$ content of plant xylem and shallow alluvium in incised alluvium sites. Rainfall, streamflow, and water content at Mohave Wash (A); $\delta^{18}O$ values at Mohave Wash (B); rainfall, streamflow, and water content at Yuma Wash (C); $\delta^{18}O$ values at Yuma Wash (D). Points are means for each species and error bars are 1 S.E. Asterisks indicate streamflow events.

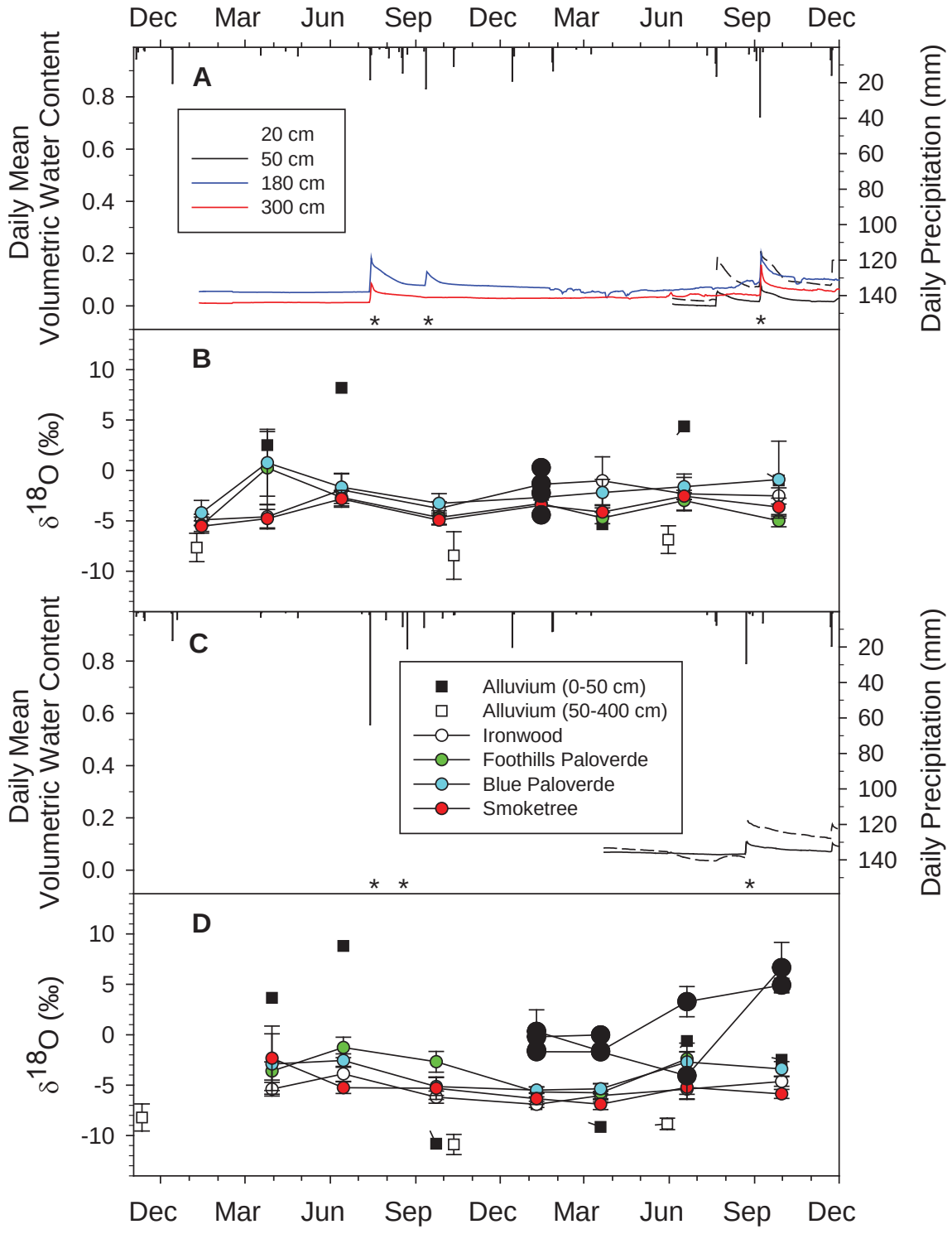

Figure 6-6. Rainfall, streamflow, water content, and $\delta^{18}O$ content of plant xylem and shallow alluvium in braided sites. Rainfall, streamflow, and water content at Mohave Wash (A); $\delta^{18}O$ values at Mohave Wash (B); rainfall, streamflow, and water content at Yuma Wash (C); $\delta^{18}O$ values at Yuma Wash (D). Points are means for each species and error bars are 1 S.E. Asterisks indicate streamflow events. Cross-hatched symbols are seedlings for each species.

Isotopic composition of xylem water in all four species was similar to shallow alluvium at the Mohave Wash braided site during the winter and fall of 2012 and 2013 (Figure 6-6B). Intermediate $\delta^{18}O$ values show that all species relied on both shallow and deep alluvium during both summers, but greater variability in water source usage occurred within and between species during each spring. In spring of 2012, mean $\delta^{18}O$ values of both paloverde species were similar to shallow alluvium, while smoketree and ironwood used water from both shallow and deep alluvium. All species relied on shallow alluvium during spring of 2013, but mean $\delta^{18}O$ values of blue paloverde and ironwood were 3 to 4 ‰ higher than shallow alluvium samples, suggesting that they used water from surficial sediments. Seedlings of all four species collected in winter of 2013 had isotopic compositions similar to shallow alluvium and mature plants, ranging from -5 to 0 ‰. High seedling mortality prevented subsequent seedling collection at this site.

At the Yuma Wash braided site, intermediate isotopic composition of all species reflected water usage from both shallow and deep alluvium during the spring and summer of 2012, and the summer and fall of 2013 (Figure 6-6D). All species used water from shallow alluvium during other sample periods. Xylem $\delta^{18}O$ values exceeded shallow alluvium samples by 6 to 8 ‰ in fall of 2012, and 3 to 4 ‰ in spring of 2013, suggesting that plants relied on surficial alluvium during these times.

Seedlings of all species collected in winter and spring of 2013 at the Yuma Wash braided site relied on water in surficial alluvium, with $\delta^{18}O$ values that exceeded shallow alluvium samples by 5 to 6 ‰ in winter and 8 to 9 ‰ in spring (Figure 6-6D). After that time, ironwood and foothills paloverde were not abundant enough sample, but blue paloverde seedlings continued to use surficial waters through the fall. In contrast, smoketree seedlings appeared to use both shallow and deep alluvial water during summer, with $\delta^{18}O$ values similar to their larger counterparts (-4 ‰). Thereafter, they relied on surficial alluvium and exhibited isotopic compositions similar to blue paloverde seedlings.

Discussion

Ironwood, foothills paloverde, blue paloverde, and smoketree exhibited broadly similar hydrologic niches across the four stream types. These trees relied primarily upon moisture within the upper 50 cm of the channel alluvium, except during seasonal drought periods, when they used a mixture of shallow and deeper alluvial waters. Following winter and spring rainfall, and occasionally after late summer floods, the trees preferentially extracted water from the uppermost sediment layers. Although our sampling could not reveal the precise depths of these surficial water sources, we infer from the highly enriched isotopic composition of xylem that trees were using water from the upper 10 to 20 cm.

We suggest that the opportunistic use of water from shallow and surficial alluvium by these riparian trees allows them to maximize nutrient uptake. Desert soils typically have low N content, and available nutrients are often concentrated near the surface (Noy-Meir 1973). Streamflow pulses provide N and labile C inputs to ephemeral stream riparian ecosystems, from direct stimulation of microbial activity as well as nutrient imports from losses throughout the watershed (Belnap et al. 2005, Harms and Grimm 2010, Larned et al. 2010). Although nitrogen fixing bacteria are known to occupy root nodules in ironwood (Felker and Clark 1981) and smoketree (Jenkins et al. 1988), nutrient pulses associated with periodic floods may provide critical resource subsidies.

Several studies have described woody phreatophytes in arid regions opportunistically using shallow soil water following warm-season rainfall in ephemeral stream (Kolb et al. 1997, Snyder and Williams 2000) and valley floor settings (Chimner and Cooper 2004, Kray et al. 2012). Similar shifts from deep to shallow soil water has also been widely observed in nonphreatophytic woody vegetation in upland settings (Williams and Ehleringer 2000, Schwinning et al. 2002, 2003, West et al. 2007). These shifts in water source usage have typically been attributed to increased water potential in near-surface sediments following infiltration, but concurrent increases in nutrient availability provide a plausible alternative explanation.

The timing and duration of water use from shallow alluvium was constrained by near-surface water availability, which varied with antecedent rainfall and streamflow. Trees in all stream types accessed both shallow and deep alluvial waters during the summer of 2012, when water availability in shallow alluvium was depleted after six months of low rainfall. In contrast, recharge from a large late-summer flood in 2012 sustained water use from only the shallow alluvium through the following summer at some sites.

The five hydrogeomorphic stream types exhibit distinctive morphology and hydraulic properties (Sutfin et al. 2014), as well as differences in alluvial depth and stratigraphy (Harry et al. *in prep.*), streamflow frequency (Faulconer et al. *in prep.*), and subsurface moisture dynamics Kampf et al. *in prep.*). These different physical environments

support distinctive riparian plant communities (Shaw and Cooper, *in prep.*). However, we did not observe systematic variation among stream types in the water sources used by riparian trees. Detection of such subtle differences likely requires more frequent sampling than the seasonal time scale we employed.

Across all stream types, waters from shallow alluvium in Yuma Wash showed greater variation and higher $\delta^{18}O$ values, and trees relied more heavily on deep alluvial water. Estimated average annual precipitation inputs to Yuma Wash have slightly higher $\delta^{18}O$ values (-2.8 ‰) than Mohave Wash (-3.2 ‰) because it is approximately 35 km closer to the Gulf of California, the primary source of warm season water vapor (Terzer et al. 2013). However, shallow alluvium in Yuma Wash consistently showed greater than ~0.5 ‰ difference within stream types, compared to Mohave Wash, suggesting that bare sediment evaporation rates are higher in Yuma Wash. Potential mechanisms for the apparently faster evaporative enrichment in Yuma Wash include higher temperatures due to approximately 0.5˚ lower latitude, and lithological differences in water retention of alluvial sediments. Bedrock in the Yuma Wash watershed is predominantly granitic, whereas the Mohave Wash watershed contains mostly rhyolite and dacite (Tosdal et al. 1989, Richard et al. 2000). These lithological disparities may influence bare sediment evaporation rates through differences in albedo and sediment texture. Finer-scale influences likely include differential shading by vegetation and local topography. These unmeasured factors may have contributed to the greater reliance of riparian trees on water from deep alluvium in Yuma Wash.

Conclusions

The dominant riparian trees in ephemeral streams of the Sonoran Desert occupy similar hydrologic niches and rely primarily on shallow alluvial water. All species used a mix of shallow and deep vadose waters during drought periods, but switched to water sources in surficial sediments following periodic rainfall and streamflow events. The timing and duration of water source usage varied considerably within and among stream types, and across watersheds, in response to hydrologic inputs.

Chapter 7. Seasonal Ecohydrological Dynamics of Riparian Trees in Ephemeral Stream Networks of the Sonoran Desert

Abstract

We examined seasonal patterns of water stress and water use in riparian trees along ephemeral streams of the Sonoran Desert in southwestern Arizona. At all sites, tree ecohydrological functioning was tightly coupled to rainfall and streamflow pulses, with the greatest water stress and lowest transpiration rates occurring during early-summer drought periods. Differences in alluvial depth and water storage capacity among stream types corresponded to variations in seasonal water relations. Water stress was more severe and more frequent in piedmont headwater and bedrock with alluvium streams, where shallow alluvium limited water storage despite more frequent streamflow. Greater subsurface water storage in braided and incised alluvium streams sustained higher plant water potentials and reduced seasonal variation in water use. In these lowland stream segments, alluvial recharge from periodic floods maintained favorable plant water status for prolonged periods.

Introduction

Although dryland trees employ a diversity of adaptations to survive droughts, physiological functioning in all species declines with increasing water stress (Szarek and Woodhouse 1976, 1978a, 1978b, Smith et al. 1997). Riparian trees in ephemeral streams of the Sonoran Desert have extensive root systems capable of accessing both shallow and deep moisture, and can tolerate prolonged drought (Turner and Brown 1994, Turner et al. 1995, Gibson 1996). Many of these species occupy hillslopes and upland surfaces within wetter portions of their ranges, but chronic water stress in marginal habitats can lead to increased plant mortality during extreme droughts (Bowers and Turner 2001, 2002).

Substrate properties and geomorphic setting profoundly influence plant water availability in drylands. Fine-textured sediments and shallow sediments magnify plant water stress during drought, but deep alluvium and fractured bedrock can provide persistent water supplies (Shreve and Wiggins 1964, McAuliffe 1994, 1999, Busch and Smith 1995). Variation in hydrologic regimes among geomorphic settings and stream network positions gives rise to divergent patterns of water stress at seasonal to multi-year timescales (Halvorson and Patten 1974, McAuliffe 1994, 1999, Sponseller and Fisher 2006). While riparian tree water use may be largely independent of precipitation patterns where stable groundwater is available (Williams et al. 2006), physiological functioning may be tightly coupled with streamflow events where subsurface moisture is limited (Horton et al. 2001, Gazal et al. 2006). These observations suggest that variation in the magnitude and frequency of streamflow events, and subsurface water storage capacity, throughout stream networks would produce distinctive seasonal patterns of water stress and water use.

Understanding the ecohydrological relations of riparian trees throughout ephemeral stream networks is necessary to designing informed management and restoration plans, and predicting potential responses to changing climate and land use. Differential patterns of plant water stress and physiological rates among stream types can be used to identify relative sensitivity to hydrologic alterations, and the relative importance of seasonal water sources will mediate tree population responses to shifts in rainfall seasonality. To clarify these issues, we examined ecohydrological relationships of ironwood, foothills paloverde, blue paloverde, and smoketree across stream types in the western Sonoran Desert.

Methods

Ecohydrological dynamics of ironwood, foothills paloverde, blue paloverde, and smoketree were examined at the eight intensive study reaches in Yuma and Mohave washes, located on the Yuma Proving Ground in southwestern Arizona. Seasonal measurements of plant water status were performed during winter (January), spring (March), summer (June), and fall (September) during 2011 to 2013, on five individual ironwood, foothills paloverde, blue paloverde, and smoketree in each reach where they occurred. Seasonal rates of water use were measured with sap flow sensors in one individual of each species within Mohave Wash, from January 2013 to May 2014. Concurrent measurements of soil moisture, stream stage, rainfall, and other meteorological variables by J. Falconer and S. Kampf were used to characterize patterns of moisture availability in each reach.

Plant water status was characterized by measuring predawn xylem pressure potential using a Model 1505D pressure chamber (PMS Instruments Inc., Albany, OR). Replicate measurements from 3-5 actively-growing terminal shoots were averaged for each plant. Predawn water potential approximates root-zone water availability, and we used this metric to describe seasonal patterns of water stress.

Temporal patterns of water use were estimated with 3-needle sap flow sensors (East 30 Sensors, Pullman, WA) that measure temperature differentials at depths of 5, 17.5, and 30 mm below bark. Temperature differentials were averaged from 60 to 100 s following an 8 s heat pulse, and measurements were stored at 15 minute intervals using AM16/32B multiplexers and CR1000 data loggers (Campbell Scientific, Logan, UT). Sensors were installed within 1 m of the ground surface, on the north side of stems within insulated protective housings to standardize errors from solar heating and circumferential variation in flow rates. Sap velocity was calculated using the Heat Ratio Method, which is capable of resolving extremely low flow rates and reverse flow (Burgess et al. 2001). In May 2014, two increment cores from each tree were used to estimate sapwood depth and moisture content. Sapwood moisture content exceeded the fiber saturation point in all trees, and thermal diffusivity was calculated following Vandegehuchte and Steppe (2012). Repeated sensor malfunctions, battery failures, and damage from floods and gnawing rodents resulted in data gaps for many trees, so we present only data from ironwood and foothills paloverde.

Sap flow rates exhibit considerable circumferential variation within individual tress, due to complex xylem architecture, hydraulic redistribution of soil moisture, and variable refilling of stem capacitance (Burgess and Bleby 2006, Kume et al. 2012, Shinohara et al. 2013). Therefore, a single sensor will likely provide misleading or imprecise estimates of whole-tree sap flux. Instead, we report water use as sap velocities measured at each sensor location. In order to compare seasonal patterns of water use across species and stream types, sap velocities were relativized by maximum values.

Results

Piedmont Headwater

Seasonal patterns of water stress in piedmont headwater streams were broadly similar in both watersheds, although predawn xylem water potentials were generally lower in Mohave Wash (Figure 7-1). The lowest observed predawn water potentials for both species occurred during the summer of 2012, averaging -2.3 MPa in Mohave Wash (Figure 7-1B) and -2.0 in Yuma Wash (Figure 7-2D). Repeated streamflow events from monsoon thunderstorms resulted in increased water potentials through the following spring in both watersheds, and during this period of increased water availability, differences in water status among species became apparent. In Mohave Wash, mean predawn water potentials for ironwood and foothills paloverde ranged from -1.6 to -1.5 and -1.1 to -1.0 MPa, respectively. Mean predawn water potentials were slightly higher in Yuma Wash, ranging from -1.4 to -1.3 MPa for ironwood and -1.1 to -0.8 MPa for foothills paloverde. High evapotranspiration rates and infrequent streamflow caused predawn water potentials to decline during the summer and fall of 2013.

Sap velocities measured from January 2013 to May 2014 at the Mohave Wash piedmont headwater site show similar seasonal variation in water fluxes between ironwood (Figure 7-2A) and foothills paloverde (Figure 7-2B). Monsoon streamflow in 2013 resulted in two sustained transpiration pulses, including the maximum observed sap velocities for ironwood (9.4 cm h^{-1}) and foothills paloverde (6.9 cm h^{-1}) at this site. Water use in response to winter precipitation and streamflow events was more variable. Ironwood sap velocities were 70 to 80 % of maximum values during January-March 2013, but rose to only 40 % in December 2013. Foothills paloverde exhibited a similar water use pattern, with winter sap velocities up to 60 % in 2013 and 40 % in 2014. Daily water use was lowest during the late-spring and early-summer drought periods, and sap velocities for both species ranged up to 20 % in 2013, and 15 % in 2014.

Bedrock with Alluvium

Differences in the frequency and timing of streamflow events at the bedrock with alluvium sites resulted in disparate temporal patterns of water stress between Mohave and Yuma Wash (Figure 7-3). A paucity of rainfall caused predawn water potentials at both sites to decline from spring 2011 through summer 2012, when all species reached their lowest observed values. Each species responded similarly to the 2012 monsoon floods, and mean predawn water potentials rose to -1.1 MPa in Mohave Wash (Figure 7-3B), and -0.8 MPa in Yuma Wash (Figure 7-3D). Although rainfall patterns during the winter of 2013 were similar in both watersheds (Figure 7-3A, 7-3C), seasonal patterns of alluvial water content and plant water status differed substantially. At Mohave Wash, mean predawn water potentials of both species declined steadily to about -2.2 MPa during the summer of 2013. In contrast, predawn water potentials remained between -1.1 and -0.9 MPa through the spring of 2013 in Yuma Wash, and declined to -2.0 MPa for ironwood and -1.5 MPa for blue paloverde during the summer. A late summer streamflow pulse increased predawn water potentials of both species to -1.0 MPa in Mohave Wash, but dry conditions at Yuma Wash resulted in water potential declines to -2.5 MPa for ironwood and -1.9 MPa for blue paloverde. At both sites,

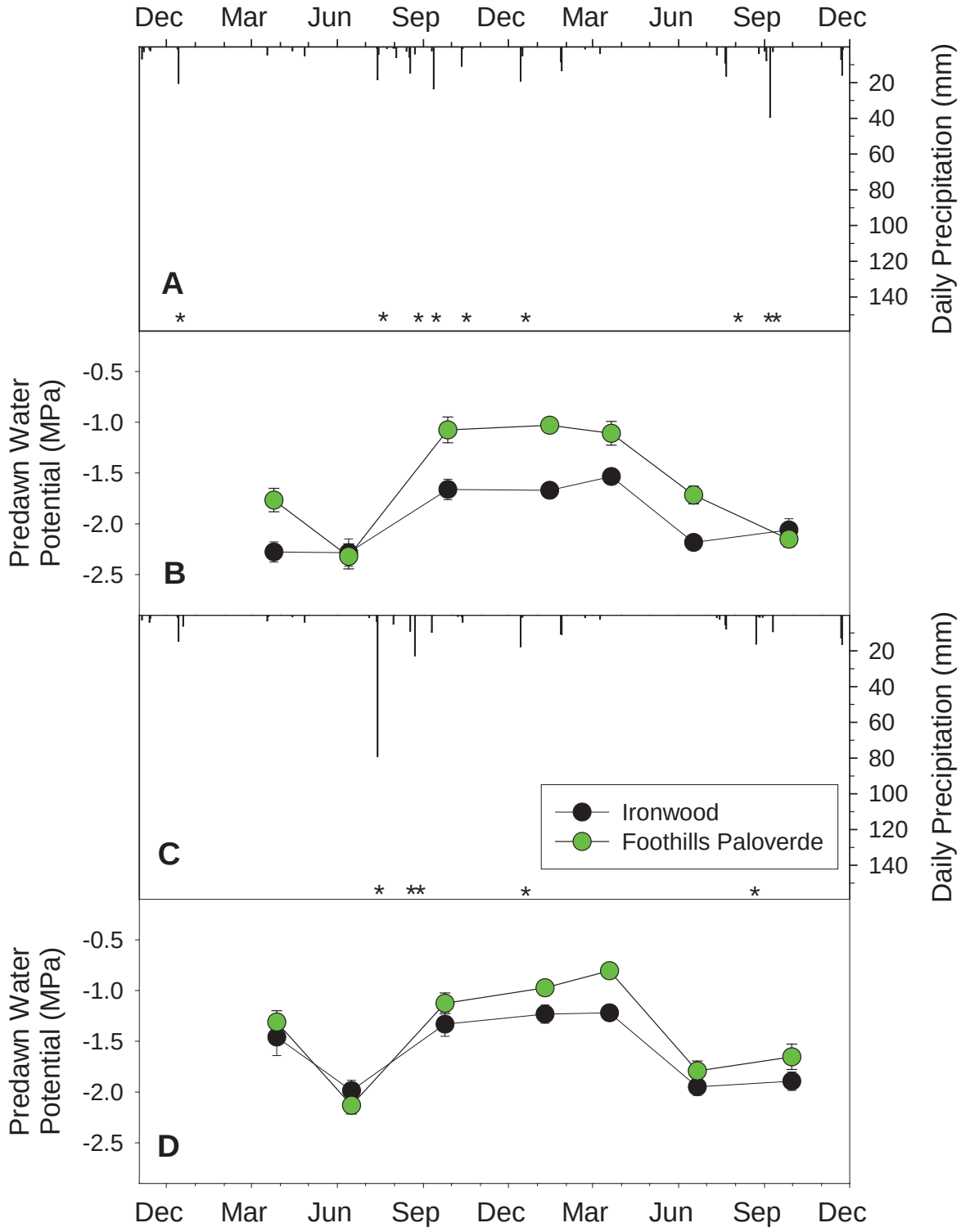

Figure 7-1. Rainfall, streamflow, and predawn plant water potential in piedmont headwater sites during 2012 and 2013. Rainfall and streamflow at Mohave Wash (A); predawn water potential at Mohave Wash (B); rainfall and streamflow at Yuma Wash (C); predawn water potential at Yuma Wash (D). Points are means for each species and error bars are 1 S.E. Asterisks indicate streamflow events.

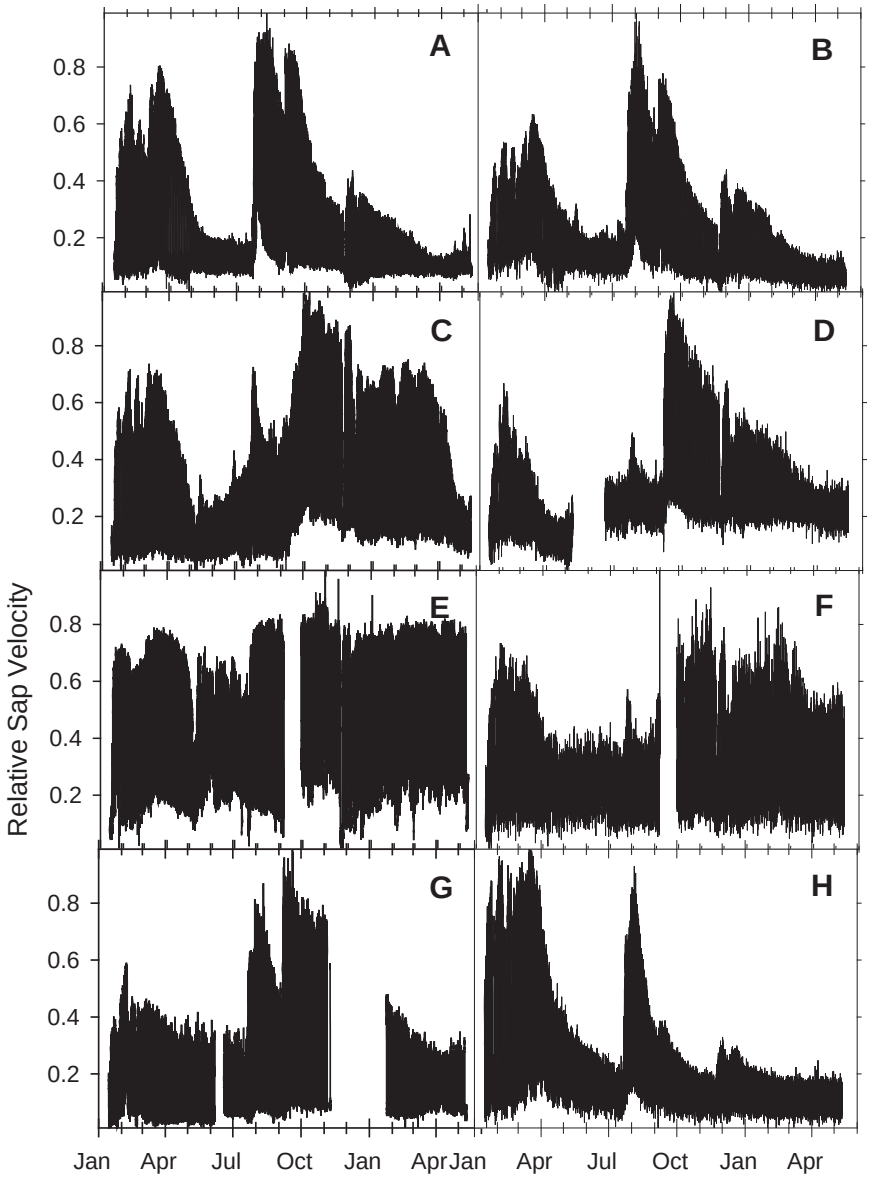

Figure 7-2. Relative sap velocity of ironwood (A, C, E, G) and foothills paloverde (B, D, F, H) from January 2013 to May 2014 in Mohave Wash. A-B, piedmont headwater; C-D, bedrock with alluvium; E-F, incised alluvium; G-H, braided.

all species exhibited similar water potentials immediately following flood events, but ironwood tended have lower water potentials than either paloverde species at all other times.

Similar to the piedmont headwater site, ironwood and foothills paloverde water use at the Mohave Wash bedrock with alluvium site was largely driven by monsoon flow pulses (Figure 7-2C, 7-2D). Water use of both species spiked following the first summer streamflow event, but maximum sap velocities for ironwood (6.6 cm h^{-1}) and foothills paloverde (4.7 cm h^{-1}) did not occur until after a second flood in September 2013. Ironwood daily sap velocities remained between 50 and 70 % until the following March (Figure 7-2C), but water use of foothills paloverde declined steadily after the September peak (Figure 7-2D). Water use of both species was 20 to 25 % of maximum during the early summer drought period.

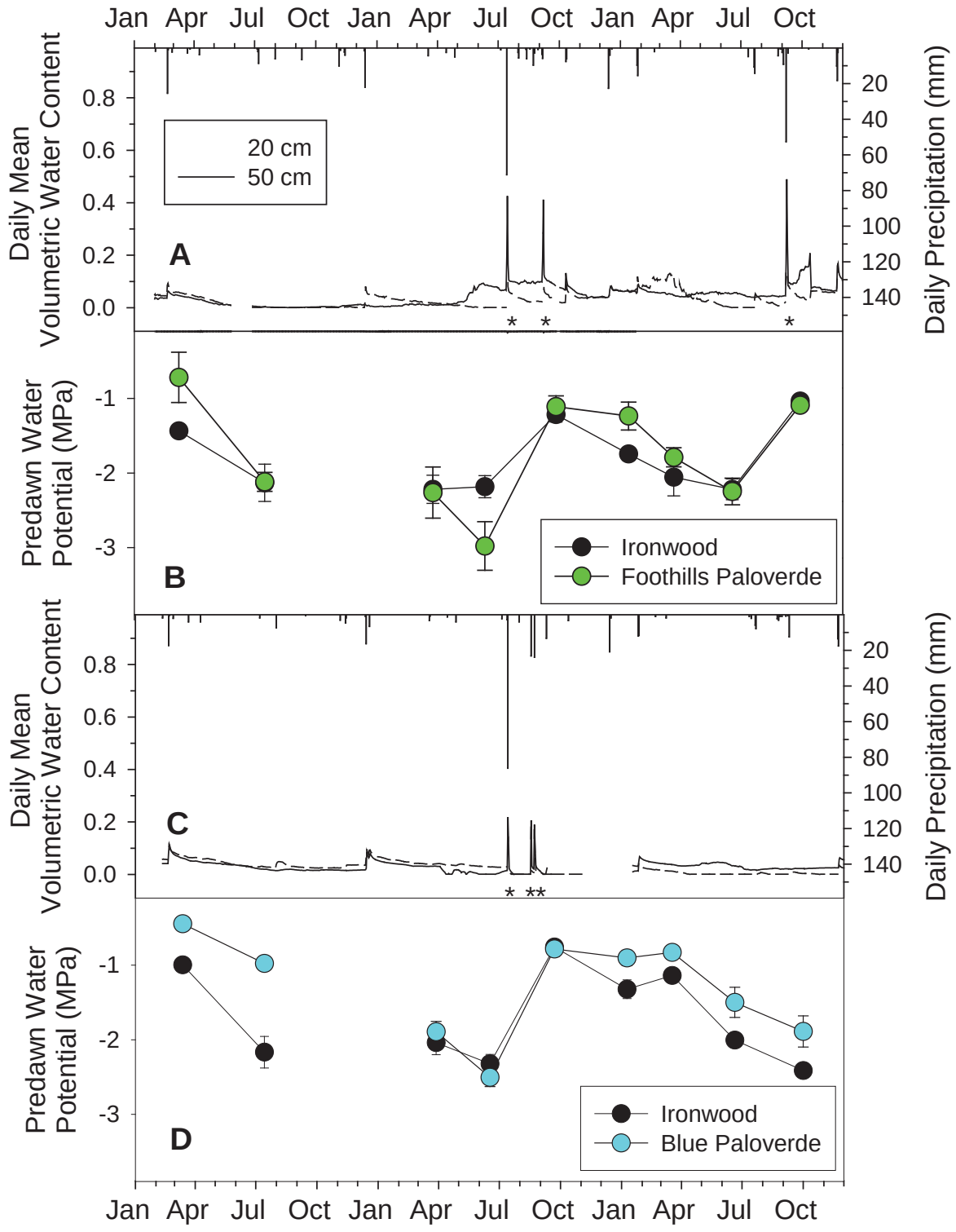

Figure 7-3. Rainfall, streamflow, water content, and predawn plant water potential in bedrock with alluvium sites from 2011 to 2013. Rainfall, water content, and streamflow at Mohave Wash (A); predawn water potential at Mohave Wash (B); rainfall, water content, and streamflow at Yuma Wash (C); predawn water potential at Yuma Wash (D). Points are means for each species and error bars are 1 S.E. Asterisks indicate streamflow events.

Incised Alluvium

Similar to the bedrock with alluvium sites, temporal variation in plant water status differed among watersheds, with the timing and magnitude of streamflow events and winter rainfall. Alluvial recharge from large winter storms in 2011 and 2012 resulted in relatively high summer predawn water potentials at Mohave Wash, although neither event produced measureable streamflow (Figure 7-4A, 7-4B). Summer predawn water potentials ranged from -1.4 to -0.8 MPa in 2011, and -1.5 to -1.0 MPa in 2012. Two monsoon flood events in 2012 increased plant water status during fall 2012, with mean predawn water potentials of -0.3 MPa for smoketree, -0.7 MPa for ironwood and blue paloverde, and -1.4 MPa for foothills paloverde. Water relations became more variable among species during the winter and spring of 2013, despite winter rainfall comparable to the previous two years, and summer mean predawn water potentials declined to -2.0 MPa for foothills paloverde, and -1.4 MPa for all others. A single monsoon streamflow event raised the water potentials of all species during the fall of 2013.

Throughout the study period, consistent differences in species water relations were apparent at Mohave Wash (Figure 7-4B). Smoketree exhibited the highest predawn water potentials, while foothills paloverde generally had the lowest. Ironwood and blue paloverde experienced similar water potentials during most seasons.

In contrast to Mohave Wash, all species at Yuma Wash exhibited similar seasonal stress patterns (Figure 7-4D). Winter storms resulted in mean predawn water potentials ranging from -1.4 to -1.2 MPa during summer 2011, while the greatest water stress occurred during summer 2012 (-2.1 to -1.8 MPa), due to lower precipitation in the preceding winter. A series of late summer and winter streamflow events maintained plant water potentials between -1.0 and -0.8 MPa through the following spring, with minor declines to -1.2 to -1.0 MPa during summer 2013. Predawn water potentials declined further to -1.5 MPa in fall 2013, despite a small streamflow event.

Temporal patterns of water use differed significantly between ironwood and foothills paloverde at the Mohave Wash incised alluvium site. Ironwood sap velocities were more uniformly distributed, ranging from 70 to 80 % of maximum (22.4 cm h^{-1}) throughout much of the study period (Figure 7-2E). Water use during the early summer drought in 2013 was between 40 and 70 % of maximum. Maximum sap velocities of foothills paloverde (4.1 cm h^{-1}) occurred after the September 2013 flood, and water use through the following spring varied between 40 and 95 % of maximum (Figure 7-2F). Daily sap velocities prior to monsoon rainfall was about 40 % in 2013 and 50 % in 2014.

Braided

Plant water status in the braided sites followed seasonal patterns similar to the incised alluvium sites in each watershed, although the timing and frequency of flood events were similar in both braided sites (Figure 7-5). In Mohave Wash, recharge from winter storms resulted in minor warm-season water stress, with mean summer predawn water potentials ranging from -1.4 to -1.9 MPa throughout the study period (Figure 7-5B). Predawn water potentials of all species increased after monsoon floods, with values during fall ranging from -1.1 to -0.5 MPa in 2012, and -1.4 MPa to -0.7 MPa in 2013. Differences in species water status were less pronounced than at the Mohave Wash incised alluvium site, and all species experienced similar water stress during summer. Smoketree exhibited higher water potentials during other seasons, while ironwood tended to have the lowest water potentials in winter and spring.

Patterns of water stress were more variable within and among species at the Yuma Wash braided site (Figure 7-5D). Mean predawn water potentials during summer 2011 were -1.8 MPa for foothills paloverde and -1.0 MPa for all others, but summer water stress declined relative to spring values for smoketree and blue paloverde. During the spring and summer of 2012, foothills paloverde water potentials were highly variable, but averaged -2.4 MPa, while the other species ranged from -1.5 to -1.1 MPa. Monsoon flood recharge during 2012 increased mean predawn water potentials of all species to -0.9 to -0.4 MPa through the following spring, with only slight declines to –1.3 to -0.9 MPa by summer 2013. Only smoketree experienced increased water potentials in fall 2013 following a minor streamflow event.

Ironwood and foothills paloverde exhibited substantially differing seasonal patterns of water use at the Mohave Wash braided site. Ironwood sap velocities (max 59.5 cm h^{-1}) peaked after the September 2013 flood, and appeared to decline steadily through the following spring (Figure 7-2G). Winter sap velocities ranged from 40 to 50 %, except for a brief spike (60%) after rainfall in February 2013, and were between 30 and 40 % during early summer droughts. In contrast to trees at other sites, sap velocities for the foothills paloverde at the braided site peaked during March 2013 (3.3 cm h^{-1}), and water use was maximal during winter and spring of 2013 (Figure 7-2H). However, lower rainfall during the winter of 2014 resulted in lower transpiration rates, up to 30 % of maximum. Sap velocity

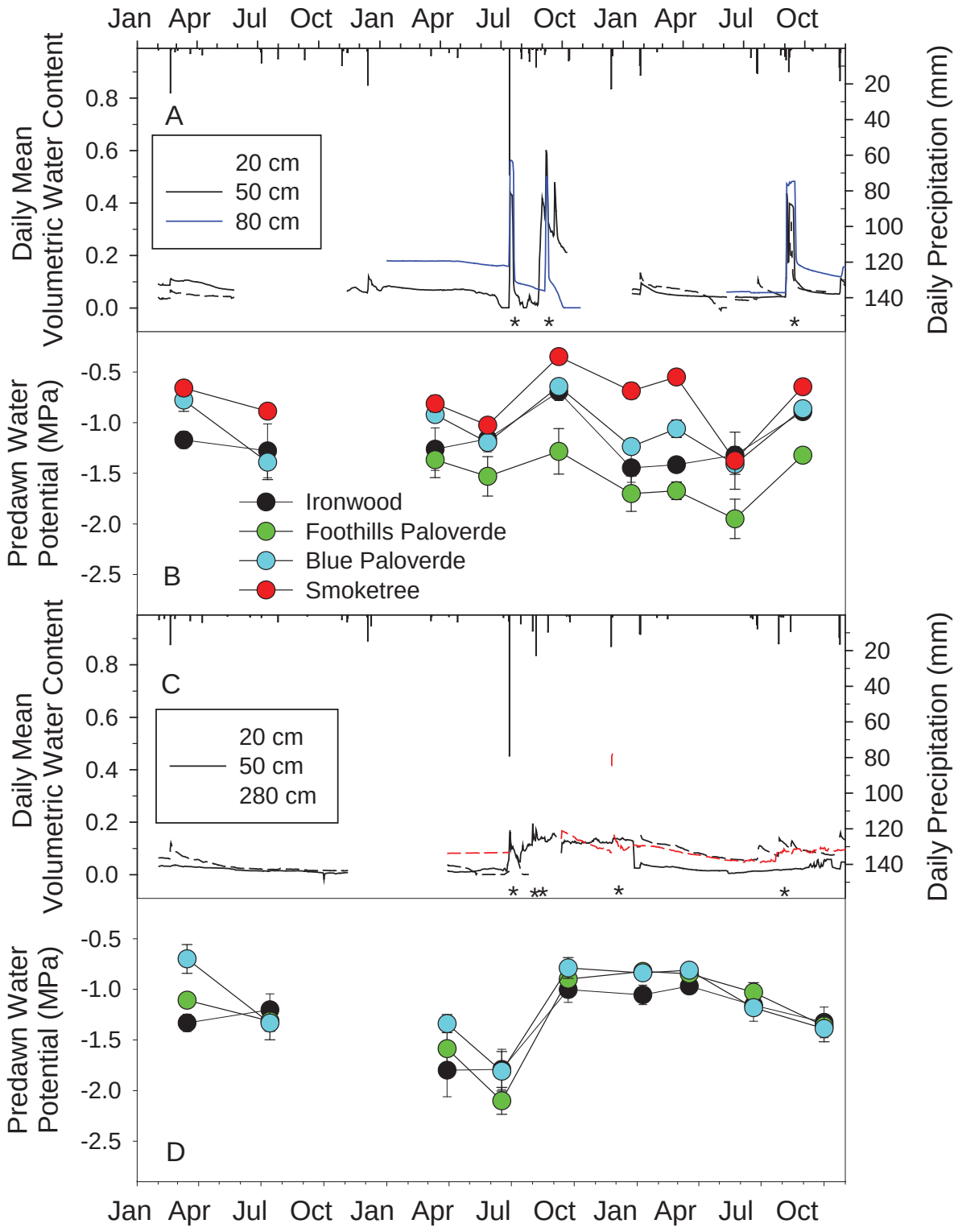

Figure 7-4. Rainfall, streamflow, water content, and predawn plant water potential in incised alluvium sites from 2011 to 2013. Rainfall, water content, and streamflow at Mohave Wash (A); predawn water potential at Mohave Wash (B); rainfall, water content, and streamflow at Yuma Wash (C); predawn water potential at Yuma Wash (D). Points are means for each species and error bars are 1 S.E. Asterisks indicate streamflow events.

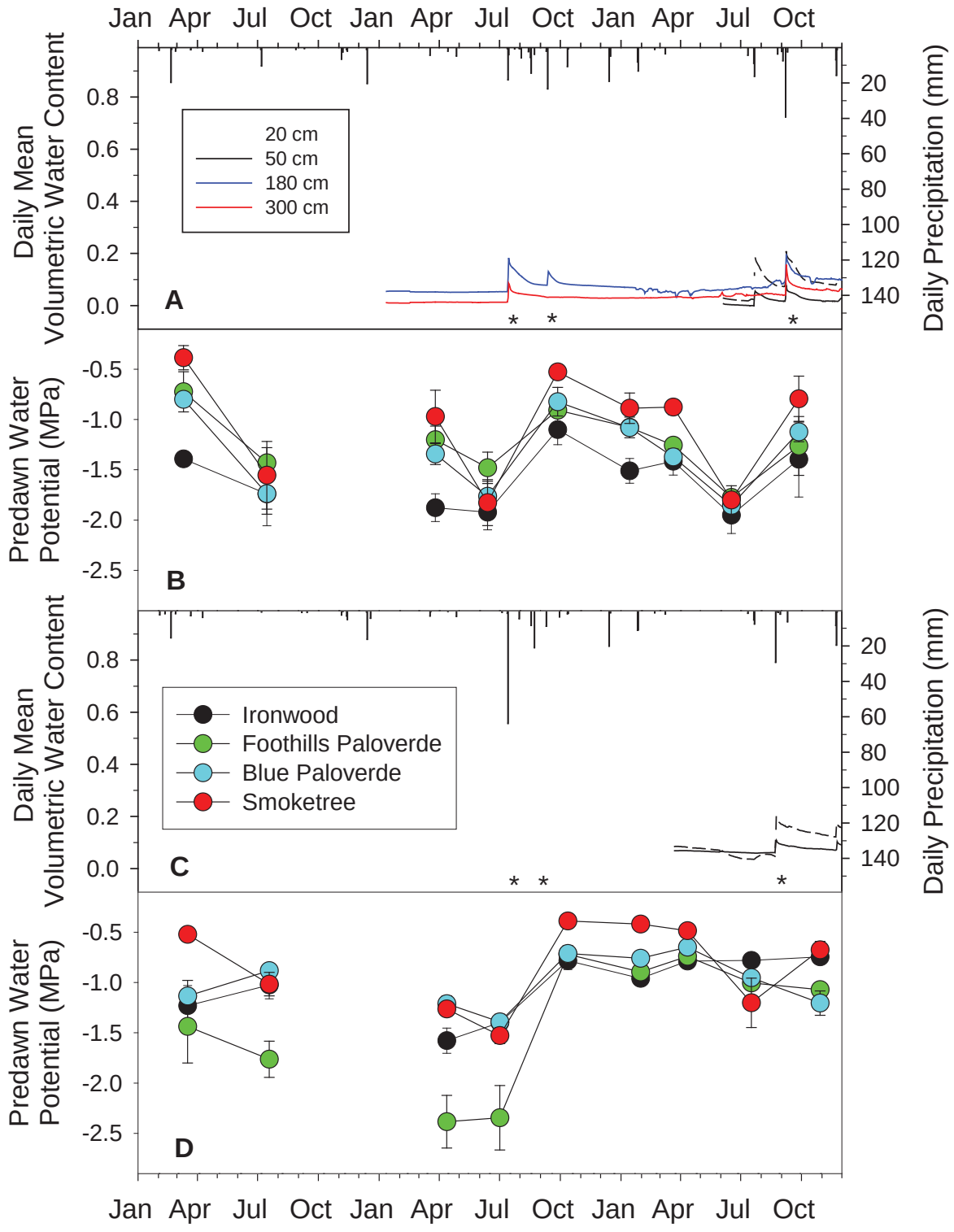

Figure 7-5. Rainfall, streamflow, water content, and predawn plant water potential in braided sites from 2011 to 2013. Rainfall, water content, and streamflow at Mohave Wash (A); predawn water potential at Mohave Wash (B); rainfall, water content, and streamflow at Yuma Wash (C); predawn water potential at Yuma Wash (D). Points are means for each species and error bars are 1 S.E. Asterisks indicate streamflow events.

increased up to 95 % during a brief spike after monsoon rainfall, and water use during drought periods was between 15 and 30 %.

Discussion

Seasonal patterns of water stress in riparian tree were driven by the timing and magnitude of hydrologic pulses. While streamflow and rainfall inputs varied among watersheds, the severity and duration of water stress differed among stream types. Trees in bedrock with alluvium and piedmont headwater sites exhibited the lowest summer water potentials (-2.0 to -3.0 MPa), despite more frequent streamflow events, while summer water stress was less severe for most species in braided and incised alluvium sites. Water potential minima for ironwood, blue paloverde, and smoketree in these stream types were between -1.4 and -1.9 MPa, but foothills paloverde exhibited greater water stress during dry seasons (-2.0 to -2.5 MPa). Although seasonal water stress varied considerably between years, winter and spring predawn water potentials were broadly similar across stream types. Increased plant water potentials following large floods also persisted longer in incised alluvium and braided streams. Overbank flooding in Yuma Wash during the fall of 2012 provided alluvial recharge that improved plant water status through the following year, and predawn water potentials at the braided and incised alluvium sites during the summer of 2013 were comparable to cool-season water potentials in other stream types. Our results are congruent with downstream decreases in riparian tree water stress observed along an intermittent stream in the northern Sonoran Desert (Sponseller and Fisher 2006).

Different patterns of riparian tree water stress and water use among stream types corresponds to variation in the depth and extent of alluvial deposits. Deeper unconsolidated alluvium in braided and incised alluvium provides greater subsurface storage capacity for infiltrated rainfall and streamflow (Harry et al. *in prep.*). In contrast, the shallow and narrow alluvial deposits in piedmont headwater and bedrock with alluvium streams have lower water storage capacities, and sustain greater evapotranspirational losses. Consequently, seasonal plant water status is highly variable, and more frequent hydrologic inputs are required to maintain water availability in these headwater channels.

Across stream types, general differences in water relations were apparent among species, although all riparian trees experienced maximum water stress during dry summers. Smoketree maintained the highest predawn water potentials in all sites where it occurred, likely reflecting its ability to minimize water stress through smaller leaf areas (Nilsen et al. 1984, 1989). In streams with shallow alluvium, ironwood often exhibited the lowest water potentials, but had water relations similar to blue paloverde in incised alluvium and braided streams. Foothills paloverde had the lowest predawn water potentials of all species in braided and incised alluvium streams. Since all species rely primarily on shallow water sources (Shaw and Cooper *in prep.*), differences in species water status at sites with deep alluvium appear to correspond with the spatial distribution of trees within the fluvial corridor. Within the study area, smoketree occurs primarily on active channel sediments, while foothills paloverde are often restricted to higher floodplain positions. Differences in alluvial recharge from streamflow events and water-holding capacity of shallow sediments in these topographic positions likely underlie the divergent seasonal water stress patterns among species.

Minimum observed predawn water potentials for the species in our study sites were slightly higher than values reported from other locations. Smoketree growing along an ephemeral wash in southern California regularly experienced predawn water potentials as low as -2.0 MPa (Nilsen et al. 1984). Ironwood leaves lose turgor at -3.7 MPa (Monson and Smith 1982, Nilsen et al. 1984), and minimum reported predawn water potentials in field studies range from -2.7 to -3.3 MPa (Szarek and Woodhouse 1977, Monson and Smith 1982, Nilsen et al. 1984), while the minimum predawn water potential of ironwood in our study was -2.3 MPa. Foothills paloverde maintains positive photosynthesis at predawn water potentials above -3.1 MPa (Szarek and Woodhouse 1978a), and experiences complete xylem embolism at -6 MPa (Pockman and Sperry 2000). In upland settings, foothills paloverde withstands predawn water potentials -3.6 MPa (Halvorson and Patten 1974). Thus, it appears that the riparian trees growing along ephemeral streams of the western Sonoran Desert are not strongly limited by physiological tolerances to water availability. However, the narrow margin between observed water status and estimated physiological limits suggest that severe or prolonged droughts could lead to tree mortality, particularly within piedmont headwater and bedrock with alluvium streams.

Conclusions

Seasonal patterns of water stress and water use in riparian trees along ephemeral streams of the Sonoran Desert are tightly coupled to rainfall and streamflow pulses. At all sites, water stress was maximal during the early summer drought period, and minimal in winter and spring. Differences in alluvial depth and water storage capacity

corresponded to variations in water status and water usage. Riparian trees experience more severe and more frequent water stress in piedmont headwater streams, while alluvial recharge from periodic floods can maintain favorable plant water status for long periods in braided and incised alluvium streams.

Chapter 8. Limitations to Seedling Establishment for Sonoran Desert Riparian Trees

Abstract

We conducted a multi-factorial field experiment over two years to understand the relative roles of herbivory, nurse plant shading, rainfall, and plant size on riparian tree seedling survival and growth in the Sonoran Desert. Herbivory by jackrabbits and cottontail rabbits was the primary limitation to seedling survival, while feral livestock and other ungulates did not affect survival rates. When protected from small herbivores, shading significantly increased survival rates. Supplemental irrigation, equivalent to an annual rainfall amount occurring once in approximately five years, substantially improved survival for shaded seedlings, and was required for any seedling survival without shade. The effects of shade and enhanced rainfall increased with seedling size. In contrast, seedling growth rates were not strongly affected by shade or irrigation. Similar responses from each species demonstrates that the dominant riparian trees in ephemeral streams of the Sonoran Desert have broadly similar regeneration niches. Their seedlings require dense nurse shrubs for shade and herbivore protection, and reproductive success is highest during unusually wet years.

Introduction

Tree recruitment in arid regions around the world is often infrequent and episodic (Shreve and Wiggins 1964, Burquez and Quintana 1994). Even when the hydrologic requirements for germination are met, first-year survival rates of woody plant seedlings are often as low as two percent, and few individuals survive to maturity (McAuliffe 1986, 1988, Bowers and Turner 2002, Bowers et al. 2004, León et al. 2011). Many desert trees are regarded as keystone species, because the fertility islands and favorable microclimates they create support numerous plant and animal taxa (Burquez and Quintana 1994, Tewksbury and Petrovich 1994, Suzan et al. 1996, Sponseller and Fisher 2006). Given the importance of woody riparian vegetation in structuring desert ecosystems, successful management and restoration of these landscapes requires a greater understanding of the factors affecting dryland tree population dynamics, especially the limitations on establishment.

Temporal patterns of tree establishment in arid landscapes are often linked to periodic hydrologic pulses. In riparian settings, establishment generally occurs where floods create patches of moist, bare sediments in topographic positions with adequate subsurface moisture, and protection from subsequent flood disturbance (Hupp and Osterkamp 1996, Scott et al. 1996). In arid regions, the timing and amount of rainfall following seedling emergence can strongly determine survival rates (Bowers et al. 2004). Unusually wet years associated with infrequent climatic conditions may be required for successful woody plant establishment (León et al. 2011).

While climatic variability is often seen as the primary driver of tree establishment in drylands, biotic interactions can strongly influence seedling survival and plant demography (Crawley 1983, Ward 2006, Butterfield et al. 2010). Herbivores directly affect population structures of large woody plants by killing seedlings (Crawley 1983, Cloudsley-Thompson 1996). In arid environments, mature trees and seedlings are commonly browsed by feral livestock (Abella 2008, Moser-Nørgaard and Denich 2011), lagomorphs such as jackrabbits and cottontail rabbits (Westoby 1980, Anderson and Shumar 1986, McAuliffe 1986, Hoagland 1992), and rodents (Vaughan and Schwartz 1980, Baxter and Hansson 2001). In all cases, defoliation through herbivory is more likely to kill plants under water stress (Crawley 1983, Ward 2006). The role of herbivory in limiting dryland tree seedling survival has been extensively studied in upland settings, while little information is available from riparian ecosystems (e.g. Moser-Nørgaard and Denich 2011).

Facilitation by nurse plants is ubiquitous in harsh environments, and where herbivore pressure is strong (Shreve and Wiggins 1964, Bertness and Callaway 1994, Butterfield et al. 2010). Tree seedlings and understory vegetation gain protection from herbivores through physical exclusion or secondary compounds produced by nurse plants (McAuliffe 1986, Cloudsley-Thompson 1996). Seedling growth and survival rates are often improved under nurse plant canopies, where shading and increased humidity reduces leaf and soil temperatures, and evapotranspiration rates (Shreve and Wiggins 1964, McAuliffe 1988, Callaway 1995, Hastwell and Facelli 2003). Only two

manipulative experiments have compared the relative importance of shading and herbivore exclusion in facilitation by nurse plants, but these were in semi-arid grasslands (Callaway 1992) and subhumid Mediterranean forests (Gómez-Aparicio et al. 2008). The facilitative mechanisms of nurse plants are likely to differ in arid desertscrub.

To understand the processes limiting dryland riparian tree establishment in the Sonoran Desert, we addressed the following questions: (1) What is the relative importance of herbivory by large ungulates and small mammals? (2) What is the relative importance of microclimatic amelioration through shading and herbivore protection by nurse plants? (3) How do infrequent wet years affect seedling growth and survival, both under nurse plants and in the open? (4) How does seedling size interact with the above factors in influence survival? We answered these questions through a multi-factorial field experiment examining the relative importance of shade, herbivory, rainfall, and seedling size to growth and survival of three dominant xeroriparian tree species of the Sonoran Desert: ironwood (*Olneya tesota*), blue paloverde (*Parkinsonia florida*), and foothills paloverde (*P. microphylla*).

Methods

Experimental plots were established on floodplain surfaces in a braided channel segment of Mohave Wash, an ephemeral tributary of the lower Colorado River within southwestern Arizona, U.S.A. (N 33.456123º, E -114.492205º; 210 m elevation). The study area is located on the U.S. Army Yuma Proving Ground within the Lower Colorado Valley subdivision of the Sonoran Desert (also known as Colorado Desert), the most arid portion of the Sonoran Desert (Shreve and Wiggins 1964, Turner and Brown 1994). In this hyperthermic arid region, monthly potential evapotranspiration exceeds precipitation throughout the year (Sellers and Hill 1974). Seasonal rainfall is derived from pacific frontal storms from November to March, while convective thunderstorms of the North American Monsoon may occur from July to September (Shreve and Wiggins 1964, Sellers and Hill 1974, Turner et al. 1995). Mean annual precipitation ranges from 93 to 103 mm and mean daily minimum and maximum temperatures are 13º C and 32º C at nearby climate stations (NCDC cooperative stations #29654, 26865). Aside from the allogenic Colorado and Gila rivers, streamflow throughout the region is ephemeral (Shreve and Wiggins 1964).

Experimental factors of shade and herbivory were applied in a randomized complete block design, with four replicate blocks located on separate floodplain surfaces. Blocks consisted of eight 24 m^2 plots, where all treatment levels of herbivory and shade were crossed. Herbivory treatments consisted of four levels, which excluded: (i) only small animals such as jackrabbits (*Lepus californicus*) and cottontail rabbits (*Silvilagus audubonii*); (ii) only large mammals such as feral burros (*Equus asinus*), feral horses (*Equus ferus caballus*), and mule deer (*Odocoileus hemionus*); (iii) all animals; and (iv) no animals (control). Small animal exclosures consisted of 60 cm tall fencing (6 mm hardware cloth) around plot perimeters, buried 30 cm below ground, following Brown and Munger (1985). Large animals were excluded by suspending polypropylene deer fencing (Tenax Corp., Baltimore, MD, USA) from 60 to 150 cm above ground. Full exclosures used both types of fencing. Shade treatments consisted of two levels, shaded and unshaded (control). Shading was accomplished by covering plots with 90 % shade cloth on frames suspended 2.4 m above ground. The shade treatment was determined by averaging photosynthetically active radiation measurements (n = 20) under two regionally common nurse plants, sweetbush (*Bebbia juncea*) and cheesebush (*Ambrosia salsola*).

Each plot was split among irrigation treatment levels (irrigated and ambient rainfall), with the three species planted in rows on each side. Irrigation treatments were applied only during the first year, as monthly additions to ambient rainfall, in order to achieve an annual total corresponding to a 5 yr recurrence interval. This amount was determined by frequency analysis of annual rainfall from 55 yr years of observation at a nearby weather station in Quartzsite, Arizona (NCDC ID 0268655; 265 m elevation), and was distributed following average monthly proportions of annual rainfall for those years. During the second year, all seedlings received ambient rainfall. Within irrigation treatment sub-plots, two sizes of seedlings were inter-planted in each species row. Eight large seedlings and 24 small seedlings were planted in each species row, allowing 900 cm^2 and 225 cm^2 for each large and small seedling, respectively. Ambient rainfall and other meteorological variables were measured at a weather station located less than 1 km from the experimental blocks (Kampf et al. *in prep*.).

Seeds collected near the study area were sown in a commercial growing medium of equal parts composted wood byproduct, peat, and perlite (Gro-Well Brands, Inc., Tempe, AZ) at a nearby nursery (Signature Botanica, Morristown, AZ). Large seedlings were grown for five months in 656 ml pots, while small seedlings were grown for four months in 164 ml pots. All plants received two applications of 21-5-20 fertilizer and one application of mycorrhizal inoculum (Myco-Drench, Tri-C Enterprises, Chino, CA) while at the nursery.

We planted the experimental plots during 11-14 January 2012 with 6144 trees, comprised of 512 large and 1536 small seedlings of each species. To minimize transplanting shock and aid establishment, all seedlings were watered in with 11 mm over three days following planting, after which time irrigation treatments were imposed. Survival rates were recorded during approximately monthly censuses over a two year period. Browsing by lagomorphs immediately after planting affected seedlings in all unprotected plots, so initial stem heights were measured only in plots with small animal exclosures (n=3072). Changes in stem height were measured annually during January 2013 and 2014. Camera traps in each study block were used to document the principle agents of herbivory.

Treatment effects on seedling survival were assessed by comparing least squares means of a generalized linear mixed model fitted to the logit of binomial survival responses using Proc GLIMMIX in SAS 9.3 (SAS Institute Inc., Carey, NC, USA). Experimental factors were considered fixed effects, while the covariance structures of study blocks and interactions between study blocks and experimental factors were treated as random effects. Analyses of survival rates were performed separately for each species, allowing for up to three-way interactions. Treatment effects on seedling growth were determined using repeated measures ANOVA (Proc GLIMMIX) on relative growth rate (change in stem height/initial height at planting). Because low survival rates resulted in few replicates, large and small seedlings of each species were pooled across subplots, allowing for two-way interactions. Similarly, large and small seedlings of each species from all unshaded plots were pooled into a single treatment. Differences in survival and growth rates among treatments after the first and second years were compared using Tukey-Kramer adjusted confidence intervals.

Results

Ambient precipitation during 2012 was 130 mm, corresponding a long-term recurrence interval of approximately 2.2 yr (exceedance probability = 0.46, Figure 8-1). A lack of winter and spring rainfall caused the first half of the year to be abnormally dry, but substantial monsoon thunderstorms raised cumulative precipitation to a typical amount after July. In irrigated subplots, monthly additions to rainfall during the dry winter and spring months resulted in an annual total of 175 mm, which corresponded to a recurrence interval of approximately 5.5 yr (exceedance probability = 0.18). In 2013, when irrigation treatments stopped and all seedlings received ambient rainfall, precipitation followed a more typical annual distribution and totaled 136 mm (exceedance probability = 0.43). Total annual potential evapotranspiration, calculated by the Penman-Monteith method, was about 2500 mm in each year.

Initial heights of blue paloverde seedlings in both size classes were larger than the other species, whereas mean initial heights of large and small seedlings were similar for ironwood and foothills paloverde (Table 8-1).

Table 8-1. Initial seedling stem heights (cm).

Species	Size	Mean	S.E.
Ironwood	Large	21.4	0.72
	Small	12.1	0.44
Blue Paloverde	Large	31.9	0.84
	Small	17.8	0.33
Foothills Paloverde	Large	20.1	0.46
	Small	13.6	0.36

Seedling Survival Rates

The effects of herbivory, shade, irrigation, and plant size on seedling survival rates through time were similar among ironwood (Figure 8-2), blue paloverde (Figure 8-3), and foothills paloverde (Figure 8-4). Immediate and intense

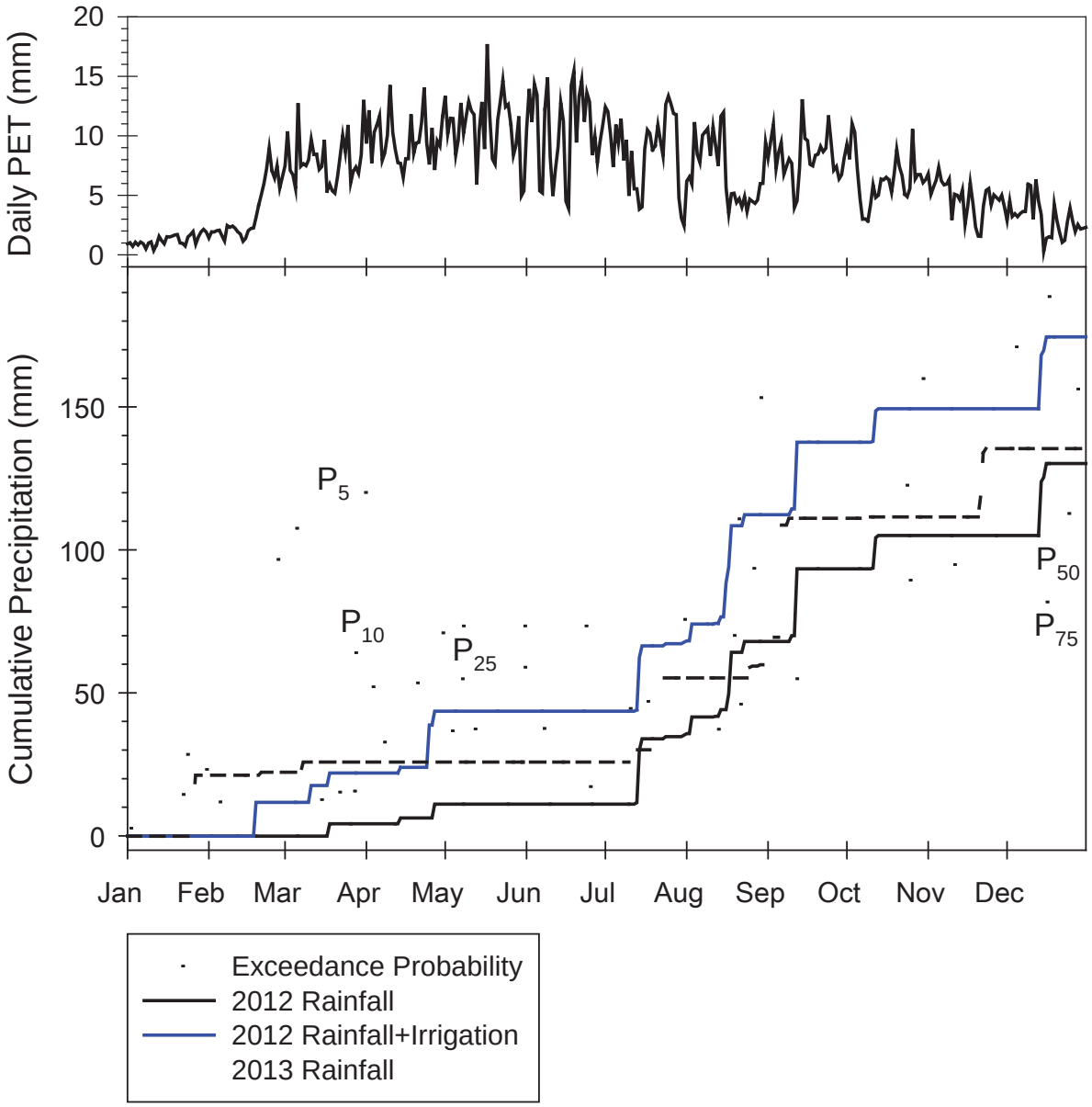

Figure 8-1. Potential evapotranspiration and cumulative precipitation at experimental plots during 2012 and 2013. Exceedance probabilities are based on 55 yr record at Quartzsite, AZ.

herbivory by lagomorphs removed the above ground biomass of nearly all seedlings in experimental plots accessible to small animals within the first few weeks. Although many browsed seedlings resprouted following rain or irrigation events, repeated browsing and desiccation killed all plants in these plots during the first year. Regardless of plant size or irrigation treatment, seedlings of all species in unshaded plots open to small animals died during the summer, while those persisted until the winter of 2012.

Herbivory by large animals did not occur in our experimental plots, and the higher survival rates in full exclosures compared to controls resulted from the exclusion of small animals. Analysis of 3187 photographs from camera traps indicated that jackrabbits and cottontail rabbits were the only herbivores to enter and consume seedlings in the experimental plots. These lagomorphs were active almost exclusively between dusk and dawn.

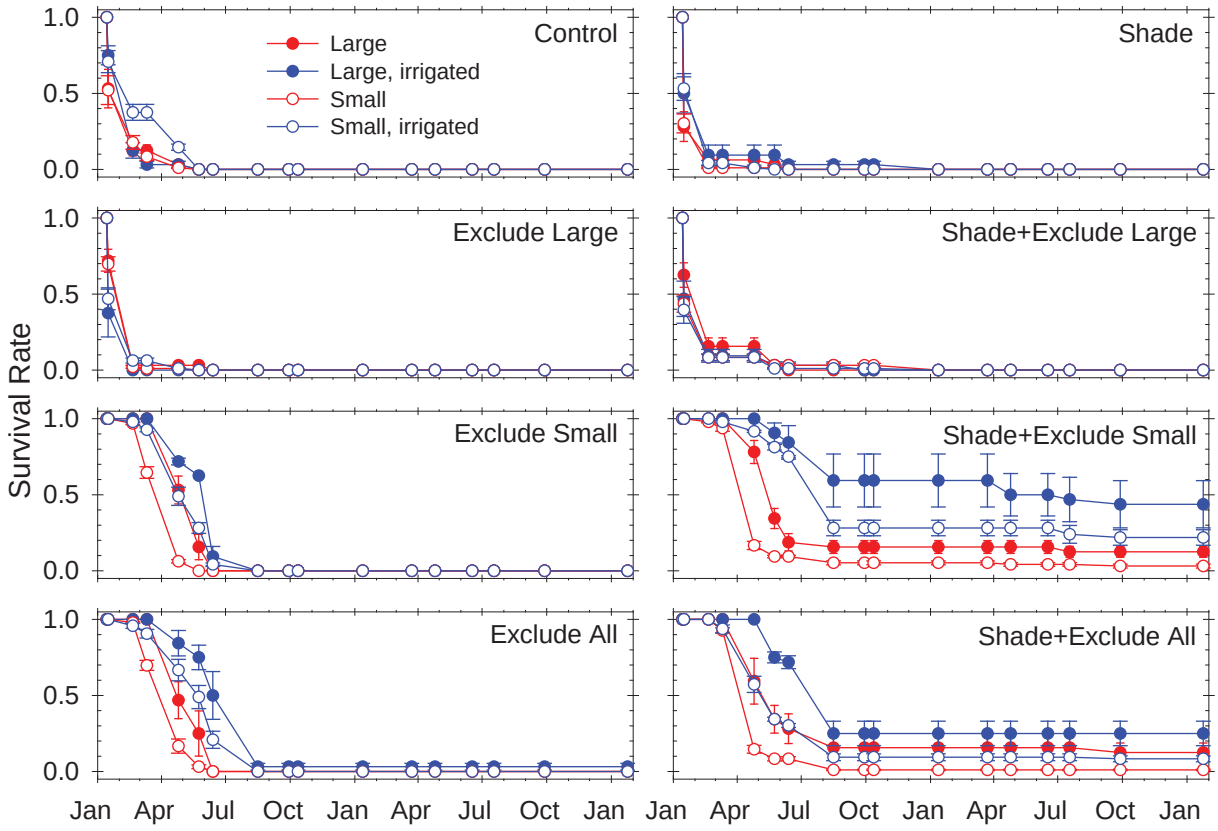

Figure 8-2. Survival rates of ironwood (Olneya tesota) seedlings in experimental plots from January 2012 to January 2014.

Table 8-2. Effects of treatment, irrigation, and plant size on seedling survival over one year. Bold p-values are significant at $\alpha = 0.05$.

		Ironwood		Blue Paloverde		Foothills Paloverde	
Effect	**DF**	**F**	**p-value**	**F**	**p-value**	**F**	**p-value**
Treatment	9	19.3	**0.0003**	122	**<0.0001**	194	**<0.0001**
Irrigation	12	2.66	0.13	782	**<0.0001**	892	**<0.0001**
Size	984	79.9	**<0.0001**	40.5	**<0.0001**	0.00	0.99
Treatment* Irrigation	12	1.05	0.38	8.31E34	**<0.0001**	1.20E35	**<0.0001**
Treatment* Size	984	Infty	**<0.0001**	7.04E34	**<0.0001**	9.47	**<0.0001**
Irrigation* Size	984	Infty	**<0.0001**	13.6	**0.0002**	50.2	**<0.0001**
Treatment* Irrigation* Size	984	Infty	**<0.0001**	6.2	**0.012**	25.4	**<0.0001**

Where small animals were excluded, desiccation-induced mortality during the first summer dramatically influenced survival rates, but this effect differed among shade and irrigation treatments, and plant sizes for all species (Table 8-2). In unshaded plots, only seedlings within irrigated subplots lived beyond the first summer, and survival rates increased with plant size (Figure 8-5). Although unshaded foothills paloverde seedling survival declined during the second summer (Figure 8-4), this effect persisted through the second year (Figure 8-6). Blue paloverde exhibited the

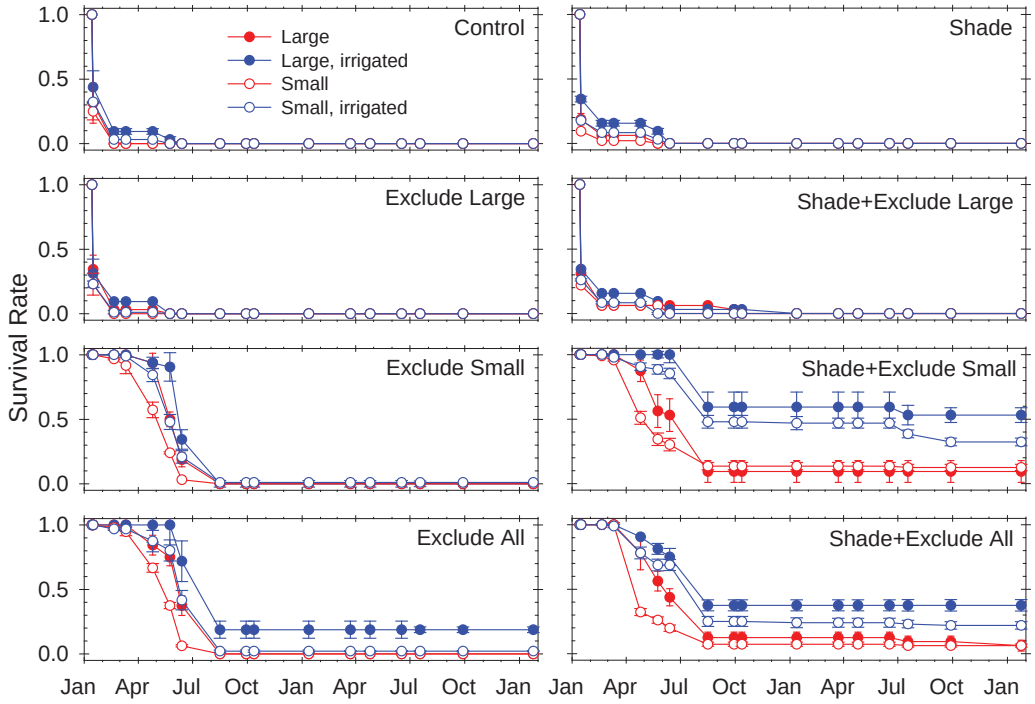

Figure 8-3. Survival rates of blue paloverde (Parkinsonia florida) seedlings in experimental plots from January 2012 to January 2014.

Table 8-3. Effects of treatment, irrigation, and plant size on seedling survival over two years. Bold p-values are significant at $\alpha = 0.05$.

		Ironwood		Blue Paloverde		Foothills Paloverde	
Effect	**DF**	**F**	**p-value**	**F**	**p-value**	**F**	**p-value**
Treatment	9	133	**<0.0001**	410	**<0.0001**	1.05E36	**<0.0001**
Irrigation	12	5.79	**0.033**	221	**<0.0001**	100	**<0.0001**
Size	984	17.9	**<0.0001**	38.1	**<0.0001**	18.5	**<0.0001**
Treatment* Irrigation	12	3.07E33	**<0.0001**	715	**<0.0001**	7.45	**0.018**
Treatment* Size	984	2.82E34	**<0.0001**	246	**<0.0001**	117	**<0.0001**
Irrigation* Size	984	0.16	0.69	304	**<0.0001**	Infty	**<0.0001**
Treatment* Irrigation* Size	984	0.39	0.68	9.86	**0.0017**	Infty	**<0.0001**

lowest mortality in unshaded plots, with 19 % of irrigated large seedlings in full exclosures and up to two percent of irrigated small seedlings surviving for two years.

Where shade was available, seedling survival in both size classes was higher in irrigated subplots, but variation among replicate blocks made these differences insignificant at $\alpha = 0.05$ during both years (Figures 8-5 and 8-6). Within each irrigation treatment, large seedlings persisted later into the first summer and had higher survival rates than small seedlings. However, the only significant differences in survival rates within shaded small animal exclosures were between irrigated large seedlings and unirrigated small seedlings. This effect was detectable for ironwood and foothills paloverde during the first year (Figure 8-5), but only foothills paloverde after two years

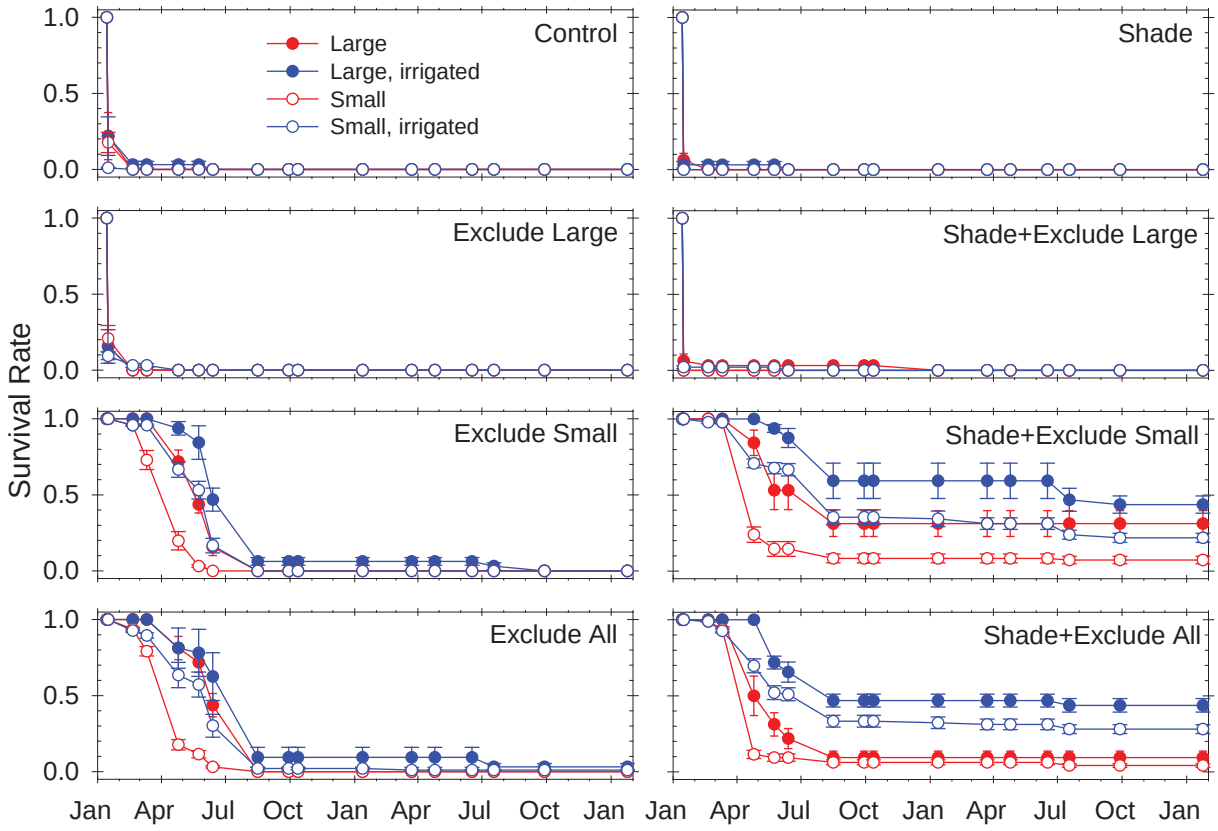

Figure 8-4. Survival rates of foothills paloverde (P. microphylla) seedlings in experimental plots from January 2012 to January 2014.

(Figure 8-6). Despite insignificant differences among many treatment combinations due to among-block variation, large differences in survival rates were apparent across irrigation and plant sizes within shaded plots.

Seedling Growth Rates

Averaged across all treatments and both seedling sizes, stem heights of surviving blue paloverde seedlings increased by 109 % during the first year, and ironwood and foothills paloverde heights increased by 82 and 47 %, respectively. After two years, mean increases in seedling heights were more similar among ironwood (129 %) and blue paloverde (155 %), while foothills paloverde stem growth averaged 77 %. Stem dieback contributed to low growth rates for ironwood and foothills paloverde.

Seedling growth rates during the first year did not differ substantially among treatments for any species (Table 8-4). Minor effects on growth rates of blue paloverde were apparent, as seedlings in unshaded plots were smaller than those in shaded plots (Figure 8-7). After two years, relative growth rates of ironwood seedlings differed among treatments, but blue paloverde and foothills paloverde growth was not significantly affected by the treatments (Table 8-5). Ironwood seedlings receiving ambient rainfall in small animal exclosures were taller than those in irrigated subplots (Figure 8-8), however this apparent height increase includes attrition of the smallest individuals through mortality during the second year. Both species of paloverde exhibited slight, but statistically insignificant,

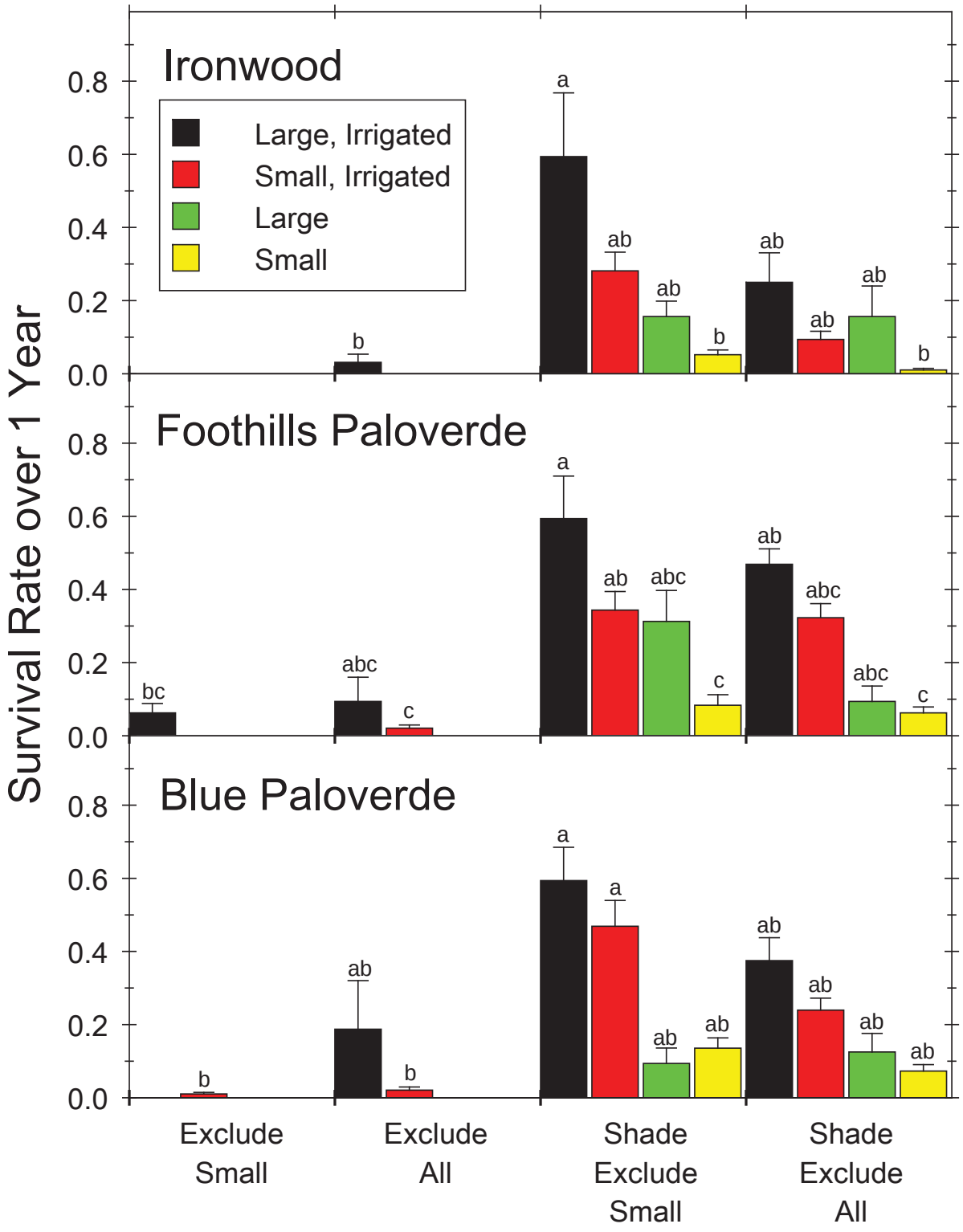

Figure 8-5. Comparison of survival rates for ironwood, blue paloverde, and foothills paloverde across treatments during the first year. Values are averaged across replicates, and error bars are 1 SE. Letters indicate significant differences at $\alpha = 0.05$.

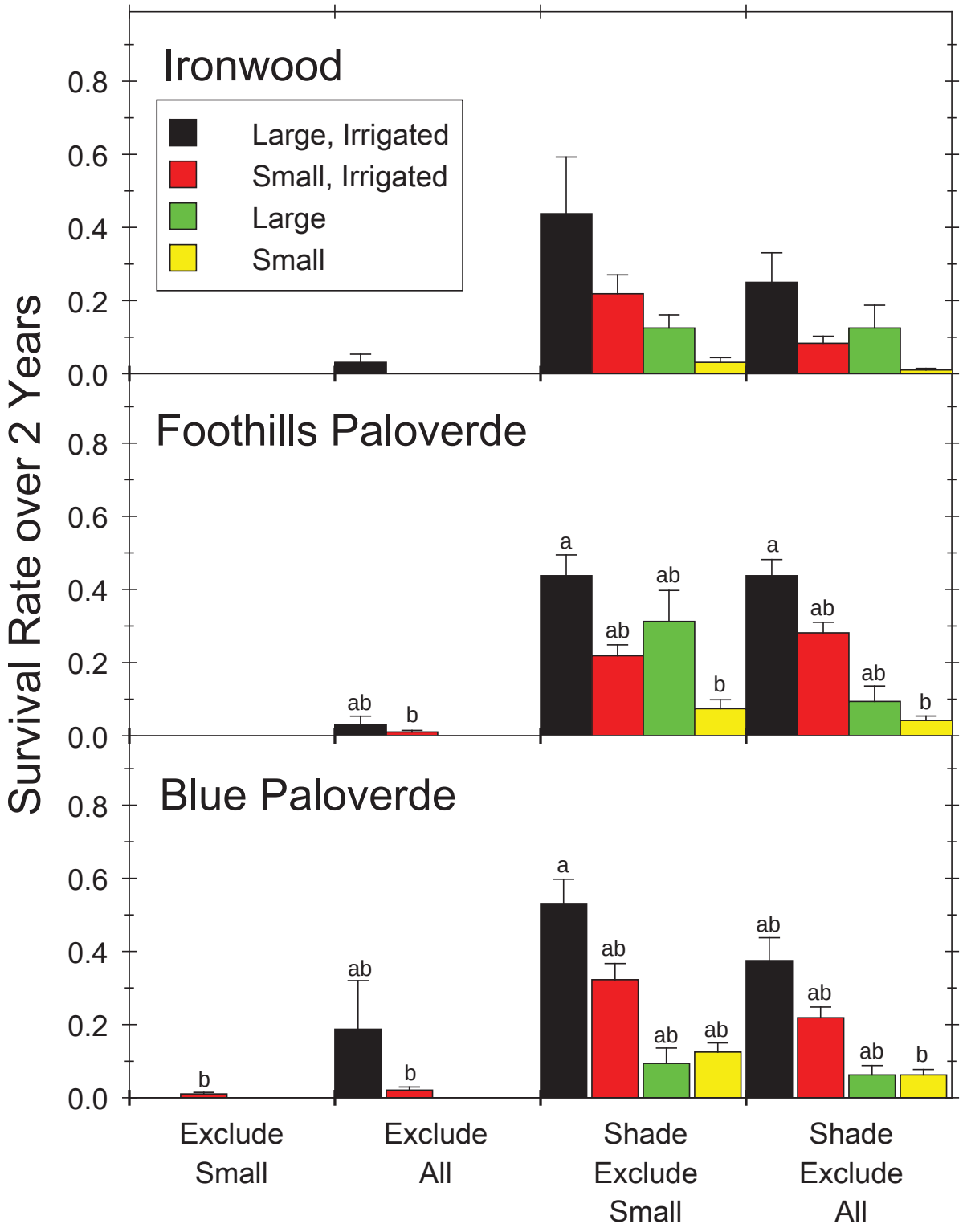

Figure 8-6. Comparison of survival rates for ironwood, blue paloverde, and foothills paloverde across treatments during two years. Values are averaged across replicates, and error bars are 1 SE. Letters indicate significant differences at $\alpha = 0.05$.

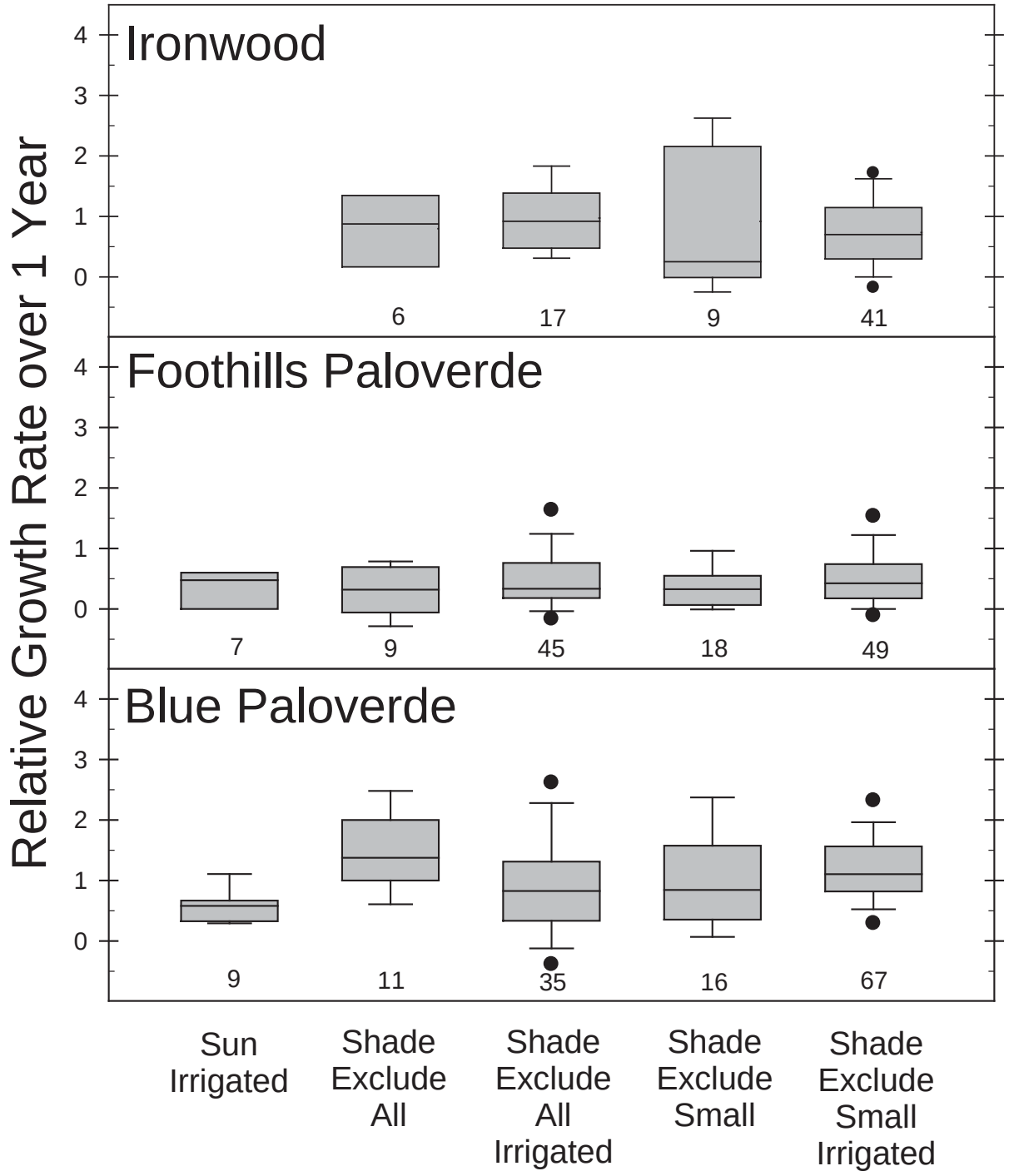

Figure 8-7. Comparison of relative growth rates for ironwood, blue paloverde, and foothills paloverde across treatments during the first year. Box plot whiskers denote 5th and 95th percentiles, dots show minima and maxima, and dashed lines indicate means. Numbers beneath boxplots indicate sample size.

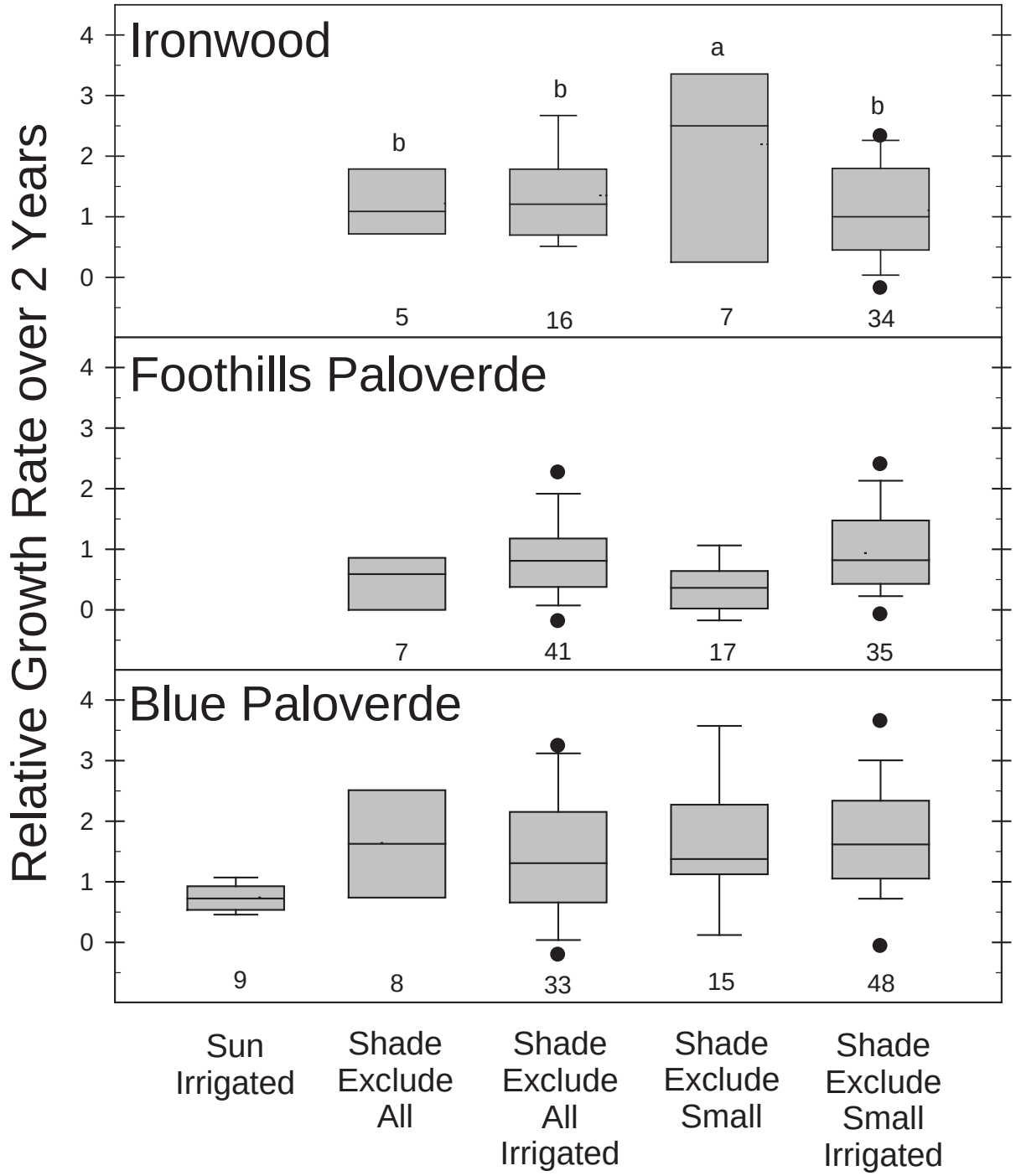

Figure 8-8. Comparison of relative growth rates for ironwood, blue paloverde, and foothills paloverde across treatments during two years. Box plot whiskers denote 5th and 95th percentiles, dots show minima and maxima, and dashed lines indicate means. Numbers beneath boxplots indicate sample size.

Table 8-4. Effects of treatment and irrigation on seedling relative growth rate over one year. Samples are pooled across seedling sizes.

	Ironwood			Foothills Paloverde			Blue Paloverde		
Effect	**DF**	**F**	**p-value**	**DF**	**F**	**p-value**	**DF**	**F**	**p-value**
Treatment	65	3.29	0.075	116	0.78	0.509	124	1.88	0.156
Irrigation	65	1.39	0.243	116	0.14	0.710	124	0.38	0.541
Treatment* Irrigation	65	1.26	0.265	116	0.00	0.975	124	3.18	0.077

Table 8-5. Effects of treatment and irrigation on seedling relative growth rate over two years. Samples are pooled across seedling sizes. Bold p-values are significant at $\alpha = 0.05$.

	Ironwood			Foothills Paloverde			Blue Paloverde		
Effect	**DF**	**F**	**p-value**	**DF**	**F**	**p-value**	**DF**	**F**	**p-value**
Treatment	53	10.66	**0.0019**	90	0.45	0.720	102	2.21	0.115
Irrigation	53	4.77	**0.033**	90	0.91	0.341	102	0.84	0.363
Treatment* Irrigation	53	11.51	**0.0013**	90	0.24	0.628	102	1.63	0.205

differences in relative growth rates among treatments. Foothills paloverde seedlings were larger in irrigated subplots, and blue paloverde seedlings were larger in shaded plots.

Discussion

Herbivory by jackrabbits and cottontail rabbits rapidly killed all seedlings in experimental plots accessible to small animals, indicating that top-down regulation is the primary constraint on tree reproduction within the study area. The effects of rainfall, shade, and plant size were only apparent when these common herbivores were excluded. The importance of lagomorphs as agents of tree seedling mortality has been shown in upland habitats elsewhere in the Sonoran Desert (McAuliffe 1986, 1988), and in the Chihuahuan Desert (Roth et al. 2007). Our findings confirm that herbivory is the primary constraint on tree seedling survival throughout the Sonoran Desert (McAuliffe 1986, 1988, Bowers et al. 2004), and the high mortality rates in our experiment are consistent with other studies of dryland woody plant establishment (Bowers and Turner 2002, Bowers et al. 2004, León et al. 2011).

Large herbivores such as horses, burros, and deer did not affect seedling survival in our experimental plots. This result was unexpected, since all three species were regularly observed within the study area, and evidence of ungulate browsing on larger saplings and mature trees occurs throughout stream networks of the region (Shaw and Cooper, *in prep.*). Feral horse and burro impacts on native vegetation within the area are significant management concerns (Abella 2008), such that their populations are actively managed through periodic culling by the Bureau of Land Management. The lack of ungulate herbivory on seedlings in our study plots may reflect vertical browsing preferences for taller vegetation (Crawley 1983, Ward 2006). Alternatively, it is possible that the experimental plots somehow deterred large herbivores, either due to periodic human presence during data collection, or modification of the local environment by our infrastructure.

The importance of herbivory in limiting dryland tree establishment varies with the density and spatial distribution of herbivores. Available data suggests that the abundance of small mammalian herbivores, and their impacts to plant populations, varies systematically across arid landscapes. The diversity and density of rodents, which can influence grassland and shrubland plant composition, varies with local-scale topography, substrate type, and plant community productivity (Brown 1975). McAuliffe (1986) observed substantially reduced herbivory on foothills paloverde by lagomorphs in rocky uplands, compared to more densely vegetated bajadas. Variation in substrate type, fluvial geomorphology, and plant communities among stream types will likely influence spatial patterns of herbivory throughout ephemeral stream networks.

Where small herbivores were excluded, the survival rates of all species were significantly increased by the presence of canopy shading. In unshaded plots, seedling survival through the first summer drought period required

supplemental irrigation. The need for both shade and herbivore protection highlights the role of shrubs as nurse plants in facilitating reproduction of desert riparian trees. Microclimates under tree canopies can provide favorable habitats by reducing insolation (Suzan et al. 1996, Reynolds and Cooper 2010), but seedlings remain vulnerable to predation. In contrast, dense shrubs provide shading and protection from herbivores through physical exclusion or secondary compounds (McAuliffe 1986, Cloudsley-Thompson 1996). These findings are consistent with growing evidence that dryland tree reproduction is controlled by synergies between abiotic conditions and biotic interactions (Crawley 1983, Bowers and Turner 2002, Ward 2006, Butterfield et al. 2010).

Combined rainfall and irrigation during the first year, equivalent to an annual total occurring on average twice in 11 years, improved seedling survival in shaded and open plots. Recent work in other dryland settings also shows that infrequent periods of high rainfall facilitate woody plant seedling survival (León et al. 2011, Matías et al. 2012). Characterizing infrequent hydrologic pulses by exceedance probabilities and associated return intervals is a common practice in hydrologic and geomorphic analyses, and its application to ecological phenomena can allow resource managers to understand the relative frequency of their occurrences. It should be noted that exceedance probabilities and return intervals describe the average expected frequency over long time intervals, and that global climatic and land cover changes are altering the magnitude and frequency of hydrologic fluxes in complex and frequently unpredictable ways. Therefore, each 11 year period may contain more or less establishment events that observed in our study, and the relative frequency of establishment can change over time with cyclical climatic variation as well as longer-term climatic trends.

Ironwood, blue paloverde, and foothills paloverde exhibited similar responses to shading and enhanced rainfall, indicating that the dominant riparian trees of ephemeral streams in the Sonoran Desert have broadly similar regeneration niches. Reproduction of these species is strongly dependent on shade and herbivore protection afforded by nurse plants, typically dense shrubs. In contrast, seedling growth rates were not significantly affected by shading or rainfall amounts, although blue paloverde were slightly taller in shaded plots. Stem height increased substantially faster for blue paloverde, while ironwood and foothills paloverde grew at similar rates.

Implications for Riparian Restoration

These findings provide guidance to increase survival rates of woody plants when revegetating disturbed riparian areas. Planted seedlings require shade and herbivore protection, which can be accomplished either by installing shaded wire cages, or planting under existing shrubs when available. Because survival rates are extremely low under typical climatic conditions, supplemental irrigation is needed during the first year. Greater irrigation than was applied here (175 mm), and irrigation beyond the first year, will likely yield further improvements in growth and survival. Planted seedlings should be as large as possible, since the effects of shading and irrigation increase with seedling size.

Conclusions

Herbivory by lagomorphs is the primary limitation to riparian tree seedling survival in ephemeral streams of the Sonoran Desert. Although species distributions differ, the dominant tree species in these communities exhibit broadly similar regeneration niches. They require dense shrubs as nurse plants to provide shade and protection from herbivory, and survival increases during unusually wet years. Improvements in survival under shade and irrigation increases with plant size.

Chapter 9. Simulating subsurface flow beneath ephemeral stream channels

Part 1, baseline simulations and sensitivity analysis

Introduction and objectives

Desert ephemeral streams flow only after rain events, but the episodic pulses of moisture during flow can be important sources of localized groundwater recharge (Renard et al. 1964; Stonestrom et al. 2004). Prior research on the water content dynamics beneath these types of streams have focused either on individual flow events (Hoffman et al. 2003; Blasch et al. 2006) or on snapshot profiles of moisture and matric potential from drill cores (Izbicki et al. 2000; Izbicki et al. 2003). More process-level research is needed to examine how the water content dynamics during flow events link with long-term redistribution of water in the subsurface.

This study has two components that examine water redistribution beneath ephemeral streams. In part 1, the primary objective is to use observed water contents from a 3-year observation study to develop a physically-based subsurface flow simulation of water content during the study time period. Part 1 also has a secondary objective of testing the sensitivity of the simulation to changes in model configuration, input, and parameter values. This sensitivity analysis is intended to help understand how sensitive the simulated water contents are to different components of the system. Part 2 uses the model developed in part 1 to examine how water contents are affected by longer-term climate patterns in both the historical record and projected future climate conditions.

Methods

Simulations of subsurface flow use the HYDRUS-2D model (Simunek et al.), which is a physically-based variably saturated flow model that solves the Richards' equation using a finite element method. In 2-D configuration, the model simulates vertical and lateral infiltration and redistribution of moisture in the subsurface, where lateral is represented as a cross section slice of the channel and surrounding alluvium. HYDRUS-2D simulates two state variables, volumetric water content (Θ) and pressure head. The model simulates redistribution of Θ continuously in response to sequences of precipitation, evaporation, and transpiration.

This modeling study builds on the stream stage and moisture observations presented in Faulconer et al. and Kampf et al. manuscripts. At six study sites, precipitation, stream stage, and subsurface moisture measurements were collected at 15-minute time steps for a three-year study time period. Calibration and testing of the HYDRUS-2D model for these sites requires continuous sequences of precipitation and stream stage. At all sites except YBA and YIA, complete sequences of precipitation and flow events were not available due to intermittent data loss. We focus here on YBA for subsurface flow modeling because it has a narrow channel, and at each monitoring location, we had only a single vertical profile of water content measurements. We found through analyses of water content profiles in wider channels, that those channels were more likely to experience flow events that did not span the full width of the channel. At the narrower YBA site, we assumed that both the stream stage and water content measurements would be a good proxy for conditions across the full channel width.

Model configuration, baseline simulations

We developed baseline simulations of Θ for the 3-year study time period at YBA using a simplified representation of each site's characteristics. Then, we tested the sensitivity of the simulations to model configuration and parameterization to evaluate how simulation results related to assumptions embedded in the model. All simulations have a 10 m wide by 10 m deep domain (Figure 9-1). The top surface has an atmospheric boundary condition, where precipitation and stream flow can be input into the domain and where potential evaporation and transpiration rates are assigned. This atmospheric boundary represents the bed of the ephemeral stream channel. The bottom boundary has a deep drainage boundary condition, and all other boundaries are no-flow. The domain has two layers, the top assumed to represent the channel bed alluvium and the bottom a less permeable layer, which may be bedrock or a finer layer of alluvium. The finite element mesh for this domain has 6199 nodes, with a target node spacing of 10 cm. Observation nodes document simulated water content and pressure head for every time step at 10, 20, 50, 100,

200, and 300 cm depth beneath the center of the channel and beneath the side of the channel. All simulations have adaptive time steps, with the length of each time step determined by the numerical solver.

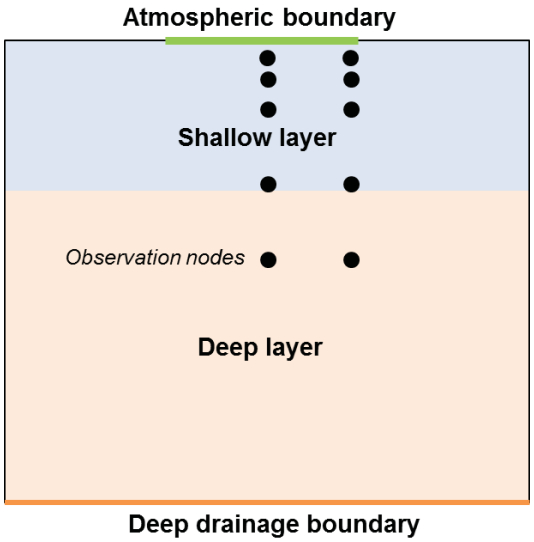

Figure 9-1 Domain configuration for HYDRUS-2D simulations.

To develop the baseline simulations for each site, we manually tested a wide range of simulation configurations and parameterizations and selected the one that best represented the observed Θ patterns over time. However, there were several problems with the Θ observations during the simulation time period. At YBA, after flow events, Θ values would show patterns that suggested that flow events scoured out the alluvium around the sensors. As a consequence, the sensors had to be replaced in the subsurface after flow events, and this led to discontinuities in the moisture values recorded over time. Because of these sensor issues, we decided not to over-fit the simulations to observed water contents but rather identify simulations that best mimicked the timing and magnitude of wetting and drying over time.

The baseline simulation configuration used for each site is summarized in Table 9-1. For YBA, the top layer depth in the baseline configuration is 2 m, and the width of the channel bed is 3 m. The van Genuchten water retention functions were used for hydraulic properties of the alluvium. Values of the residual water content, Θ_r, were set to 0.01 which is below the minimum values of Θ recorded by the sensors, excluding measurements flagged as recording errors. Similarly, values of the saturated water content, Θ_s, were set to 0.33 based on maximum values of water content typically recorded by the sensors, excluding measurements flagged as recording errors. The remaining hydraulic parameter values were identified through manual calibration of parameter values in the shallow layer. Parameter values in the deep layer were set to have lower saturated hydraulic conductivity, K_s, to represent a partial barrier to deep infiltration through either a layer of compacted sediment or bedrock. Deep layer water retention was set to have α and n parameter values similar to a sand, as the numerical solver of the program would crash when parameters of the deep layer differed dramatically from those of the shallow layer. Simulating water uptake through transpiration requires parameterizing a root water uptake function. For the baseline simulation we used the Feddes root water uptake function with HYDRUS default parameter values. Roots were distributed throughout the top layer of alluvium with the density of roots decreasing with depth below the surface.

The model was initialized with a linear distribution of Θ, with values increasing from 0.05 at the top surface of the domain to 0.15 at the base of the domain. These initial conditions produced water contents similar to the observations at the start of the simulation. Simulations began on May 1, 2011 and ended April 30, 2014. Precipitation rates were input through the atmospheric boundary condition at a 15-minute time step. For flow events, the observed flow stage was also input through the atmospheric boundary condition also at 15-minute time step. In the baseline simulation, potential evapotranspiration was calculated on a daily time step using the Penman-Monteith equation option in HYDRUS-1D using observed meteorological observations from the weather station at the Mohave Braided channel monitoring site, supplemented by data from the Blythe airport NCDC weather station. Inputs to the Penman-Monteith equation were net radiation, daily maximum and minimum temperature, relative

humidity, and wind speed. Calculated daily values of potential evapotranspiration were multiplied by a surface cover fraction of 0.1 and input into the transpiration boundary condition for the HYDRUS-2D simulations.

Table 9-1 Baseline model configuration for YBA simulations from May 2011-Apr 2014.

Model feature	YBA
Configuration	2D 2 m top layer, 10 m total depth 3 m channel width
Boundary conditions	Atmospheric over channel. Deep infiltration at base
Hydraulic parameters, shallow layer	$\Theta_r = 0.01$ $\Theta_s = 0.33$ $\alpha = 0.06$ cm^{-1} n = 2 $K_s = 50$ cm hr^{-1}
Hydraulic parameters, deep layer	$\Theta_r = 0.01$ $\Theta_s = 0.33$ $\alpha = 0.145$ cm^{-1} n = 2.68 $K_s = 0.1$ cm hr^{-1}
Root water uptake	Feddes root water uptake function with default parameters P0 = -10 Popt = -25 P2H = -200 P2L = -800 P3 = -8000 Root distribution parameters Max rooting depth = 200 cm Depth of max intensity = 0 cm Pz =5
Initial conditions	Linear distribution of water content from 0.05 at the surface to 0.15 at base
Input, precipitation and flow Input, transpiration	15-minute time step Daily time step, calculated using Penman-Monteith equation in HYDRUS-1D and multiplied by 0.1 surface cover fraction 0.1

Model configuration, sensitivity tests

Because of the complexity of the HYDRUS-2D model, we conducted a series of tests to evaluate how decisions about model configuration and parameterization in the baseline simulation affected simulation results (Table 9-2). These test scenarios each modified one component of the simulation configuration from the baseline simulation. Tests of model configuration changed the depth of the shallow alluvium layer and the width of the channel. We also compared HYDRUS-2D simulation results to those of a 1D model configuration. Additional tests modified the hydraulic parameters of both the shallow and deep layers, the root distribution, and the root water uptake function and associated parameters. We tested two different initial condition scenarios at the wet and dry end of the range used in the baseline simulation. Finally, we conducted a series of tests that modified input through the atmospheric boundary condition. For tests modifying evapotranspiration (ET) input, we increased transpiration by increasing the surface cover fraction (ET1), assumed no losses through either evaporation or transpiration (ET2), and assigned the same values of transpiration used in the baseline simulation to evaporation (ET3). We conducted one test modifying precipitation and flow input by using a daily time step instead of the 15-minute time step used in the baseline scenarios.

Table 9-2 Scenarios for model sensitivity analysis.

Model feature modified	Scenario	Modification from baseline
Model configuration	C1	Depth of shallow alluvium 1m
	C2	Depth of shallow alluvium 3 m
	C3	Channel width 5 m
	C4	Channel width 1 m
	C5	1D simulation
Hydraulic properties, shallow alluvium	HPs1	Sand, alpha 0.145, n 2.68
	HPs2	Alpha 0.05, n 3
	HPs3	Ks = 1 cm hr^{-1}
	HPs4	Ks = 100 cm hr^{-1}
Hydraulic properties, deep layer	HPd1	Alpha 0.06, n 2
	HPd2	Alpha 0.05, n 3
	HPd3	Ks = 0.001 cm hr^{-1}
	HPd4	Ks = 1 cm hr^{-1}
Evaporation, transpiration	ET1	Increase T, Surface cover fraction 0.5
	ET2	No ET
	ET3	Assign PM from baseline to E only
	ET4	Root distribution a. Uniform top 200 cm b. Depth max intensity 200 cm c. Max depth 500 cm
	ET5	Alternate RWU parameters a. S-shape, P50 -800 cm, P3 3 cm, PW -1e10 cm b. P50 -100 cm c. P50 -2000 cm
	ET6	Feddes, altered parameters a. P2H = -100 cm b. P2H = -300 cm c. P2L = -600 cm d. P2L = -1000 cm e. P3 = -5000 cm f. P3 = -11000 cm
Initial conditions	IC1	a. Uniform 0.05 throughout b. Uniform 0.15 throughout
Input (precipitation and flow)	I1	Daily time step

Baseline simulations

The baseline simulations show similar water content patterns to the observations in timing and magnitude of response to inputs, with some notable differences. Figure 9-2 shows two examples of the baseline simulation results for YBA. The first example is for the first year of simulation, which was relatively dry with no flow events. Both the observations and simulations respond to rain events on July 31, Nov 4, and Nov 12, 2011, with the largest response during several consecutive days of rain in December 2011. The range of water content values in the simulations is similar to the observed values, except the observed values have greater differences in water content with depth than the simulations.

The bottom example in Figure 9-2 shows the observed and simulated response to a flow event on August 17, 2012. Not the difference in y-axis scales for the bottom plot as compared to the top plot. Water content rapidly increases to saturation during flow for both the simulation and observations, with saturated conditions in the observed data indicated by relatively constant VWC values between 0.26-0.34. The observed Θ values have some oscillations near the beginning and end of the period of saturation, and they drop rapidly back to low Θ values after this period of saturation. In contrast, the simulation does not stay saturated as long, and Θ values drop more gradually after the flow event. Similar discrepancies between simulations and observations were observed for the two other flow events at this site. Through tests of different simulation configurations, we found configurations that better represented the duration of saturation observed at the site, as shown in the next section, but improved simulation of saturation during flow resulted in poorer simulations between flow events. We did not find a set of hydraulic parameters that would reproduce either the rapid oscillations in VWC near saturation or the abrupt drops in moisture after saturation recorded in the observations. The event shown in Figure 9-2 followed another large flow event, which probably scoured out the sensors, giving unrealistically low baseline VWC values prior to the August 17 event. Therefore, we concluded that the observed VWC patterns during flow events were not necessarily representative of the actual water contents at 10-50 cm depth. Selection of hydraulic parameters for the baseline simulations focused on identifying parameter values that would best capture the timing of the rising limb during a flow event rather than the falling limb.

Over the 3-year time period, the mean Θ values in the simulations were higher than the observed values by 0.003-0.008 (Figure 9-3). Because the observations appear to have unrealistically low values between flow events due to sensor disturbance (Figure 9-2), we concluded that the slightly higher mean values in the simulations were reasonable representations of actual VWC at these sites. The lateral position of observation nodes does have a small effect on VWC values as well, with nodes beneath the center of the channel slightly wetter than those at the side of the channel. Sensors were installed closer to the sides of the channels.

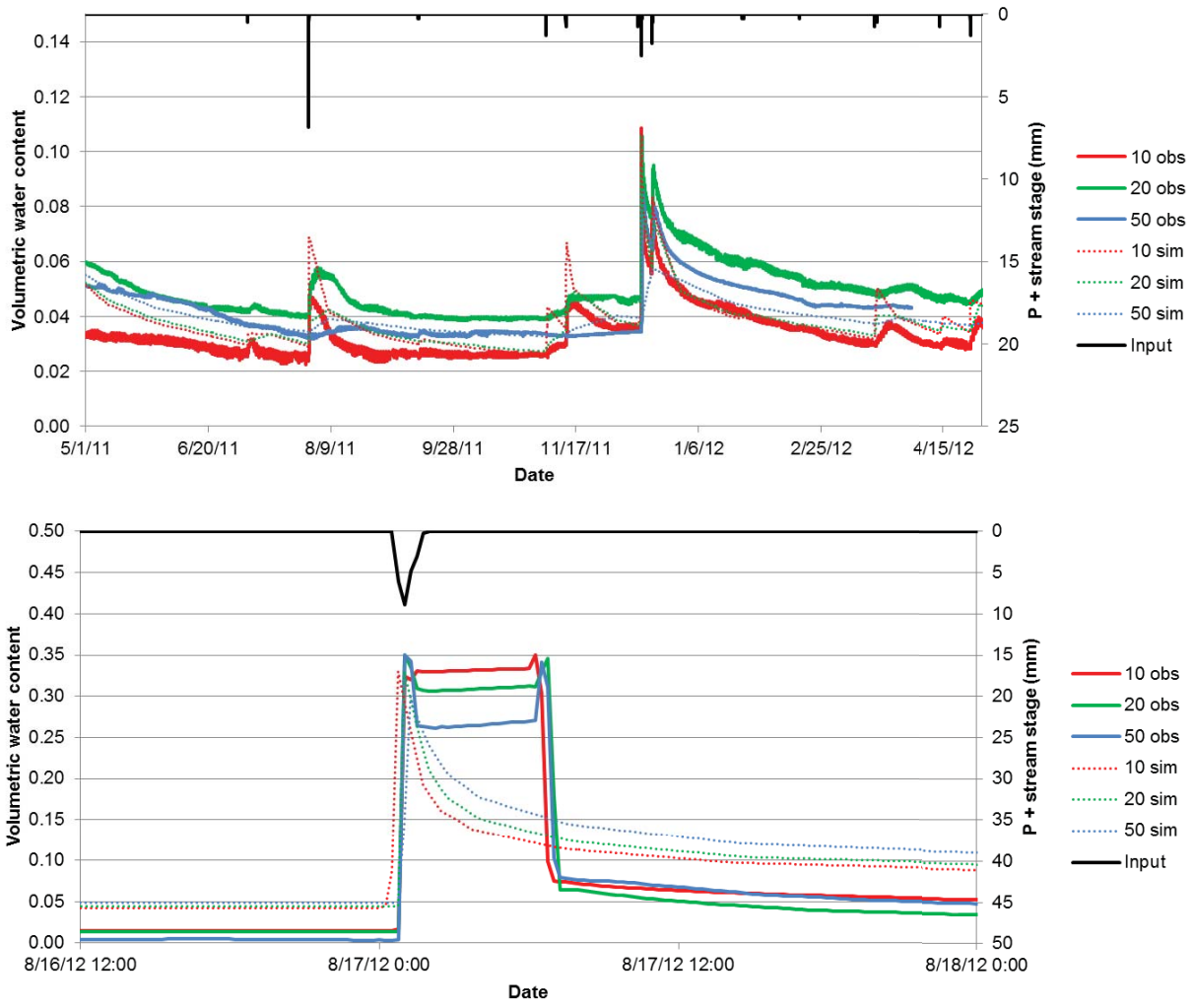

Figure 9-2 Example comparisons of simulations and observations for the baseline HYDRUS simulation at YBA. Top plot shows a relatively dry year with only rain events, and bottom plot shows an example flow event.

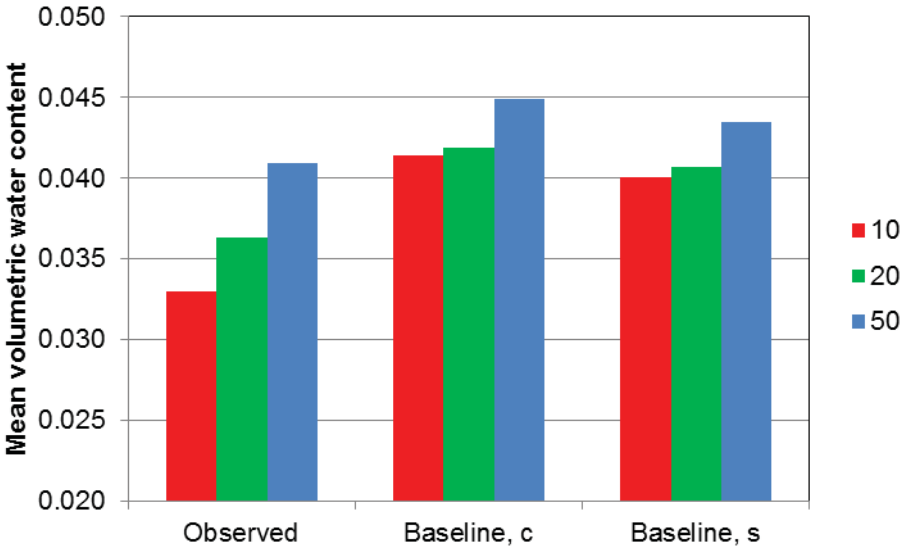

Figure 9-3. Mean volumetric water content over 3-year simulation time period for observations and baseline simulations at observation nodes beneath the center of the channel (c) and side of the channel (s).

Sensitivity tests

Sensitivity tests show how differences in model configuration, parameters, and input affect simulated water content. Tests are summarized in Table 9-3, which shows the difference in mean depth-integrated water content (0-300 cm) between each sensitivity scenario and the baseline simulation. Decreasing the depth of the shallow layer (scenario C1) led to elevated moisture because the lower K_s of the deep layer inhibited deep infiltration, keeping higher water contents in the shallower subsurface (Figure 9-4). During the initial dry time period of the simulation, the effects of the shallow layer depth were relatively small, but after the three flow events during the middle of the simulation, the shallow top layer in scenario C1 stayed substantially wetter than in the baseline scenario. Creating a deeper top layer (scenario C2) had the opposite effect on average water content, with drier conditions than the baseline because water traveled more easily down through the high K_s surface layer than through the lower K_s deep layer. Creating a wider channel at the surface of the domain (C3) had minimal effect on the simulated water content, but creating a 1 m wide channel (C4) reduced average water content because the domain received substantially less water input through the narrow channel.

Several simulation tests were conducted in HYDRUS-1D before deciding to use HYDRUS-2D for the baseline simulation. The 1D simulation results (C5) are similar to those in 2D except during and after flow events, when 2D simulations re-distribute water laterally, particularly at the interface between the higher Ks shallow layer and the lower Ks deep layer (Figure 9-5). As a consequence, a 1D simulation with the same K_s as a 2D simulation will have more water retained in the domain because no lateral redistribution is possible. This actually improves the simulated duration of saturation during flow events (Figure 9-6) because water can only redistribute vertically. In natural conditions, more lateral redistribution is likely because sediments within and beside the channels remain unsaturated, and we found that lateral redistribution of water was necessary to simulate large flow events at one of the other larger channel sites, MIA. Therefore we concluded that even though the ability to simulate sustained saturation during flow was improved in the 1D scenarios in this case, the mechanism of doing this through impeded lateral redistribution is unrealistic. Overall, 1D simulations (C5) are wetter than the baseline because of no possibility for lateral redistribution (Table 9-3).

Table 9-3 Change in depth-integrated (0-300 cm) mean volumetric water content for each model sensitivity test relative to the baseline scenario. Values in bold are scenarios with the largest changes from the baseline values.

Model feature modified	Scenario	Change in depth integrated Θ from baseline
Model configuration	C1	**0.019**
	C2	**-0.021**
	C3	0.007
	C4	**-0.023**
	C5	**0.038**
Hydraulic properties, shallow alluvium	HPs1	Crash
	HPs2	Crash
	HPs3	-0.002
	HPs4	-0.002
Hydraulic properties, deep layer	HPd1	0.026
	HPd2	0.002
	HPd3	**0.041**
	HPd4	**-0.021**
Evaporation, transpiration	ET1	**-0.026**
	ET2	**0.016**
	ET3	0.006
	ET4	0.000-0.003
	ET5	0.000-0.011
	ET6	0.000
Initial conditions	IC1	-0.007-**0.017**
Input (precipitation and flow)	I1	0.004

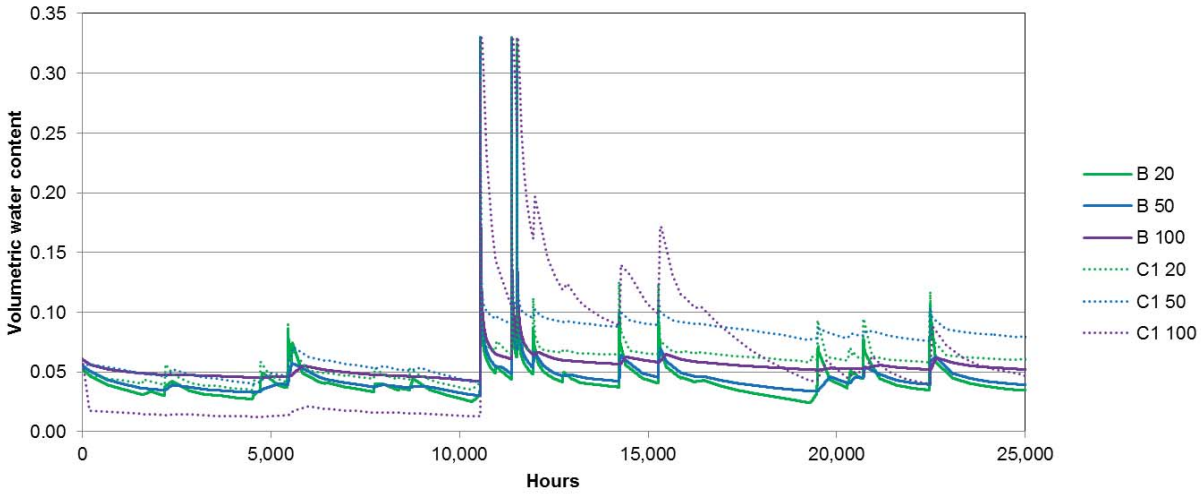

Figure 9-4. Comparison of simulation C1 (reduced depth of shallow layer) to baseline simulation at 20, 50, and 100 cm depth.

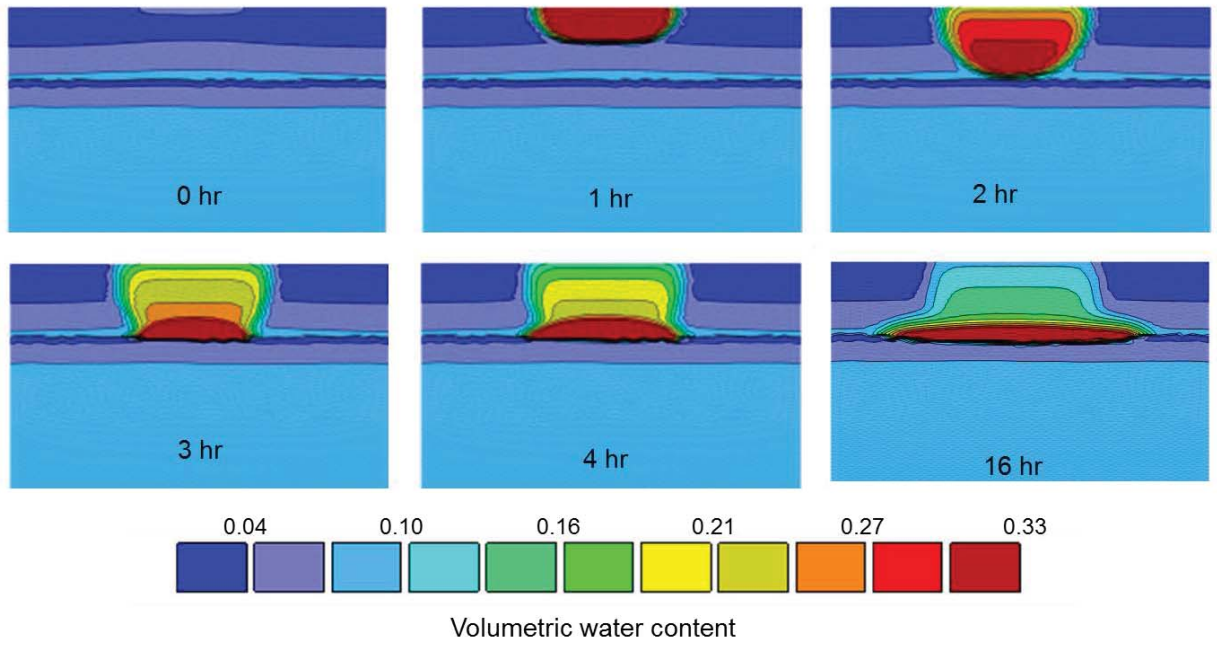

Figure 9-5. Baseline scenario simulation of July 13, 2012 flow event. Water infiltrates rapidly through the top layer, with minimal lateral redistribution until the wetting front reaches the interface with the lower K_s deep layer, where a perched saturated zone builds up at the interface between the layers, and water begins to redistribute laterally.

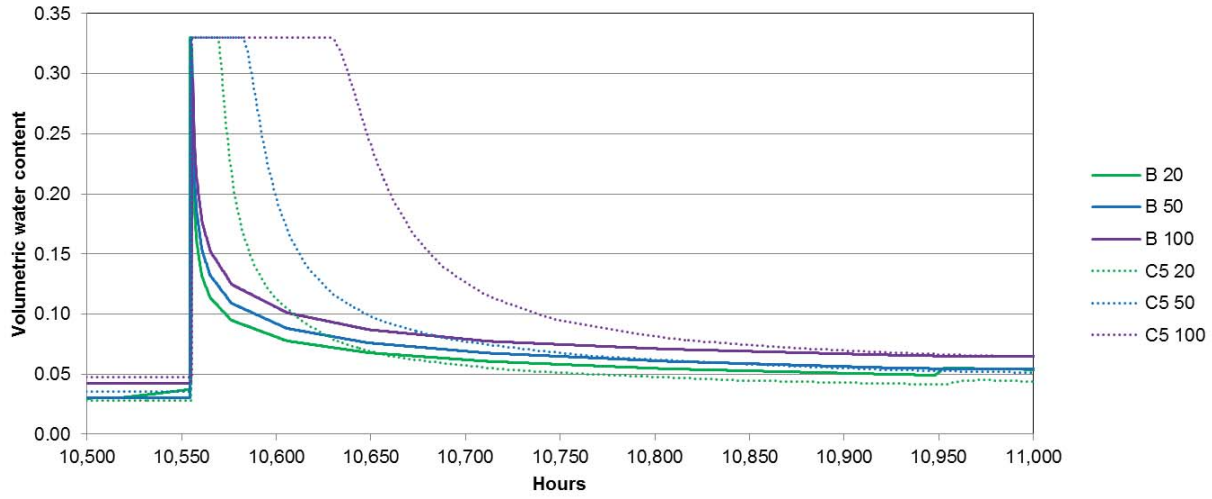

Figure 9-6. Comparison of baseline simulation to the 1D scenario C5 at 20, 50, and 100 cm depth for the flow event shown in Figure 1.5. The 1D simulation does not allow lateral redistribution of water during the flow event, so saturated conditions persist longer than in the baseline 2D simulation.

Hydraulic parameters that best simulate water content patterns in the shallow alluvium have low water retention, and we found that modifying the water retention curvature parameters (α and n) in this range would often produce problems with the numerical solver in HYDRUS. As a result, comprehensive testing of model sensitivity to hydraulic parameters was not feasible, particularly for the shallow layer. Note the simulation crashes for two of the shallow parameter scenarios (HPs1, HPs2, Table 9-3). The simulations were not very sensitive to Ks values in the shallow layer, where conditions were unsaturated most of the time. The simulated water contents were more sensitive to the value of Ks in the deep layer, with lower Ks producing wetter conditions (HPd3) because deep

infiltration was impeded. Higher Ks (HPd4) produced drier conditions because this allowed more infiltration of water deeper into the subsurface.

Increasing ET led to drier conditions (ET1), and eliminating ET led to wetter conditions (ET2), though eliminating ET only elevated average VWC by 0.02 (Figure 9-7, Table 9-3). Assigning ET to evaporation instead of transpiration (ET3) changed the distribution of water in the near-surface, with drier conditions closer to the land surface, but had minimal effect on the 0-300 cm depth-integrated VWC. The simulations were relatively insensitive to the root water uptake functions, parameters, and root distribution (ET4-6). In all cases, the simulated root water uptake was substantially lower than the potential ET, indicating moisture-limited conditions (Figure 9-8). The high transpiration scenario (ET1) illustrates the effects of moisture limitation, with high transpiration (shown as root water uptake) during time periods with moisture availability. The higher transpiration can then reduce water content enough that transpiration periodically shuts down in the high transpiration scenario. As a consequence, the pattern of transpiration over time is not clearly related to the seasonal pattern of potential ET.

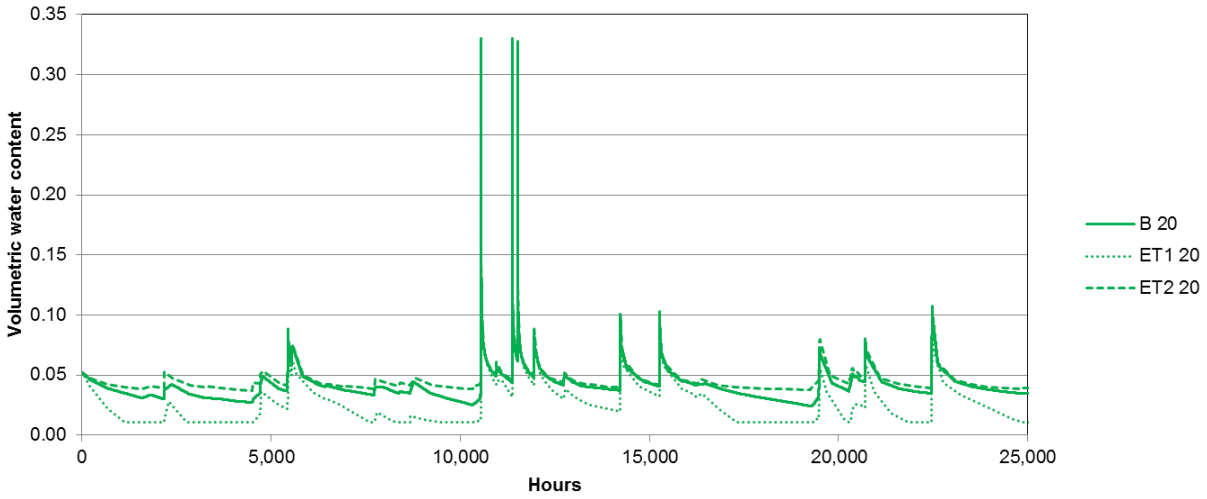

Figure 9-7. Comparison of simulations ET1 (increased transpiration) and ET2 (no ET) to the baseline simulation of VWC at 20 cm depth. Increased transpiration in ET1 brings shallow VWC down to the residual water content during dry periods; eliminating ET in ET2 leads to slightly higher water content than in the baseline scenario.

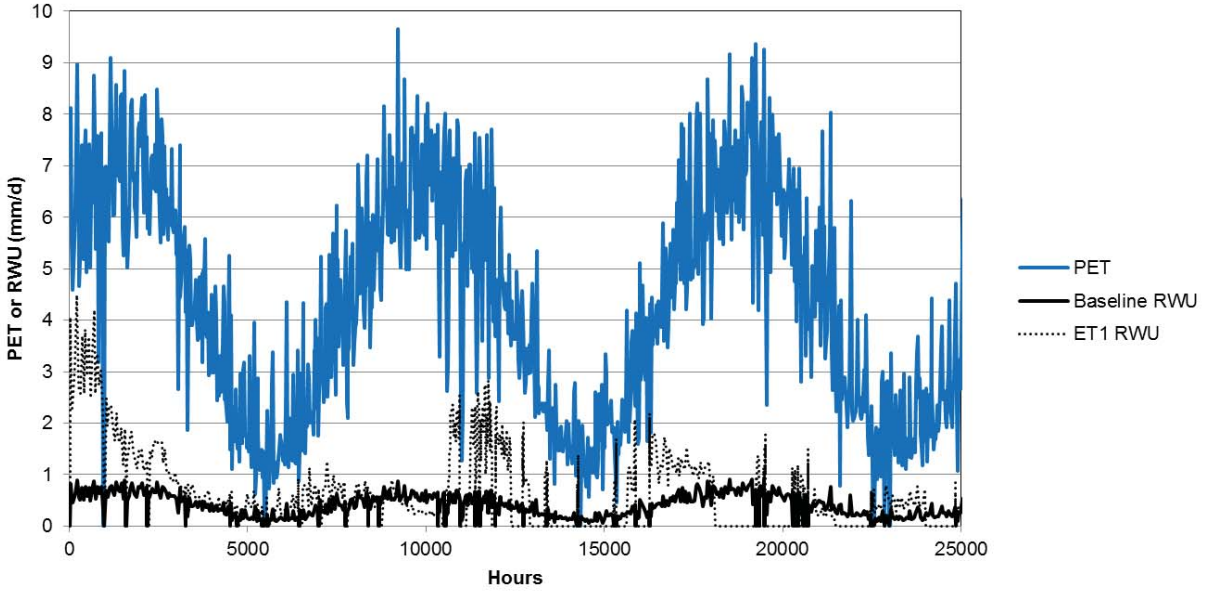

Figure 9-8. Comparison of root water uptake (RWU) in the baseline and ET1 scenarios relative to potential ET calculated by the HYDRUS model using the Penman-Monteith equation.

Changing initial conditions (IC1) had the expected effect, with drier initial conditions leading to drier average water content and wetter initial conditions leading to higher average water contents (Table 9-3). Changing the input of precipitation and flow to a daily time step (I1) had minimal effect on the long-term mean water content, and differences from the baseline simulation were only evident during flow events, when the timing and redistribution patterns of VWC differed because moisture was input over a 24-hour period rather than during the short pulses of flow observed in the finer temporal resolution data (Figure 9-9). For the largest flow event shown in Figure 9-9 (7/13/12 event), distributing the large input over a daily time step resulted in an extended period of saturation relative to the baseline because input was high enough to sustain saturated conditions. In contrast, for the two smaller flow events shown in Figure 9-9, distributing the input over a longer period of time meant that saturated conditions did not develop with daily time step input. Because the baseline simulation had input concentrated in a shorter period of time, saturated conditions did develop briefly in response to the flow events.

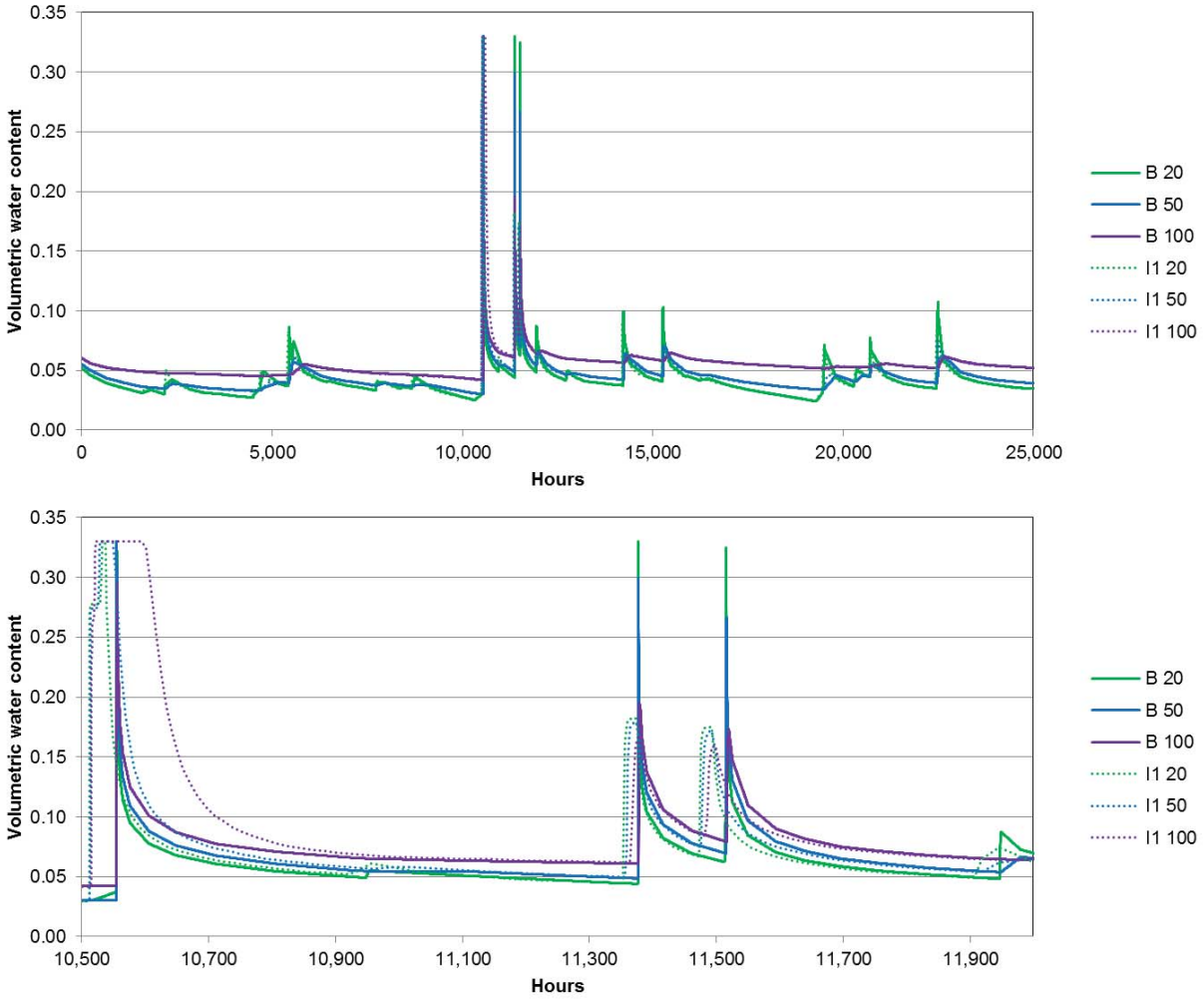

Figure 9-9. Comparison of simulation I1 (daily time step input) to the baseline simulation at 20, 50, and 100 cm depth for the 3-year simulation (top) and for the summer 2012 flow events (bottom).

Discussion

HYDRUS simulations reproduce the dominant patterns of water content with depth and over time for the YBA site. Simulated water contents respond rapidly to rain events and increase to saturation during flow events, as observed in the measurements at this site. The simulations track water content dynamics at this site for the period of observation, indicating that they are suitable for examining how water contents might change over time under different climate and flow scenarios. Similar simulation configurations work for the other study sites tested, suggesting that the model configuration is a good representation of water content dynamics in ephemeral stream channels for this study area. In this discussion, we focus on the results of the sensitivity analyses and what these tests indicate about how the baseline simulation configuration will affect results of longer-term simulations of water content under changing climate conditions.

Sensitivity to stratigraphic configuration

Sensitivity tests indicate that water contents are most sensitive to the depth of the top layer of shallow alluvium and to the Ks of the deeper layer below it. The interface between the higher Ks shallow layer and the lower Ks deeper layer is where a water table perches after flow events (Figure 9-5), so changing the depth of this layer or its ability to take in more water (Ks) will change the water contents in the shallow layer. We can identify combinations of layer depths and deep layer Ks that best reproduce the observed water contents, but because these two components of the model interact with one another, a model configuration with good performance is not necessarily unique. For example, we could produce wetter water contents in the shallow layer either by decreasing the shallow layer depth or by decreasing the Ks of the deep layer. At the YBA site, we know that the alluvium rests on less permeable bedrock, but we lack information about the hydraulic properties of this bedrock. While geophysical surveys gave some information about layering at the site that informed our selection of the shallow layer depth (Harry et al. manuscript), geophysical results were not conclusive about whether moisture, cementation, or stratigraphy caused layering at the study sites. Further, flow events can change the depth of the alluvium, so the top layer in reality does not have a constant depth. Flow events may also change hydraulic properties of alluvium through fine sediment clogging (Hoffman et al. 2003). In long-term climate scenarios, a climate that generates high runoff could result in systematic incision of channel bed alluvium, decrease of the shallow layer depth, and potentially changes in hydraulic properties if channel bed sediment composition changes. As a result, long-term simulations using the baseline HYDRUS simulation configuration are best suited for runoff conditions that do not differ substantially from those that have resulted in the current depth of alluvium in the YBA channel.

The HYDRUS simulations are also affected by the ability of water from runoff events to redistribute laterally, rather than just vertically beneath the channel bed. When there are only rain events without runoff, 1D vertical simulations are nearly identical to 2D simulations, but with high water input during flow events, water contents stay higher in 1D because lateral redistribution of water is inhibited. Other studies have highlighted the importance of lateral spreading of water after flow events in ephemeral streams (Izbicki et al. 2000; Eastoe et al. 2004), and we have also seen evidence of lateral spreading of water in the deep subsurface at one of the other monitoring sites (Kampf et al. manuscript). The problem with representing this lateral redistribution of water accurately in simulations is that we have limited information about the subsurface stratigraphy beneath channel banks, which will also affect lateral spreading. We have also simplified the shape of the channel in the simulation, and the actual channel cross section shape will affect how water enters the subsurface. Because HYDRUS only allows a single atmospheric boundary condition, we do not input rain water or transpiration rates at the land surface on either side of the channel bed, potentially leading to drier conditions in the side channel sediments than would be present in reality. In cases of discontinuous flow along the channel, there could also be longitudinal spreading (upstream-downstream) of water, which is not represented in a 2D simulation. We expect that long-term simulations will not be sensitive to lateral flow during low or no-runoff conditions, but they will be affected during time periods with high runoff.

Sensitivity to evapotranspiration

Through simulation tests, we found that ET had to be quite low relative to potential ET to be able to reproduce the observed water content patterns (Figure 9-8). In initial development of the baseline configuration, we were able to develop good simulations of water content by excluding ET entirely. When we increased transpiration above the baseline value, the patterns of water content were no longer consistent with observations. When we shifted

atmospheric losses from transpiration to evaporation, the vertical patterns of water content diverged from the observations. This gives us confidence that the rate of transpiration assigned in the model is reasonable. Simulations were insensitive to root distribution and to root water uptake parameters in the ranges tested.

Conclusions

This chapter describes configuration and testing of a variably saturated subsurface flow model that represents water redistribution continuously in response to rain events, runoff events, and transpiration at an ephemeral stream channel. The model reproduces the dominant features of water flow in this system, where water contents in the shallow subsurface increase rapidly in response to rain events then dry gradually from transpiration and redistribution into the deeper subsurface. Infrequent flow events cause rapid saturation of the shallow sediments, with water percolating into the deeper subsurface, where it develops a perched water table and spreads laterally at the contact with a lower permeability layer. Sensitivity tests of the model indicate that its water content simulations are relatively insensitive to the model configuration during rain-only events and dry periods. During and after flow events, the simulations are more sensitive to how the subsurface stratigraphy is represented in the model. Simulations that best match observations have low atmospheric losses through transpiration.

Part 2, climate change scenarios

Introduction and objectives

The three-year time period of observations used to configure the model in part 1 is a relatively small window of time in which to evaluate the water content dynamics of ephemeral streams, particularly because flow is so infrequent. In this portion of the study, we use the baseline model configuration to evaluate how water contents are affected by longer-term climate conditions. Long-term climate scenarios can be developed using either historical observations or general circulation model (GCM) simulations. GCMs have been applied to predict future climate conditions, so they potentially allow us to assess how future climate will affect runoff and subsurface flow. This portion of the study has three objectives (1) evaluate how well GCMs reproduce precipitation characteristics of the study area, (2) develop a method for simulating runoff magnitude as a function of precipitation, and (3) use the results of (1) and (2) to develop scenarios for testing how long-term precipitation and runoff patterns affect subsurface water content.

Methods

Precipitation

To address objective 1, we first compiled historical precipitation observations from the long-term weather stations near the study area and compared these to GCM precipitation. Historical climate data (H) come either from the Blythe airport (b) or Yuma Proving Grounds (y) stations, using the data archives in the National Climatic Data Center. We compared these data to GCM output for 1950-1999. This time period corresponds to the "observation" time period for the World Climate Research Programme's (WCRP's) Coupled Model Intercomparison Project phase 3 (CMIP3). Previous research on the performance of GCMs from the CMIP3 project in the southwestern U.S. region (Dominguez et al. 2010) identified significant problems in the models, which generally do not capture either the seasonality or magnitude of precipitation in the region. The models tend to over-estimate winter precipitation, and most fail to capture the summer peak in precipitation from the North American Monsoon. Therefore, before selecting a GCM for detailed comparison with observations, we examined seasonal patterns in the updated CMIP5 GCM simulations. This initial analysis showed the same problems highlighted by Dominguez et al. (2010), with most models missing the monsoonal moisture peak entirely. Dominguez et al. (2010) scored GCM model performance based on monthly precipitation, temperature, and large-scale climatological features, and they identified two models that performed the best, the Max-Planck-Institute for Meteorology model (mpi_echam5) and the UK Met. Office model (ukmo_hadcm3).

Because most GCMs do not capture the monsoonal moisture pattern that produces most of the runoff in the study area, we elected to examine only the MPI model, which scored high in the Dominguez et al. (2010) evaluation of CMIP3 models and was the model that best represented a summer precipitation peak in our initial GCM assessment. We evaluated both the CMIP3 and the CMIP5 versions of the MPI model, using both the original model output, the bias-corrected (bc) products, and the bias-corrected and spatially disaggregated products (bcsd) available through the Downscaled CMIP3 and CMIP5 Climate and Hydrology Projections Archive (http://gdodcp.ucllnl.org/downscaled_cmip_projections). The bias-correction uses the gridded climate data from Maurer et al. (2002) and described in Brekke et al. (2013). To evaluate how the GCMs compare to the observed climate record, we compared them to the mean monthly precipitation at the weather stations. We also compared the frequency of precipitation events exceeding thresholds for runoff production between weather stations and GCMs.

Based on the comparison of the GCM and observed precipitation, we selected versions of the GCM to use in future climate scenarios. Following the CMIP3 format, we evaluate two future climate time periods, 2046-2065 (F1) and 2081-2099 (F2) and the emissions scenarios developed by CMIP5. These emission scenarios are Representative Concentration Pathways (rcp) 2.6, 4.5, and 8.5, where the numbers refer to the increase in radiative forcing in 2100 in W m^{-2} (van Vuuren et al. 2011). For CMIP5, there are six model runs for each emission pathway (rcp26, rcp45, and rcp85). Three of the six runs are a low-resolution (lr) configuration of the model with a 1.9 degree horizontal resolution, and the remaining three are mixed resolution (Giorgetta et al. 2013).

Runoff

To develop a method for simulating runoff magnitude as a function of precipitation, we build on the results of Faulconer et al., who found that the occurrence of flow in channels with contributing areas less than around 3 km^2 is linked to a threshold rain intensity, with rain intensities above the threshold causing flow. The finest temporal resolution of both long-term precipitation records and GCM output is daily, so we need a method to predict runoff occurrence as a function of daily precipitation. Faulconer et al. found that a threshold rain event magnitude can also predict flow occurrence with 95.5% accuracy. Therefore, if we assume that daily total precipitation is a good approximation for event total precipitation, then we can use daily precipitation magnitude to predict whether or not runoff is generated each day.

For the YBA site (drainage area 2.2 km^2), which is the focus for subsurface flow modeling, Faulconer et al. identified a runoff threshold between 21-23 mm of precipitation. Other study sites had runoff thresholds between 5-51 mm. The thresholds at the lower end of the range correspond either to small contributing area (<0.1 km^2) headwater sites or to a larger contributing area site (YIA1) where a headwater tributary entered a larger channel just upstream of the flow monitoring location. The upper end of the range corresponds to sites with larger contributing areas. Given this range of thresholds at the measurement sites, we create five possible runoff scenarios with thresholds (T) at 5, 22, and 50 mm of daily precipitation (T5, T22, T50). In the runoff simulation, any days with precipitation above the threshold will generate runoff; days with precipitation below the threshold will not generate runoff.

For days with precipitation greater than the runoff threshold, we estimate the magnitude of runoff using a runoff ratio (fraction of daily precipitation that becomes runoff). Calculating runoff ratios from observed stream stage records requires estimation of event discharge. At the stage monitoring sites in the study area, we did not measure discharge because flow events are rare and brief, inhibiting field measurements. Therefore, for each site with stage measurements, we developed a stage-discharge rating curve using channel cross section geometry (Sutfin et al. 2014) and the Manning flow resistance equation:

where Q is the discharge in $m^3\ s^{-1}$; A is the cross section area in m^2; R is the hydraulic radius, calculated as A divided by the wetted perimeter; S is the slope of the hydraulic grade line, and n is the Manning coefficient.

Each monitoring site had 4-5 separate cross section surveys. To develop synthetic stage-discharge rating curves, we first interpolated each cross section survey to a common horizontal base spacing of 0.1 m using a linear interpolation function. Then, we identified the portion of the cross section that would be inundated at different stage heights, also calculated in increments of 0.1 up to a maximum of 2 m. For each increment of stage height, we calculated A, P, and R. We assumed that S at each cross section was equal to the slope of the channel bed, and we calculated a range of possible Q values at each stage height using n=0.03-0.06.

This procedure produced a series of 8-10 separate possible rating curves for each stage monitoring site. From those, we selected the curves that represented the lowest, highest, and middle range of discharge estimates. We fit a function to each of the rating curves and used these functions to calculate discharge for the observed stage values during flow events. We estimated low, medium, and high total discharge magnitudes for each observed flow event at each site.

To simulate runoff magnitude for days with threshold-exceeding precipitation, we need to estimate the runoff ratio (Q/P) for each event, calculated as total event discharge (Q) over total event precipitation (P). To determine a possible range of runoff ratios, we used the calculated discharge magnitudes from the monitoring sites and watershed average precipitation corresponding to each of these flow events. We estimated watershed average precipitation using inverse distance weighting of daily precipitation totals from the rain gauges at our study sites (Faulconer et al.), rain gauges operated by Yuma Proving Grounds, and the two closest long-term weather stations, Blythe Airport and Yuma Proving Grounds. For each day that runoff was generated at any study site, we created an interpolated field of daily precipitation totals over the entire study area. From this field, we extracted the average precipitation for each watershed where flow was observed.

Given the range of observed runoff ratios at the study sites, we examined how the runoff ratios vary by study site and with event total precipitation. Based on this analysis, we selected low, average, and high runoff ratios to represent the range of possible runoff generation for a given rain event. These runoff ratios then create a series of

flow magnitudes for each sequence of precipitation and runoff threshold evaluated. Figure 9-10 illustrates the order of calculations to produce precipitation and runoff scenarios.

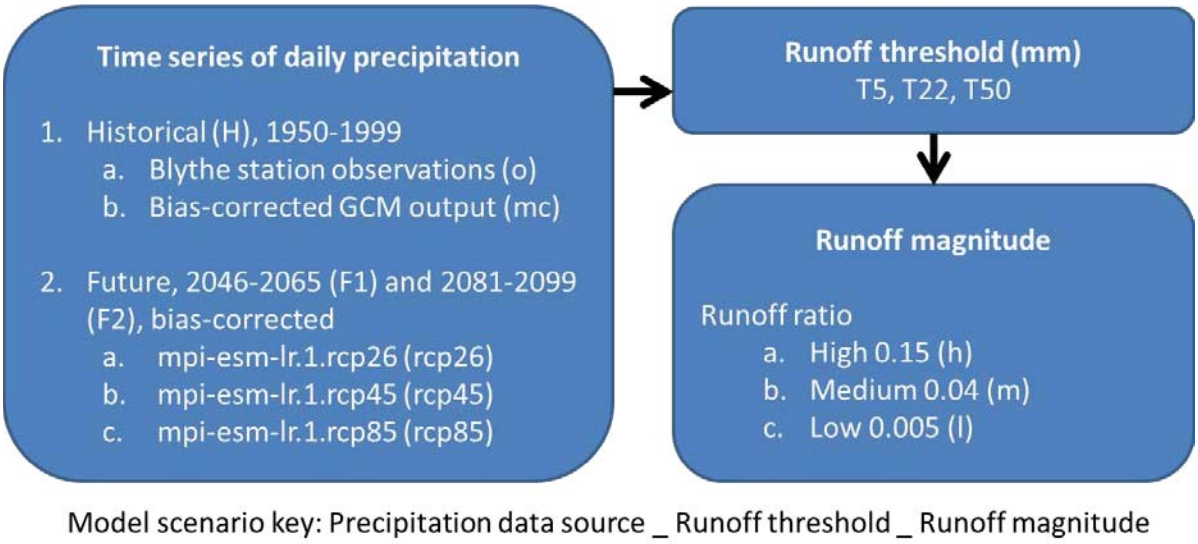

Figure 9-10.Precipiration and runoff

Subsurface water content

To simulate how different precipitation and runoff scenarios affect subsurface water content, we used the baseline configuration of the HYDRUS model for YBA described in part 1 of this chapter. Using this configuration, we force the model with a series of different precipitation and runoff inputs representing historical and future climate. First, for a reference set of simulations, we compare the baseline simulation for the study time period (STb) to a simulation for the same time period that excludes the additional input from flow events (STnf). This first test allows us to evaluate the sensitivity of the subsurface water content to the magnitude of runoff.

Next, we developed a series of historical scenarios for the period of record (1950-2013) using precipitation observations from Blythe (Ho); note that while we ran the simulation for the period of record, results for the historical time period are always reported just for 1950-1999 (Figure 9-10). To test the sensitivity of simulated water content to the magnitude of runoff, for each set of observed precipitation inputs, we created three runoff scenarios that represent high, low, and average runoff. For high runoff, we used T=5 mm and Q/P = 0.15 (T5_l); for average runoff T=22 mm and Q/P = 0.04 (T22_m), and for low runoff T=50 mm and Q/P = 0.005 (T50_l).

We also developed both historical and future climate scenarios using simulated precipitation from the mpi-esm-lr.1 model, both original (Hm) and bias corrected (Hmc). For historical climate, we simulated the same period of record as the observations (1950-2013). For future climate, we reinitialized the HYDRUS model in 2014 and used the mpi-esm-lr.1 model precipitation as inputs for 2014-2099. We ran two future climate scenarios were run, one with the low emissions scenario (F_rcp26) and the other with the high emissions scenario (F_rcp85). For each set of climate model input scenarios, we simulated runoff used the average runoff threshold and runoff ratio (T22_m).

For each of these scenarios, HYDRUS simulations are run with daily time step input. To configure the runoff scenarios for input to HYDRUS, we converted the predicted runoff in mm to a daily average discharge, then used the inverse of the stage-discharge rating curve to compute a daily average stage depth. This stage depth was added to the precipitation as an input through the atmospheric boundary for the simulation.

HYDRUS also requires time series of evaporation and transpiration as inputs to the simulation. The simulation approach we used in the baseline simulations in part 1 of this chapter calculates potential ET using the Penman-Monteith equation, then multiplies this PET by a surface cover fraction to calculate the transpiration boundary condition for the HYDRUS simulation. Through the initial set of model tests in part 1 of this chapter, we found that a low surface cover fraction (0.1 in the baseline simulation) was needed to keep water contents in the range of observations. This means that transpiration assigned at the atmospheric boundary condition was only a tenth of the PET. ET in this hyper-arid climate is moisture-limited, not energy-limited, and this condition is not likely to change

in future warmer climates. Therefore, for all HYDRUS simulations we chose to keep transpiration input the same as in the baseline scenario. For each year simulated, the daily PET was taken from the 2012 PET used in the baseline simulation.

Results

Precipitation

The historical climate in the study area extremely arid, with mean annual precipitation of 94-95 mm at the Blythe Airport and Yuma Proving Ground stations. The two weather stations have very similar seasonal patterns in mean monthly precipitation, with the highest precipitation in August during the North American Monsoon and another peak in precipitation in December-January due to winter frontal storms (Figure 9-11). The MPI GCMs produce substantially wetter conditions for the historical (1950-1999) time period, with mean annual precipitation ranging from 269-281 mm, more than double the observed precipitation. The model runs all do capture a summer monsoon peak in precipitation, but in contrast to the observations, the winter precipitation peak is much higher than the summer peak in all model runs. The model runs vary in the magnitudes of mean monthly precipitation, but they all predict similar seasonal patterns. Bias correction of the MPI model give mean monthly precipitation patterns closer to the observations, with mean annual precipitation ranging from 102-136 mm. We found that the bias-corrected precipitation matched the observations at coarse resolution (2 degrees for CMIP3 and 1 degree for CMIP5) better than the spatially disaggregated (bcsd) products, so we used GCM output at the original spatial resolution without spatial disaggregation for further comparison and for runoff and subsurface flow simulations.

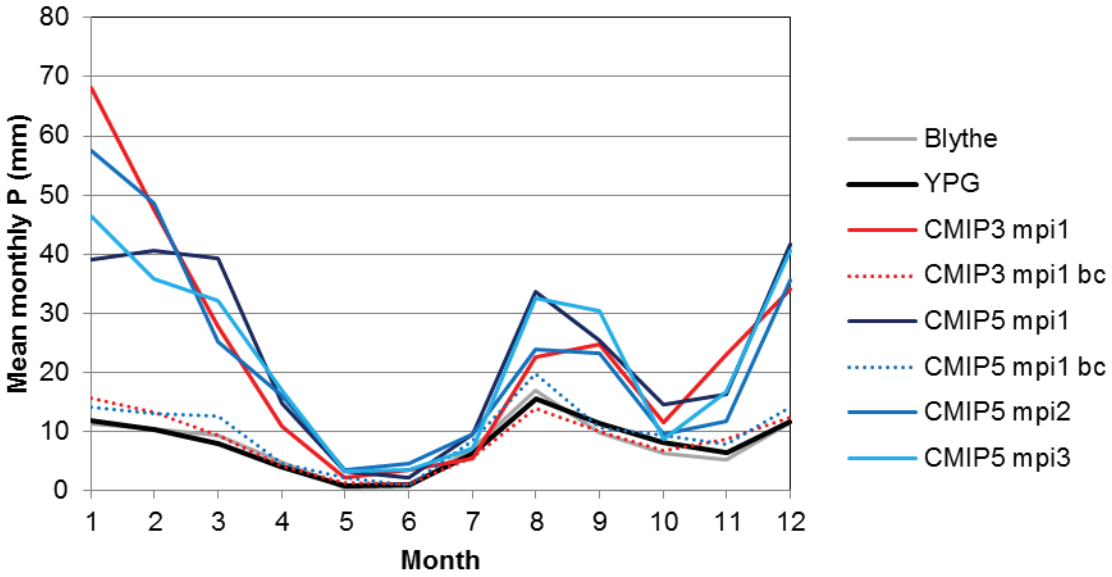

Figure 9-11. Observed historical mean monthly precipitation from Blythe Airport and Yuma Proving Ground (YPG) stations compared to the MPI GCM simulated precipitation from the CMIP3 and CMIP5 projects. CMIP5 model lines are three iterations of the LR model runs. CMIP series labeled bc have been bias-corrected. All means are for the 1950-1999 time period except YPG (starts 1955) and CMIP3 (starts 1961).

Because our simulation procedure uses precipitation thresholds for runoff generation, we evaluated how the frequency of threshold-exceeding precipitation events compares between the GCM runs and the observations (Figure 9-12). The GCM runs have higher precipitation overall, so they have a greater number of events exceeding all precipitation threshold values. Bias-correction brings the frequency of threshold-exceeding events closer to the observations. The bias-corrected GCM runs tend to distribute the precipitation into a greater number of small depth events and under-predict the number of larger rain events relative to the observations.

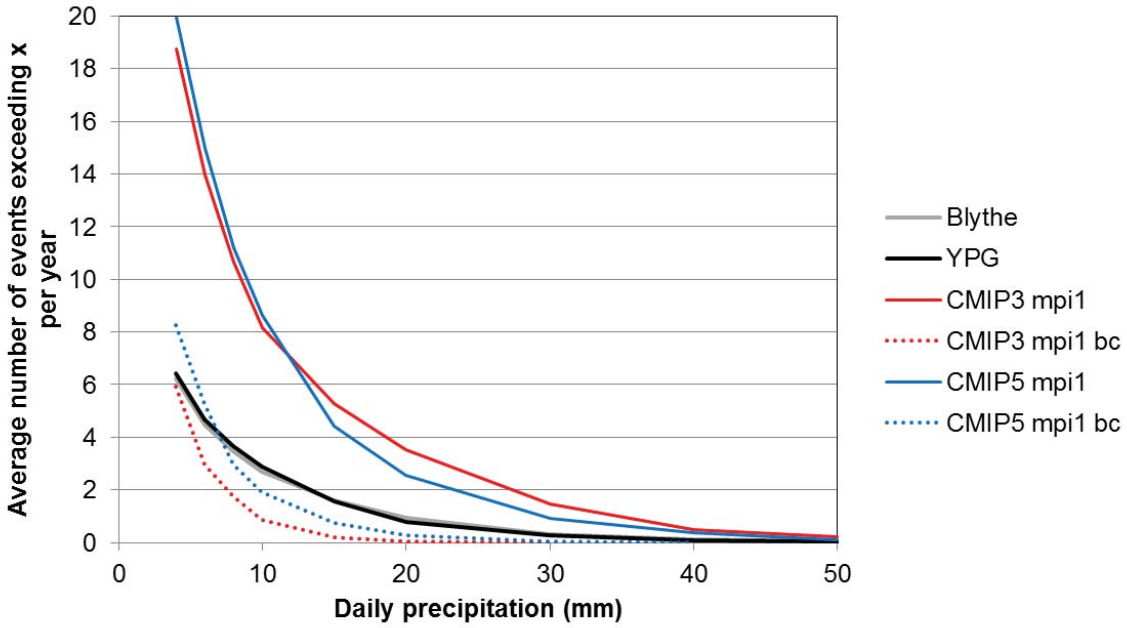

Figure 9-12. Average number of days per year with runoff generation, given daily precipitation thresholds on the x-axis for the historical time period. See Figure 9-10 caption for descriptions of data series.

Because CMIP3 and CMIP5 simulation results were similar for the historical time period, we show only CMIP5 results for future time periods, focusing on the LR1 runs. Relative to the historical time period, the 2046-2065 time period has declining summer monsoon precipitation for the low emissions scenario (rcp26) but increasing monsoon precipitation for the high emissions scenario (rcp85) (Figure 9-13). The 2081-2099 time period shows less change in the magnitude of the monsoon precipitation, but the simulations consistently show higher winter precipitation. The bias-corrected values preserve the same types of changes in precipitation simulated in the original model output.

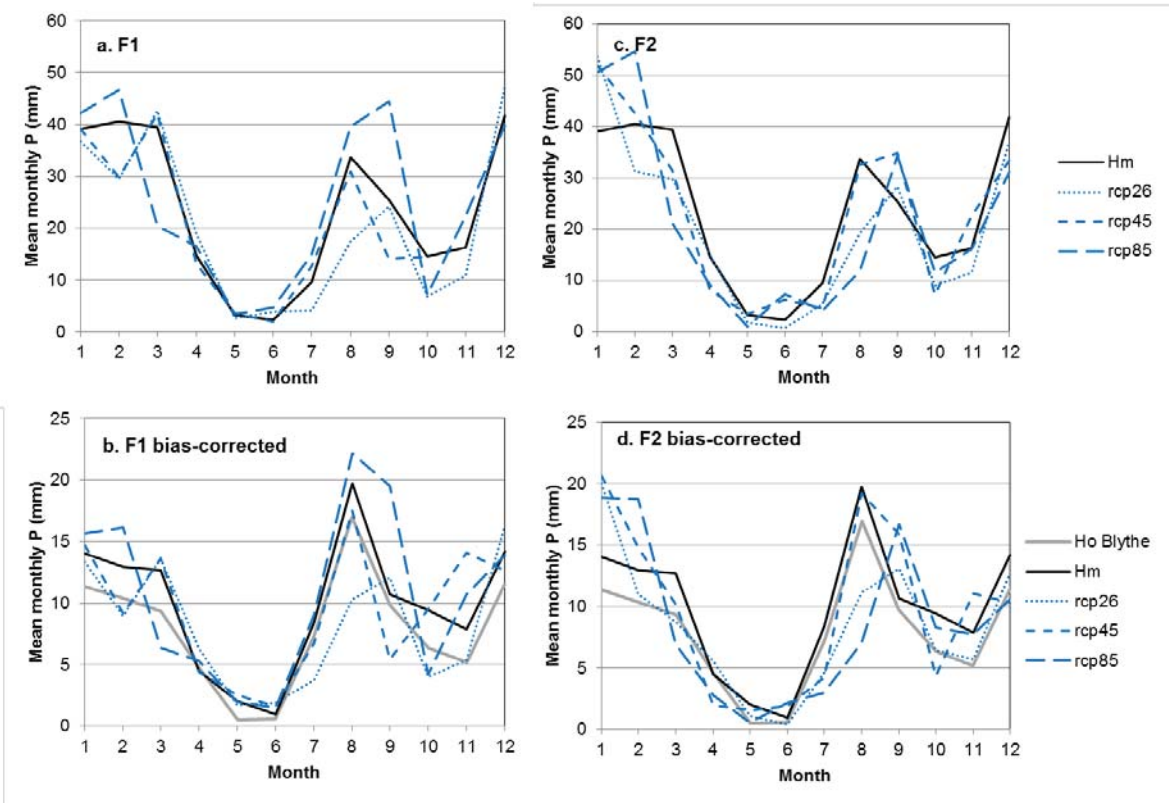

Figure 9-13. Mean monthly precipitation for 2046-2065 (F1) and 2081-2099 (F2) simulated by the mpi-esm-lr.1 model using three different emissions scenarios (rcp26,45,85) as compared to the same model run for the 1950-1999 time period (Hm) and the observed mean monthly precipitation from the Blythe station (Ho).

The future climate scenarios generally increase the frequency of large magnitude rain events and decrease the frequency of smaller events in both original and bias-corrected GCM output (Figure 9-14). In 2046-2065, the shift in frequency is greatest in the high emissions scenario (rcp85) and negligible in the other scenarios relative to 1950-1999 For 2081-2099 all emissions scenarios predict decreased frequency of small events (<15 mm in original simulations and <4 mm in bias-corrected simulations) and increased frequency of larger events relative to the 1950-1999 time period.

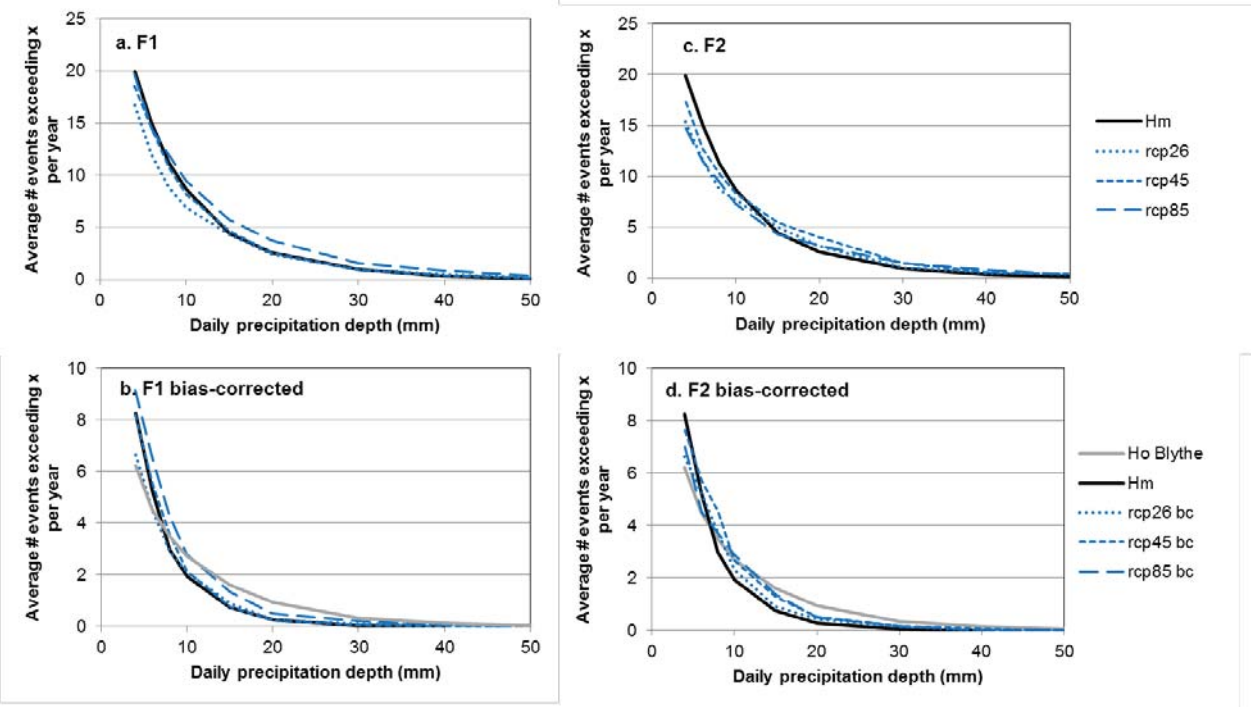

Figure 9-14. Average number of days per year with runoff generation, given daily precipitation thresholds on the x-axis for future time periods 2046-2065 (F1) and 2081-2099 (F2). See Figure 9-12 caption for descriptions of data series.

Runoff

Event runoff ratios for the study sites ranged from 0.005 to 0.831, with the highest runoff ratios at piedmont headwater channel types (Figure 9-15). High runoff ratios at piedmont headwater sites suggest that these sites are important sources of runoff to downstream channel. At bedrock, bedrock with alluvium, and incised alluvium sites shown in Figure 9-15, estimated runoff ratios never exceeded 0.11. At the reference site for subsurface flow modeling, YBA, the highest runoff ratio (0.11) was during the extreme storm on July 13, 2012, when estimated catchment total precipitation was 85 mm. This event also produced the highest runoff ratio for the YIA site. The average runoff ratio estimated at YBA is 0.04. We used the range of runoff ratios in the bedrock, bedrock with alluvium, and incised alluvium sites to set the range of runoff ratios in runoff modeling. For a low runoff scenario, we used the minimum runoff ratio (0.005); for average runoff, we used the average runoff ratio at YBA, 0.04, and for high runoff, we used a value slightly higher than the maximum runoff ratio (0.15).

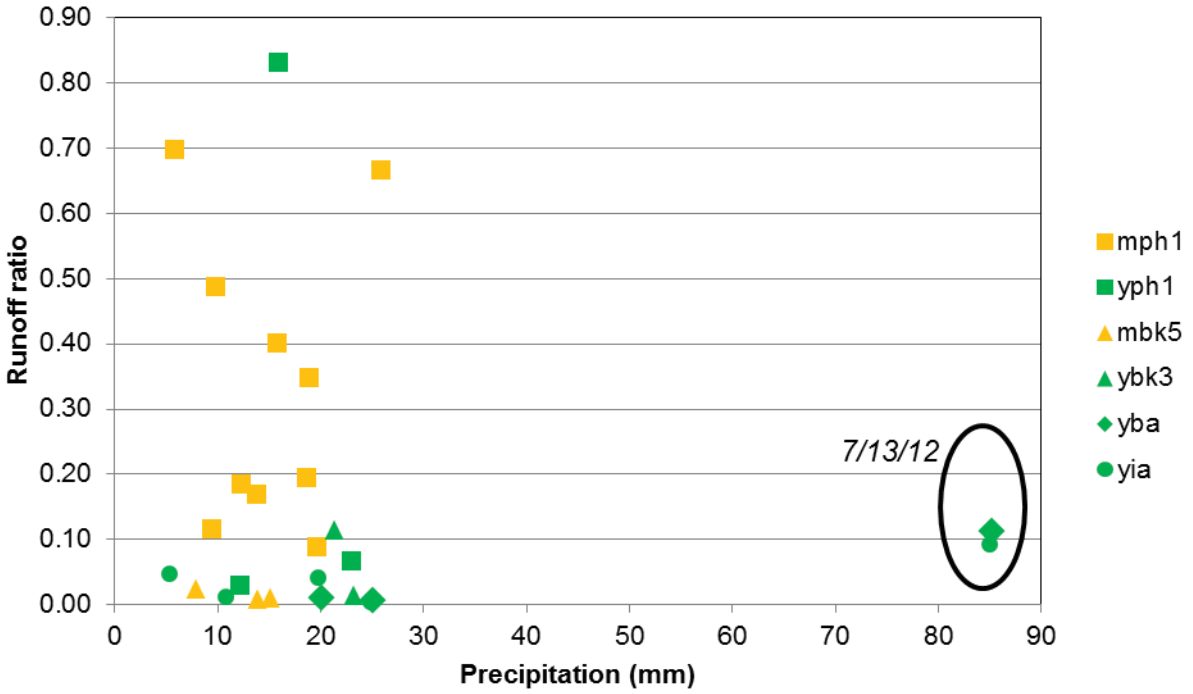

Figure 9-15. Estimated event runoff ratios for study sites with stage monitoring. Runoff ratios are event total discharge over event total precipitation. Discharge is estimated using stage measurements and synthetic rating curves. Event total precipitation is estimated through inverse distance weighting interpolation of daily precipitation totals over the study area.

To simulate runoff generation, we used the series of scenarios described in Figure 9-10. Historical scenarios based on observations (Ho) use the Blythe station because this station had the longest period of record. GCM scenarios use the MPI lr1 model output with bias correction (Hmc). We chose not to use the original model output because of the high bias in precipitation. Both the Ho and Hmc precipitation scenarios are then run with three different runoff thresholds and three different fixed runoff ratios. Mean annual runoff for each of these scenarios is shown in Figure 9-16. The greatest mean annual runoff is produced in the simulations with lowest runoff thresholds and highest runoff ratios; this likely over-estimates runoff substantially, as the upper end of runoff ratios were from the extreme 7/13/12 storm. Based on the 3-year study time period the scenario that is most closely linked to observations is Ho_T22_m, the scenario with the runoff threshold measured at YBA and the average runoff ratio for the YBA site. This scenario produced only 1 mm of mean annual runoff for the historical record. The bias-corrected GCM scenarios produced even less runoff overall than the observed record because of the lower frequency of large events (Figure 9-12). These GCM scenarios produced no runoff for the highest runoff threshold (50 mm) because there were no rain events in the bias-corrected GCM records with magnitudes greater than 50 mm.

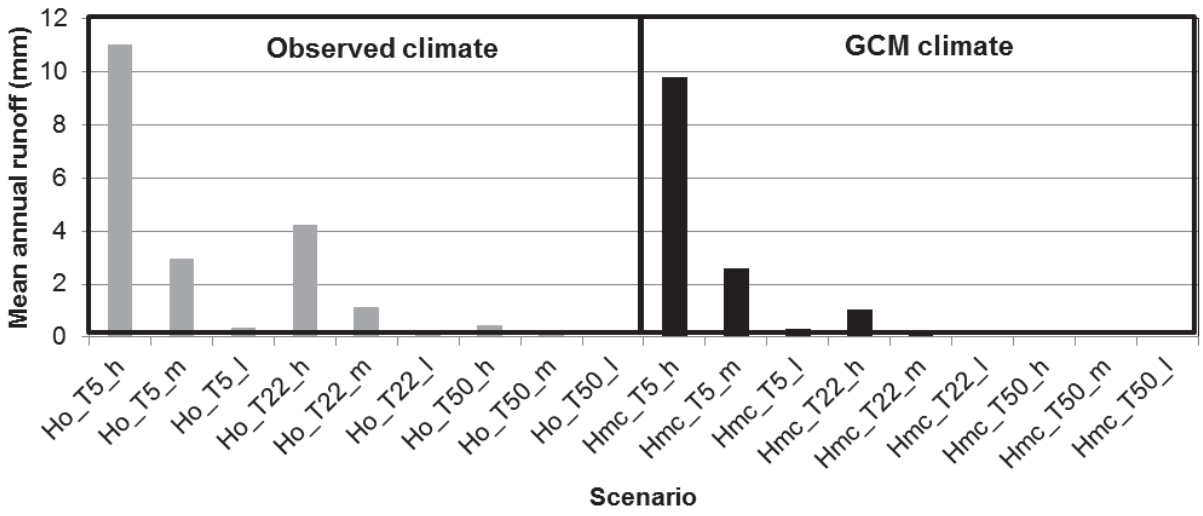

Figure 9-16. Mean annual runoff simulated for the historical (1950-1999) time period using observed precipitation (Ho) and GCM bias-corrected precipitation from the mpi-esp-lr.1 model (Hmc), three different runoff thresholds (T5,T22,T50), and three different runoff ratios (l=0.005, m=0.04,h= 0.15).

All runoff predictions from the bias-corrected MPI GCM are lower than those predicted from the observations, as shown in Figure 9-17, which compares the simulated future runoff using climate time series from the bias-corrected GCM to historical mean annual runoff for the average scenario (T22_m). Runoff is higher in the scenario using observed precipitation because of the greater frequency of high precipitation events (Figure 9-14). Although the bias-corrected GCMs in many cases have higher precipitation totals than the 1950-1999 observed precipitation (Figure 9-13), that higher precipitation is distributed into a greater number of small events than in the observed record.

Comparing just the GCM scenarios to one another, the 2081-2099 time period generates more runoff than the 2046-2065 time period due to greater frequency of high precipitation events. Similarly, the greater frequency of high precipitation events in the most extreme emissions scenario (rcp85) leads to greatest runoff generation during both future time periods analyzed. Relative to the historical time period in the simulations, the 2046-2065 time period has a slight reduction in runoff for the rcp26 and rcp45 scenarios and an increase in runoff for the rcp85 scenarios. The 2081-2099 time period shows an increase in runoff relative to 1950-1999 for all three emissions scenarios.

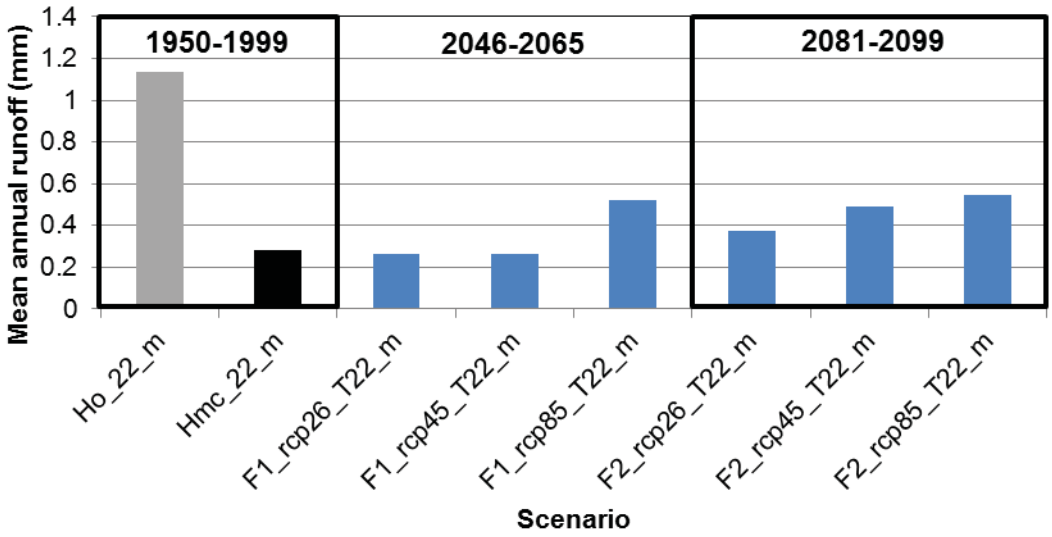

Figure 9-17. Mean annual runoff simulated for the historical (1950-1999) time period using observed precipitation (Ho) and GCM bias-corrected precipitation from the mpi-esp-lr.1 model (Hmc). These historical scenarios are compared to bias-corrected future simulations of precipitation for 2046-2065 (F1) and 2081-2099 (F2) from the mpi-esp-lr.1. All simulations use the T22_m runoff scenario.

To illustrate how the select time periods analyzed relate to the entire historical and future dataset, Figure 9-18 plots annual precipitation and runoff predicted from the T22_m scenarios. Over the historical time period, the MPI bias-corrected model results generally have lower variability in runoff than the observed precipitation records, and because of the lower frequency of high magnitude precipitation, runoff predicted using the historical MPI climate is lower than predicted using observed precipitation (Table 9-4). For 1950-1999, Blythe and YPG stations had 94-96 mm of mean annual precipitation and 1 mm of runoff, whereas the bias-corrected MPI model had 118 mm of mean annual precipitation and only 0.3 mm of runoff. In the MPI bias-corrected model, mean annual precipitation was higher than the observations for all future scenarios.

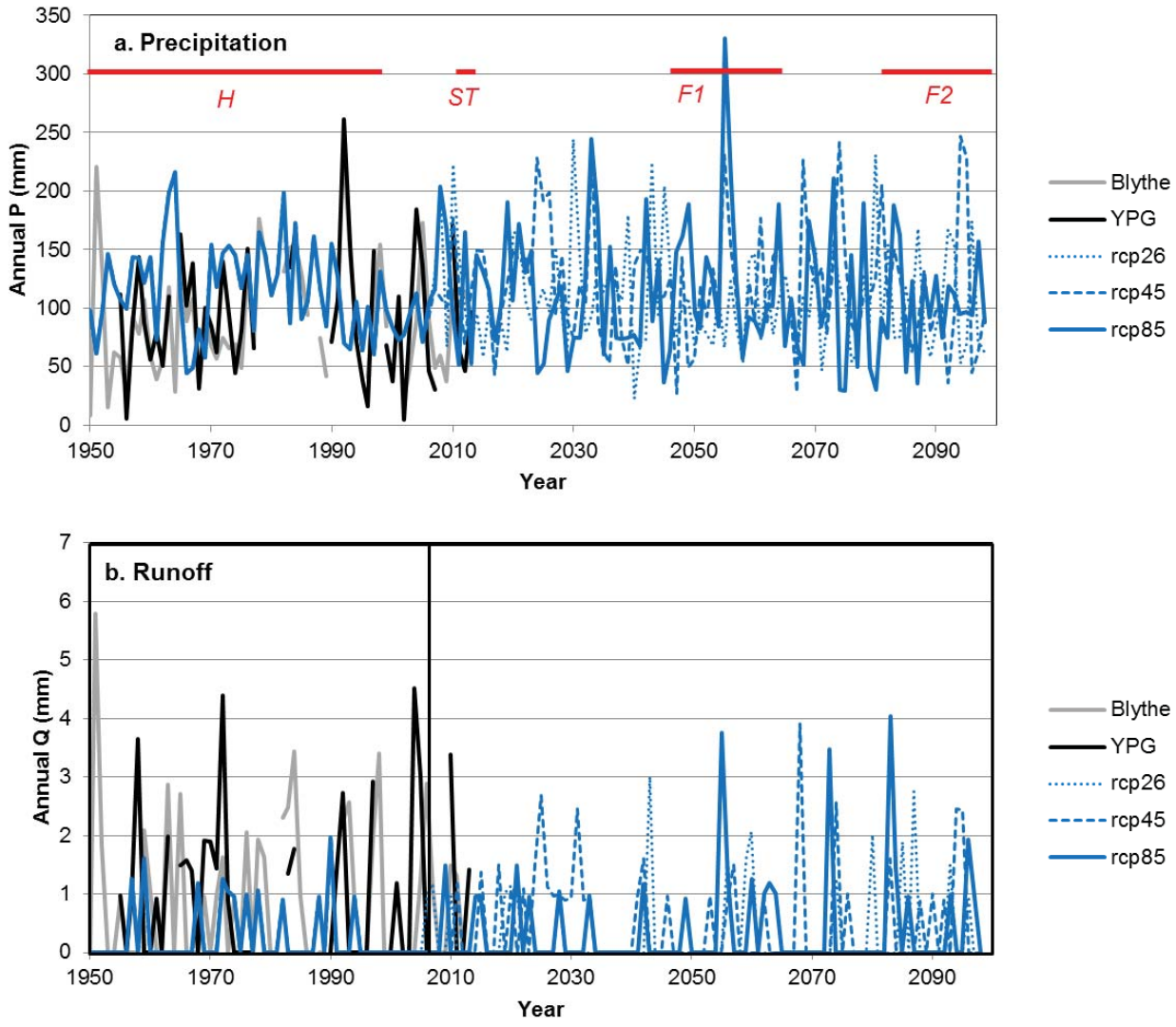

Figure 9-18. Annual precipitation and predicted runoff (Q) in T22_m scenarios. Blythe and YPG lines show observed precipitation and runoff; other lines are from the bias-corrected mpi-esp-lr.1 model. The model runs are the same from 1950-2006, after which they diverge based on three emissions scenarios (rcp26, rcp45, rcp85). The red lines highlight the historical time period (H), study time period (ST), 2046-2065 (F1), and 2081-2099 (F2) time periods analyzed in previous figures.

Table 9-4. Comparison of mean annual P and Q for the 1950-1999 (H) and 2012-2013 (ST) time periods between observed precipitation records and the bias-corrected mpi-esp-lr.1 model. All values in mm, and all Q simulated with the T22_m scenario.

	Blythe		YPG		Model	
	P	Q	P	Q	P	Q
H	93.6	1.1	96.4	1.0	117.5	0.3
ST	99.7	0.0	71.7	0.7	83.9	0.0

For the two complete calendar years in our monitoring study at YPG (2012-2013), annual precipitation was slightly higher than average at Blythe and lower than average at YPG station (Table 9-4). At the monitoring site, YBA, which we used to develop the HYDRUS simulation of subsurface flow in part 1 of this chapter, the annual precipitation in 2012 was 192 mm, substantially higher than the 114 mm recorded at Blythe and 46 mm recorded at YPG (Table 9-5). Our related research identified an orographic increase in precipitation in this region (Kampf et al. manuscript), indicating that the long-term weather stations likely under-report the magnitude of precipitation falling at higher elevations including YBA. During 2012, the YBA site also experienced an extreme precipitation event on July 13, with 86 mm falling in one day. During this storm, the Blythe station only received 19 mm of precipitation, and no precipitation was recorded at the YPG station. This extreme event at YBA elevated both the precipitation and runoff totals at that site relative to those reported for Blythe and YPG in 2012 (Table 9-5). The magnitude of daily precipitation at YBA on 7/13/12 exceeded the maximum daily total precipitation at both Blythe and YPG over the period of record (76-77 mm). In 2013, the YBA site did not experience an extreme rain event, and no runoff was detected. During this year, the annual precipitation total (96 mm) was closer to that of Blythe (86 mm) and YPG (97 mm). The short period of observations at YBA makes it difficult to determine how well the long-term weather stations represent precipitation conditions at that site, but it appears that long-term simulations using the observed record from weather stations may result in less runoff generation than actually occurs at this site.

Table 9-5. Comparison of observed annual precipitation (P) and runoff (Q) at the YBA monitoring site to the observed P and simulated Q for the long-term weather stations. All values in mm, and all Q simulated with the T22_m scenarios.

	YBA		Blythe		YPG	
	P	Q	P	Q	P	Q
2012	192.0	9.8	113.9	0.0	46.3	0.0
2013	96.0	0.0	85.5	0.0	97.0	1.4

Subsurface water content

For the three-year study time period, there were three flow events at the reference site, YBA, in summer 2012. To evaluate the sensitivity of the subsurface water content to runoff, we first changed the baseline simulation to exclude the three runoff events. Excluding these flow events only affected simulated VWC during the second half of the simulation, when water contents stayed slightly drier in the no-flow scenario (Figure 9-19). Although water contents were substantially drier during the individual flow events (Figure 9-19, lower plot), the low water retention of the alluvium kept the drier conditions from having much of an effect on long-term water contents in the top meter of alluvium.

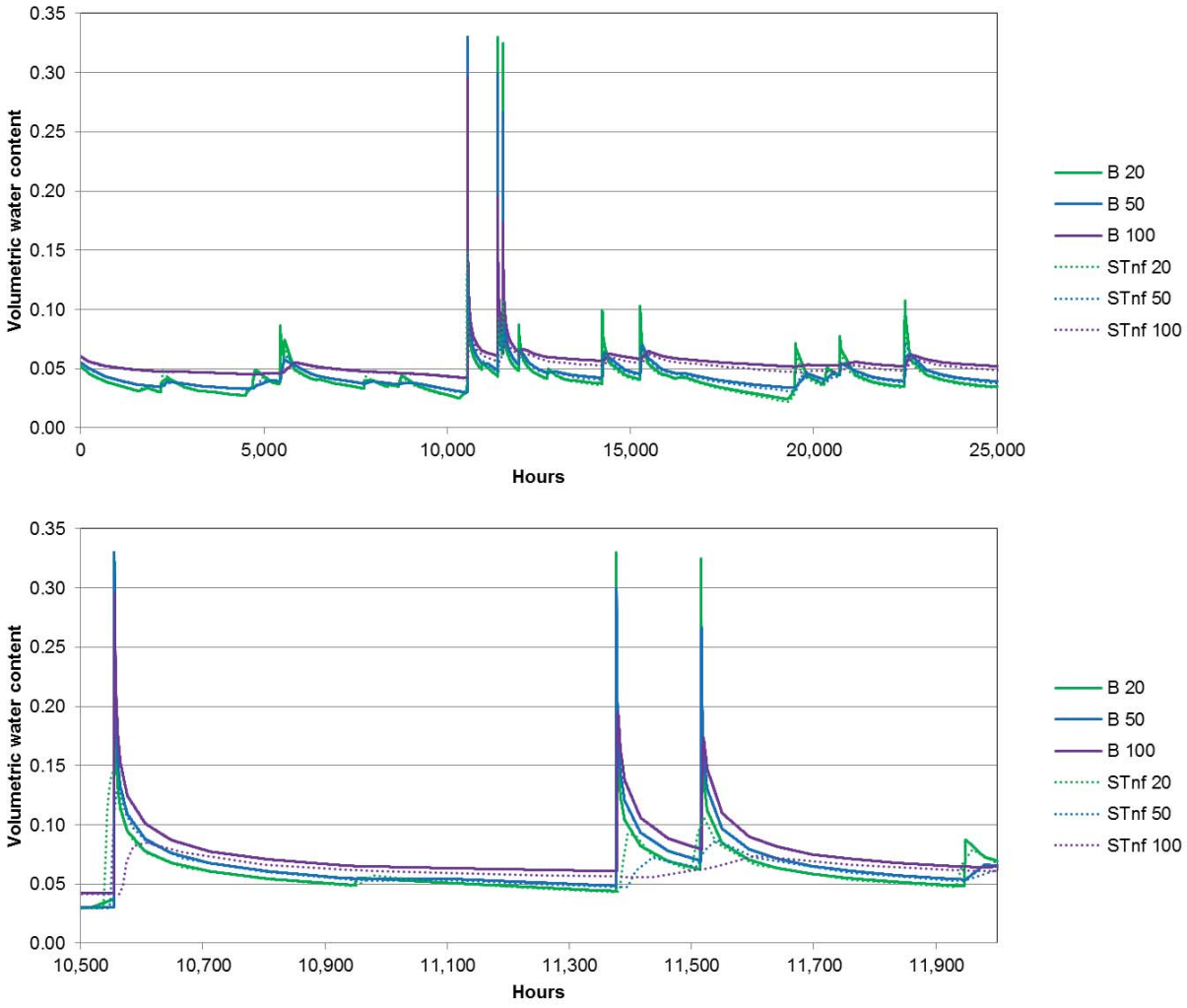

Figure 9-19. Comparison of baseline simulation at YBA to a no-flow scenario (STnf) for the 3-year study time period (top) and the three summer 2012 flow events (bottom) at 20, 50, and 100 cm depth.

In the deeper subsurface (layer 2), the effects of including or excluding the flow events were more evident (Figure 9-20). The sequence of flow events led to an extended period of elevated water content in the deep layer, whereas water contents remained low in the deep layer for the no-flow scenario. Over the study time period, mean depth-integrated VWC was drier than in the baseline scenario by 0.02, mostly due to reduced water contents in the deep layer. These examples show that simulated water contents in the top meter of alluvium are relatively insensitive to runoff magnitudes, whereas water contents in the deeper subsurface typically only increase in response to flow events, making them much more sensitive to the magnitude of runoff.

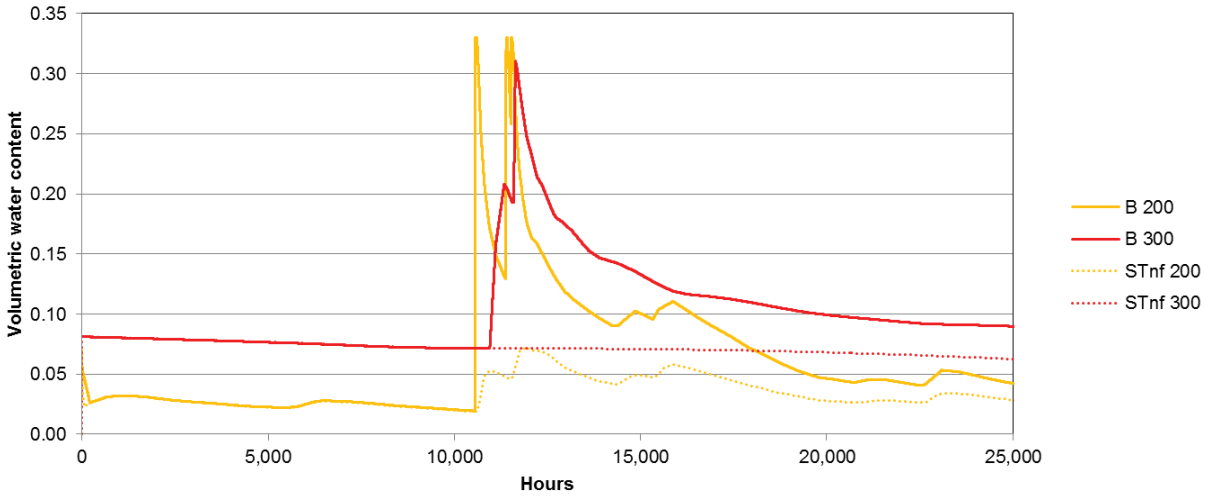

Figure 9-20. Comparison of baseline simulation at YBA to a no-flow scenario (STnf) for the 3-year study time period at 200 and 300 cm depth.

Long-term HYDRUS simulations also show that the effects of higher runoff are most evident at greater depths below the surface. Figure 9-21 compares the mean water contents for the historical time period (1950-1999) in the three HYDRUS simulations different runoff magnitudes: high (T5_h), average (T22_m), and low (T50_l). Mean water content increases with higher runoff at all depths, but this increase is small (<0.01) at depths below 1 m. At the deepest observation point (3 m), the mean VWC was 0.08 higher in the high runoff scenario than in the low runoff scenario. These three scenarios are all forced with the same precipitation sequence (Ho), and where precipitation is held constant, the mean VWC increases linearly with mean annual runoff (Figure 9-21), with the rate of increase becoming greater deeper in the subsurface.

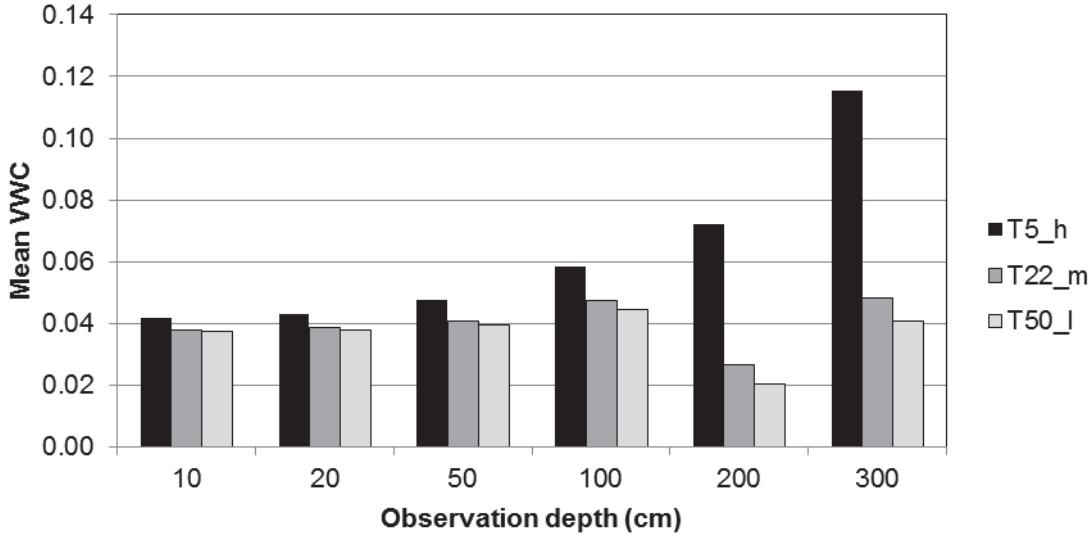

Figure 9-21. Mean volumetric water content (VWC) for the historical time period (1950-1999) in Ho scenarios with three different runoff magnitudes. T5_h is high runoff, with T=5 mm and Q/P=0.15; T22_m is average runoff with T=22 mm and Q/P=0.04; T50_l is low runoff with T=50mm and Q/P=0.005.

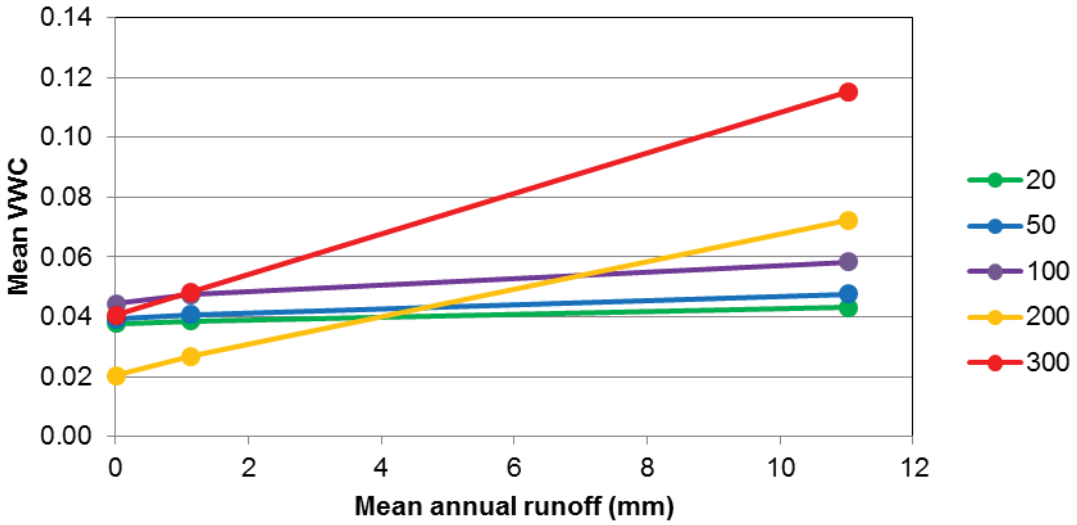

Figure 9-22. Mean annual VWC vs. mean annual runoff for the historical time period (1950-1999) in Ho precipitation scenarios with varying runoff magnitudes (see Figure 9-20 caption for details on runoff scenarios).

In the high runoff scenario shown in Figure 9-21 (T5_h), the domain saturates at 3 m at the end of the historical time period (Figure 9-23). This saturation develops after a sequence of runoff events in winter 1994-1995, and once saturation develops, it persists for the rest of the simulation time period (through 2013). Saturated conditions develop in the simulation starting at the bottom of the domain, with the water table gradually rising to shallower depths if high water input persists. As the domain becomes saturated at the bottom, simulations show a gradual increase in water content at shallower depths, as shown in Figure 2.14 starting around 1975. In the simulation, these saturated conditions spread laterally to the no-flow boundary conditions at the sides of the domain, and when that happens, water is only able to leave the domain through the deep drainage boundary condition at the bottom or through root water uptake. If the domain had been deeper or wider, it would have taken longer for the saturated conditions to develop. Without more information about the subsurface stratigraphy in the study area, we do not know whether the simulation configuration is reasonable for simulating longer-term flow patterns. However, conceptually the wet simulation shows that persistent input in excess of the deep infiltration rate can lead to development of a shallower water table.

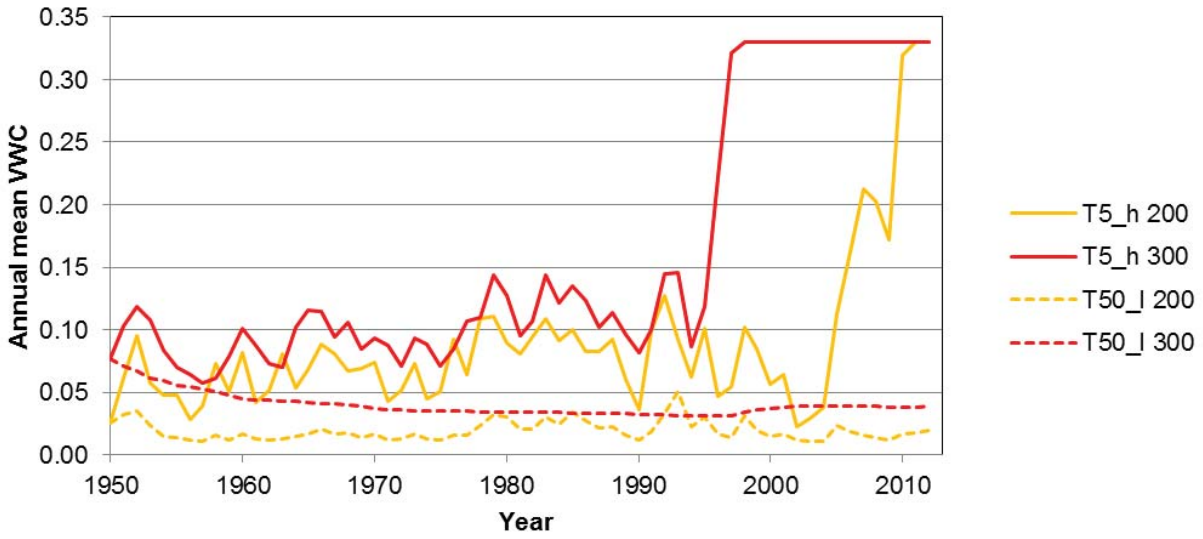

Figure 9-23. Annual mean VWC for HYDRUS simulations forced with precipitation data from the Blythe station and simulated runoff for a high runoff scenario (T5_h) and low runoff scenario (T50_l). Series labels give the depth of observation in cm.

To compare the HYDRUS simulations forced with observed precipitation to those forced with GCM precipitation, we used only the average runoff scenario (T22_m). For the historical time period, we tested the raw MPI model precipitation, which is biased high relative to observed precipitation. This higher precipitation and resulting higher runoff led to the domain fully saturating with water within the first four decades of simulation. Figure 2.15 shows this domain saturation effect at different depths of observation. Saturation began at the bottom of the domain (10 m depth), and it reaches 3 m depth by 1978; 2m depth by 1982, and 1 m depth by 1988. In 1988, the simulation could no longer compute a solution because of the nearly saturated domain. Because of the low water retention of the subsurface materials, each depth relatively rapidly shifts from low water contents to fully saturated conditions. This domain saturation effect indicates that the MPI model precipitation without bias correction is too high to run with this domain configuration, so for all additional HYDRUS simulations using MPI model precipitation, we used the bias-corrected precipitation.

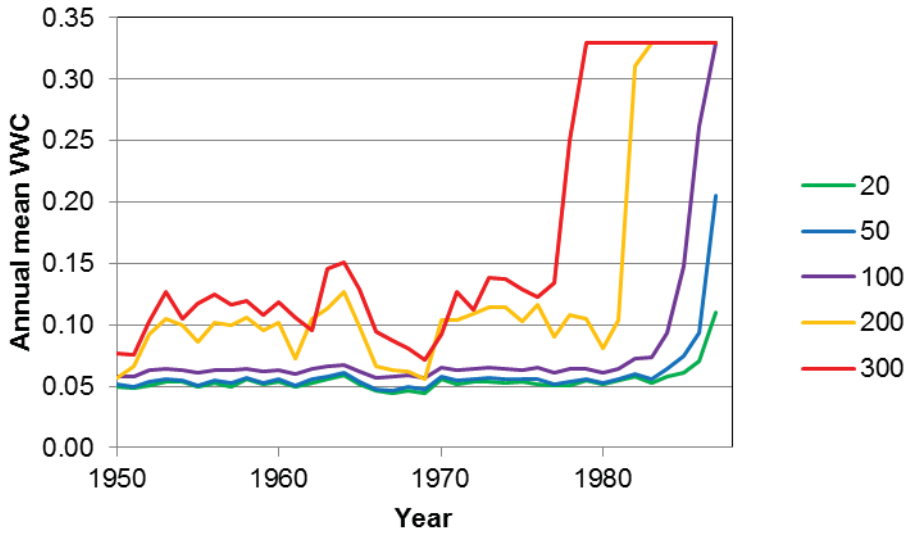

Figure 9-24. Annual mean VWC for a HYDRUS simulation forced with precipitation from the mpi-esp-lr.1 model and runoff from the T22_m scenario. Series labels give the observation depth in cm.

Comparing HYDRUS simulations forced with the bias-corrected MPI model precipitation (Hmc) produces a similar vertical water content distribution as in the simulation forced with observed precipitation (Ho) (Figure 9-25). The Hmc model has higher total precipitation but lower total runoff for the historical time period than the observations. The mean annual precipitation was 118 mm for the Hmc model and 94 mm for the Blythe station. Higher precipitation leads to slightly higher water contents (difference of 0.004-0.006) in the HYDRUS Hmc scenario at all depths except 3 m. At 3 m depth, higher runoff in the Ho scenario leads to slightly higher water contents because water from runoff events are more likely to percolate into the deeper subsurface before being lost to root water uptake. The Ho scenario had 1.1 mm of mean annual runoff compared to 0.3 mm of runoff in the Hmc scenario. This is a small difference in total depth of runoff, so the differences in deep water content between the two scenarios is only 0.001 at 3 m, less than the magnitude of the precipitation-induced differences in water content at shallower depths.

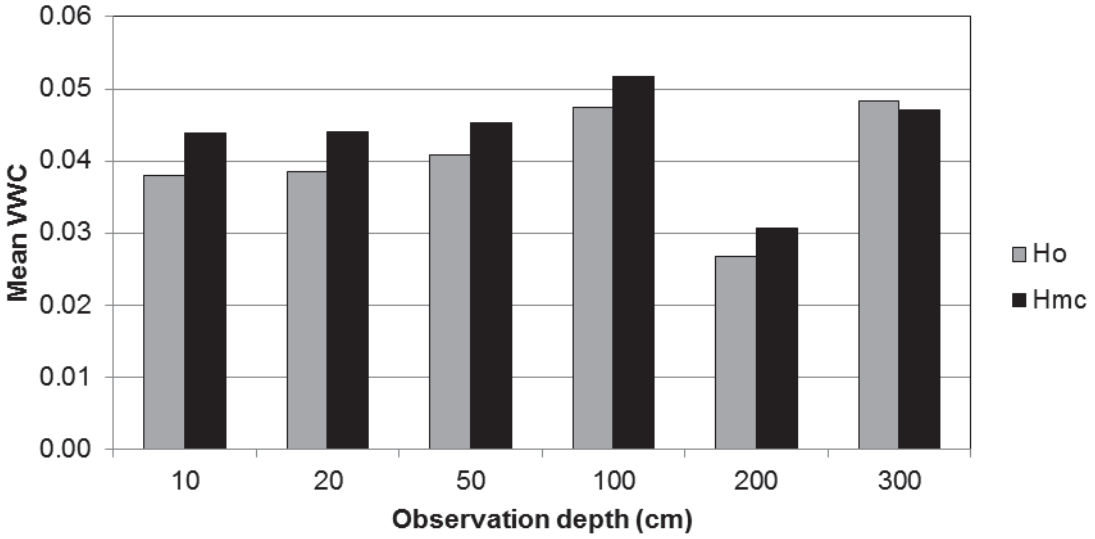

Figure 9-25. Mean volumetric water content (VWC) for the historical time period (1950-1999) in HYDRUS simulations with observed precipitation from the Blythe station (o) and with precipitation from the bias-corrected mpi-esp-lr.1 model (mc). Both simulations shown have average runoff, simulated using T=22 mm and Q/P=0.04.

Relative to the Hmc scenario (historical time period, model precipitation bias-corrected), the future climate scenarios have both lower and higher average water contents (Figure 9-27). At 20 and 100 cm depth, the differences in water content between scenarios are linked to mean annual precipitation, with higher precipitation scenarios generally having higher mean water contents. Differences between scenarios are greatest at 300 cm depth, and for both future time windows, the higher emissions precipitation scenario (rcp85) has higher water content at 300 cm. As shown in the previous examples, this higher water content relates to runoff magnitude. The rcp85 scenarios generally have greater frequencies of high magnitude precipitation events than the rcp26 scenarios (Figure 9-14).

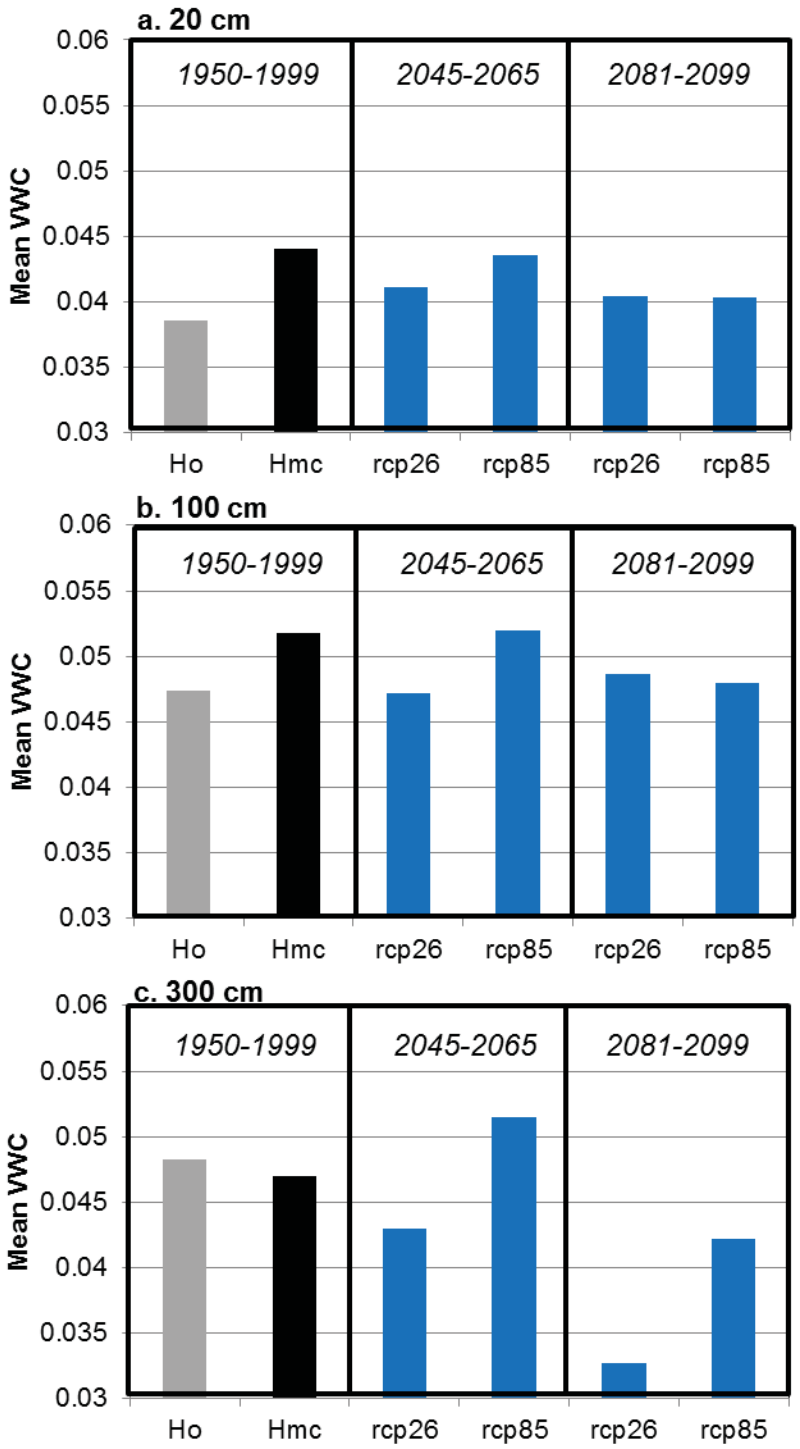

Figure 9-26. Mean VWC for H, F1, and F2 time periods from HYDRUS simulations with observed precipitation from the Blythe station (o) and with precipitation from the bias-corrected mpi-esp-lr.1 model (mc) under two emissions scenarios, low (rcp26) and high (rcp85). All simulations shown have average runoff, simulated using T=22 mm and Q/P=0.04.

Table 9-6. Average annual precipitation (P), runoff (Q), and volumetric water content (VWC) for HYDRUS simulation scenarios. See Figure 2.1 for descriptions of scenario abbreviations. All scenarios simulate runoff with T22_m.

Scenario	P (mm)	Q (mm)	VWC 20 cm	VWC 100 cm	VWC 300 cm
H_o	94	1.1	0.039	0.047	0.048
H_mc	118	0.3	0.044	0.052	0.047
F1_rcp26	98	0.3	0.041	0.047	0.043
F1_rcp85	127	0.5	0.044	0.052	0.051
F2_rcp26	102	0.4	0.041	0.049	0.033
F2_rcp85	106	0.6	0.040	0.048	0.042

Figure 9-17 illustrates how water contents change over time in the historical and future HYDRUS scenarios. In the top meter, water contents vary from year to year, but they do not exhibit systematic wetting or drying trends in any of the scenarios. At 2 m depth, the contact between the upper and lower layers in the simulation, water contents are much more variable, and particularly in the historical simulations, they show persistent multi-year periods of drier or wetter conditions. At 3 m depth in the deep layer, patterns of moisture variability are much lower frequency, and in all cases shown, the 3 m water content gradually dries for the duration of the simulation unless runoff events cause water to percolate to that depth. In the scenario with observed precipitation, there were two threshold-exceeding precipitation events in 1952, leading to runoff elevated water contents at 3 m early in the simulation. The historical model scenario with bias-corrected precipitation did not have a runoff event until 7 years into the simulation. Because of the lower frequency variability at 3 m, the average water contents over H, F1 and F2 time periods capture a combination of the effects of runoff events during those time periods and the longer-term drying pattern at that depth.

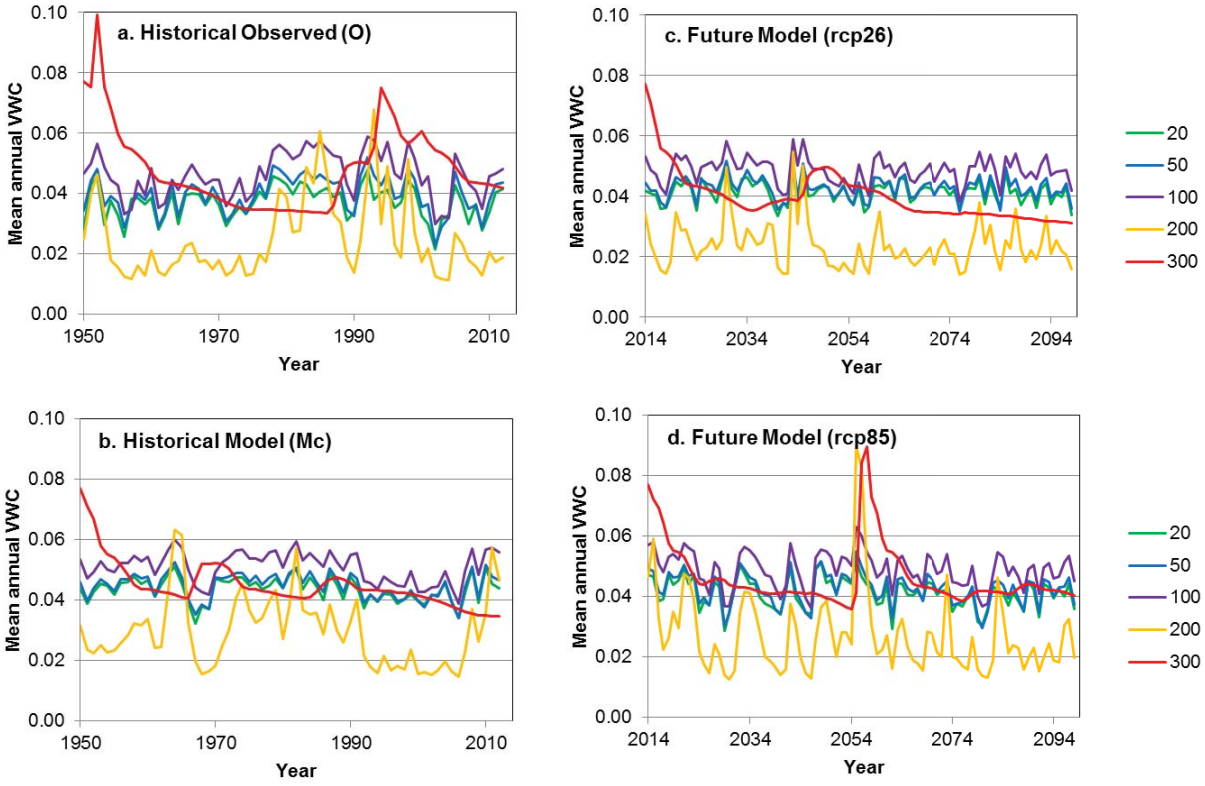

Figure 9-27. Mean annual VWC from HYDRUS simulations over the period of record (1950-2013) and future (2014-2099) forced with observed precipitation from the Blythe station (o) and with precipitation from the bias-corrected mpi-esp-lr.1 model (mc) under two emissions scenarios, low (rcp26) and high (rcp85). All simulations shown have average runoff, simulated using T=22 mm and Q/P=0.04. For future time period model runs,

simulations with model precipitation were reinitialized using the same initial conditions as in the historical simulations.

Discussion

Precipitation and runoff

The historical climate in the study area has been arid since 1950, with annual precipitation always less than 250 mm, except in one extreme year (Figure 9-18). Annual precipitation has been highly variable, with some years experiencing almost no precipitation. In the historical climate record, highest precipitation in the study area is during the late summer monsoon season, with a secondary peak in precipitation during the winter. In our related observation research, we found that most runoff events are in the summer season, with winter rain events occasionally generating runoff in headwater streams. These runoff events are related to thresholds of precipitation, with lowest thresholds in headwater catchments and higher thresholds in larger catchments. For the reference modeling site, YBA, the runoff threshold is 22 mm. In the historical precipitation record, daily total precipitation exceeded 22 mm less than once per year on average. The long-term weather stations (Blythe, YPG) may under-represent precipitation at higher elevations like the YBA site, but results of the historical climate analysis do suggest that threshold-exceeding rain events have been rare in this region throughout the period of record.

GCMs generally do not reproduce the seasonal pattern of precipitation in the study area, with most missing the monsoonal precipitation peak entirely. The GCM we selected for further analysis, the MPI model, does capture a monsoon peak in precipitation, but the monsoon peak is smaller than the winter precipitation peak. In all historical MPI model scenarios analyzed, the precipitation is biased high, more than double the observed precipitation. The bias-corrected precipitation product for this model reproduces the seasonal pattern in precipitation and reduces the high bias in mean annual precipitation to 25 % of mean annual precipitation. However, bias correction of the MPI model produces a frequency distribution of daily precipitation that is different from the historical record, assigning more precipitation to small events and less to large events. This means that historical runoff simulations using the MPI model predict less runoff than those using the observations.

Because the frequency of large, threshold-exceeding rain events is essential for understanding runoff generation in this area, the bias-corrected MPI model is not a good proxy for the historical precipitation characteristics of the region. As a result, we have low confidence that future climate projections will reproduce the seasonality and frequency distribution of future precipitation. Future climate scenarios are also uncertain because of the assumptions made in creating the emissions scenarios that force the future climate simulations. Nevertheless, comparing different precipitation scenarios derived from the MPI model runs does provide some insight into how runoff and subsurface water content respond to different types of precipitation patterns. Higher emissions scenarios for future climate predict a greater frequency of large magnitude rain events, which would mean a greater likelihood of runoff generation in this region. These types of shifts in precipitation patterns toward more extreme events have been predicted for many parts of the world (IPCC 2014), and should this occur in the study region, runoff would be more likely in the future. However, because the region is so arid, circulation patterns that influence whether water is available for precipitation are key controls on precipitation patterns. Without strong prediction of monsoonal precipitation in this region, GCMs may not be adequately capturing the processes that determine precipitation occurrence.

Our approach for estimating future runoff scenarios relies on the runoff thresholds identified in our related observation study. The presence of a strong threshold for runoff generation suggests that runoff comes from infiltration excess overland flow during extreme events. The desert pavement and bedrock surfaces in the study area have low permeability, which leads to overland flow during high rains. If the climate stays persistently arid in the future, we expect that runoff would continue to be threshold-dependent. However, changes in land cover could modify the runoff process and thresholds for runoff generation. For example, we found that the desert pavement surfaces have the lowest runoff thresholds and highest runoff ratios, making them important sources of water to channels further downstream. Disturbance of the desert pavement could lead to greater infiltration and less runoff generation from these surfaces and, as a consequence, less runoff in channels further downstream.

The actual magnitude of runoff predicted for different climate scenarios is fairly uncertain, as a number of assumptions are embedded in our method of predicting runoff. First, we derived runoff ratios using synthetic stage-

discharge rating curves, which are coarse estimates of discharge magnitudes for each site. From these synthetic rating curves, we found a wide range of possible runoff values across the study area, suggesting that runoff ratios are not consistent between rain events. Future research could expand to develop a more physically-based model of runoff generation and explore how the precipitation event characteristics and antecedent wetness may affect runoff during each event.

Subsurface water content

HYDRUS simulations for both historical and future climate scenarios suggest that water contents in the top meter of alluvium are consistent across a wide range of precipitation and runoff conditions. Higher precipitation leads to slightly higher near-surface water contents, but above 1 m depth, the difference in average water contents between scenarios was always less than 0.01. Differences in average water content between scenarios were only greater than 0.01 at depths 1 m or greater.

In contrast, water contents deeper alluvium and underlying materials are much more variable between precipitation and runoff scenarios because water contents in deeper layers respond only to runoff events, not precipitation events alone. Higher runoff increases the likelihood of deep infiltration, so the occurrence of runoff in future climates determines whether or not water percolates past the shallow alluvium and recharges groundwater. Simulations showed that high runoff could lead to development of a water table that gradually rises over time; these conditions only developed in the high runoff or high precipitation scenarios. In the high runoff scenario (Ho_T5_h), mean annual runoff was an order of magnitude higher than in the average runoff scenario. In the high precipitation scenario, (Hm_T22_m), mean annual precipitation was more than double those of the observed climate record. This suggests that large changes in precipitation and runoff are needed for the alluvium in the ephemeral channel to become wet enough for a shallower water table to develop. In reality, development of a perched water table in this area will depend also on the permeability of deep subsurface materials, which is unknown for our study area. Other studies in wetter parts of the Sonoran Desert have reported water tables rising closer to the surface than observed in our study area (e.g. Renard et al. 1964).

The subsurface flow simulations assume no changes in either potential transpiration, surface area fraction covered by vegetation, or root water uptake parameters. Because potential evapotranspiration is high in this dry, sunny region, losses of water to the atmosphere are not energy-limited, and we assume that changes in potential transpiration in a future climate will not be as important to future transpiration patterns as changes in water availability. The HYDRUS simulations do not represent feedback with vegetation as water availability changes such as changes in surface area fraction or root distribution. Future research could expand analyses of how subsurface water contents interact with transpiration using an ecohydrological model that can explore such feedbacks.

Conclusions

Ephemeral streams in the study area are most likely to flow during extreme precipitation events. As a result, climate conditions with higher frequency of extreme events are predicted to have greater runoff. Subsurface flow modeling suggests that water only percolates into the deep subsurface during runoff events, so climates with more extreme precipitation may also be more likely to have deep infiltration and groundwater recharge. Shallow water contents are less sensitive to changing precipitation and runoff conditions and stay consistently dry even as precipitation magnitude and event frequency patterns change.

The GCM evaluated in this study predicts increased frequency of high magnitude precipitation events in the future, which would imply that runoff could be more frequent in future climate conditions. However, future climate projections for this region are uncertain because of uncertainties in both future emissions pathways driving the simulations and in the ability of the GCM to reproduce patterns of localized monsoonal precipitation. Unless future precipitation patterns differ substantially from the historical climate record, this area is likely to continue to have limited and infrequent runoff. Therefore, land management should focus on minimizing disturbance to desert pavement areas with high runoff generation, as these areas are critical for supplying the water that reaches further downstream in the channel network.

Chapter 10. Conclusions and Implications for Future Research and Implementation

The preceding chapters in this report met the objectives by clarifying variation in the form and function of dryland ephemeral streams, and provided insight into the effects of hydrologic alteration by climate change on ephemeral stream systems. While specific physical and biotic attributes of each stream type will vary across regions with differing geology, climatic patterns, biogeography, and land use, the observed patterns in geomorphic, hydrologic, and ecological process domains within the hydrogeomorphic stream classification provides a robust conceptual framework for understanding spatio-temporal dynamics in desert fluvial ecosystems. This framework can be used to inform management and restoration activities, and guide future research.

This hydrogeomorphic stream classification formed the basis for stream classifications used in other SERDP-sponsored desert stream research. Stromberg et al. (RC-1726) used similar stream types in their investigation of riparian ecological dynamics across streamflow gradients ranging from perennial to ephemeral within the Sonoran Desert. Levick et al. (RC-1727) applied our stream typology to dryland regions throughout the southwestern United States. Using a considerably larger sample size across the Mohave, Sonoran, and Chihuahuan deserts, they identified additional stream types that may be considered sub-types within the broader framework we describe in this report. Similarly, additional stream types not described within our classification are likely to be encountered in other dryland settings. For example, floodout zones are un-channelized sheetflow systems that occur where streams terminate into ephemeral playas or eolian sand sheets (Tooth 2000). A few channel reaches of this type occur, such as Growler Wash on the Barry M. Goldwater Range, but this stream type was not present within our study areas.

Differences in channel planform, lateral confinement, and boundary materials reflect distinctive geomorphic process domains within ephemeral watersheds, resulting in consistent patterns of channel morphology and hydraulics (Sutfin et al. 2014, Chapter 1). Steep and highly-confined bedrock streams efficiently route sediment to downstream segments. Progressively decreased transport capacity due to lower channel gradients and confinement in bedrock with alluvium, incised alluvium, and braided streams results in wider channels with greater alluvial storage capacity.

Patterns in subsurface stratigraphy and alluvial characteristics were evident at broader spatial scales (Harry et al. *in prep.*, Chapter 2). Incised alluvium and braided streams that occur within lowland valley settings contain deep (~1 m) active alluvial deposits, underlain by consolidated sedimentary strata. Bedrock with alluvium streams in narrow mountain valleys exhibit thinner active alluvium and complex subsurface stratigraphy bounded by bedrock. Bedrock and piedmont headwater channels lack persistent alluvium, and were not investigated. These subsurface characteristics provide context for understanding variations in hydrologic responses of desert watersheds.

Differences in stream flow responses to precipitation events among stream types correspond to network position and channel boundary materials (Faulconer et al. *in prep.*, Chapter 3). Bedrock and piedmont headwater streams, which drain small watersheds with low infiltration rates, experience runoff most frequently. Despite differences in watershed surface properties, these stream types exhibit similar responses to rainfall depth and intensity. Streamflow occurs less frequently in channels containing unconsolidated alluvial deposits, such as bedrock with alluvium, incised alluvium, and braided streams. Floods in these middle and lower portions of arid watersheds occur almost exclusively during intense summer thunderstorms. Upstream transmission losses and asynchronous tributary inflows decrease streamflow frequency in the downstream direction, and the depth and intensity required to generate runoff increases with drainage area (Goodrich et al. 1997).

Direct precipitation from storm events greater than 10 mm increase water content for relatively short periods of time within the upper 100 cm of alluvial deposits, but deep recharge occurs only after periodic summer floods (Kampf et al. *in prep*., Chapter 4). In all stream types, streamflow and saturation of shallow alluvium typically lasts for only a few hours, but deeper recharge (2-3 m) beneath incised alluvium and braided streams can persist for months after flow events. Where active alluvium is underlain by impermeable sedimentary strata, localized perched groundwater may occur. Subsurface moisture dynamics below channels did not appear to be strongly affected by sediment characteristics, but fine-grained floodplain surfaces likely receive deep recharge only during overbank floods.

Differences in riparian plant community composition closely mirror the distinctive morphological attributes of stream types, highlighting the critical role of geomorphic disturbance in shaping riparian vegetation of arid ephemeral streams (Shaw and Cooper *in prep*., Chapter 5). Vegetation is sparse and highly variable in bedrock streams, where minimal water storage capacity and frequent flood disturbance exceeds the physiological tolerances of many taxa. Bedrock with alluvium and incised alluvium channels support similar community types distinguishable by species densities, and large woody plants are important community members. Drought deciduous shrubs dominate piedmont headwater streams, although trees such as ironwood and foothills paloverde do occur in these stream types. Community composition is similar across braided stream types, where evergreen and photosynthetic-stem trees comprise most of the canopy cover. Compositional differences among stream types correspond primarily to variation in channel gradient and width:depth.

Within the study area, large woody plants rely primarily on water from near-surface (0-50 cm) alluvial sediments (Shaw and Cooper, *in prep*., Chapter 6). Riparian trees access water from different depths, following seasonal shifts in water availability. Recharge from large floods reduces seasonal water stress (Shaw and Cooper, *in prep*, Chapter 7), and trees use water from surficial sediments when it is available. All riparian trees access water from greater depths during drought periods, when plant water stress is greatest. In braided and incised alluvium streams, periodic large floods can improve riparian tree water status for several seasons, while limited storage capacity in the shallow substrate of bedrock with alluvium and piedmont headwater streams results in more regular seasonal dynamics. The highest summer water stress occurs in these smaller channels, despite more frequent streamflow inputs.

Although water availability is a fundamental control on desert plant populations, herbivory by small mammals appears to be the primary limitation to riparian tree establishment within the study area (Shaw and Cooper, *in prep*., Chapter 8). Significant seedling survival requires protection from herbivores and shading by nurse plants, both of which can be provided by shrubs with dense canopies. Infrequent wet years substantially increase seedling survival rates, and likely influence desert tree population dynamics over timescales of decades to centuries. The dominant riparian trees of Sonoran Desert ephemeral streams occupy similar regeneration niches, but differ in seedling growth rates.

Implications for a Changing Climate

Projected increases in temperatures and reduced winter precipitation are expected to result in vegetation changes throughout the southwestern United States (Notaro et al. 2012). Due to limited subsurface water storage capacity and a greater reliance on winter storm inputs (Chapter 5), distal portions of stream networks such as piedmont headwaters, bedrock, and bedrock with alluvium streams are likely to experience the most immediate hydrologic effects of climatic shifts. Amplified seasonal droughts could result in riparian tree dieback in these stream types, where summer water stress is greatest (Chapter 8). The ability to access more stable water sources in deeper alluvium may buffer riparian trees in incised alluvium and braided streams from short-term droughts, but reduced near-surface water availability may cause declines in the abundances of shallow-rooted plants such as herbs, cacti, and subshrubs. Prolonged and severe droughts could result in compositional shifts throughout ephemeral stream networks.

The effects of more frequent and intense extreme storm events on channel morphology and riparian vegetation are expected to differ among stream types. Increased flood disturbance will probably not cause significant changes in bedrock streams, where channel boundaries are resistant to erosion, but alluvial stream segments could experience vertical and lateral adjustment to changing water and sediment fluxes. If sediment transport capacity is significantly increased by these regime shifts, alluvial export through channel scouring and bed degradation could gradually change bedrock with alluvium streams into bedrock channels. Less cohesive channel banks will permit lateral adjustments in braided and incised alluvium channels, with potential responses including channel widening and increased sinuosity (Knighton 1998). Channel widening and bank erosion may have the greatest impact on riparian vegetation in incised alluvium streams, particularly where channel confinement is high and floodplain surfaces are limited to narrow benches. Lateral channel adjustment from periodic large floods is a common feature of braided streams, so we expect lesser changes in this stream type.

Management Considerations

Since our hydrogeomorphic stream classification characterizes spatial patterns in the physical and biotic attributes of stream networks, it can be used to improve the efficacy of many resource management activities. These stream types provide a mechanistic basis for stratification in resource assessments and mapping, and biotic inventories. Since stream types exhibit distinctive characteristics, resource managers can estimate the physical and biotic properties for a stream segment of interest, based on the qualitative features of channel confinement, planform, and boundary materials.

Differences in geomorphology, streamflow regime, and riparian vegetation suggest that sensitivity to disturbance will vary among stream types. These characteristics can provide a foundation for managing the location and types of land use and anthropogenic disturbance, in order to minimize ecological impacts. Resistant channel boundaries in bedrock and bedrock with alluvium streams make these channel types the least sensitive to physical disturbances. Erodible boundaries along incised alluvium, braided, and piedmont headwater streams would exhibit the greatest changes from vehicle maneuvering and other land disturbance. Destruction of vegetation in piedmont headwater streams will likely have long-lasting effects, since limited water availability in these channels impair plant establishment.

Hydrologic alterations from earth moving, roads, and other infrastructure will probably have the largest ecological impacts in piedmont headwater and bedrock with alluvium streams. Seasonal variations in water availability and plant water stress are greatest in these channel types, so stream crossings and other impediments to streamflow will strongly affect vegetation dynamics. The larger incised alluvium and braided streams would probably be less affected by localized topographic changes, since streamflow in these network locations occurs as periodic large floods capable of bypassing stream crossings and small berms. However, the cumulative impacts of numerous smaller flow impediments could have widespread effects, even on these larger channels.

Restoration Considerations

Stream types can be used to determine reference conditions for ephemeral stream restoration. Appropriate channel dimensions and hydraulic geometry in disturbed channels, as well as plant community composition and density of species, can be estimated from unimpacted locations from the same stream type (Chapter 2 and 6). This approach will provide realistic restoration targets, enhancing the likelihood of success.

Understanding the limitations to woody plant establishment will also facilitate revegetation efforts (Chapter 8). Our data indicates that protection from herbivores and shading are critical requirements for tree seedling survival within the western Sonoran Desert. Multiple approaches could be used to provide these conditions, ranging from shaded cages and tree shelters, to phased planting plans beginning with pioneer shrubs before tree seedlings. Plantings should consist of the largest seedlings possible, since they have the highest survival rates under all conditions. Supplemental irrigation is needed to maximize transplant survival under typical climatic conditions, but logistical constraints and additional costs may limit the feasibility of this technique at remote or extensive sites.

Remaining Research Questions

Our results help to sharpen the focus on, and provide a conceptual framework to address, key remaining research questions in ephemeral stream systems of the southwestern United States. Additional stream types that were not present within our study areas likely exist in other dryland regions. Physical and ecological characteristics of the stream types described here will also vary across regions with differing climatic, geologic, and physiographic properties. Application of this conceptual framework to other regions will provide a greater understanding of variation in ephemeral stream systems, and enable direct comparisons across broad geographic scales.

While we identified distinctive patterns in hydrologic behavior throughout ephemeral stream networks, additional data on streamflow and subsurface moisture dynamics are needed to further understand spatial and temporal variation in contemporary ephemeral stream hydrology. In particular, longer streamflow and subsurface monitoring records will clarify spatial patterns in the timing, magnitude, and duration of streamflow events, and how they impact groundwater and vadose zone dynamics. Longer periods of record across larger spatial scales will also facilitate modeling endeavors to predict the impacts of climate change.

The effects of invasive species and disturbance associated with military training and testing also requires further study. Invasive plants were absent or present at negligible levels within our study area, but are more abundant in less arid drylands, where they create significant management challenges. Potential effects of human disturbance from infrastructure development and military training activities on ephemeral stream form and function may be inferred from our results, but focused and detailed studies are needed to more fully understand the ecological impacts, as well as implications for management and restoration. For example, the concepts developed here and reconnaissance performed at YPG and BMGR, resulted in the funding of a two-year study of the impacts of road crossings on ephemeral streams at DoD installations across the southwestern United States (DoD Legacy cooperative agreement HQ0034-15-2-0005). This work will identify the prevalence, extent, and causal mechanisms of hydrogeomorphic and ecological alterations associated with stream crossings across a range of climate, geology, and land uses. Such information will be used to develop guidelines to avoid future degradation and target restoration activities in degraded areas.

Potential for Implementation by DoD and Others

The hydrogeomorphic stream classification and other findings described in this work can be readily applied by DoD personnel and others to infer basic physical and ecological properties of ephemeral stream systems, guide management decisions, and inform appropriate restoration activities. Easily observed qualitative physical descriptors can be used to determine the relevant stream types other areas, thereby providing a rapid assessment of ecological potential and probable sensitivity to various stressors and disturbance. The restoration considerations developed from our analysis of limitations on woody plant establishment can be implemented to increase the efficacy of revegetation projects in drylands throughout the southwestern United States.

Literature Cited

Abdel Khalik, K., M. El-Sheikh, and A. El-Aidarous. 2013. Floristic diversity and vegetation analysis of Wadi Al-Noman, Mecca, Saudi Arabia. Turkish Journal of Botany 37:894–907.

Abella, S. R. 2008. A systematic review of wild burro grazing effects on Mojave Desert vegetation, USA. Environmental Management 41:809–19.

Al Wadie, H. 2002. Floristic composition and vegetation of Wadi Talha, Aseer Mountains, southwest Saudi Arabia. OnLine Journal of Biological Sciences 2:285–288.

Al-Rowaily, S.L., El-Bana, M.I., Al-Dujain, F.A.R., 2012. Changes in vegetation composition and diversity in relation to morphometry, soil and grazing on a hyper-arid watershed in the central Saudi Arabia. Catena 97, 41-49.

Alatar, A., M. a El-Sheikh, and J. Thomas. 2012. Vegetation analysis of Wadi Al-Jufair, a hyper-arid region in Najd, Saudi Arabia. Saudi Journal of Biological Sciences 19:357–368.

Ali, M. M., G. Dickinson, and K. J. Murphy. 2000. Predictors of plant diversity in a hyperarid desert wadi ecosystem. Journal of Arid Environments 45:215–230.

Allan, J.D., 1995. Stream Ecology: Structure and Function of Running Waters. Chapman and Hall, New York.

Anders, M. D., et al. (2005), Pleistocene geomorphology and geochronology of eastern Grand Canyon: linkages of landscape components during climate changes, *Quaternary Science Reviews*, *24*, 2428-2448.

Anderson, J. E., and M. L. Shumar. 1986. Impacts of black-tailed jackrabbits at peak population densities on sagebrush-steppe vegetation. Journal of Range Management 39:152–156.

Anderson, M.J., 2001. A new method for non-parametric multivariate analysis of variance. Austral Ecology 26, 32-46.

Anderson, M.J., 2005. PERMANOVA: a FORTRAN computer program for permutational multivariate analysis of variance. Department of Statistics, University of Auckland, New Zealand.

Anderson, M. J. 2006. Distance-based tests for homogeneity of multivariate dispersions. Biometrics 62:245–53.

Angiolini, C., A. Nucci, F. Frignani, and M. Landi. 2011. Using multivariate analyses to assess effects of fluvial type on plant species distribution in a Mediterranean river. Wetlands 31:167–177.

Arcement Jr., G.J., Schneider, V.R., 1989. Guide for selecting Manning's roughness coefficients for natural channels and flood plains. United States Geological Survey Water-supply Paper 2339.

Archie, G. E. (1942), The electrical resistivity log as an aid in determining some reservoir characteristics, *Petroleum Technology*, *5*, 54-62.

Arizona Geological Survey (AGS), 2000. Digital Geologic Map (DGM-17) (1:1,000,000-map scale). http://www.azgs.az.gov/services_azgeomap.shtml

Arizona Land Resource Information System (ALRIS), 2012. Ten-meter digital elevation model of Maricopa, Pinal, and Pima counties. Data acquired through written request and mail services.

Babcock, H.M., Cushing, E.M., 1941. Recharge to ground water from floods in a typical desert wash, Pinal County. Arizona. American Geophysical Union Transactions 23, 49-56.

Bacon, S.N., McDonald, E.V., Baker, S.E., Caldwell, T.G., Stullenbarger, G., 2008. Desert terrain characterization of landforms and surface materials within vehicle test courses at U.S. Army Yuma Proving Ground, U.S.A. Journal of Terramechanics 45, 167-183.

Baker, W. L. 1989. Macro- and micro-scale influences on riparian vegetation in western Colorado. Annals of the Association of American Geographers 79:65–78.

Balding, F. R., and G. L. Cunningham. 1974. The influence of soil water potential on the perennial vegetation of a desert arroyo. The Southwestern Naturalist 19:241–248.

Baldwin, B. G., S. Boyd, B. J. Ertter, R. W. Patterson, T. J. Rosatti, D. H. Wilken, and M. Wetherwax. 2002. The Jepson Desert Manual: Vascular Plants of Southeastern California. University of California Press, Berkeley, California.

Baxter, R., and L. Hansson. 2001. Bark consumption by small rodents in the northern and southern hemispheres. Mammal Review 31:47–59.

Beechie, T.J., Sear, D.A., Olden, J.D., Pess, G.R., Buffington, J.M., Moir, H., Roni, P., Pollock, M.M., 2010. Process-based principles for restoring river ecosystems. Bioscience 60(3), 209-222.

Belnap, J., J. R. Welter, N. B. Grimm, N. Barger, and J. A. Ludwig. 2005. Linkages between microbial and hydrologic processes in arid and semiarid watersheds. Ecology 86:298–307.

Benda, L., Hassan, M.A., Church, M., May, C.L. 2005. Geomorphology of steepland headwaters: The transition from hillslopes to channels. Journal of the American Water Resources Association 41(4), 835-851.

Benda, L., N. L. Poff, D. Miller, T. Dunne, G. Reeves, G. Pess, and M. Pollock. 2004. The Network Dynamics Hypothesis: how channel networks structure riverine habitats. BioScience 54:413–427.
Bendix, J. 1994. Among-site variation in riparian vegetation of the southern California Transverse Ranges. American Midland Naturalist 132:136–151.
Bendix, J. 1997. Flood disturbance and the distribution of riparian species diversity. Geographical Review 87:468–483.
Bendix, J., and C. R. Hupp. 2000. Hydrological and geomorphological impacts on riparian plant communities. Hydrological Processes 14:2977–2990.
Benhouhou, S. S., N. Boucheneb, Q. Kerzabi, and O. Sassi. 2003. Plant communities of several wadi types in the Tassili N'Ajjer, central Sahara, Algeria. Phytocoenologia 33:49–69.
Bertness, M. D., and R. M. Callaway. 1994. Positive interactions in communities. Trends in Ecology & Evolution 9:191–193.
Bevens, K., 2002. Runoff generation in semi-arid areas. In: Bull, L.J., Kirkby, M.J. (Eds), Dryland Rivers: Hydrology and Geomorphology of Semi-Arid Channels. John Wiley and Sons, Chichester, pp. 57-105.
Birkeland, G.H., 1996. Riparian vegetation and sandbar morphology along the lower Little Colorado River, Arizona. Physical Geography 17, 534-553.
Blasch KW, Ferré TPA, Hoffmann JP, Fleming JB, 2006. Relative contributions of transient and steady state infiltration during ephemeral streamflow. Water Resources Research 42, W08405, doi:10.1029/2005WR004049.
Bonnin, G.M., Marin, D., Lin, B., Parzybok, T., Yekta, M., Riley, D., 2011. NOAA Atlas 14 Precipitation-Frequency Atlas of the United States, Volume 1 Version 5.0: Semiarid Southwest (Arizona, Southeast California, Nevada, New Mexico, Utah). U.S. Department of Commerce, National Oceanic and Atmospheric Administration, National Weather Service.
Bowers, J. E., and R. M. Turner. 2001. Dieback and episodic mortality of Cercidium microphyllum (foothill paloverde), a dominant Sonoran Desert tree. Journal of the Torrey Botanical Society 128:128–140.
Bowers, J. E., and R. M. Turner. 2002. The influence of climatic variability on local population dynamics of Cercidium microphyllum (foothill paloverde). Oecologia 130:105–113.
Bowers, J. E., R. M. Turner, and T. L. Burgess. 2004. Temporal and spatial patterns in emergence and early survival of perennial plants in the Sonoran Desert. Plant Ecology 172:107–119.
Breiman, L., Friedman, J.H., Olshen, R.A., Stone, C.J., 1984. Classification and regression trees. Chapman & Hall, New York.
Brekke L, Thrasher BL, Maurer EP, Pruitt T, 2013. Downscaled CMIP3 and CMIP5 climate projections. Release of downscaled CMIP5 climate projections, comparison with preceding information, and summary of user needs. http://gdo-dcp.ucllnl.org/downscaled_cmip_projections/techmemo/downscaled_climate.pdf
Brierley, G.J., Fryirs, K.A., 2005. Geomorphology and river management: applications of the River Styles framework. Blackwell Publishing, Oxford, UK.
Brooks, J.R., Barnard, H.R., Coulombe, R., McDonnell, J.J., 2009. Ecohydrologic separation of water between trees and streams in a Mediterranean climate. Nature Geosciences 3, 100-104
Brown, D.E., Unmack, P.J., Brennan, T.C., 2007. Digitized map of biotic communities for plotting and comparing distributions of North American animals. The Southwestern Naturalist 52, 610-616.
Brown, J. H. 1975. Geographical ecology of desert rodents. Pages 315–341 *in* M. L. Cody and J. M. Diamond, editors. Ecology and Evolution of Communities. Harvard University Press, Cambridge, Massachusetts.
Brown, J. H., and J. C. Munger. 1985. Experimental manipulation of a desert rodent community: Food addition and species removal. Ecology 66:1545–1563.
Bull, L.J., Kirkby, M.J., 2002. Dryland river characteristics and concepts. In: Bull, L.J., Kirkby, M.J. (Eds), Dryland Rivers: Hydrology and Geomorphology of Semi-Arid Channels. John Wiley and Sons, Chichester, pp. 3-15.
Bull, W. B. (1991), *Geomorphic Responses to Climate Change*, 326 pp., Oxford University Press, New York.
Bull, W. B., and A. P. Schick (1979), Impact of climatic change on an arid watershed: Nahal Yael, southern Israel, *Quaternary Research*, *11*, 153-171.
Bull, W.B., 1977. The alluvial fan environment. Progress in Physical Geography 1, 222-270.
Bull, W.B., 1979. Threshold of critical power in streams. Geological Society of America Bulletin, Part I 90, 453-464.
Bull, W.B., 1997. Discontinuous ephemeral streams. Geomorphology 19, 227-276
Burgess, S. S. O., and T. M. Bleby. 2006. Redistribution of soil water by lateral roots mediated by stem tissues. Journal of Experimental Botany 57:3283–3291.

Burgess, S. S. O., M. A. Adams, N. C. Turner, C. R. Beverly, C. K. Ong, A. A. H. Khan, and T. M. Bleby. 2001. An improved heat pulse method to measure low and reverse rates of sap flow in woody plants. Tree physiology 21:589–98.

Burquez, A., and M. A. Quintana. 1994. Islands of diversity: ironwood ecology and the richness of perennials in a Sonoran Desert biological reserve. Pages 9–28 *in* G. P. Nabhan and J. L. Carr, editors. Ironwood: An Ecological and Cultural Keystone of the Sonoran Desert. Conservation International Occasional Paper 1, Washington, DC.

Busch, D. E., and S. D. Smith. 1995. Mechanisms associated with decline of woody species in riparian ecosystems of the southwestern U.S. Ecological Monographs 65:347–370.

Butterfield, B. J., and J. M. Briggs. 2011. Regeneration niche differentiates functional strategies of desert woody plant species. Oecologia 165:477–87.

Butterfield, B. J., J. L. Betancourt, R. M. Turner, and J. M. Briggs. 2010. Facilitation drives 65 years of vegetation change in the Sonoran Desert. Ecology 91:1132–9.

Callaway, R. M. 1992. Effect of shrubs on recruitment of Quercus douglasii and Quercus lobata in California. Ecology 73:2118–2128.

Callaway, R. M. 1995. Positive interactions among plants. Botanical Review 61:306–349.

Campbell, C. J., and W. Green. 1968. Perpetual succession of stream-channel vegetation in a semiarid region. Journal of the Arizona Academy of Science 5:86–98.

Camporeale, C., Perucca, E., Ridolfe, L., gurnell, A.M., 2013. Modeling the interactions between river morphodynamics and riparian vegetation. Reviews of Geophysics 51, 379-414.

Canadell, J., R. B. Jackson, J. R. Ehleringer, H. A. Mooney, O. E. Sala, and E. D. Schulze. 1996. Maximum rooting depth of vegetation types at the global scale. Oecologia 108:583–595.

Chabot, B. F., and D. J. Hicks. 1982. The ecology of leaf life spans. Annual Review of Ecology and Systematics 13:229–59.

Chiang, F., and L. R. Landrum. 2009. Vascular plants of Arizona: Solanaceae, part three: Lycium. CANOTIA 5(1):17-26.

Chimner, R. A., and D. J. Cooper. 2004. Using stable oxygen isotopes to quantify the water source used for transpiration by native shrubs in the San Luis Valley, Colorado U.S.A. Plant and Soil 260:225–236.

Christie, K., M. Currie, L. S. Davis, M. Hill, S. Neal, and T. Ayers. 2006. Vascular plants of Arizona: Rhamnaceae. CANOTIA 2(1):23-46.

Christy, C. M., D. Damrel, A. M. Henry, A. E. T. Nare, R. Puente-Martinez, and G. M. Walters. 2003. Lamiaceae mint family: part 1. Agastache Gronov., Hyptis Jacq., Lamium L., Leonurus L., Marrubium L., Monarda L., Monardella Benth., Nepeta L., Salazaria Torr., Stachys L., Teucrium L., and Trichostema L. Journal of the Arizona-Nevada Academy of Science 35(2):151-169.

Clapp, E. M., et al. (2000), Sediment yield exceeds sediment production in arid region drainage basins, *Geology*, *28*, 995-998.

Clarke, K. R. 1993. Non-parametric multivariate analyses of changes in community structure. Australian Journal of Ecology 18:117–143.

Clarke, K. R., and M. Ainsworth. 1993. A method of linking multivariate community structure to environmental variables. Marine Ecology Progress Series 92:205–219.

Cloudsley-Thompson, J. L. 1996. Biotic Interactions in Arid Lands. Springer-Verlag, Berlin, Germany.

Coffin, A.W. 2007. From roadkill to road ecology: A review of the ecological effects of roads. Journal of Transport Geography 15: 396-406.

Comporeale, C., Perona, P., Ridolfi, L., 2006. Hydrological and Geomorphological significance of riparian vegetation in drylands. In: D'Odorico, P., Porporato, A. (Eds), Dryland Ecohydrology, pp. 161-179.

Constantz, J., Thoma, C.L., Zellweger, G., 1994. Influence of diurnal variations in stream temperature on streamflow loss and groundwater recharge. Water Resources Research 30(12), 3253-3264.

Cooke, R.U., Warren, A., 1973. Geomorphology in deserts. University of California Press. Berkeley and Los Angeles.

Coplen, T. B. 1988. Normalization of oxygen and hydrogen isotope data. Chemical Geology 72:293–297.

Cornelissen, J. H. C., P. Castro-Diez, and R. Hunt. 1996. Seedling growth, allocation and leaf attributes in a wide range of woody plant species and types. Journal of Ecology 84:755–765.

Cornish, J.H., 1961. Flow Losses in Dry Sandy Channels. Journal of Geophysical Research 66, 1845-1853.

Costelloe JF, Grayson RB, Argent RM, McMahon TA, 2003. Modelling the flow regime of an arid zone floodplain river, Diamantina River, Australia. Environmental Modelling & Software 18, 693-703.

Costelloe, J. F., E. Payne, I. E. Woodrow, E. C. Irvine, A. W. Western, and F. W. Leaney. 2008. Water sources accessed by arid zone riparian trees in highly saline environments, Australia. Oecologia 156:43–52.
Crawley, M. J. 1983. Herbivory: The Dynamics of Animal-Plant Interactions. University of California Press, Berkeley, California.
Davis, S. D., and H. A. Mooney. 1986. Water use patterns of four co-occurring chaparral shrubs. Oecologia 70:172–177.
Dawson, T. E., S. Mambelli, A. H. Plamboeck, P. H. Templer, and K. P. Tu. 2002. Stable isotopes in plant ecology. Annual Review of Ecology and Systematics 33:507–559.
De'ath, G., Fabricius, K.E., 2000. Classification and regression trees: A powerful yet simple technique for ecological data analysis. Ecology 81(11), 3178-3192.
Diaz, S., and M. Cabido. 2001. Vive la différence: plant functional diversity matters to ecosystem processes. Trends in Ecology & Evolution 16:646–655.
Dominguez F, Canon J, Valdes J, 2010. IPCC-AR4 climate simulations for the Southwestern US: the importance of future ENSO projections. Climatic Change 99, 299-514.
Duniway, M.C., and J.E. Herrick. 2011. Disentangling road network impacts: The need for a holistic approach. Journal of Soil and Water Conservation 66(2): 31-36.
Dunkerley, D., 2008. Identifying individual rain from pluviograph records: a review with analysis of data
Dunkerley, D., Brown, K., 1999. Flow behaviour, suspended sediment transport and transmission losses in a small (sub-bank-full) flow event in an Australian desert stream. Hydrological Processes 13: 1577–1588.
Dunne, T., Leopold, L.B., 1978. Water in Environmental Planning. W.H. Freeman and Company, New Yok.
Dust, D.W., Wohl, E.E., 2010. Quantitative technique for assessing the geomorphic thresholds for floodplain instability and braiding in the semi-arid environment. Natural Hazards 55, 145-160.
Eastoe CJ, Gu A, Long A, 2004. The origins, ages and flow paths of groundwater in Tucson Basin: Results of a study of multiple isotope systems. Groundwater Recharge in a Desert Environment: The Southwestern United States, edited by JF Hogan, FM Phillips, BR Scanlon. Water Science and Application 9. Washington DC, American Geophysical Union.
Eberly, L. D., and T. B. Stanley. 1978. Cenozoic stratigraphy and geologic history of southwestern Arizona. Geological Society of America Bulletin 89:921–940.
Ehleringer, J. R., and C. B. Osmond. 1989. Stable isotopes. Pages 281–300 *in* R. W. Pearcy, J. Ehleringer, H. A. Mooney, and P. W. Rundel, editors. Plant Physiological Ecology: Field Methods and Instrumentation. Chapman & Hall.
El Ghazali, G. E. B., A. R. A. Al-Soqeer, and G. E. A. El Tayeb. 2013. Floristic and ecological studies on the plant cover of Wadi Al Rummah, Qassim Region, Saudi Arabia. International Research Journal of Plant Science 4:310–318.
Ellsworth, P. Z., and D. G. Williams. 2007. Hydrogen isotope fractionation during water uptake by woody xerophytes. Plant and Soil 291:93–107.
Faulconer et al.manuscript (currently Faulconer thesis). Thresholds for runoff generation in ephemeral streams with varying morphology in the Sonoran Desert in Arizona, USA.
Felker, P., and P. R. Clark. 1981. Nodulation and nitrogen fixation (acetylene reduction) in desert ironwood (Olneya tesota). Oecologia 48:292–293.
Fisher, S. G., J. B. Heffernan, R. a. Sponseller, and J. R. Welter. 2007. Functional ecomorphology: Feedbacks between form and function in fluvial landscape ecosystems. Geomorphology 89:84–96.
Flora of North America Editorial Committee. 1993+. Flora of North America North of Mexico. 16+ vols. New York and Oxford.
Flores, J., O. Briones, A. Flores, and S. Sánchez-Colón. 2004. Effect of predation and solar exposure on the emergence and survival of desert seedlings of contrasting life-forms. Journal of Arid Environments 58:1–18.
Forman, R.T.T., and L.E. Alexander. 1998. Roads and their major ecological effects. Annual Review of Ecology and Systematics 29: 207-231.
Friedman, J.M., Lee, V.J., 2002. Extreme floods, channel change, and riparian forest along ephemeral streams. Ecological Monographs 72, 409-425.
From an Australian dryland site. Hydrological Processes; 22:5024-5036.
Frostick, L. E., and I. Reid (1977), The origin of horizontal laminae in ephemeral stream channel-fill, *Sedimentology*, *24*, 1-9.
Fryirs, K., Brierley, G.J., 2010. Antecedent controls on river character and behavior in partly confined valley settings: Upper Hunter catchment, NSW, Australia. Geomorphology 117, 106-120.

Fryxell, P.A. 1993. Malvaceae mallow family: part 1. All genera except Sphaeralcea St.-Hil. Journal of the Arizona-Nevada Academy of Science 27(2):222-236.
Fu, P., and P. M. Rich. 1999. Design and implementation of the Solar Analyst: an ArcView extension for modeling solar radiation at landscape scales. Proceedings of the 19th Annual ESRI User Conference. San Diego, California.
Gazal, R. M., R. L. Scott, D. C. Goodrich, and D. G. Williams. 2006. Controls on transpiration in a semiarid riparian cottonwood forest. Agricultural and Forest Meteorology 137:56–67.
Gibson, A. C. 1996. Structure-function relations of warm desert plants. Page 216. Springer-Verlag, Berlin, Germany.
Giorgetta MA, Jungclaus J, Reick CH, Legutke S, Bader J, Böttinger M, Brovkin V, Crueger T, Esch M, Fieg K, Glushak K, Gayler V, Haak H, Hollweg H, Ilyina T, Kinne S, Kornblueh L, Matei D, Mauritsen T, Mikolajewicz U, Mueller W, Notz D, Pithan F, Raddatz T, Rast S, Redler R, Roeckner E, Schmidt H, Schnur R, Segschneider J, Six KD, Stockhause M, Timmreck C, Wegner J, Widmann H, Wieners K, Claussen M, Marotzke J, Stevens B, 2013. Climate and carbon cycle changes from 1850 to 2100 in MPI-ESM simulations for the Coupled Model Intercomparison Project phase 5.Journal of Advances in Modeling Earth Systems 5(3), 572-597.
Giorgetta MA, Roeckner E, Mauritsen T, Stevens B, Crueger T, Esch M, Rast S, Kornblueh S, Schmidt H, Kinne S, Möbis B, Krismer T, Reick C, Raddatz T, Gayler V, 2012. The atmospheric general circulation model ECHAM6 - Model description. Max-Planck-Institut fur Meteorologie. ISSN 1614-1199.
Gómez-Aparicio, L., R. Zamora, J. Castro, and J. A. Hódar. 2008. Facilitation of tree saplings by nurse plants: microhabitat amelioration or protection against herbivores? Journal of Vegetation Science 19:161–172.
Gonfiantini, R. 1978. Standards for stable isotope measurements in natural compounds. Nature 271:534–536.
Goodrich, D. C., L. J. Lane, R. M. Shillito, S. N. Miller, and A. Woolhiser. 1997. Linearity of basin response as a function of scale watershed located in southeastern drainage areas range channels a critical transition threshold area occurring roughly around the range causes of increasingly nonlinear response are the 33:2951–2965.
Goodrich, D.C., Lane, L.J., Shillito, R.M., Miller, S.N., Syed K.H., Woolhiser, D.A., 1997. Linearity of basin response as a function of scale in a semiarid watershed. Water Resources Research 33(12), 2951-2965.
Graf, W.L., 1981. Channel instability in a braided, sand bed river. Water Resources Research 17(4), 1087-1094.
Graf, W. L. (1987), Late Holocene sediment storage in canyons of the Colorado Plateau, *Geol. Soc. Am. Bull.*, *99*, 261-271.
Graf, W.L., 1988a. Fluvial Processes in Dryland Rivers. Springer-Verlag, Berlin.
Graf, W.L., 1988b. Definition of flood plains along arid-region rivers. In: Baker, V.R., Kochel, R.C., Patton, P.C. (Eds), Flood Geomorphology. Wiley, New York, pp. 231-242.
Grandmaison, D.D. 2012. Landscape-level habitat associations and phylogenetics of desert tortoises on southwestern Arizona military ranges managed by the Army, Air Force, and Marines. Department of Defense, Legacy Resource Management Program, Project 09-385.
Gregory, S. V, F. J. Swanson, W. A. Mckee, and K. W. Cummins. 1991. An ecosystem perspective of riparian zones. Bioscience 41:540–551.
Grenfell, S.E., 2012. Morphodynamics of a gully and floodout system in the Sneeuberg Mountains of the semi-arid Karoo, South Africa: implications for local landscape connectivity. Catena 89, 8-21.
Gucinski, H., M.J. Furniss, R.R. Ziemer, and M.H. Brooks. 2001. Forest roads: A synthesis of scientific information. USDA Forest Service, Pacific Northwest Research Station. General Technical Report PNW-GTR-509.
Hallack-Alegria, M., and Watkins, D.W. Jr., 2007. Annual and Warm Season Drought Intensity-Duration-Frequency Analysis for Sonora, Mexico. Journal of Climate. American Meteorological Society; 27:1897-1909
Halvorson, W. L., and D. T. Patten. 1974. Seasonal water potential changes in Sonoran Desert shrubs in relation to topography. Ecology 55:173–177.
Harms, T. K., and N. B. Grimm. 2010. Influence of the hydrologic regime on resource availability in a semi-arid stream-riparian corridor. Ecohydrology 359:349–359.
Hassan, M.A., 1990. Observations of desert flood bores. Earth Surface Processes and Landforms 15, 481-485.
Hastwell, G. T., and J. M. Facelli. 2003. Differing effects of shade-induced facilitation on growth and survival during the establishment of a chenopod shrub. Journal of Ecology 91:941–950.
Hoagland, D. B. 1992. Feeding ecology of an insular population of the black-tailed jackrabbit (Lepus californicus) in the Gulf of California. The Southwestern Naturalist 37:280–286.
Hoffman JP, Blasch KW, Ferré TP, 2003. Combined use of heat and soil-water content to determine stream/ground-water exchanges, Rillito Creek, Tucson, Arizona. Ch. 7 in Heat as a tool for studying the movement of ground water near streams. Circular 1260. United States Geological Survey. Edited by DA Stonestrom, J Constantz.

Hogan, J.F., Philips, F.M. and Scanlon, B.R. (Editors) 2004. Groundwater recharge in a desert environment: The southwestern United States. Water Science and Applications Ser.9. American Geophysical Union, Washington, DC

Hooke, R.L., 1967. Processes on arid-region alluvial fans. Journal of Geology 75, 438-460.

Horton, J. L., T. E. Kolb, and S. C. Hart. 2001. Leaf gas exchange characteristics differ among Sonoran Desert riparian tree species. Tree Physiology 21:233–241.

Hughes, D.A., Sami, K., 1992. Transmission Losses to alluvium and associated moisture dynamics in a semiarid ephemeral channel system in southern Africa. Hydrological Processes 6, 45-53.

Hupp, C. R. 1982. Stream-grade variation and riparian-forest ecology along Passage Creek , Virginia. Bulletin of the Torrey Botanical Club 109:488–499.

Hupp, C. R. 1986. Upstream variation in bottomland vegetation patterns, northwestern Virginia. Bulletin of the Torrey Botanical Club 113:421–430.

Hupp, C. R., and W. R. Osterkamp. 1996. Riparian vegetation and fluvial geomorphic processes. Geomorphology 14:277–295.

Izbicki JA, Radyk J, Michel RL, 2000. Water movement through a thick unsaturated zone underlying an intermittent stream in the western Mojave Desert, southern California, USA. Journal of Hydrology 238, 194-217.

Izbicki JA, Radyk J, Michel RL, 2003. Movement of water through the thick unsaturated zone underlying Oro Grande and Sheep Creek washes in the western Mojave Desert, USA. Hydrogeology Journal 10, 409-427.

Jaeger, K. L., and Olden, J. D., 2012. Electrical resistance sensor arrays as a means to quantify longitudinal connectivity of rivers. River Research and Applications; 28:1843-1852.

Jenkins, M. B., R. A. Virginia, and W. M. Jarrell. 1988. Rhizobial ecology of the woody legume Psorothamnus spinosus in a Sonoran Desert arroyo. Plant and Soil 105:113–120.

Johnson, A.S. 1989. The thin green line: riparian corridors and endangered species in Arizona and New Mexico. InL Mackintosh, G. (ed.), In defense of wildlife: preserving communities and corridors. Defenders of Wildlife, Washington, D.C.

Kampf et al. manuscript. Subsurface water content dynamics beneath ephemeral stream channels.

Kassas, M., and M. Imam. 1954. Habitat and plant communities of the Egyptian Desert: III. The wadi bed ecosystem. Journal of Ecology 42:424–441.

Kearny, T. H. and R. H. Peebles. 1960. Arizona Flora. University of California Press. Berkeley and Los Angeles, California.

Keppel, R.V., Renard, K.G., 1962. Transmission Losses in Ephemeral Stream Beds. Journal of the Hydraulics Division 8(HY3), 59-68.

Kidron, G.J., and Pick, K., 2000. The limited role of localized convective storms in runoff production in the western Negev Desert. Journal of Hydrology 229:281-289.

Kirkpatrick, C., C.J. Conway, and D. LaRoche. 2009. Quantifying impacts of ground water withdrawal on avian communities in desert riparian woodlands of the southwestern U.S. Department of Defense, Legacy Resource Management Program, Project 08-290.

Knighton AD, Nanson GC, 1994. Flow transmission along an arid zone anastomosing river, Cooper Creek, Australia. Hydrological Processes 8, 137-154.

Knighton, D. 1998. Fluvial Forms and Processes: A New Perspective. Oxford University Press, New York.

Kolb, T. E., S. C. Hart, and R. Amundson. 1997. Boxelder water sources and physiology at perennial and ephemeral stream sites in Arizona. Tree Physiology 17:151–160.

Kondolf, G.M., Smeltzer, M.W., Railsback, S.F., 2001. Design and performance of a channel reconstruction project in a coastal California gravel-bed stream. Environmental Management 28, 761-776.

Kray, J. a., D. J. Cooper, and J. S. Sanderson. 2012. Groundwater use by native plants in response to changes in precipitation in an intermountain basin. Journal of Arid Environments 83:25–34.

Kruskal, J. B., and M. Wish. 1978. Multidimensional Scaling. Sage Publications, Beverly Hills, California.

Kume, T., K. Otsuki, S. Du, N. Yamanaka, Y.-L. Wang, and G.-B. Liu. 2012. Spatial variation in sap flow velocity in semiarid region trees: its impact on stand-scale transpiration estimates. Hydrological Processes 26:1161–1168.

Lane, L.J., Diskin, M.H., Renard, K.G., 1971. Input-output relationships for an ephemeral stream channel system. Journal of Hydrology 13, 22-40.

Lange, J., 2005. Dynamics of transmission losses in a large arid stream channel. *Journal of Hydrology* 306: 112–126.

Larned, S. T., J. Schmidt, T. Datry, C. P. Konrad, J. K. Dumas, and J. C. Diettrich. 2011. Longitudinal river ecohydrology : flow variation down the lengths of alluvial rivers 548:532–548.

Larned, S. T., T. Datry, D. B. Arscott, and K. Tockner. 2010. Emerging concepts in temporary-river ecology. Freshwater Biology 55:717–738.
Lavorel, S., S. McIntyre, J. Landsberg, and T. D. A. Forbes. 1997. Plant functional classifications: from general groups to specific groups based on response to disturbance. Trends in Ecology & Evolution 12:474–478.
Lee, K., et al. (2003), *Hydrogeology Laboratory Manual*, *2nd Edition*, 151 pp., Prentice Hall, Upper Saddle River, New Jersey.
León, M. F., F. a. Squeo, J. R. Gutiérrez, and M. Holmgren. 2011. Rapid root extension during water pulses enhances establishment of shrub seedlings in the Atacama Desert. Journal of Vegetation Science 22:120–129.
Leopold, L.B., Miller, J.P., 1956. Ephemeral streams – hydraulic factors and their relation to the drainage net. US Geological Survey Professional Paper 282-A, p. 36
Leopold, L.B., Wolman, M.G., Miller, J.P., 1964. Fluvial Processes in Geomorphology. W.H. Freeman and Company, San Francisco.
Levick, L., J. Fonseca, D. Goodrich, M. Hernandez, D. Semmens, J. Stromberg, R. Leidy, M. Scianni, D. P. Guertin, M. Tluczek, and W. Kepner. 2008. The Ecological and Hydrological Significance of Ephemeral and Intermittent Streams in the Arid and Semi-arid American Southwest. U.S. Environmental Protection Agency and USDA/ARS Southwest Watershed Research Center, EPA/600/R-08/134, ARS/233046, 116 pp.
Levin, G. A. 1995. Euphorbiaceae spurge family: part 1. Acalypha and Cnidoscolus. Journal of the Arizona-Nevada Academy of Science 29(1):18-24.
Lite, S. J., and J. C. Stromberg. 2005. Surface water and ground-water thresholds for maintaining Populus–Salix forests, San Pedro River, Arizona. Biological Conservation 125:153–167.
Loke, M. H. (2014), RES2DINVx32: Rapid 2-D Resistivity & IP inversion using the least-squares method, edited, Geotomo Software, LTD.
Loke, M. H., and R. D. Barker (1995), Least-squares deconvolution of apparent resistivity pseudosections, *Geophysics*, *60*(6), 1682-1690.
Loke, M. H., and R. D. Barker (1996), Rapid least-squares inversion of apparent resistivity pseudosections by a quasi-Newton method, *Geophysical Prospecting*, *44*, 131-152.
Loke, M. H., and T. Dahlen (2002), A comparison of the Gauss-Newton and quasi-Newton methods in resistivity imaging inversion, *Journal of Applied Geophysics*, *49*, 149-162.
Loke, M. H., et al. (2003), A comparison of smooth and blocky inversion methods in 2D electrical imaging surveys *Exploration Geophysics*, *34*, 182-187.
Manly, B.F.J., 2000. Multivariate statistical methods: A primer. Chapman and Hall/CRC, Boca Raton.
Marshall, R.M., S. Anderson, M. Batcher, P. Comer, S. Cornelius, R. Cox, A. Gondor, D. Gori, J. Humke, R. Paredes Aguilar, I.E. Parra, S. Schwartz. 2000. An ecological analysis of conservation priorities in the Sonoran Desert. Department of Defense, Legacy Resource Management Program, Project 001703.
Mason, C. T. 1999. Fouquieriaceae ocotillo family. Journal of the Arizona-Nevada Academy of Science 32(1):55-56.
Matías, L., R. Zamora, and J. Castro. 2012. Sporadic rainy events are more critical than increasing of drought intensity for woody species recruitment in a Mediterranean community. Oecologia 169:833–44.
McAuliffe, J. R. (1994), Landscape evolution, soil formation, and ecological patterns and processes in Sonoran Desert bajadas, *Ecological Monographs, 64*, 112-148.
McAuliffe, J. R. 1986. Herbivore-limited establishment of a Sonoran Desert tree, Cercidium microphyllum. Ecology 67:276–280.
McAuliffe, J. R. 1988. Markovian dynamics of simple and complex desert plant communities. American Naturalist 131:459–490.
McAuliffe, J. R. 1994. Landscape evolution, soil formation, and ecological patterns and processes in Sonoran Desert bajadas. Ecological Monographs 64:112–148.
McAuliffe, J. R. 1999. The Sonoran Desert: landscape complexity and ecological diversity. Pages 68–114 *in* R. H. Robichaux, editor. Ecology of Sonoran Desert Plants and Plant Communities. University of Arizona Press, Tucson, Arizona.
McCune B., Mefford M.J., 1999. PC-ORD, multivariate analysis of ecological data, version 4.14. MjM Software Design, Gleneden Beach, OR.
McCune, B., and J. B. Grace. 2002. Analysis of Ecological Communities. MjM Software Design, Gleneden Beach, Oregon.
McDonald, A., Hernandez, R. (email exchange), 2011. Five-meter digital terrain model (DTM) of Yuma Army Proving Ground. Optics Division, U.S. Army Yuma Test Center.

McDonald, E., Hamerlynck, E., McAullife, J., and Caldwell, T. 2004. Analysis of desert shrubs along first-order channels on desert piedmonts: Possible indicators of ecosystem condition and historical variation. SERDP Seed project #CS1153, Final Technical Report.
McDonald, E.V., Dalldorf, G.K., Bacon, S.N., 2009. Landforms and surface cover of US Army Yuma Proving Ground. Desert Research Institute Final Report, DRI/DEES/TAP—2009-R44-Final.
McFadden, L. D., Wells, S. G., Jercinovich, M. J., 1987. Influences of eolian and pedogenic processes on the origin and evolution of desert pavements. Geology; 15:504-508.
McFadden, L.D., McDonald, E.V., Wells, S.G., Anderson, K., Quade, J., Forman, S.L., 1998. and Jercinovich, M.J., The vesicular layer and carbonate collars of desert soils and pavements: formation, age, and relation to climate change. Geomorphology 24, 101-145.
Meinzer, O.E. 1923. Outline of ground-water hydrology, with definitions. U.S. Geological Survey Water Supply Paper 494.
Melton, M. A. (1965), The geomorphic and paleoclimatic significance of alluvial deposits in southern Arizona, *Journal pf Geology*, *73*, 1-38.
Merritt, D. M. and E. Wohl. 2003. Downstream hydraulic geometry and channel adjustment during a flood along an ephemeral, arid-region drainage. *Geomorphology* 52: 165–180.
Merritt, D. M., M. L. Scott, L. N. Poff, G. T. Auble, and D. A. Lytle. 2010. Theory, methods and tools for determining environmental flows for riparian vegetation: riparian vegetation-flow response guilds. Freshwater Biology 55:206–225.
Metzger, D. G. (1968), The Bouse Formation (Pliocene) of the Parker-Blythe-Cibola area, Arizona and California, *USGS Professional Paper*, *600-D*, 126-136.
Miall, A. D. (1977), A review of the braided-river depositional environment, *Earth Science Reviews*, *13*, 1-62.
Millennium Ecosystem Assessment, (2005) Ecosystems and Human Well-being: Desertification Synthesis. World Resources Institute, Washington, DC, http://www.millenniumassessment.org/documents/document.355.aspx.pdf
Miller, S.N., Guertin, D.P., Goodrich, D.C., 1996. Investigating stream channel morphology using a geographic information system. Environmental Systems Research Incorporated Users Conference Proceedings. http://gis.esri.com/library/userconf/ proc96/TO300/PAP291/P291.htm.
Mitchell, P. J., et al. (2008), Using multiple trait associations to define hydraulic functional types in plant communities of south-western Australia, *Oecologia*, *158*, 385-397.
Monson, R. K., and S. D. Smith. 1982. Seasonal water potential components of Sonoran Desert plants. Ecology 63:113–123.
Montgomery, D. R. (1999), Process domains and the river continuum, *Journal of the American Water Resources Association*, *35*, 397-410.
Montgomery, D.R., Buffington, J.M., 1997. Channel-reach morphology in mountain drainage basins. Geological Society of America Bulletin, 109(5), 596-611.
Montgomery, D. R., and J. M. Buffington. 1998. Channel processes, classification, and response. Pages 13–42 *in* R. J. Naiman and R. Bilby, editors. River Ecology and Management. Springer-Verlag, New York.
Morin E, Grodek T, Dahan O, Benito G, Kulls C, Jacoby Y ,van Langenhove G, Seely M, Enzel Y, 2009. Flood routing and alluvial aquifer recharge along the ephemeral arid Kuiseb River, Namibia. Journal of Hydrology 368, 262-275.
Moser-Nørgaard, P. M., and M. Denich. 2011. Influence of livestock on the regeneration of fodder trees along ephemeral rivers of Namibia. Journal of Arid Environments 75:371–376.
Murphey, J.B., Wallace, D.E., Lane, L.J., 1977. Geomorphic parameters predict hydrograph characteristics in the southwest. *Water Resources Bulletin* 13: 25–38.
Naeem, S., and J. P. Wright. 2003. Disentangling biodiversity effects on ecosystem functioning: deriving solutions to a seemingly insurmountable problem. Ecology Letters 6:567–579.
Naimen, R. J., D. G. Lonzarich, T. J. Beechie, and S. C. Ralph. 1992. General principles of classification and the assessment of conservation potential in rivers. Pages 93–124 *in* P. J. Boon, P. Callow, and G. E. Petts, editors. River Conservation and Management. John Wiley and Sons, West Sussex, England.
Nanson, G. C., S. Tooth, and A. D. Knighton. 2002. A global perspective of dryland rivers: perceptions, misconceptions, and distinctions. Pages 17–54 *in* L. J. Bull and M. J. Kirkby, editors. Dryland Rivers: Hydrology and Geomorphology of Semi-arid Channels. John Wiley and Sons, West Sussex, England.
National Weather Service, Arizona climate summaries, Yuma Proving Ground. National Oceanic and Atmospheric Administration: http://www.esrl.noaa.gov/psd/cgi-

bin/data/usclimate/city.pl?state=AZ&lane=fast&itypea=1&loc.x=68&loc.y=363&.cgifields=itypea, accessed October 17, 2012.
Newson, M. D., and C. L. Newson. 2000. Geomorphology, ecology and river channel habitat: mesoscale approaches to basin-scale challenges. Progress in Physical Geography 24:195–217.
Nilsen, E. T., F. C. Meinzer, and P. W. Rundel. 1989. Stem photosynthesis in Psorothamnus spinosus (smoke tree) in the Sonoran desert of California. Oecologia 79:193–197.
Nilsen, E. T., M. R. Sharifi, and P. W. Rundel. 1984. Comparative water relations phreatophyes in the Sonoran Desert of California. Ecology 65:767–778.
Notaro, M., A. Mauss, and J. W. Williams. 2012. Projected vegetation changes for the American Southwest: combined dynamic modeling and bioclimatic-envelope approach. Ecological Applications 22:1365–1388.
Noy-Meir, I. 1973. Desert ecosystems: environment and producers. Annual Review of Ecology and Systematics 4:25–51.
Nucci, A., C. Angiolini, M. Landi, and G. Bacchetta. 2012. Influence of bedrock-alluvial transition on plant species distribution along a Mediterranean river corridor. Plant Biosystems 146:564–575.
Oksanen, J., Blanchet, F.G., Kindt, R., Legendre, P., Minchin, P.R., O'Hara, R.B., Simpson, G.L., Solymos, P., Stevens, M.H.H., Wagner, H., 2011. Package VEGAN 2.0-9: Community Ecology Package. R package version 2.0-2. http://CRAN.R-project.org/package=vegan
Oldenburg, D. W., and Y. Li (1999), Estimating depth of investigation in DC resistivity and IP surveys, *Geophysics*, *64*(2), 403-416.
Osborn, H.B. 1964. Effect of storm duration on runoff from rangeland watersheds, in the semiarid southwetern United States. International Association of Scientific Hydrology IX (4), 40-47.
Osborn, H.B., and Lane, L.J., 1969. Precipitation-runoff relations for very small semiarid rangeland watersheds. Water Resources Research 5 (2), 419-425.
Parker, K. C. 1988. Environmental relationships and vegetation associates of columnar cacti in the northern Sonoran Desert. Vegetatio 78:125–140.
Patton, P.C., Schumm, S.A., 1981. Ephemeral-stream processes: Implications for studies of Quaternary valley fills. Quaternary Research 15, 24-43.
Perucca, E., Camporeale, C., Ridolfe, L., 2007. Significance of the riparian vegetation dynamics on meandering river morphodynamics. Water Resources Research 43(W03430), 1-10. doi:10.1029/2006WR005234
Petchey, O. L., and K. J. Gaston. 2006. Functional diversity: back to basics and looking forward. Ecology Letters 9:741–58.
Phillips FM, Walvoord MA, Small EE, 2004. Effects of environmental change on groundwater recharge in the desert southwest. Groundwater Recharge in a Desert Environment: The Southwestern United States, edited by JF Hogan, FM Phillips, BR Scanlon. Water Science and Application 9. Washington DC, American Geophysical Union.
Phillips, D. L., and J. W. Gregg. 2001. Uncertainty in source partitioning using stable isotopes. Oecologia 127:171–179.
Phillips, D. L., S. D. Newsome, and J. W. Gregg. 2005. Combining sources in stable isotope mixing models: alternative methods. Oecologia 144:520–527.
Picard, M. D., and L. R. High (1973), *Sedimentary Structures of Ephemeral Streams*, 222 pp., Elsevier, Amsterdam.
Pockman, W. T., and J. S. Sperry. 2000. Vulnerability to xylem cavitation and the distribution of Sonoran Desert vegetation. American Journal of Botany 87:1287–1299.
Poff, N.L. 1996. A hydrogeography of unregulated streams in the United States and an examination of scale-dependence in some hydrological descriptors. Freshwater Biology 36: 71-91.
Polvi, L.E., Wohl, E.E., Merritt, D.M., 2011. Geomorphic and process domain controls on riparian zones in the Colorado Front Range. Geomorphology 125(4), 504-516.
Pool DR, 2005. Variations in climate and ephemeral channel recharge in southeastern Arizona, United States. Water Resources Research 41, W11403, doi:10.1029/2004WR003255.
Poole, G. C. 2010. Stream hydrogeomorphology as a physical science basis for advances in stream ecology. Journal of the North American Benthological Society 29:12–25.
Powell, D.M., Brazier, R., Wainwright, J., Parsons, A., Kaduk, J., 2005. Streambed scour and fill in low-order dryland channels. Water Resources Research 41(W05019), 1-13. doi:10.1029/2004WR003662.
Powell, D.M., Reid, I., Laronne, J.B., Frostick, L.E., 1998. Cross-stream variability of bedload flux in narrow and wide ephemeral channels during desert flash floods. In: Klingeman, P.C., Beschta, R.L., Komar, P.D. and Bradley, J.B. (Eds.), Gravel-bed rivers in the environment. Water Resources Publications, Highlands Ranch, Colorado, pp. 177-196.

R Core Team, 2012. R: A language and environment for statistical computing. R Foundation for Statistical Computing. Vienna, Austria. http://www.R-project.org

Reid, I., Frostick, L.E., 2011. Channel form, flows, and sediment of endogenous ephemeral rivers in deserts. In: Thomas, D.S.G. (Ed.), Arid Zone Geomorphology: Process, Form, and Change in Drylands, 3rd edition. Wiley and Sons, Chichester. pp. 301-332.

Reid, I., Laronne, J.B., 1995. Bedload sediment transport in an ephemeral stream and a comparison with seasonal and perennial counterparts. Water Resources Research 31(3), 773-781.

Renard KG, Keppel RV, Hickey JJ, Wallace DE, 1964. Performance of local aquifers as influenced by stream transmission losses and riparian vegetation. Transactions of the ASAE 7(4), 471-474.

Revesz, K. M., B. Buck, and T. B. Coplen. 2012. Determination of the δ2H and δ18O of soil water and water in plant matter; RSIL Lab Code 1700. *in* K. M. Revesz and T. B. Coplen, editors. Methods of the Reston Stable Isotope Laboratory: U.S. Geological Survey Techniques and Methods, Book 10. U.S. Geological Survey, Reston, Virginia.

Revesz, K., and P. H. Woods. 1990. A method to extract soil water for stable isotope analsis. Journal of Hydrology 115:397–406.

Reynolds JF, Kemp PR, Ogle K, Fernández RJ, 2004. Modifying the 'pulse-reserve' paradigm for deserts of North America: precipitation pulses, soil water, and plant responses. Oecologia 141, 194-210.

Reynolds, L. V., and D. J. Cooper. 2010. Environmental tolerance of an invasive riparian tree and its potential for continued spread in the southwestern US. Journal of Vegetation Science 21:733–743.

Rhodes, S., J. Beasley, and T. Ayers. 2011. Vascular plants of Arizona: Fabaceae. CANOTIA 7:1-13.

Richard, S. M., et al. (2000), Geologic Map of Arizona, Arizona Geological Survey, Tucson, AZ.

Richard, S. M., S. J. Reynolds, J. E. Spencer, and P. A. Pearthree. 2000. Geologic Map of Arizona. Arizona Geological Survey Map 35, 1 sheet, scale 1:1,000,000, Tucson, Arizona.

Ripley, B. Venables, B., Bates, D.M., Hornik, K., Gebhardt, A., Firth, D., 2012. Package MASS version 7.3-29: Support functions and datasets for venables and ripley's MASS. R package version 2.0-2. http://CRAN.R-project.org/package=vegan

Ronan, A.D., Prudic, D.E., Thodal, C.E., Constantz, J., 1998. Field study and simulation of diurnal temperature effects on infiltration and variably saturated flow beneath an ephemeral stream. Water Resource Research 34(9), 2137-2153.

Rosgen, D.L., 1994. A classification of natural rivers. Catena 22, 169-199.

Roth, G. A., W. G. Whitford, and Y. Steinberger. 2007. Jackrabbit (Lepus californicus) herbivory changes dominance in desertified Chihuahuan Desert ecosystems. Journal of Arid Environments 70:418–426.

Salford Predictive Modeler v6.6, 1998. *Salford Systems*, San. Diego, CA, USA.

Sandercock, P. J., and J. M. Hooke. 2010. Assessment of vegetation effects on hydraulics and of feedbacks on plant survival and zonation in ephemeral channels. Hydrological Processes 24:695–713.

Schenk, H. J., and R. B. Jackson. 2002. Rooting depths, lateral root spreads and below-ground/above-ground allometries of plants in water-limited ecosystems. Journal of Ecology 90:480–494.

Schick, A.P., 1986. Surface runoff in the desert: hydrological concepts and applications in extremely arid areas. Beiträge zur Hydrologie 6, 151-160.

Scholes, R. J., G. Picket, W. N. Ellery, and A. C. Blackmore. 1997. Plant functional types in African savannas and grasslands. Pages 255–268 *in* T. M. Smith, H. H. Shugart, and F. I. Woodward, editors. Plant Functional Types: Their Relevance to Ecosystem Properties and Global Change. Cambridge University Press, Cambridge, UK.

Schreiber, H.A., and Kincaid, D.R., 1967. Regression models for predicting on-site runoff from short-duration convective storms. Water Resources Research 3(2), 389-395.

Schumm, S.A., 1977. The Fluvial System. Wiley-Interscience, New York.

Schwinning, S., B. I. Starr, and J. R. Ehleringer. 2003. Dominant cold desert plants do not partition warm season precipitation by event size. Oecologia 136:252–260.

Schwinning, S., K. Davis, L. Richardson, and J. R. Ehleringer. 2002. Deuterium enriched irrigation indicates different forms of rain use in shrub/grass species of the Colorado Plateau. Oecologia 130:345–355.

Scott RL, Shuttleworth WJ, Keefer TO, Warrick AW, 2000. Modeling multiyear observations of soil moisture recharge in the semiarid American Southwest. Water Resources Research 36(8), 2233-2247.

Scott, M. L., J. M. Friedman, and G. T. Auble. 1996. Fluvial process and the establishment of bottomland trees. Geomorphology 14:327–339.

Sellers, W. D., and R. H. Hill. 1974. Arizona Climate 1931-1972, 2nd edition. University of Arizona Press, Tucson, Arizona.

Shannon, J., R. Richardson, and J. Thornes, 2002. Modelling event-based fluxes in ephemeral streams. Chapter 5 in *Dryland Rivers: Hydrology and geomorphology of semi-arid channels*, edited by L.J. Bull and M.J. Kirkby, pp. 129-172.Shreve, F., and I. L. Wiggins. 1964. Vegetation and Flora of the Sonoran Desert. Stanford University Press, Stanford, California.

Shaw, J.R., Cooper, D.J., 2008. Linkages among watersheds, stream reaches, and riparian vegetation in dryland ephemeral stream networks. Journal of Hydrology 350, 68-82.

Shinohara, Y., K. Tsuruta, A. Ogura, F. Noto, H. Komatsu, K. Otsuki, and T. Maruyama. 2013. Azimuthal and radial variations in sap flux density and effects on stand-scale transpiration estimates in a Japanese cedar forest. Tree physiology 33:550–8.

Shmida, A., and T. L. Burgess (1988), Plant growth-form strategies and vegetation types in arid environments, in *Plant Form and Vegetation Structure: Adaptation, Plasticity and Relation to Herbivory*, edited by M. J. A. Werger, et al., SPB Academic Publishing, The Hague, Netherlands.

Shreve, F., and I. L. Wiggins. 1964. Vegetation and Flora of the Sonoran Desert. Stanford University Press, Stanford, California.

Sidorchuk, A. 2003. Floodplain sedimentation: inherited memories. Global and Planetary Change 39, 13-29.

Sieben, E. J. J., L. Mucina, and C. Boucher. 2009. Scaling hierarchy of factors controlling riparian vegetation patterns of the Fynbos Biome at the Western Cape, South Africa. Journal of Vegetation Science 20:17–26.

Simanton, and J.R., Osborn, H.B., 1983. Runoff estimates for thunderstorm rainfall on small rangeland watersheds. Hydrology and Water Resources in Arizona and the Southwest. Proceedings of the 1983 Meetings of the Arizona Section, American Water Resources Association and the Hydrology Section, Arizona, Nevada Academy of Sciences, Flagstaff, Arizona, April 16.

Simon, A., W. Dickerson, A. Heins, 2004. Suspended-sediment transport rates at the 1.5-year recurrence interval for ecoregions of the United States; transport conditions at the bankfull and effective discharge? Geomorphology 58, 243-262.

Simons, D. B., et al. (1965), Sedimentary structures generated by flow in alluvial channels, in *Primary Sedimentary Structures and their Hydrodynamic Interpretation*, edited, pp. 34-52, Society of Economic Paleontologists and Mineralogists, Tulsa, OK.

Simunek J, van Genuchten M, Sejna M, 2012. The HYDRUS software package for simulating the two- and three-dimensional movement of water, heat, and multiple solutes in variably-saturated porous media. Technical Manual version 2.0.

Small EE, 2005. Climatic controls on diffuse groundwater recharge in semiarid environments of the southwestern United States. Water Resources Research 41, W04012, doi:10.1029/2004WR003193.

Smith, S. D., D. A. Devitt, A. Sala, J. R. Cleverly, and D. E. Busch. 1998. Water relations of riparian plants from warm desert regions. Wetlands 18:687–696.

Smith, S. D., R. K. Monson, and J. E. Anderson. 1997. Physiological Ecology of North American Desert Plants. Springer-Verlag, Berlin, Germany.

Snyder, K. A., and D. G. Williams. 2000. Water sources used by riparian trees varies among stream types on the San Pedro River, Arizona. Agricultural and Forest Meteorology 105:227–240.

Sorman, A.U., Abdulrazzak, M.J., Morel-Seytoux, H.J., 1997. Groundwater recharge estimation from ephemeral streams. Case study: Wadi Tabalah, Saudi Arabia. *Hydrological Processes* 11: 1607–1619.

Sperry, J. S., and U. G. Hacke. 2002. Desert shrub water relations with respect to soil characteristics and plant functional type. Functional Ecology 16:367–378.

Sponseller, R. A., and S. G. Fisher. 2006. Drainage size, stream intermittency, and ecosystem function in a Sonoran Desert landscape. Ecosystems 9:344–356.

Springer, M.E., 1958. Desert Pavement and Vesicular Layer of Some Soils of the Desert of the Lahontan Basin, Nevada. Soil Science Society of America Journal. Soil Science Society Proceedings. 22(1), 63-66.

Stanley, E.H., Fisher, S.G., Grimm, N.B., 1997. Ecosystem expansion and contraction in streams. BioScience 47(7), 427-435.

Stear, W. M. (1985), Comparison of the bedform distribution and dynamics of modern and ancient sandy ephemeral flood deposits in the southwestern Karoo region, South Africa, *Geology*, *45*, 209-230.

Stonestrom DA, Prudic DE, Laczniak RJ, Akstin KC, 2004. Tectonic, climatic, and land use controls on groundwater recharge in an arid alluvial basin: Amargosa Desert, USA. Groundwater Recharge in a Desert Environment: The Southwestern United States, edited by JF Hogan, FM Phillips, BR Scanlon. Water Science and Application 9. Washington DC, American Geophysical Union.

Stromberg, J. C. 2013. Root patterns and hydrogeomorphic niches of riparian plants in the American Southwest. Journal of Arid Environments 94:1–9.

Stromberg, J. C. 2013. Root patterns and hydrogeomorphic niches of riparian plants in the American Southwest. Journal of Arid Environments 94:1–9.
Sundell, E. 1993. Asclepiadaceae milkweed family. Journal of the Arizona-Nevada Academy of Science 27(2):169-187.
Sutfin, N. A., J. Shaw, E. E. Wohl, and D. Cooper. 2014. A geomorphic classification of ephemeral channels in a mountainous, arid region, southwestern Arizona, USA. Geomorphology 221:164–175.
Suzan, H., G. P. Nabhan, and D. T. Patten. 1996. The importance of Olneya tesota as a nurse plant in the Sonoran Desert. Journal of Vegetation Science 7:635–644.
Syed, K. H., Goodrich, D. C., Myers, D. E., & Sorooshian, S. 2003. Spatial characteristics of thunderstorm rainfall fields and their relation to runoff. Journal of Hydrology, 271:1–21.doi:http://dx.doi.org/10.1016/S0022-1694(02)00311-6
Szarek, S. R., and R. M. Woodhouse. 1976. Ecophysiological studies of Sonoran Desert plants. I. Diurnal photosynthesis patterns of Ambrosia deltoidea and Olneya tesota. Oecologia 26:225–234.
Szarek, S. R., and R. M. Woodhouse. 1977. Ecophysiological studies of Sonoran Desert Plants. II. Seasonal photosynthesis patterns and primary production of Ambrosia deltoidea and Olneya tesota. Oecologia 28:365–375.
Szarek, S. R., and R. M. Woodhouse. 1978a. Ecophysiological studies of Sonoran Desert plants. III. The daily course of photosynthesis for Acacia greggii and Cercidium microphyllum. Oecologia 35:285–294.
Szarek, S. R., and R. M. Woodhouse. 1978b. Ecophysiological studies of Sonoran Desert plants. IV. Seasonal photosynthetic capacities of Acacia greggii and Cercidium microphyllum. Oecologia 37:221–229.
Telford, W. M., et al. (1990), *Applied Geophysics*, Cambridge University Press, Cambridge, England.
Terzer, S., L. I. Wassenaar, L. J. Araguas-Araguas, and P. K. Aggarwal. 2013. Global isoscapes for delta18O and delta2H in precipitation: improved prediction using regionalized climatic regression models. Hydrology and Earth System Sciences 17:1–16.
Tewksbury, J. J., and C. A. Petrovich. 1994. The influences of ironwood as a habitat modifier species: a case study on the Sonoran Desert coast of the Sea of Cortez. Pages 29–54 *in* G. P. Nabhan and J. L. Carr, editors. Ironwood: An Ecological and Cultural Keystone of the Sonoran Desert. Conservation International Occasional Paper 1, Washington, DC.
Thorp, J. H., M. C. Thoms, and M. D. Delong. 2006. The riverine ecosystem synthesis: biocomplexity in river networks across space and time. River Research and Applications 22:123–147.
Tinkler, K.J., Wohl, E.E., 1998. A primer on bedrock channels. In: Tinkler, K.J., Wohl, E.E., (Eds), Rivers over rock. American Geophysical Union, Washington, DC, pp. 1-18.
Tooth, S., 1999. Downstream changes in floodplain character on the Northern Plains of arid central Australia. In: Smith, N.D., Rogers, J. (Eds), Fluvial Sedimentology VI., Special Publications of the International Association of Sedimentologists 28, 93-112.
Tooth, S., 2000. Process, form and change in dryland rivers: a review of the research. Earth-Science Reviews 51, 67-107.
Tooth, S., Nanson, G.C., 2000. The role of vegetation in the formation of anabranching channels in an ephemeral river, Northern plains, arid central Australia. Hydrological Processes 14, 3099-3117.
Tosdal, R. M., G. B. Haxel, and J. E. Wright. 1989. Jurassic geology of the Sonoran Desert region, southern Arizona, southeast California, and northernmost Sonora: Construction of a continental-margin magmatic arc. Arizona Geological Society Digest 17:397–434.
Trombulak, S.C., and C.A. Frissell. 2000. Review of ecological effects of roads on terrestrial and aquatic communities. Conservation Biology 14 (1): 18-30.
Tucker, G.E., Arnold, L., Bras, R.L., Flores, H., Istanbulluoglu, E., Sólyom, P., 2006. Headwater channel dynamics in semiarid rangelands, Colorado high plains, USA. Geological Society of America Bulletin 118, 959-974.
Tunbridge, I. P. (1981), Sandy high-energy flood sedimentation - Some criteria for recognition, with an example from the Devonian of S.W. England, *Sedimentary Geology*, *28*, 79-95.
Turk J K, Graham R C. 2011. Distribution and Properties of Vesicular Horizons in the Western United States. Soil Science Society of America journal; 75(4):1449-1461.
Turner, R. M., and D. E. Brown. 1994. Sonoran Desertscrub. Pages 181–221 *in* D. E. Brown, editor. Biotic Communities: Southwestern United States and Northwestern Mexico. University of Utah Press, Salt Lake City, Utah.
Turner, R. M., J. E. Bowers, and T. L. Burgess. 1995. Sonoran Desert Plants: An Ecological Atlas. University of Arizona Press, Tucson, Arizona.

Turner, R.M., Webb, R.H., Bowers, J.E., and Hastings, J.R., 2003. The changing mile revisited, University of Arizona Press, Tucson.
United States Department of Agriculture's Farm Service Agency's National Agriculture Imagery Program (NAIP), Aerial Photography Field Office, June 9, 2013.
Van Coller, A. L., K. H. Rogers, and G. L. Heritage. 1997. Linking riparian vegetation types and fluvial geomorphology along the Sabie River within the Kruger National Park, South Africa. African Journal of Ecology 35:194–212.
van Vuuren DP, Edmonds J, Kainuma M, Riahi K, Thomson A, Hibbard K, Hurtt GC, Kram T, Krey V, Lamarque J, Masui T, Meinshausen M, Nakicenovic N, Smith SJ, Rose SK, 2011. The representative concentration pathways: an overview. Climatic Change 109:5–31, DOI 10.1007/s10584-011-0148-z.
Vandegehuchte, M. W., and K. Steppe. 2012. Improving sap flux density measurements by correctly determining thermal diffusivity, differentiating between bound and unbound water. Tree physiology 32:930–42.
Vaughan, T. A., and S. T. Schwartz. 1980. Behavioral ecology of an insular woodrat. Journal of Mammalogy 61:205–218.
Walters, M.O., 1989. Transmission losses in arid region. Journal of Hydraulic Engineering 116, 129-138.
Walter, M.O., 1990. Transmission losses in arid region. *Journal of Hydraulic Engineering* 116: 129–138.
Ward, D. 2006. Long-term effects of herbivory on plant diversity and functional types in arid ecosystems. Pages 142–169 *in* K. Danell, P. Duncan, R. Bergstrom, and J. Pastor, editors. Large Herbivore Ecology, Ecosystem Dynamics and Conservation. Cambridge University Press, Cambridge, Massachusetts.
Waters, M.R. and Haynes, C.V., 2001. Late Quaternary arroyo formation and climate change in the American Southwest, *Geology* 29: 399-402.
Waters, T.F., 1995. Sediment in streams: sources, biological effects, and control. American Fisheries Society, Bethesda, MD, Monograph 7.
Wentworth, C.K., 1922, A scale of grade and class terms for clastic sediments: Journal of Geology 30, 377-392.
West, A. G., K. R. Hultine, K. G. Burtch, and J. R. Ehleringer. 2007. Seasonal variations in moisture use in a piñon-juniper woodland. Oecologia 153:787–798.
Western Regional Climate Center. Gila Bend, Arizona (023393), Period of record monthly climate summaries: http://www.wrcc.dri.edu/cgi-bin/cliMAIN.pl?azgila. Accessed October 17, 2012b.
Western Regional Climate Center. Yuma Proving Ground (029654), Period of record monthly climate summaries: http://www.wrcc.dri.edu/cgi-bin/cliMAIN.pl?azyupg. Accessed October 17, 2012a.
Western Regional Climate Center. Yuma Proving Ground (029654), Period of record monthly climate summary: http://www.wrcc.dri.edu/cgi-bin/cliMAIN.pl?az9654. Accessed 18 June 2013.
Westoby, M. 1980. Black-tailed jack rabbit diets in Curlew Valley, northern Utah. Journal of Wildlife Management 44:942–948.
Wilcox, B.P., Newman, B.D., Brandes, D., Davenport, D.W., Reid, K. 1997. Runoff from a semiarid ponderosa pine hillslope in New Mexico. Water Resources Research, 33(10):2301-2314.
Williams, D. G., and J. R. Ehleringer. 2000. Intra- and interspecific variation for summer precipitation use in pinyon-juniper woodlands. Ecological Monographs 70:517–537.
Williams, D. G., R. L. Scott, T. E. Huxman, D. C. Goodrich, and G. Lin. 2006. Sensitivity of riparian ecosystems in arid and semiarid environments to moisture pulses. Hydrological Processes 20:3191–3205.
Williams, D.D. 2006. The Biology of Temporary Waters. Oxford University Press.
Williams, G.P., 1978. Bank-full discharge of rivers. Water Resources Research 14(6): 1141-1154.
Wohl, E., David, G.C.L., 2008. Consistency of scaling relations among bedrock and alluvial channels. Journal of Geophysical Research 113, F04013, doi:10.1029/2008JF000989.
Wood, Y.A., Graham, R.C., and Wells, S.G., 2005. Surface control of desert pavement pedological process and landscape function, Cima Volcanic field, Mohave desert California. Catena 59, 205-230.
Yair, A., and Lavee, H., 1985. Runoff generation in arid and semi-arid zones. Hydrological Forecasting, edited by M.G. Anderson and T.P. Burt. John Wiley, New York, 183-220.
Yang, T. W., and C. H. Lowe (1956), Correlation of major vegetation climaxs with soil characteristics in the Sonoran Desert, *Science*, *123*, 542.
Youberg, A., et al. (unpublished), Geologic map of the Arizona part of the Cibola 7.5' Quadrangle, La Paz County, Arizona, Arizona Geological Survey, Tucson, AZ.
Youberg, A., Guertin, D.P., Ball, G.L., 1998. Developing stream-watershed relationships for selecting reference site characteristics using ArcInfo. Environmental Systems Research Incorporated Users Conference Proceedings. http://gis.esri.com/library/userconf/proc98/TO450/PAP407/ P4071.htm.

Young, M.H., McDonalds, E.V., Caldwell, T.G., Benner, S.G., and Meadows, D.G., 2004. Hydraulic properties of a desert soil chronosequence in the Mohave desert, USA. Vadose Zone Journal 3, 956-963.
Zimmerman, J.C., DeWald, L.E., Rowlands, P.G., 1999. Vegetation diversity in an interconnected ephemeral riparian system of north-central Arizona, USA. *Biological Conservation* 90: 217–228.
Zimmerman, R.C., 1969. Plant ecology of an arid basin – Tres Alamos-Redington area southeastern Arizona. US Geological Survey Professional Paper 485-D. p. 51.

Appendix A. Supporting Data

Appendix A-1. Details of Geophysical Data Processing and Laboratory Methods

A-1.1. Ground Penetrating Radar

The GPR data were collected using a Sensors & Software Pulse Ekko Pro system with 100 MHz antennae and a record length of 400 ns. This resulted in a nominal recording depth of 3.5 m with a bed thickness resolution of 0.16 m (based on an average radar velocity of 0.045 m ns^{-1} and a dominant frequency of 70 MHz, as discussed below). A minimum of four common offset profiles were collected at each site, with three profiles crossing the drainage perpendicular to the channel, and one trending parallel and intersecting the other three profiles. The common offset surveys provide a radar image of the subsurface stratigraphy at 25 cm intervals. The transmitting and receiving antennas were oriented parallel to the profile azimuth and were separated by 1 m. Common Midpoint (CMP) surveys were collected at each of the study sites to obtain subsurface radar velocity estimates. In the CMP surveys, the spacing between the transmitting and receiving antennae was incrementally increased by 20 cm while keeping the midpoint between the antennae fixed.

The GPR data was processed using EKKO_View Deluxe software by Sensors & Software Inc. Data processing included application of a DEWOW filter to remove low frequency noise, a gain to enhance deep reflections, and, where the data was available, a topographic correction. Both Automatic Gain Control (AGC) and Spherical and Exponential Divergence Correction (SEC) gained radar profiles were used in the interpretation. The former proved most suitable for delineating reflection patterns, whereas the latter revealed differences in reflection amplitudes that were found to be lithologically significant. Gain parameters were empirically tested to identify those which produced the most interpretable GPR profiles. Optimal parameters for the AGC gain were a window length of 14 ns and a maximum gain of 250 times the original signal strength. The optimal SEC gain is obtained with a gain at time 0 ns of 0.75 times the original signal strength, an increase in gain of 0.5 dB ns^{-1}, and a maximum gain of 500.

A-1.2. DC Electrical Resistivity

DC Electrical Resistivity surveys were collected along profiles coincident with all but one of the GPR profiles (the narrowness of the channels at the Yuma Wash bedrock with alluvium site precluded collection of ERT data at the upstream end of the reach). The data were collected with a 10-channel 48 electrode Syscal Pro system. A dipole-dipole array was used with a 2 m electrode spacing except for two profiles at the Yuma Wash bedrock with alluvium site, where a 1 m electrode spacing was tested to verify that the electrode spacing was capturing subsurface heterogeneity at the bedform scale. Output voltage for the Syscal Pro was set to 200 volts. A minimum of 3 measurements were averaged for each electrode pair, with measurements repeated until either a measurement standard deviation of <5% was achieved or 10 measurements were recorded. At the incised alluvium and braided stream sites a roll-along technique was used to extend profiles beyond the length spanned by the 48 electrodes available, extending the profile by one fourth of the spread length (12 electrodes) for each roll-along.

The subsurface resistivity structure was estimated by tomographic inversion using the Res2D software by Geotomo Software, Ltd. [*Loke and Barker*, 1996; *Loke and Dahlen*, 2002]. Prior to inversion, measurements with voltage drops within 10% of the self potential (deemed to be the result of poor signal strength), measurements with a standard deviation greater than 5% (indicative of poor repeatability), and measurements visually identified as outliers on the basis of their large difference in apparent resistivity from neighboring measurements were eliminated. In sum, these data filtering processes reduced the dataset for each profile by approximately 44% on average. A rectangular mesh was used to parameterize the subsurface during the tomographic inversion. The thickness of the rows in the mesh is 0.2 times the electrode spacing near the surface and increases 10% with each row of the mesh down to a maximum depth of 30 m. The width of the columns in the mesh is equal to the electrode spacing. A finer mesh with block widths and thickness reduced by half was tested on two of the ERT profiles. This yielded similar results to the courser mesh, so the coarse mesh was deemed sufficient.

Tomographic inversions based on minimization of model L1 and L2 norms were examined. The L1 inversion yielded an inverse model that produced a sharp gradient in resistivity coinciding with the depth at which the radar amplitudes change abruptly, whereas the L2 norm yields a much more gradational change in resistivity [*Loke et al.*,

2003]. Because the sharp resistivity gradient is correlates in most places with a sharp reduction in the GPR signal strength, the L1 norm was chosen as the basis for interpretation. Other key parameter choices in the inversion include relative weighting between smoothing in the vertical and horizontal directions and the amount of damping used in the inversion. These parameters were varied systematically in different inverse models for two test profiles to identify parameters that led most rapidly to low-variance solutions (see [*Loke*, 2014] for parameter definitions). Based on these empirical tests, the smoothing filters were evenly weighted (with a value of 0.1). An initial damping factor (0.16) was selected that heavily weights fitting the data over the starting model and allows relatively large resistivity changes in the model with each iteration. The damping factor is refined after each iteration. RMS misfits between the models and the data range from 4-40%, and were typically obtained after 4-6 iterations of the inversion. In all models, further iterations resulted in only a marginal reduction of the misfit, but produced increasingly higher variance in the resistivity models. Inverse models with misfits >20% between the data and model were not used for quantitative analysis.

The fidelity of the inverse models is assessed by calculating the sensitivity of the predicted surface voltage drops to variations in the resistivity within each portion of the model mesh [*Loke and Barker*, 1995], and by examining the Depth of Investigation (DOI) Index [*Oldenburg and Li*, 1999], which identifies portions of the model domain in which the solution is heavily dependent upon the initial model (and is therefore deemed to be poorly constrained). Both the DOI Index and the model sensitivity are relatively uniform at depths shallower than about 3.5 m, and diminish rapidly at greater depths. Consequently, we confine our interpretation of the ERT data to depths shallower than 3.5 m.

A-1.3. Grain Size Distribution, Laboratory Resistivity Measurements, and Moisture Estimation

Sediment samples were collected by shovel in all of the active channels except the Mohave Wash bedrock with alluvium site, where the channel was composed primarily of large cobbles. Samples were also collected from adjacent flood plains and/or bars at all sites except the Yuma Wash bedrock with alluvium and incised alluvium sites. The samples were sieved to determine the grain size distribution by weight (Fig. 2). Porosity was determined by volumetric balance [*Lee et al.*, 2003] for three portions of each sample. These were averaged to determine a mean porosity for the sediment at each sample location (Table 1).

Resistivity for each of the samples was measured using a protocol similar to that described by [*Telford et al.*, 1990]. Portions of each sample were placed in a 42.5 cm long acrylic tube with a diameter of 6 cm. Copper plates capping the ends of the sample are wired in series with a 22 k-ohm resistor and a 12 V DC power supply. The current through the sample is calculated from Ohm's Law using the voltage drop measured across the 22 k-ohm resistor. The resistivity of the sample is given by

Eqn. 1

where A is the cross-sectional area of the sample, L is the length of the sample (nominally 35 cm), V is the voltage drop between the copper end-plates, and I is the current [*Telford et al.*, 1990]. Resistivity values were measured at pore volume water saturations of 0, 3, 6, 9, 12, 15 and 100% using tap water as the pore fluid with a measured resistivity of 1040 ohm-m. The amount of water added to each sample to achieve the desired saturation was determined by multiplying the sample volume by the sample porosity to obtain the total pore volume of the sample. To obtain even wetting, the sample was well mixed after wetting and prior placing the sample in the acrylic tube. A simplified form of Archie's Law [*Archie*, 1942] is used to describe the relationship between resistivity and saturation:

Eqn. 2 $\rho = B \times S^{-n} \times \rho_w$

where ρ is the sample bulk resistivity, S is the volumetric pore saturation, and ρ_w is the resistivity of the pore fluid. B and n are empirically determined coefficients that were estimated by least squares regression (Table 1). All of the samples displayed behaviors that are reasonably well fit with this form of Archie's Law at saturations above 2% (Fig. 2). Equation 2 is used derive an estimate of the sediment moisture content at each site based on the ERT data.

Appendix A-2. Designation of Plant Functional Groups

Table A-2.1. Plant species and a priori plant functional groups. EGTR = evergreen tree, PSTR = photosynthetic stem tree, WDTR = winter deciduous tree, COCA = columnar cactus, EGSH = evergreen shrub, DDSH = drought deciduous shrub, PSSH = photosynthetic stem shrub, WDSH = winter deciduous shrub, CASH = shrubby cactus, EGSS = evergreen subshrub, DDSS = drought deciduous subshrub, PSSS = photosynthetic stem subshrub, WDSS = winter deciduous subshrub, CASS = low cactus, VINE = vine, HERB = herbaceous, GRAS = grass, PARA = epiphytic parasite.

Species	Growth Form	Sources
Acalypha californica Benth.	DDSH	**1,7,8,11**
Acacia constricta Benth.	WDSH	**7,11,13**
Acacia greggii A. Gray	WDSH	**1,7,11,13**
Adenophyllum porophylloides (A. Gray) Strother	DDSS	**1,5,11**
Ambrosia ambrosiodes (Cav.) W.W. Payne	EGSS	**5,7,11,13**
Ambrosia deltoidea (Torr.) W.W. Payne	DDSS	**5,7,11,13**
Ambrosia dumosa (A. Gray) Payne	DDSS	**1,5,7,11,13**
Ambrosia salsola (Torrey & A. Gray) Strother & B.G. Baldwin	DDSH	**5,7,11,13**
Argythamnia lanceolata (Müll. Arg.) Pax & K. Hoffmann	DDSS	**1,11**
Aristida purpurea Nutt.	GRAS	**1,11**
Argythamnia serrata (Torr.) Müll. Arg.	DDSS	**1,7,11**
Ayenia microphylla A. Gray	WDSS	**11**
Bahiopsis parishii (Greene) E.E. Schilling & Panero	DDSH	**1,5,7,11,13**
Baccharis sarothroides A. Gray	PSSH	**1,5,7,11**
Bebbia juncea var. aspera Greene	DDSH	**1,5,11**
Brickellia coulteri A. Gray	DDSS	**7,11**
Carlowrightia arizonica A. Gray	PSSS	**1,5,7,11**
Calliandra eriophylla Bentham	WDSH	**7,11,13**
Carnegiea gigantea (Engelm.) Britton & Rose	COCA	**1,5,11,13**
Celtis pallida Torr.	EGSH	**7,11,13**
Chilopsis linearis (Cav.) Sweet	WDTR	**1,7,11,13**
Colubrina californica I.M. Johnston	WDSH	**1,3,7,11,13**
Condalia globosa var. pubescens I.M. Johnston	EGTR	**7,11**
Cottsia gracilis (A. Gray) W.R. Anderson	VINE	**7,11**
Commicarpus scandens (L.) Standl.	DDSS	**7,11**
Cylindropuntia acanthocarpa var coloradensis (L.D. Benson) D.J. Pinkava	CASH	**5,11**
Cylindropuntia ramosissima (Engelm.) F.M. Knuth	CASH	**1,5,7,11,13**
Daucus pusillus Michx.	HERB	**1**
Echinocactus polycephalus Engelm. & J.M. Bigelow	CASS	**1,5,11,13**
Encelia farinosa A. Gray ex Torrey	DDSS	**7,11,13**
Encelia frutescens (A. Gray) A. Gray	DDSS	**5,13**
Ephedra aspera Engelm. ex S. Watson	PSSH	**1,5,7,11,13**
Eriogonum inflatum Torrey & Fremont	HERB	**1,5,7,11**
Euphorbia polycarpa var. polycarpa	HERB	**1,5,7,11**
Fagonia laevis Standley	DDSS	**7,11**
Fagonia pachyacantha Rydberg	DDSS	**7,11**
Ferocactus cylindraceus (Engelm.) Orcutt	CASH	**1,5,11,13**
Fouquieria splendens (Engelm.)	DDSH	**1,7,9,11,13**
Heteropogon contortus (L.) P. Beauvois ex Roem. & Schult.	GRAS	**1,11**
Hibiscus denudatus Bentham	DDSS	**1,6,7,11**
Hilaria rigida (Thurb.) Benth. ex Scribn.	GRAS	**1,11,13**
Horsfordia newberryi (S. Watson) A. Gray	EGSH	**6,13**

Hyptis emoryi Torrey	EGSH	**1,4.7,11,13**
Justicia californica (Bentham) D.N. Gibson	PSSH	**1,5,7,11,13**
Krameria erecta Willd. ex Schult.	PSSH	**1,7,9,11**
Krameria grayi Rose & Painter	PSSH	**1,7,9,11**
Larrea tridentata (Sesse & Moc. Ex DC.) Coville	EGSH	**1,7,11,13**
Lycium andersonii A. Gray	DDSH	**1,2,7,11**
Lycium berlandieri Dunal	DDSH	**2,7,11**
Lycium fremontii A. Gray	DDSH	**1,2,7,11**
Lycium macrodon A. Gray	DDSH	**2,7,11**
Lycium parishii A. Gray	DDSH	**1,2,7,11**
Lycium torreyi A. Gray	DDSH	**1,2,7,11**
Mammillaria dioica K. Brandegee	CASS	**1,5,11**
Menodora scabra A. Gray	DDSS	**1,7,11**
Mirabilis laevis var. villosa (Kellogg) Spellenberg	DDSS	**1,5,7,11**
Muhlenbergia microsperma (DC.) Kunth	GRAS	**1,11**
Muhlenbergia porteri Scribn. ex Beal	GRAS	**1,11**
Olneya tesota A. Gray	EGTR	**1,7,11,13**
Opuntia basilaris Englem. & J.M. Bigelow	CASS	**11,13**
Opuntia echinocarpa (Engelm. & Bigelow) F.M. Knuth	CASH	**1,5,11**
Opuntia leptocaulis (DC.) Knuth	CASH	**5,11,13**
Parkinsonia florida (Benth. ex A. Gray) S. Watson	PSTR	**1,7,11,13**
Parkinsonia microphylla (Torrey) Rose & I.M. Johnston	PSTR	**1,7,11,13**
Peniocereus greggii (Engelm.) Britton & Rose	CASS	**11**
Penstemon parryi (A. Gray) A. Gray	HERB	**7,11**
Peucephyllum schottii A. Gray	EGSH	**1,5,7,11,13**
Phoradendron californicum Nuttall	PARA	**1,7,11,12**
Pleurocoronis pluriseta (A. Gray) R.M. King & H.E. Robinson	DDSS	**1,11**
Porophyllum gracile Bentham	PSSS	**1,5,7,11**
Prosopis velutina Wooton	WDTR	**7,11,13**
Psorothamnus spinosus (A. Gray) Barneby	PSTR	**1,7,10,11,13**
Sarcostemma cynanchoides ssp Hartwegii (Vail) R. Holm	VINE	**7,11,12**
Salazariia mexicana Torrey	DDSS	**7,11**
Sebastiania bilocularis S. Watson	EGTR	**7,11**
Senna covesii (A. Gray) H.S. Irwin & Barneby	HERB	**7,11**
Simmondsia chinensis (Link) C.K. Schneider	EGSH	**1,7,11,13**
Sphaeralcea ambigua A. Gray	HERB	**1,7,11**
Stephanomeria pauciflora (Torr.) A. Nelson	DDSS	**1,5,7,11**
Tetracoccus fasciculatus var. hallii (Brandegee) Dressler	DDSH	**1,7,11**
Tiquilia canescens (A. DC.) A.T. Richardson	EGSS	**1,7,11**
Trixis californica Kellogg	DDSH	**1,7,11,13**
Tridens muticus (Torr.) Nash	GRAS	**1,11**
Xanthisma spinulosum var. gooddingii (A. Nelson) D.R. Morgan & R.L. Hartman	DDSS	**1,5,7,11**
Ziziphus obtusifolia var. canescens (A. Gray) M.C. Johnston	PSSH	**1,3,5,7,11,13**

Literature Cited

1. Baldwin, B. G., S. Boyd, B. J. Ertter, R. W. Patterson, T. J. Rosatti, D. H. Wilken, and M. Wetherwax. 2002. The Jepson Desert Manual: Vascular Plants of Southeastern California. University of California Press. Berkeley, California.
2. Chiang, F., and L. R. Landrum. 2009. Vascular plants of Arizona: Solanaceae, part three: Lycium. CANOTIA 5(1):17-26.
3. Christie, K., M. Currie, L. S. Davis, M. Hill, S. Neal, and T. Ayers. 2006. Vascular plants of Arizona: Rhamnaceae. CANOTIA 2(1):23-46.

4. Christy, C. M., D. Damrel, A. M. Henry, A. E. T. Nare, R. Puente-Martinez, and G. M. Walters. 2003. Lamiaceae mint family: part 1. Agastache Gronov., Hyptis Jacq., Lamium L., Leonurus L., Marrubium L., Monarda L., Monardella Benth., Nepeta L., Salazaria Torr., Stachys L., Teucrium L., and Trichostema L. Journal of the Arizona-Nevada Academy of Science 35(2):151-169.
5. Flora of North America Editorial Committee. 1993+. Flora of North America North of Mexico. 16+ vols. New York and Oxford.
6. Fryxell, P.A. 1993. Malvaceae mallow family: part 1. All genera except Sphaeralcea St.-Hil. Journal of the Arizona-Nevada Academy of Science 27(2):222-236.
7. Kearny, T. H. and R. H. Peebles. 1960. Arizona Flora. University of California Press. Berkeley and Los Angeles, California.
8. Levin, G. A. 1995. Euphorbiaceae spurge family: part 1. Acalypha and Cnidoscolus. Journal of the Arizona-Nevada Academy of Science 29(1):18-24.
9. Mason, C. T. 1999. Fouquieriaceae ocotillo family. Journal of the Arizona-Nevada Academy of Science 32(1):55-56.
10. Rhodes, S., J. Beasley, and T. Ayers. 2011. Vascular plants of Arizona: Fabaceae. CANOTIA 7:1-13.
11. Shreve, F. and I. L. Wiggins. 1964. Vegetation and Flora of the Sonoran Desert. Volume 1-2. Stanford University Press. Stanford, California.
12. Sundell, E. 1993. Asclepiadaceae milkweed family. Journal of the Arizona-Nevada Academy of Science 27(2):169-187.
13. Turner, R. M., J. E. Bowers, and T. L. Burgess. 1995. Sonoran Desert Plants: An Ecological Atlas. University of Arizona Press. Tucson, Arizona.

Appendix B. List of Scientific Publications

Publications

Sutfin, N. A., J. Shaw, E. E. Wohl, and D. Cooper. 2014. A geomorphic classification of ephemeral channels in a mountainous, arid region, southwestern Arizona, USA. Geomorphology 221:164–175.

Manuscripts in Preparation

Faulconer, J., S. Kampf, and J.R. Shaw. *In prep*. Thresholds for Runoff Generation in Ephemeral Streams with Varying Morphology in The Sonoran Desert In Arizona, USA

Harry, D.L., N.A. Sutfin, J.R. Shaw, J. Faulconer, A. Genco, E.E. Wohl, S. Kampf, and D.J. Cooper. *In prep*. Alluvial Stratigraphy of Ephemeral Streams in the Sonoran Desert, southwestern Arizona, USA: Constraints form DC Electrical Resistivity and Ground Penetrating Radar

Kampf, S. *In prep.* Subsurface moisture dynamics beneath ephemeral stream channels

Shaw, J.R., and D.J. Cooper. *In prep*. Ecological significance of a hydrogeomorphic stream classification: riparian plant community composition.

Shaw, J.R., and D.J. Cooper. *In prep.* Limitation to seedling establishment for Sonoran Desert riparian trees.

Shaw, J.R., and D.J. Cooper. *In prep.* Seasonal water relations of riparian trees in dryland ephemeral stream networks.